UNIVERSTY OF SOUTHAMPTON

FACULTY OF ENGINEERING, SCIENCE & MATHEMATICS

School of Chemistry

Towards separation of Platinum Group Metal anions from feed solutions

by

Josep Vicent Colomer i Martínez

Thesis for the degree of Doctor of Philosophy

February 2005

UNIVERSITY OF SOUTHAMPTON

ABSTRACT

FACULTY OF ENGINEERING, SCIENCE & MATHEMATICS

SCHOOL OF CHEMISTRY

Doctor of Philosophy

TOWARDS SEPARATION OF PLATINUM GROUP METAL ANIONS FROM FEED SOLUTIONS

By

Josep Vicent Colomer i Martínez

This thesis concerns the synthesis of new solid supports for anion separation. X-ray crystallographic studies of hexachloroplatinate(VI) show that hydrogen bond donor groups such as guanidinium and amidinium complex this anion in the solid state. Novel solid supports bearing the guanidinium group, with either a single, double or triple arm motif have been prepared. Also several solid supports bearing isothiouronium groups with either a single, double or triple arm motifs have been synthesised and their performance as chromatographic media has been evaluated. The solid supports are capable of forming multiple hydrogen bonds interactions with simple anions such as Br^-, I^-, SCN^-, NO_3^-, $H_2PO_4^-$, $S_2O_3^{2-}$, SO_4^{2-}, HPO_4^{2-}, AMP^{2-}, ADP^{2-}, ATP^{2-}, and PO_4^{3-}. These supports displayed longer retention times compared with solid supports which cannot bind anions via multiple hydrogen bonds. The thiourea modified supports showed shorter retention times when compared to guanidinium based resins.

Chromatographic separation of platinum group metal (PGM) feed on the resins containing thiourea showed no retention for any PGMs. The exception was Pd which was very strongly co-ordinated to the resin through the sulfur atom. Single guanidinium arm functionalised silica gel strongly retained ruthenium on the column. Methacrylate guanidinium single arm resin showed separation of Pt from the rest of the PGMs. The triple arm guanidinium support was capable of separating Pd from the rest of the PGMs. New elution orders for the PGMs were also found when triple arm guanidinium support was used.

Finally, anion complexation studies have been carried out on isophthalamides derivatives amidopyridines and 3,4-diphenylamidopyrrole clefts, in order to investigate whether these compounds could behave as efficient receptors of MCl_6^{2-} anions.

Aquesta tesi està dedicada als meus germans Juan i Carol

Chapter 1

Introduction

Chapter 2

Strategies for binding $[MCl_6]^{2-}$ anions and the synthesis and characterisation of new polymer solid-supported guanidine resins

Chapter 3

Synthesis and characterisation of new polymer solid-supported thiourea resins

Chapter 4

Separation of PGM anions feed by new solid-supports media

Chapter 5

Selective receptors for hexachloroplatinate (IV)

Chapter 6

Experimental

Appendix

Acknowledgments

I would like to thank Dr. Philip A. Gale for allowing me to work in his research group and for his supervision and help over the past three years.

Many thanks must go to Dr. Francesco Bernardis and Mr. Richard Grant from Johnson Matthey Technology Centre, for their advice and encouragement throught the last three years.

I must also thank the EPSRC Crystallographic Centre, Dr. Mark Light and Dr. Simon Coles who solved all the structures contained in this thesis and who possibly helped my samples to jump to the front of the queue and also to Prof. Mike Hursthouse.

My thanks go to the past and present members of the Gale group. Among them I would especially like to thank Dr. Korakot Navakhun for his advice in the lab, his "no worries" and "tomorrow will be another day" attitude. Also Lady Louise Sarah Evans for her company during the long, long, coffee breaks (I hope Phil does not read this part) and for her patience while proof reading my thesis, and Simon "cool" Brooks for teaching me some of the important words in English. Thanks also for the successful solvents exchange program that we carried out in the lab. I am grateful to have had their friendship.

Thanks to my football team (Juanjo, Andrea, Phil, Patrik, Luciano, Michael, Romain, Laurent, Edgard, Guilhem) for the enjoyable and tiring matches that we played. Thanks to the Bradley group for allowing me to use their equipment and some of their chemicals and for the company on Friday evening in the Staff Club. Thanks, most importantly though, for their friendship. Special thanks must go to Juanjo, Rosario, Mathilde and Jasmine.

Last but not least, I would like to thank to my parents Juan and Joaquina, my grandma Monica, my brother Juan and his lovely wife Celia and of course my admirably lovely sister Carol and her fiancé Paco for their continued support throughout my studies. Also I would like to thank my Aunt Lola and Cousins Monica and Paco for their support over the past three years. Finally, thanks to all my friends in Benitatxell for their support and the numerous welcome and leaving parties.

Glossary

	Polystyrene based resin
	Methacrylate based polymer
δ	Chemical shift (ppm)
ADP	Adenosine 5-diphosphate
AEM	2-Amino ethyl methacrylate
AIBN	2,2´-azobis-isobutyryl nitrile
AMP	Adenosine 5-monophosphate
Ar	Aryl
ATP	Adenosine 5-triphosphate
br	Broad resonance (NMR)
Calcd.	Calculated
d	Doublet (NMR)
DCM	Dichloromethane
Decomp.	Decomposition
DIEA	Diisopropylehtylamine
DMAP	Dimethylaminopyridine
DMF	Dimethylformamide
DMSO	Dimethylsulphoxide
DNA	Deoxyribonucleic acid
DVB	Divinyl benzene
EGDM	Ethylene glycol dimethacrylate
ES^+/ES^-	Positive/Negative electrospray
Et_2O	Diethyl eter
EtOH	Ethanol
FTIR	Fourier transform infrared
h	Hours.
IC	Ion chromatography
ICP-OES	Inductively coupled plasma optical emission spectroscopy
ISP	Inverse suspension polymerisation

J	Coupling constant
m	Multiplet (NMR) / medium (FTIR)
mg	Milligram
mL	Millilitre
Mp	Melting Point
MeCN	Acetonitrile
MeOH	Methanol
MHz	Megahertz
NMP	N-Methyl pyrrolidin-2-one
NMR	Nuclear magnetic resonance
Obs.	Observed
PBP	Phosphate binding protein
SBP	Sulphate binding protein
PEGDM	Poly(ethylene glycol) dimethacrylate
PGMs	Platinum group metals
ppm	Part per million
ppte	Precipitate
PS	Polystyrene
PTSA	*p*-Toluene sulfonic acid
PVA	Polyvinyl alcohol
RT	Room temperature
s	Singlet (NMR) / strong (FTIR)
SP	Suspension polymerisation
Span80	Sorbitan monooleate
t	Triplet (NMR)
TBA	Tetrabutylammonium
THF	Tetrahydrofuran
t_R	Retention time
V-50	2,2'-azobis(2-methylpropioamidine) dihydrochloride
VBC	Vinyl benzyl chloride
VBDA	Vinyl benzyldiamine monomer
w	weak (FTIR)

Chapter 1

Introduction

1.1 Supramolecular chemistry

The field of supramolecular chemistry has been defined by Jean-Marie Lehn[1] as "chemistry beyond the molecule". It investigates molecular systems in which the host and guest molecules are held together by reversible non-covalent interactions.

A supermolecule can be thought of as an organised structure consisting of two or more chemical species. These species are not covalently bound and form stable complexes in solution and in solid state. The host-guest interactions can occur through particular binding sites and generally most synthetic receptors are based on a similar design; consisting of a cavity, which approximates the size and shape of the potential guest molecule and incorporates some chemical features that are complementary to those displayed by the guest. This idea was described by Fischer[2] as the *"Lock and Key"* principle. The arrangement of binding sites in the host is complementary to the guest both sterically and electronically.

The double-helical structure of DNA (Figure 1.1) is probably the most famous example of complementarity in Nature. It carries genetic code information and therefore an alteration of its structure can be the cause of many diseases. The double helix combines two antiparallel strands which are held together by complementary hydrogen bounds between the base pairs.

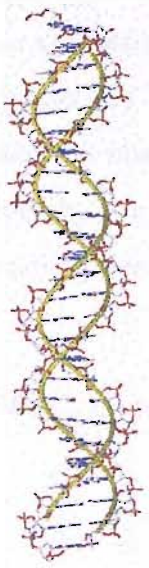

Figure 1.1 DNA helix

Supramolecular chemists working in this area can be thought of as architects combining individual convalently bonded molecular building blocks with a range of guests, designed to be held together by intermolecular forces. There are a number of such interactions that can be utilized: electrostatic interactions (ion-ion, ion-dipole and dipole-dipole), hydrogen bonds, π-stacking, Van der Waals forces, Lewis acids and hydrophobic effects. They can be used either in combination or individually to make a selective receptor.

The rapid growth in the area of anion binding is due to the realization of the many roles that anions play in medicine[3], biology[4,5], catalysis[6] and in the environment[7-9]. It is interesting to note that anion binding by proteins is most often achieved by way of neutral amide functions employing the hydrogen bond acceptor properties of the amido group[10].

1.2 Anion Coordination

Over the last 30 years, the area of anion coordination has not attracted much attention from the supramolecular chemistry community. It was 1968 when Park and Simmons[11] reported the synthesis of the first synthetic anion receptor. The co-ordination of anionic species presents a number challenges for supramolecular chemist. The variety of geometries (spherical for halides, linear for hydroxide, tetrahedral for phosphate, octahedral for hexachloroplatinate, etc.) makes the coordination a challenging task, because the receptors must be designed to be complementary to the guest. In addition the choice of solvent can also be important,

as some solvents are able to accept or donate hydrogen bonds, and may compete with the anion for the binding sites in the receptor.

The majority of enzyme substrates and co-factors are anionic. Anions are involved in many processes in biological systems such as the transport of hormones, protein synthesis and DNA regulation. The inherited genetic disorder cystic fibrosis, is characterised by a chloride inbalance in cells resulting from the mis-regulation of chloride ion channels in cell membranes[12]. The coordination of chloride has been achieved by many receptors but currently no such chloride transport system has been successfully demonstrated in vivo (Figure 1.2).

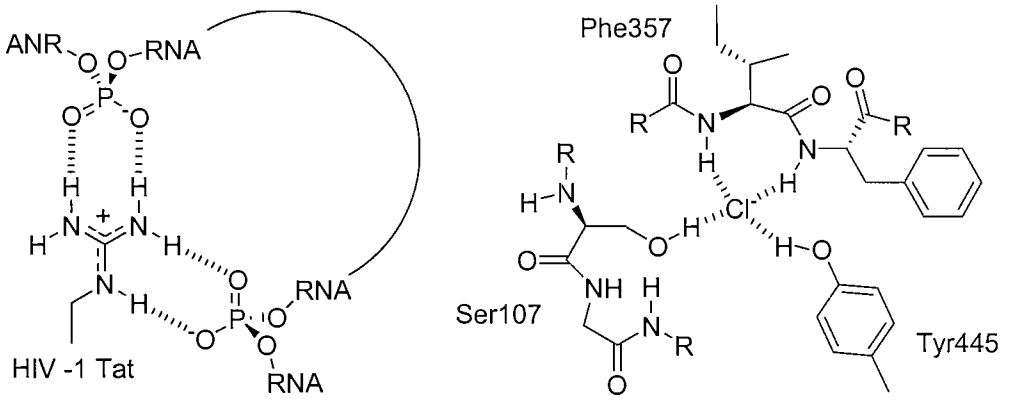

Figure 1.2: Arginine fork motif (left) and chloride anions channels (right).

The guanidinium group from the HIV-1 Tat protein bridges two phosphate anions in an interaction referred to as the "arginine fork" (Figure 1.2). The close proximity of the two phosphate residues forms a space that is complementary to a guanidinium group. This cavity should be present near RNA loops and bulges and not within double-stranded A-form RNA. Frankel and co-workers found that the guanidinium group from the HIV-1 Tat protein bridges between phosphate groups present in RNA, and the resulting hydrogen bond network allows the protein to distinguish selectively between different regions of RNA[13].

Other examples of anion recognition in biological systems occur in proteins and enzymes. The principal characteristic of enzymes is that they posses high selectivity to the substrate that they bind. Good examples of high selectivity in biological system are shown by the phosphate binding proteins (PBP)[14] and sulfate binding proteins (SBP)[15] (Figure 1.3). The ability of SBP and PBP to distinguish between

sulphate and hydrogen phosphate ions is believed to be due to the fact that at physiological pH hydrogen phosphate remains mono-protonated whereas sulfate does not (Figure 1.4)[5].

Figure 1.3: Crystal structures of the PBP (left) and SBP (right).

The PBP contains a hydrogen bond acceptor which allows the hydrogen phosphate donate a hydrogen bond to an Asp residue (marked in blue), however the SBP does not have a hydrogen bond acceptor group in the binding site, resulting in selectivity for SO_4^{2-}.

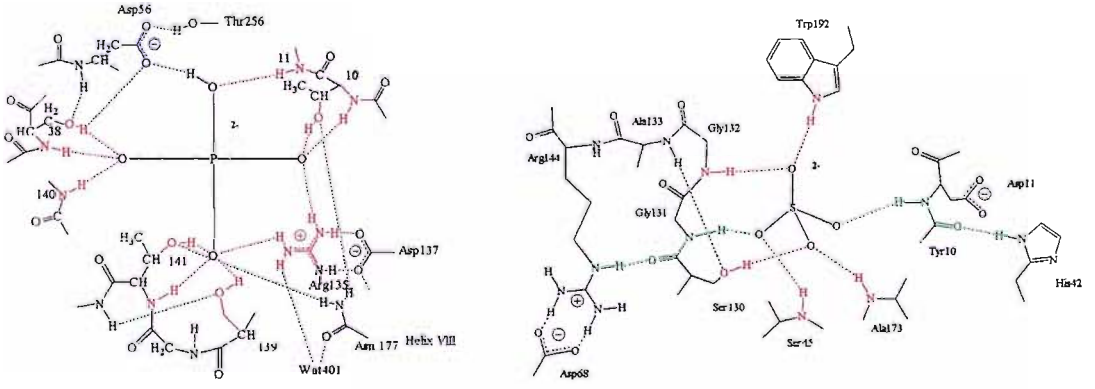

Figure 1.4: The binding motif of the complex PBP (left) and complex SBP (right).

Reactions in which oxygen and metal centres are involved always are going to be problematic, due to the tendency of oxygen to react irreversibly with the metal

centre, forming dioxo species. However Nature provides an excellent example of a functional and selective supramolecular receptor: haemoglobin. The role of the haem centre in haemoglobin[16] is to ensure not only that the oxygen binding is reversible, but also that complexation and release occur rapidly and at the correct concentrations. Furthermore, oxygen binding must occur selectively from amongst other components such as water, nitrogen, carbondioxide, and even stronger ligands for Fe(II) such as CO.

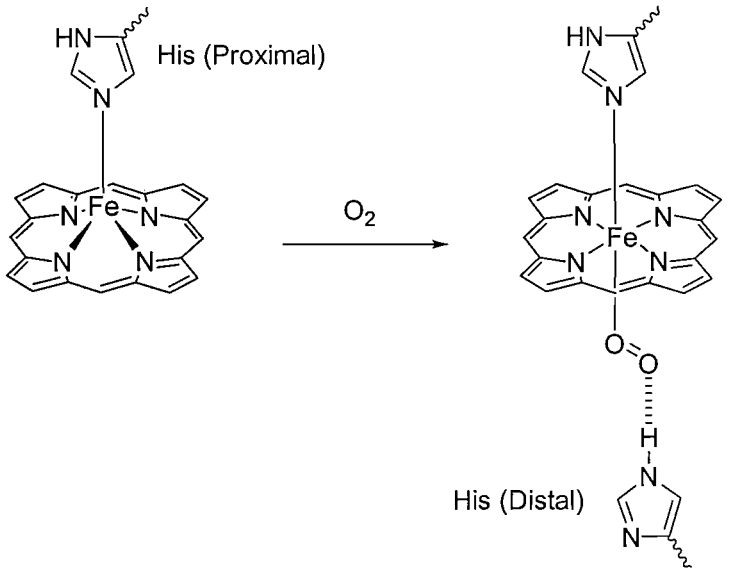

Figure 1.5: Porphyrin doming relaxes upon O_2 Binding.

The environment is another challenging area in which anion coordination can play an important role. Many of the fertilisers available contain nitrates and phosphates that can cause eutrofication[8] of lakes and rivers.

1.3 Hydrogen bond mediated anion co-ordination chemistry

The particular properties of the anions throughout biological systems, and the fact that the majority of enzymes substrates and co-factors are anionic, has influenced the sudden interest in anion complexation over the last 15 years. As previously discussed, the synthetic chemist can employ different interactions into any

designed receptor (Figure 1.6). The strength of a single covalent chemical bond is around ~ 350 $kJmol^{-1}$ rising to 942 $kJmol^{-1}$ for the triple bond in N_2. A non-covalent interaction is much weaker than a regular bond, at around 2 to 250 $kJmol^{-1}$. Although these interactions, when considered individually, are weak compared to covalent bonds their effects can still be dramatic. Electrostatic interactions (ion-ion, ion-dipole and dipole-dipole), hydrogen bonds, π-stacking, Van der Waals forces, Lewis acids and hydrophobic effects can all be utilised.

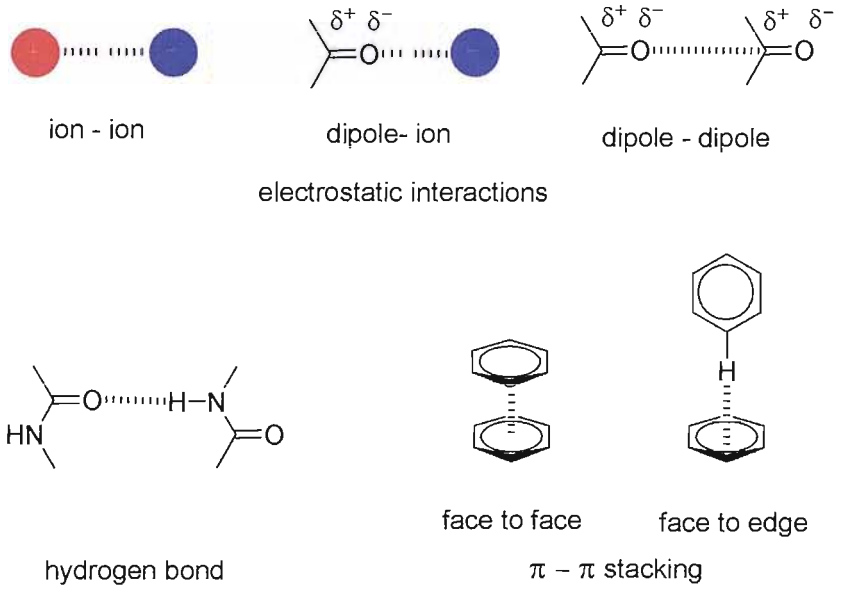

Figure 1.6: Non covalent interactions that can be used in the design of new receptors.

Typical interaction strengths of different non-covalent interactions are: electrostatic interactions such as ion-ion, ion-dipole and dipole-dipole (50-200 $kJmol^{-1}$); hydrogen bonds (4-120 $kJmol^{-1}$); π-stacking (2-50 $kJmol^{-1}$); Van der Waals forces (<5 $kJmol^{-1}$).

Another important issue for designing new anion receptors is the geometry of the guest. Anionic species have a wide range of geometries (Figure 1.7) and therefore a high degree of design may be required to make receptors complementary to their anionic guest.

Hydrophobic, hydrophilic interactions and pH also have an important role in anion recognition. Anions can be sensitive to small changes of pH, becoming protonated at low pH whilst anion receptors may themselves become deprotonated at high pH. For example, this can be a problem when using ammonium groups to bind

anions. Moreover, hydrophobic and hydrophilic interactions[17] can effect the selectivity between receptor and the anion, generally hydrophobic anions are bound more strongly in hydrophobic binding sites.

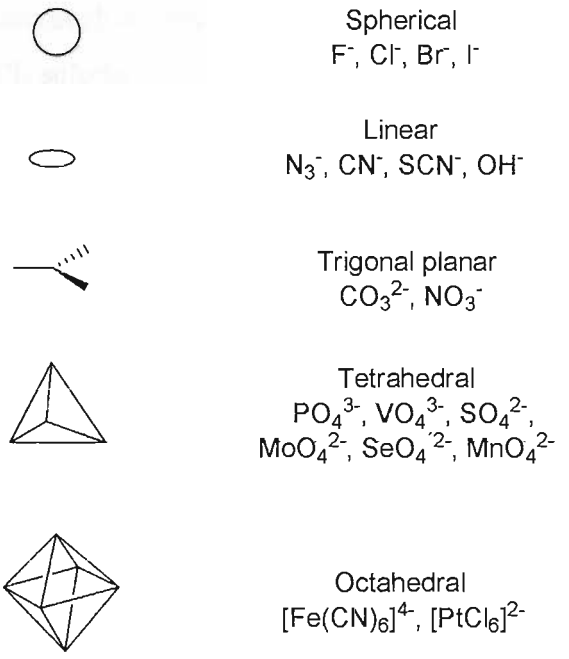

Figure 1.7: The structural variety of anions.

Hydrogen bonds are one of the principal interactions involved in the formation of supramolecular complexes, although these interactions when considered individually are weak compared to covalent bonds. We can generalize the hydrogen bond interaction through the representation below (Figure 1.8).

X = O, N (also F, Cl, Br, P, S, C)

Y = N, O, F, Cl, Br, I, S or P (C only when in π-system)

Figure 1.8: Representation of the hydrogen bond.

The amide group is one of the most commonly used functional groups to produce new anion receptors, such receptors can often utilise either only hydrogen bonding or

a combination of hydrogen bonding and electrostatic interactions. The amide binding units are most commonly preorganized to act together.

Hamilton[18] incorporated three amide groups into macrocycles **1** and **2** to produce receptors designed to bind tetrahedral anions. Binding studies showed that compound **1** bound spherical anions such as iodide and chloride, and planar anion such as nitrate in 2% DMSO-d_6/$CDCl_3$ solution.

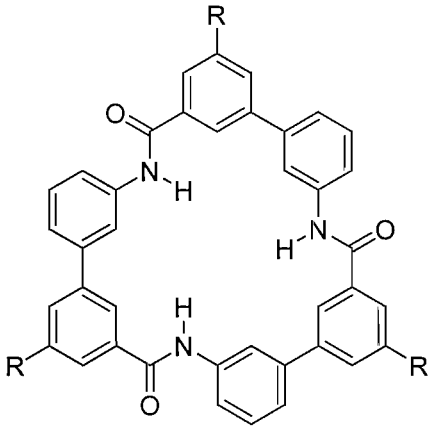

1 R=CO_2Et
2 R=NHBoc

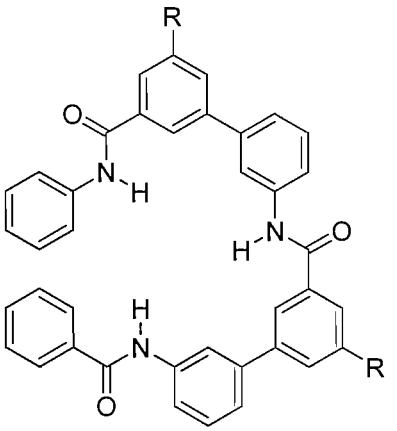

3 R=CO_2Me

Until addition of 0.5 equivalents of anion, 2:1 receptor:anion ratio was found, and 1:1 ratio after this point. When the anions were titrated in 100% DMSO-d_6 the 2:1 ratio was not found. Selectivity was observed for iodide over chloride; with binding constants of 1.3×10^5 M^{-1} and 8.8×10^3 M^{-1} respectively. Variation of the R group did not affect the binding properties. However, compound **3** showed only a weak affinity for anions with a stability constant of 120 M^{-1} for iodide in 2% DMSO-d_6/$CDCl_3$ solution.

Ungaro[19] et al. designed calix[4]arene based receptors **4** and **5** containing two alanine units used to form macrocycle. These preorganized receptors bound carboxylate anions with an association constants from 4900 to 44000 M^{-1} in acetone-d_6 solution. Furthermore, it was found that compounds **4** and **5** showed selectivity for benzoate due to their ability to π-stack with the aromatic rings of the calixarene.

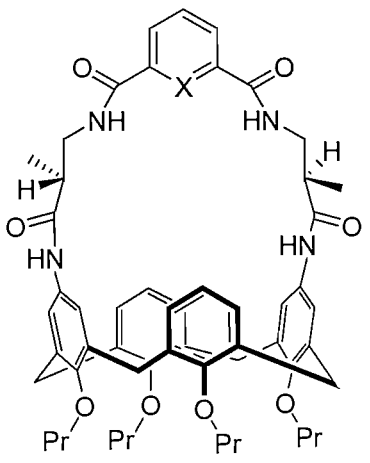

4 X= CH
5 X= N

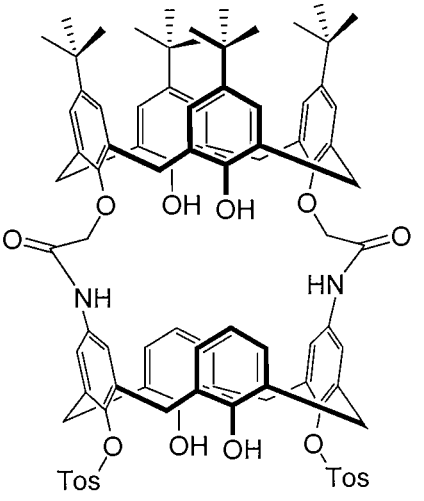

6

Beer[20] and co-workers developed calixarene **6** that bound fluoride with a stability constant of 1330 M^{-1} compared with 172 M^{-1} for chloride. The reason for this behaviour is that the calixarene was functionalized at the lower rim by two amide groups with another calixarene in the upper rim, so the resulting cavity was too small for chloride but was good to match for fluoride.

The guanidinium moiety forms strong non-covalent interactions with anionic groups such as carboxylates, phosphates, sulfates and nitrates through hydrogen bonding and charge pairing interactions. The ability of the guanidinium group to bind anions relies on the groups ability to remain protonated over a wide range of p*H* range, and the geometrical orientation of this functional group is such that it aligns with the anionic groups.

Compound **7** was designed by de Mendoza[21] and co-workers to bind amino acids through interactions between the ammonium group and the host crown, carboxylate with the guanidinium group and π-stacking interactions between the aromatic groups. Compound **7** was found to bind selectively amino acids with aromatic side chains such as phenylalamine and tryptophan over those with aliphatic chains. Other evidence which supports the formation of all three interactions in the host-guest complex was the selectivity for L-tryptophan over D-tryptophan.

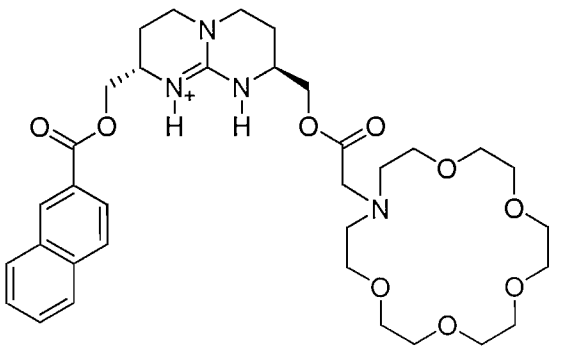

7

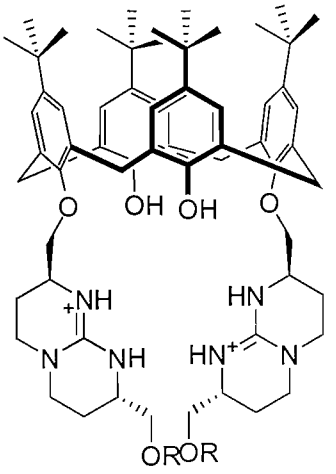

8 R= $Si(C_6H_5)_2{}^tBu$

More recently Fang[22] et al. produced an example of bicyclic guanidiniums functionalising a calix[4]arene. Receptor **8** and the corresponding monoguanidinium were found to enantioselectively extract amino acids into organic solvent. The results indicated selectivity for both binding and extraction of the L-phenylalanine over the D-isomer.

Thiourea[23,24] and urea have been employed to produce new anion receptors, in particular thiourea shows stronger affinities to bind anionic species due to the more acidic NH protons than the NH protons on urea.

Examples of thiourea derivatives are compounds **9** and **10** which have been synthesised by Tobe[25] and co-workers. These receptors display a binding motif of two thiourea groups connected through various spacers which are *meta-* and *ortho-*substituted. Binding studies showed selectivity for $H_2PO_4^-$ with both receptors. Also it was found that *meta-* and *ortho*-substituted aromatic linkers have higher binding affinity with $1.2x10^4$ M^{-1} for $H_2PO_4^-$ in DMSO-d_6 solution than the other analogous receptors.

Two new macrocycles, **11** and **12** containing the thiourea binding motif have been synthesised by Lee[26] et al. In this case, two different linkers have been used to connect the binding motif. 1,3,5-Triethylbenzene was selected as the spacer group to hold the six hydrogen bond donors in the optimal anion binding position. The complexation properties showed increased binding affinities compared with the unpreorganized spacer **12**. The association constants for acetate were found to be 5300 and 320 M^{-1} respectively in DMSO-d_6 solution.

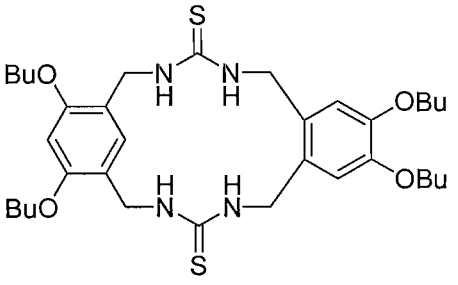

9

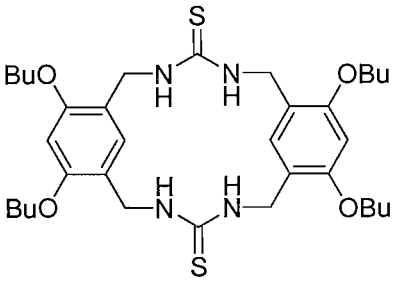

10

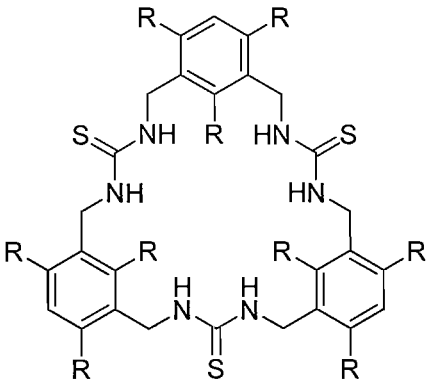

11 R= Et
12 R= H

1.4 Chromatographic separation of cations and anions

Methods of chemical analysis are generally selective, but not many are truly specific. Consequently, the separation of the analyte from the possible interfering species is often a stage of vital importance in the analytical procedure. Further, the method most commonly used to carry out analytic separations is chromatography, a method that has applications in all areas of science.

The liquid chromatography column was invented and named at the beginning of the last century by the Russian botanist Mikhail Tswett. He used the technique to separate several vegetable pigments, such as chlorophylls and xantophylls. The separate species appeared as bands of colour in the column, which justifies the name that he chose for the method (of the Greek *chroma* that means "colour", and *graphein* that means "write").

Basically we can find four different types of chromatography:

1) Gas chromatography (GC) which makes use of a pressurized gas cylinder and a carrier gas, such as helium, to carry the solute through the column. There are three types of gas chromatography: gas adsorption, gas liquid and capillary gas chromatography. The invention of the GC is generally attributed to James and Martin[27]. They reported the separation of volatile fatty acids by partition chromatography with nitrogen gas as the mobile phase and a stationary phase of silicone oil/ stearic acid supported on diatomaceous earth.

The main item is the column, originally a tube packed with a solid support coated with the stationary liquid, but now a fine tube with the liquid coated on the inner surface. The carrier gas, at first nitrogen, but now helium or hydrogen, passes from a cylinder through a pressure or flow-rate-controlling device to the sample injector at the column inlet. An important factor influencing column performance is its temperature; for most mixtures, it is necessary to work at higher temperatures, and good temperature control is always important, originally achieved by enclosing the column in a thermostatted block, but now in a hot air oven.

2) Liquid chromatography[28,29], there are a variety of types; they are reverse phase, high performance and size exclusion liquid chromatography, along with supercritical fluid chromatography. Reverse phase chromatography is a powerful analytical tool and involves a hydrophobic, low polarity stationary phase which is chemically bonded to an inert solid such as silica. The separation is essentially an extraction operation and is useful for separating non-volatile components. Size exclusion chromatography, also known as gel permeation or filtration chromatography does not involve any adsorption and is extremely fast. The packing is a porous gel, and is capable of separating large molecules from smaller ones. The larger molecules eluete first since they can not penetrate the pores. This method is common in protein separation and purification. Supercritical fluid chromatography is a relatively new analytical tool. In this method, the carrier is a supercritical fluid, such as carbon dioxide mixed with a modifier. This type of chromatography has not yet been implemented on a large scale. Probably one of the most important is the High Performance Liquid Chromatography (HPLC). It is similar to reverse phase, only in this method, the process is conducted at a high velocity and pressure drop. The column is shorter and has a small diameter, but it is equivalent to possessing a large number of equilibrium stages. HPLC is powerful analytical tool and involves a

hydrophobic low polarity stationary phase which is chemically bonded to an inert solid such as silica.

3) Affinity chromatography[28,29] involves the use of packing which has been chemically modified by attaching a compound with a specific affinity for the desired molecules, primarily biological compounds. The packing material used, called the affinity matrix, must be inert and easily modified. Agarose is the most common substance used. The ligands that are inserted into the matrix can be genetically engineered to possess a specific affinity. In a process similar to ion exchange chromatography, the desired molecules adsorb to the ligand on the matrix until a solution of high salt concentration is passed through the column. This is the most selective type of chromatography employed. It utilises the specific interaction between one kind of solute molecule and a second molecule that is immobilised on a stationary phase.

4) The basic principles in ion exchange chromatography consist of the attractive forces (electrostatic interactions) between the sample and gel matrix.

1.4.1 Ion exchange chromatography

Ion chromatography developed by Small[30] et al. in 1975 is now recognized as a very powerful method for the analysis of anions and cations in a variety of aqueous solutions. The basic principles of ion exchange chromatography consist of the attractive forces (electrostatic interactions) between the sample and gel matrix. The analyte to separate must have an opposite charge to the gel matrix. The ionic groups of exchanger columns are covalently bound to the gel matrix and are compensated by counter anions. Sample is added to the column, and exchange with the weakly bound counter ions takes place.

There are two exchanger types: basic (positively charged) and acidic (negatively charged). They in turn can be divided into those with weakly basic and weakly acid. With strongly basic or acidic, the majority of all functional groups are always present in ionized form, independent from the p*H* value in the specified operating range. For example, the quaternary amino group (R_3N^+-) are positively charged, while sulfonic acid groups (-SO_3^--) are negatively charged. The pK_a values of the quaternary amino groups are around 14, those of the sulfonate residues are below 1. In addition, weakly

basic types (pK_a values between 8 and 11) and weakly acidic types (between 4 and 6) exist.

Ion chromatography is widely used, especially as a convenient method for inorganic anion analysis, in the fields of environmental, industrial, clinical and food analysis[31-34].

Novel ion chromatography using a cationic coordination-unsaturated (hydrated) complex immobilized on a packing material as an anion-exchange group was investigated by Umehara[35] and co-workers. They reported the anion exchange property of an "on column" formed divalent metal complex with pyridine and quinoline derivatives. The material is packed into a column then a solution containing the salt of a divalent Lewis acidic metal cation (M^{2+}) and a suitable counter anion (A^-) is pumped through. The bis(2-pyridylmethyl)amino (bpa) group (or similar) is converted into a charged complex anion-exchange group (CCAGs).

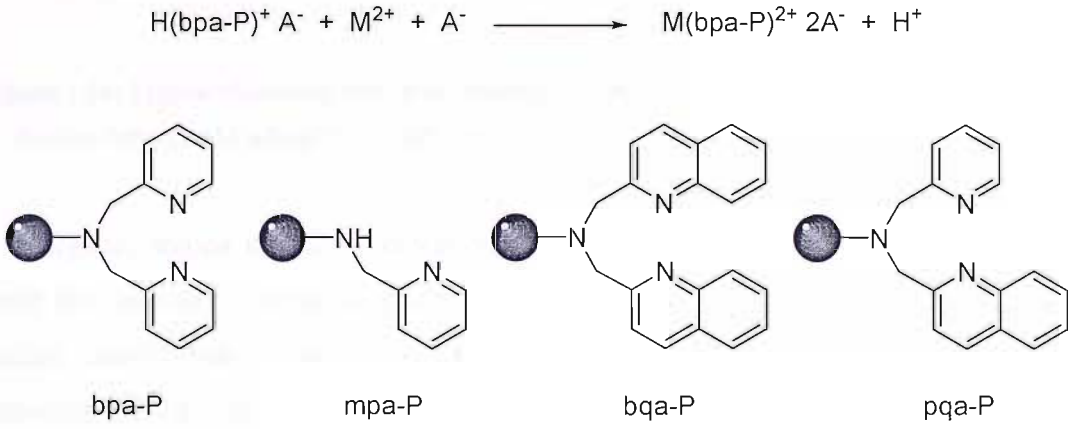

Figure 1.9: Functionalized packing materials. Solid circle means vinyl polymer gel.

It was found that the hardness and softness of the central metal cations as Lewis acids in charged complex anion exchange group (CCAGs) and the steric structure of the formed CCAGs had the greatest influence on the elution order.

The results showed an elution order of the anions with use of $H(bpa\text{-}P)^+$ which agreed with the Hofmeister[17] selectivity sequence ($Cl^- < NO_2^- < Br^- < NO_3^- < I^- < SCN^- < ClO_4^-$). $Cu(bpa\text{-}P)^{2+}$ showed anti-Hofmeister type chromatographic selectivity patterns (typical chromatograms of Cl^- and NO_3^- using $H(bpa\text{-}P)^+$ and $Cu(bpa\text{-}P)^{2+}$ anion exchange groups are shown in Figure 1.10). Umehara reported

that for the supports $H(pqa\text{-}P)^+$ and $H(bqa\text{-}P)^+$ the elution order of the anions seemed to originate from the difference in size of these protonated exchange groups. Also, it was found that the hardness/softness of the central cations in charged complex anion-exchange group (CCAGs) and the steric structure of the formed CCAGs mainly influence the property.

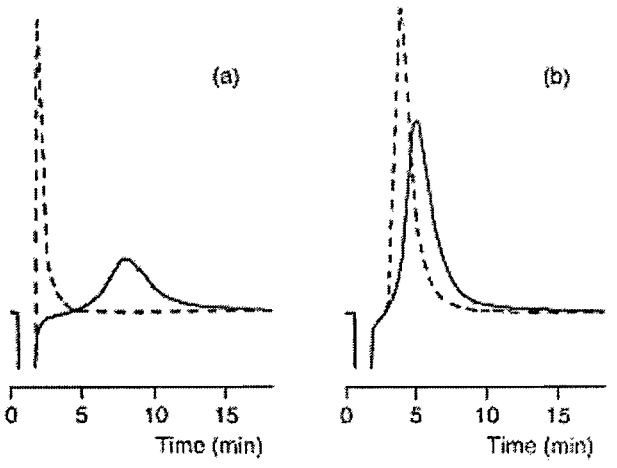

Figure 1.10: Typical chromatograms of (a) chloride and (b) nitrate. Anion exchange group: $H(bpa\text{-}P)^+$ (broken curve), and $Cu(bpa\text{-}P)^{2+}$ (solid curve). Eluent: 10 mmol dm^{-3} benzenesulfonate (pH 5.0).

Organic anions in tea are considered to be important from the point of view of taste and quality[36]. Inorganic and carboxylic acids contribute to the final acidity of coffee, acidity being associated with a better flavour and aroma[37]. Pablos[38] et al. reported an ion chromatographic method for the simultaneous determination of organic acids and inorganic ions present in both coffee and tea.

Acetic acid, ascorbic, citric, malic and succinic acids, Cl^- and $H_2PO_4^-$ were analyzed by ion chromatography using an isocratic elution with phthalate/phtalic acid (0.6 mM)/4% acetonitrile as the mobile phase and conductimetric detection. A chromatogram corresponding to a sample of coffee is shown in figure 1.11. It was found that succinic acid was not detected in any of the analyzed coffee samples, due to degradation occurring during the roasting process. Also, they reported the loss of volatile components during the roasting process which resulted in weight loss of the coffee beans and consequently the concentration on the non-volatile components such as chlorides and phosphates were higher in roasted coffees.

Pablos and co-workers analyzed three different varieties of tea: non-fermented, fermented and semi-fermented. Similar chromatograms (Figure 1.12) were obtained

for the three kinds of tea. They found that the concentration of succinic acid present in fermented tea is larger than the non-fermented tea. Also, they found a higher concentration of $H_2PO_4^-$ than Cl^-, irrespective of whether the tea was fermented or non-fermented.

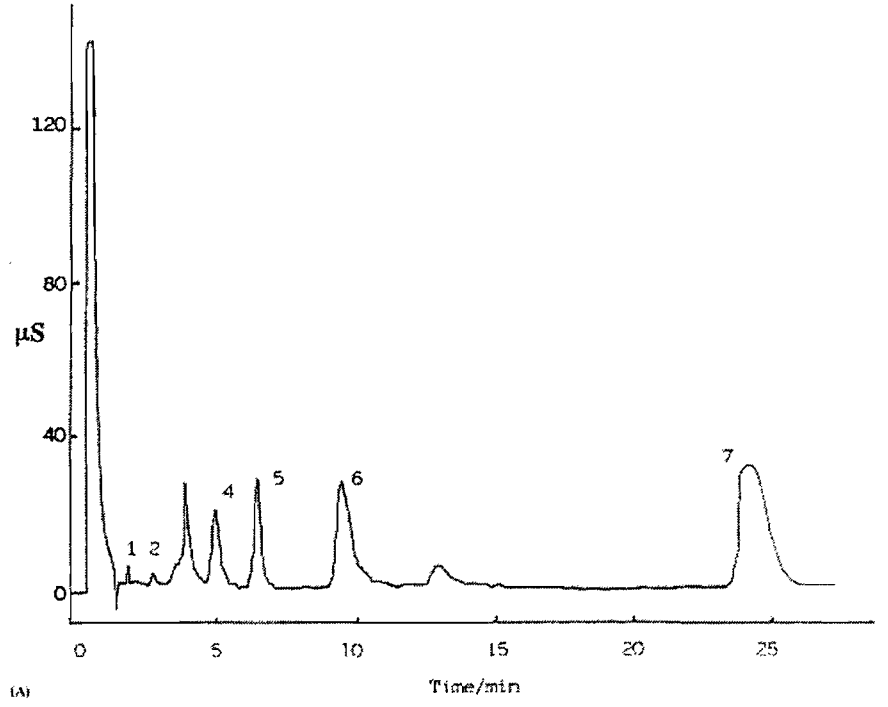

Figure 1.11: Chromatogram of roasted coffee sample. Peaks: (1) acetic; (2) ascorbic; (3) succinic; (4) $H_2PO_4^-$; (5) Cl^-; (6) malic; (7) citric.

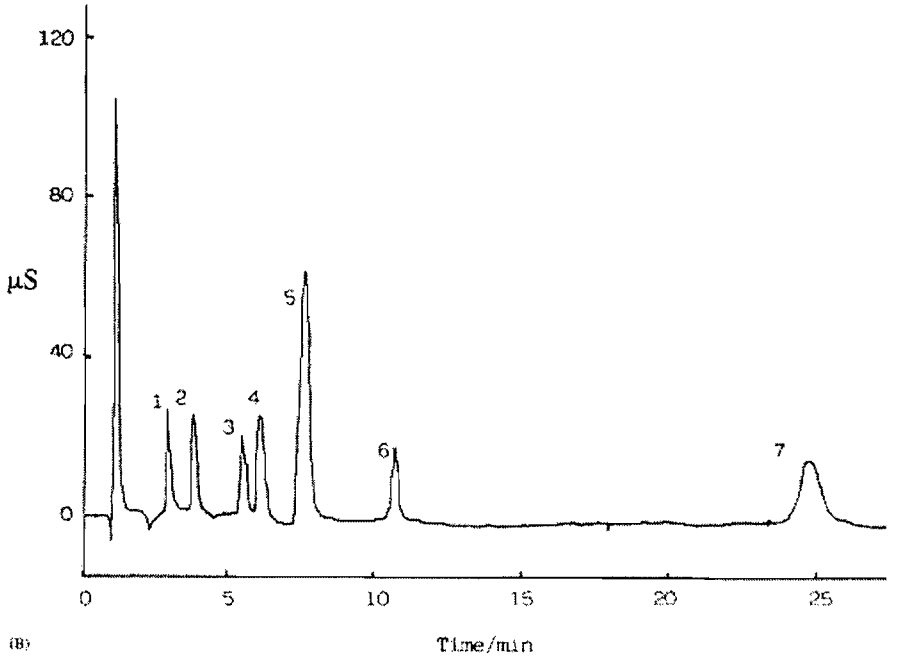

Figure 1.12: Chromatogram of tea sample. Peaks: (1) acetic; (2) ascorbic; (3) succinic; (4) $H_2PO_4^-$; (5) Cl^-; (6) malic; (7) citric.

In many cases, ion chromatography has been used to determine anions and cations separately using different separation systems. These approaches involve the use of a mixed bed of anion exchange and cation exchange materials[39,40] and anion exchange and cation exchange columns in tandem[41-44].

The effects of the order of ion exchange columns in series have been studied by Takeuchi[45] et al. They reported that only four cations could be detected since calcium ions were overlapping with bromide and nitrate ions when columns were connected in the series of cation exchange followed by anion exchange (Figure 1.13). Other anions such as iodate, bromate and nitrite were not included because they were detected in the first ten minutes and overlapped with the cations. They also found that the peak shapes and the resolution of cations deteriorated in Figure 1.13 compared to those in Figure 1.14 that have been analysed using additives in to the mobile phase.

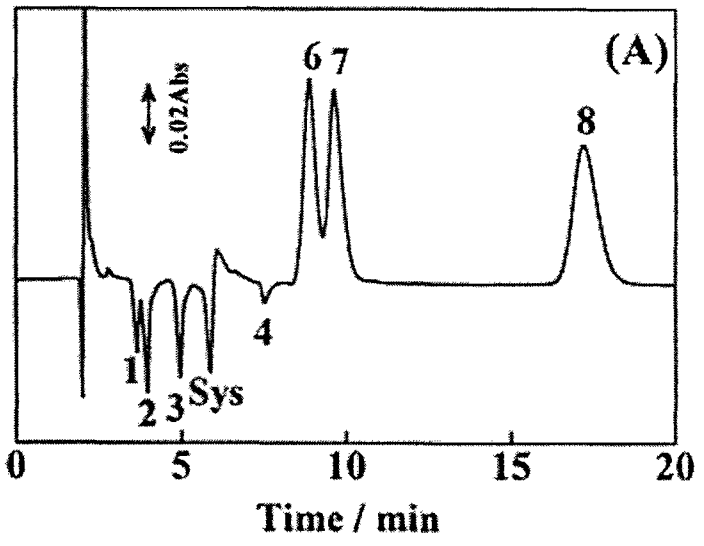

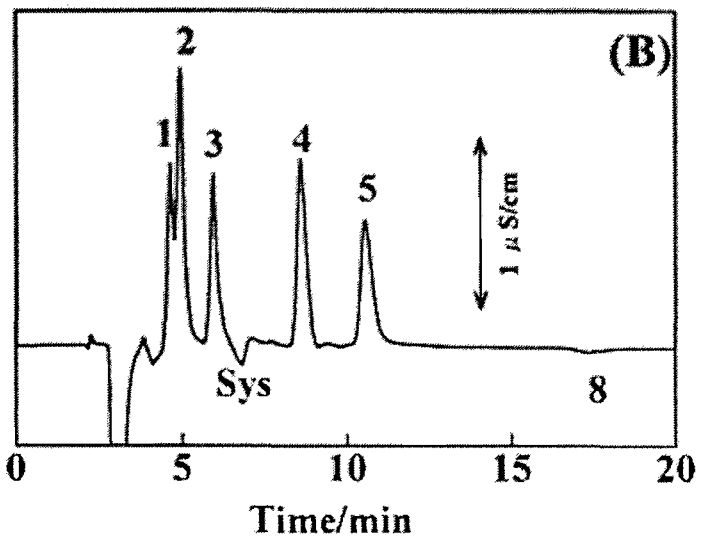

Figure 1.13: Simultaneous separation of both anions and cations on cation-exchange and anion-exchange columns in series. Detection of cations and anions for UV (A) and CD detection (B). Eluent, 1.0 mM H_2SO_4 containing 0.1 mM *L*-His. Flow rate, 1.0 $mLmin^{-1}$. Columns: TSK_{gel} Super IC-Cation (150x4.6 mm I.D.) and : TSK_{gel} IC-Anion-SW (50x4.6 mm I.D) connected in series. Analytes: 1 Na^+; 2 NH_4^+; 3 K^+; 4 Mg^{2+}; 5 Ca^{2+}; 6 Br^-; 7 NO_3^-; 8 I^-. Injection volume: 20μL. UV detection at 210 nm.

The effects of additives to the mobile phase such as amino acids, have also been reported by Takeuchi[45] and co-workers. Several amino acids such *L*-His, *L*-Arg, *L*-Trp, *L*-Ala and *L*-Phe were used to visualise analytes and to improve the shape of the cation peaks. They found that when *L*-His was not added to the mobile phase there was no identification of cations by the UV detection (Figure 1.14 A). Conversely, the cations were detected by conductivity detection (CD), independent of the presence or absence of *L*-His. When *L*-His was included in the mobile phase, cations can also be seen by UV detection (Figure 1.14 A) showing longer retention time.

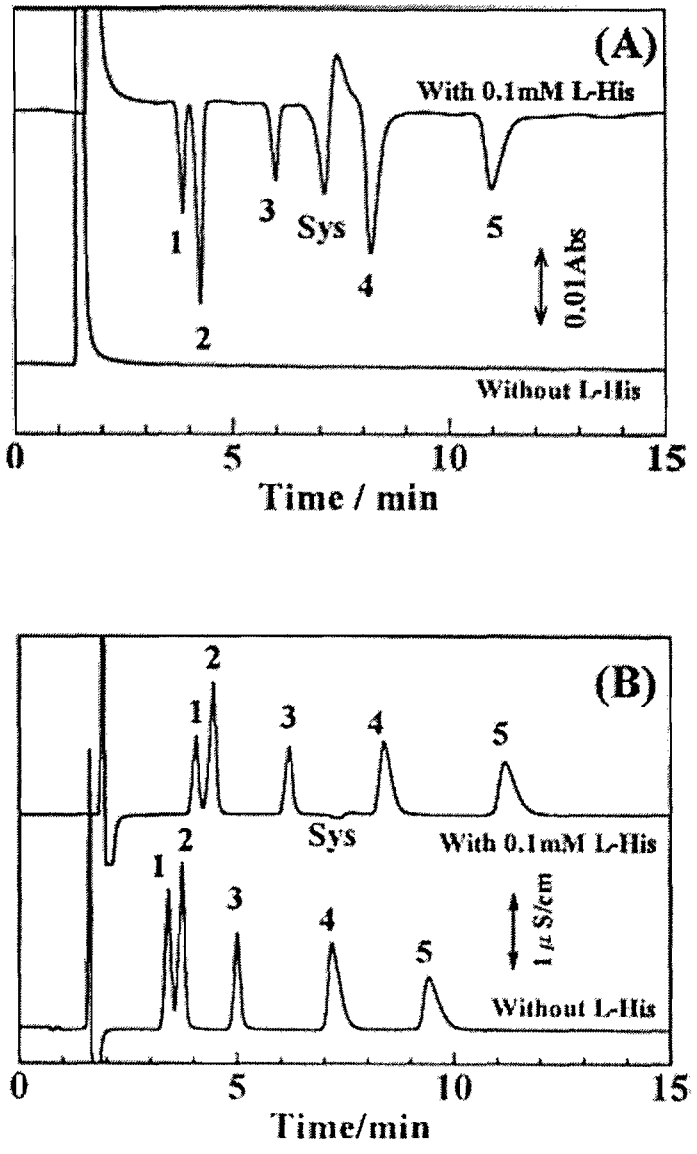

Figure 1.14: Effects of L-His on the retention and detection of cations for UV (A) and CD detection (B). Eluent, 1.0 mM H_2SO_4 with or without 0.1 mM L-His. Column: TSK_{gel} super IC-cation (150x4.6 mm I.D.). Flow rate, 1.0 $mLmin^{-1}$. Analytes: 1 Na^+; 2 NH_4^+; 3 K^+; 4 Mg^{2+}; 5 Ca^{2+}. Injection volume; 20μL. UV detection at 210 nm.

1.4.2 Ionic strengths in ion exchange chromatography

As in all forms of liquid chromatography, conditions are employed that permit the sample components to move through the column with different speeds. At low ionic concentration, all components with affinity for the ion exchanger will be

absorbed and nothing will remain in the mobile phase. When the ionic strength of the mobile phase is increased by employing more competitive eluent (neutral salt), the salt anions will compete with the sample anions for the binding sites, the sample components will be partially desorbed and start moving through the column. Increasing the ionic strength even more causes a larger proportion of the sample components to be desorbed, and speed of the movement through the column will increase. Ideally equilibrium between the sample anions and the mobile phase (eluent), the sample should be strong enough to exchange with the anion present in the matrix for itself, and the eluent should be strong enough to exchange again with the anion in the matrix producing desired anion exchange (Figure 1.15).

Figure 1.15: Proposed ion-exchange mechanism

1.5 The importance of the PGMs

Platinum Group metals (PGMs) are platinum Pt, palladium Pd, rhodium Rh, iridium Ir, ruthenium Ru and osmium Os. Their low natural abundance, the complex processes required for their extraction and refining and the important properties which they possess have resulted in PGMs having a great importance in industry.

Platinum[46] is a hard and extremely dense metal. Indeed platinum, and its associated metals, iridium and osmium, are the most dense metals known to man (platinum is nearly twice as dense as lead and 11% more dense than gold). It has a high melting point of 1772 °C, high temperature stability and is corrosion resistant. Platinum in certain compounds can inhibit the growth of cancerous cell growth. Platinum gives an important contribution to the environment, through its use as an efficient catalyst employed in motor cars, greatly reducing air pollution and greenhouse gases. Furthermore, the high recyclability of PGMs means they can be reused many times.

Palladium has the lowest melting point of all PGMs at 1554 °C and is also the least dense. Its melting point is still high when compared with other metals such as lead, and it has high temperature stability and corrosion resistance. It is also a good oxidation catalyst, is conductive, oxidation resistant and ductile when annealed. But it most incredible property is the ability to absorb 900 times its own volume of hydrogen at room temperature[46]. This makes palladium an efficient and safe hydrogen storage medium and purifier. Palladium's catalytic qualities result in it playing a key role in catalytic converters and air purification equipment. Its chemical stability and electrical conductivity make it more effective and durable plating than gold in electronic components.

Rhodium also has excellent catalytic activity. Many complex chemical compounds have been developed to be used as catalysts, especially in the organic chemicals industry. Rhodium-platinum gauzes are used in the production of nitric acid[46]. Rhodium's high melting point of 1963 °C, high temperature stability and corrosion resistance make it key to many industrial processes such as glass and glass fibre production. Rhodium's hardness makes it an excellent alloying agent to harden platinum.

Ruthenium is rarely used by itself because it is extremely difficult to work. It remains hard and brittle even at temperatures as high as 1500 °C. Ruthenium is, however, a useful addition to platinum and palladium to impart hardness in certain jewellery alloys and to improve resistance to abrasion in electrical contact surfaces.

The rarest of the PGMs, iridium is second only to osmium as the densest element and is the most corrosive resistant metal known. It is extremely hard (over four times that of platinum itself) and with its high melting point, temperature stability and corrosion resistance, it is used in high-temperature equipment such as the crucibles used to grow crystals for laser technology.

Osmium[46] is the densest substance know and the hardest of all the platinum group metals. It is ten times harder than platinum. Osmium also has a higher melting point than the other platinum group metals of 3050 °C. Like the other PGMs it is an extremely efficient oxidation catalyst and is used in fuel cells. This quality is

uniquely applied in forensic science for staining fingerprints and DNA (osmium tetroxide).

The demand[47,48] for the various platinum group metals by some of the most in important applications are presented in table 1.1.

Demand	Pt	Pd	Rh	Ir[(a)]	Ru[(a)]
Total demand (oz)	6.4 M	6.1 M	680000	103000	496000
Applications					
Autocatalyst	53%	60%	80%	-	-
Jewellery	34%	12%	-	-	-
Dental materials	-	14%	5%	-	-
Chemical	5%	4%	-	19%	28%
Electrical	4%	-	1%	-	-
Glass	4%	-	6%	-	-
Petroleum	2%	-	-	-	-
Investment	1%	-	-	-	-
Electrochemical	-	-	-	22%	24%
Electronics	-	15%	-	31%	32%
Other	8%	4%	2%	27%	16%

Table 1.1: Demand and end use patterns of PGMs in 2004. (a) Data 2003. Source: Johnson Matthey.

As a result of the growth in the number of applications of these technologically important metals, the production of PGMs has increased over the years.

1.6 Properties of the PGMs

1.6.1 General

The chemistry of PGMs is obviously of great importance in designing any separation and purification scheme. PGMs differ from base transition metals such as copper, iron and nickel, by forming more stable complexes. This is due to better metal ligand (nucleophilic group) orbital overlap arising from the spatially larger 4d and 5d orbitals osthe PGM. The most stable PGM complexes contain heavier donor atoms with the approximate overall order of S ~ C > I > Br > Cl > N > O > F. This particularly applies to Pt and Pd.

Mn	Fe	Co	Ni	Cu
Tc	**Ru**	**Rh**	**Pd**	Ag
Re	**Os**	**Ir**	**Pt**	Au

Figure 1.16: Periodic table.

The propensity for slow reactions is due to the relatively inert nature of heavier transition metals[49,50]. Inertness to substitution varies for comparable complexes of transition metals such that 3rd row > 2nd row > 1st row. The actual rate varies with the electron configuration Co(III), Rh(III), Ir(III) and Pt(IV) are d^6 and particularly inert while Ni(II), Pd(II) and Pt(II) are d^8 relatively more labile.

1.6.2 Chloro complexes

PGMs form a range of complexes with a variety of different ligands. The PGM chloro[51,52] complexes are the most effective medium in which all the PGMs can be brought into solution and concentrated, normally using high HCl concentration (approximately 6M). This is possible because the number of PGMs aquo species is reduced at this concentration, the most commonly encountered chloro species of the PGMs are listed in Table 1.2.

PGM	Major chloro species	Oxidation state
Platinum	$[PtCl_4]^{2-}$	Pt (II)
	$[PtCl_6]^{2-}$	Pt (IV)
Palladium	$[PdCl_4]^{2-}$	Pd (II)
	$[PdCl_6]^{2-}$	Pd (IV)
Iridium	$[IrCl_6]^{3-}$	Ir (III)
	$[IrCl_5(H_2O)]^{2-}$	
	$[IrCl_4(H_2O)_2]^{-}$	
	$[IrCl_6]^{2-}$	Ir (IV)
Rhodium	$[RhCl_6]^{3-}$	Rh (III)
	$[RhCl_5(H_2O)]^{2-}$	
	$[RhCl_4(H_2O)_2]^{-}$	
	$[RhCl_6]^{2-}$	Rh (IV)
Ruthenium	$[RuCl_6]^{3-}$	Ru (III)
	$[RuCl_5(H_2O)]^{2-}$	
	$[RuCl_4(H_2O)_2]^{-}$	
	$[RuCl_3(H_2O)_3]$	
	$[RuCl_6]^{2-}$	Ru (IV)
	$[Ru_2OCl_{10}]^{4-}$	
	$[Ru_2OCl_8(H_2O)_2]^{2-}$	
Osmium	$[OsCl_6]^{3-}$	Os (III)
	$[OsCl_5(H_2O)]^{2-}$	
	$[OsCl_4(H_2O)_2]^{-}$	
	$[OsCl_6]^{2-}$	Os (IV)

Table 1.2: Chloro species of the PGMs.

Whilst the majority of PGMs form full chloro complexes, the trivalent metals form mixtures of chloro aquo species in equilibria with each other. Ruthenium (IV) differs from the rest of the PGMs by forming oxo bridged dimers. Recovery of hexachloro species can be achieved very easily with ammonium salts.

$$2NH_4^+Cl^- + [MCl_6]^{2-} \rightleftharpoons [NH_4]_2[MCl_6] + 2Cl^-$$

PGMs chloro complexes are in general less reactive than the base metals. The order of increasing reactivity is $[MCl_6]^{2-} > [MCl_6]^{3-} > [MCl_4]^{2-}$.

1.6.3 Ion exchange reactions

The PGMs chloro complexes are normally anionic species and over the years many techniques have been employed to investigate the differences in anion exchange behaviour. These anionic species are able to undergo ion exchange reactions with different organic bases.

$$nRH^+Cl^- + [MCl_6]^{n-} \rightleftharpoons [RH]_n[MCl_6] + nCl^-$$

The order of ion pair formation with anion exchangers depends on the charge density of the anionic species. So species with low charge density are more easily paired than species with higher charge density, also the fact that it is harder to pack three large bulky organic cations around $[MCl_6]^{3-}$ anion than two around $[MCl_4]^{2-}$. These steric effects may also partly explain the fact that the tendency to form ion pairs with anion exchanger follows the pattern of $[MCl_6]^{2-} > [MCl_4]^{2-} > [MCl_6]^{3-} >$ aquo species.

In general there are two types of anion exchangers, the strong and weak base extractants. The strong base extractants are amines and quaternary ammonium salts, they can be very easily protonated even by contact with a weak hydrochloric acid solution. Weak base extractants need a higher acid concentration to be protonated. We can summarize that, strong base extractants can behave as ion exchangers at relatively low acid concentration while weak base extractants only at high acid concentration can they behave as ion exchangers.

The relative strength of extraction of the PGMs by different classes of amine follows the pattern $R_4N^+Cl^- > R_3NH^+Cl^- > R_2H_2N^+Cl^- > RH_3N^+Cl^-$. This is because the strength of extraction of the chloride ion improves along the series. This is a result of the greater hydrogen bonding ability, which in turn is due to the increasing number of amino hydrogens in the organic cation.

A typical strong base anion exchange extractant is trioctylamine, and a typical weak base anion exchange extractant is tributylphosphate. As an example, $[IrCl_6]^{2-}$ has a high distribution on ion exchangers while $[IrCl_6]^{3-}$ is very poorly extracted under the same conditions.

1.6.4 Oxidation states

As previously reported, heavy transition metals such as the PGMs exhibit a wider range of stable oxidation states than lighter metals.

The PGMs redox behaviour shows that the stability of the higher oxidation states tends to decrease as one moves across the periodic table from left to right, and they increase when going from the second to the third row (Table 1.3).

Ruthenium		**Rhodium**		**Palladium**	
Ru (III)	$[RuCl_5(H_2O)]^{2-}$				
	↕ 0.83V	Rh (III)	$[RhCl_6]^{3-}$	Pd (II)	$[PdCl_4]^{2-}$
Ru (IV)	$[Ru_2OCl_{10}]^{4-}$		↕ >1.4V		↕ 1.29V
	↕ >1.4V				
Ru (VIII)	RuO_4	Rh (IV)	$[RhCl_6]^{2-}$	Pd (IV)	$[PdCl_6]^{2-}$
Osmium		**Iridium**		**Platinum**	
Os (III)	$[OsCl_6]^{3-}$				
	↕ 0.42V	Ir (III)	$[IrCl_6]^{3-}$	Pt (II)	$[PtCl_4]^{2-}$
Os (IV)	$[OsCl_6]^{2-}$		↕ 0.96V		↕ 0.74V
	↕ 1.0V				
Os (VIII)	OsO_4	Ir (IV)	$[IrCl_6]^{2-}$	Pt (IV)	$[PtCl_6]^{4-}$

Table 1.3: Redox behaviour of the PGMs in acidic chloride media.

Kinetic and thermodynamic factors are also involved in the equilibrium redox potentials. Kinetic factors are related to the electronic configuration and hence oxidation state so reaction rates tend to decrease in the order $d^5 > d^3 > d^4 > d^6$ for octahedral complexes. Reaction rates for square planar d^8 complexes vary such that Pd(II) > Au (III) > > Pt(II). For example[53], the Ir(IV)/Ir(III) couple has a redox

potential of -0.87V and the Pt(IV)/Pt(II) couple has similar redox potencial of -0.74V, but the d^6 configuration of Pt(IV) means that the rate of reduction is much slower than for Ir(IV) d^5.

Manipulation of oxidation states can be used to achieve separations, particularly for third row transition metals such as Os, Ir and Pt which are more stable than the second row, Ru, Rh and Pd metals.

1.7 Chromatographic separation of the PGMs

Until the 1970's the separation of the PGMs was achieved using a series of precipitation reactions. However, relatively poor selectivity was obtained for many of the precipitation steps. This problem was overcome by using the solvent extraction technique. Pioneering contributions on the use of liquid amines for PGMs analysis and recovery were made in the Soviet Union by Gindin[54] et al. and Dolgikh[55] et al. A good review was also published on the use of ternary[54-56] and quaternary amines[57]. These efforts led to industrial application of amines (octylamine) in PGMs recovery[58]. This latter technique offers a number of advantages with respect to the precipitation methods, such as higher selectivity and purity.

More recently the chromatographic separation of the PGMs was proposed as a new alternative technique. This technique involves the anion exchange method to selectively extract the PGMs in their tetravalent oxidation state.

As previously mentioned, due to their low natural abundance and the complex processes required for their extraction and refining the isolation techniques of the PGMs are of great importance. The important properties which they possess and the wide use of palladium and platinum not only in automotive catalytic converters but as a drug (Pt) and in food production (Pd)[59] has led to more uncontrolled release of these metals in to the environment, which further increases the importance of such isolation techniques.

Many research groups have being investigating different ways to analyse and isolate the PGMs. In particular Rehkämper[60] and co-workers have been developing new ion-exchange techniques for the separation of the PGMs and other siderophile elements from geological samples. They investigated two ion-exchange separation

procedures that are suitable for the isolation of Zn, Cd, Ag, Re, Ru, Pd, Ir and Pt from 5 to 10g silicate rock samples. The experimental details of the two protocols "Method 1 and 2" are summarized in Tables 1.4 and 1.5 respectively.

Eluent	Volume (mL)	Eluted
Sample solution in 1M HCl + 10% Br_2	~5-10	Bulk matrix
0.5 M HCl+10% Br_2	2	Bulk matrix
0.8 M HNO_3+10% Br_2	0.5	Bulk matrix
0.8 M HNO_3+10% Br_2	5	Zn, Cd
11 M HCl	2	Ag
11 M HCl	10	Ru
8 M HNO_3	10	Pd, Re
13.5 M HNO_3	14	Ir, Pt

Table 1.4: Elution sequence of ion-exchange procedure "Method 1" for the separation of Zn, Cd, Ag, Re, Ru, Pd, Ir and Pt from geological samples.

Eluent	Volume (mL)	Eluted
Sample solution in 1M HCl + 10% Br_2	~5-10	Bulk matrix
0.5 M HCl+10% Br_2	2	Bulk matrix
0.8 M HNO_3+10% Br_2	0.5	Bulk matrix
0.8 M HNO_3+10% Br_2	5	Zn, Cd
8 M HNO_3	10	Ru, Re
13.5 M HNO_3	14	Pt, Ir
11 M HCl	2	Ag
11 M HCl, 13.5 M HNO_3	8, 5	Pd

Table 1.5: Elution sequence of ion-exchange procedure "Method 2" for the separation of Zn, Cd, Ag, Re, Ru, Pd, Ir and Pt from geological samples.

Both separation procedures use the same ion-exchange columns utilising quartz-glass columns (6mm diameter) fitted with acid-cleaned quartz-wool plugs for the support of the resin bed. The columns were filled with 1.25 mL of Bio-Rad AG1X8 (200-400 mesh). The same acids were used for the loading of the sample solutions (5-10mL 1M HCl + 10% Br_2) and the initial rinse (2mL 0.5 M HCl + 10% Br_2, 0.5 mL 0.8M HNO_3 + 10% Br_2). While the ion-exchange procedure of Method 2 (Table 1.5) uses the same acids as Method 1 (Table 1.4) they are applied in a different order and this results in different elemental elution sequences being obtained. This can be significant, and allows Method 2 to produce the separation of Pd from Ru, which is not possible with Method 1.

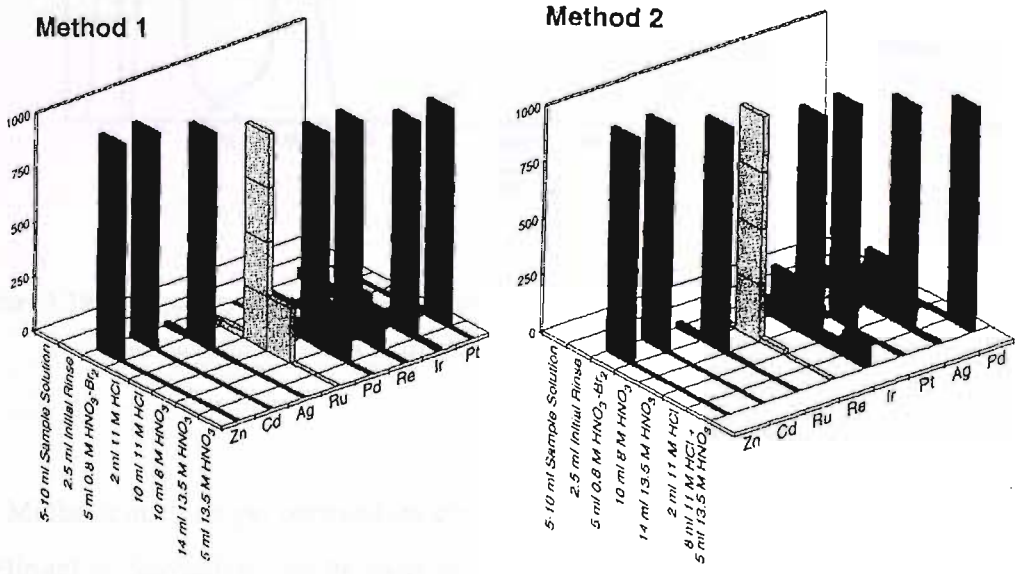

Figure 1.17: Elution of Zn, Cd, Ag, Re and the PGMs Ru, Pd, Ir and Pt during anion exchange separation of standard rock SU-1a using "Method 1" and "Method 2". Effluent fractions with no data where not analysed. 2.5 mL initial rise = 2 mL 0.5 M HCl + 10% Br_2 followed by 0.5 mL 0.8 M HNO_3 + 10% Br_2.

A method for the separation of the PGMs from a gold free halide solution using at least one chromatographic column has been developed by Schmuckler[61] (when gold is present with the PGMs, its prior removal is required by an additional chromatographic column containing an absorbent based on polystyrene divinyl benzene). The solution is passed through a column containing a solid absorbent

whereby the PGMs are absorbed. The loaded absorbent is eluted by a halide salt solution, producing well-spaced fractions, each containing only one single noble metal, eluting in the order: Ru, Pd, Pt, Ir and Os (Figure 1.19).

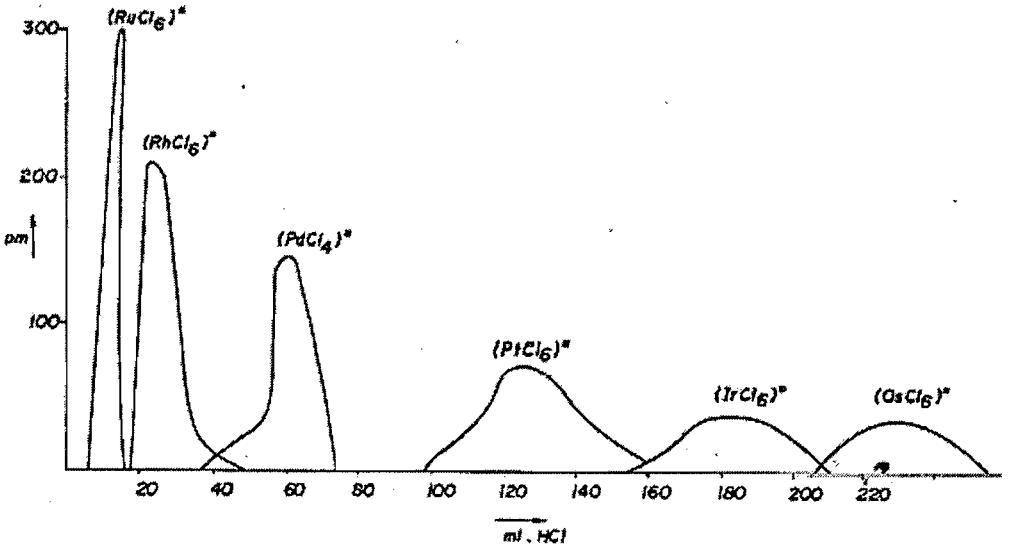

Figure 1.19: Chromatographic separation graph of a mixture of Rh, Pd, Pt, Ir, Os on Sephadex G-10. Columns dimensions, 300x10 mm. Flow rate, 0.5mL/min. Eluent, 1M HCl.

Methods such as gel permeation chromatography, in which hydrophilic gels such as Biogel or Sephadex, can be used to achieve separation of Rh from the rest of the PGMs as they bypass the difficulties involved in the separation and purification by solvent extraction. With gel permeation chromatography, separation of the chlorocomplexes of Rh, Pd and Pt occurs gradually. Rhodium emerges first, followed by palladium and finally by platinum. Schmuckler[62] and co-workers found that small inorganic molecules have much higher distribution coefficients (K_d>1), indicating more specific interactions such as ion exclusion, H-bonding, adsorption, hydration and dipole-dipole interactions. The trend of increasing distribution coeficient (Rh K_d=1.5; Pd K_d=5.1; Pt K_d=9.4) in the distribution data from Rh to Pt can largely be explained by hydrogen bonding interactions between the chloride and hydrogens on the sephadex gel. These bonds are specific and weak and thus make for

easy elution of the metal complexes from the chromatographic columns by aqueous salt solutions (Figure 1.20).

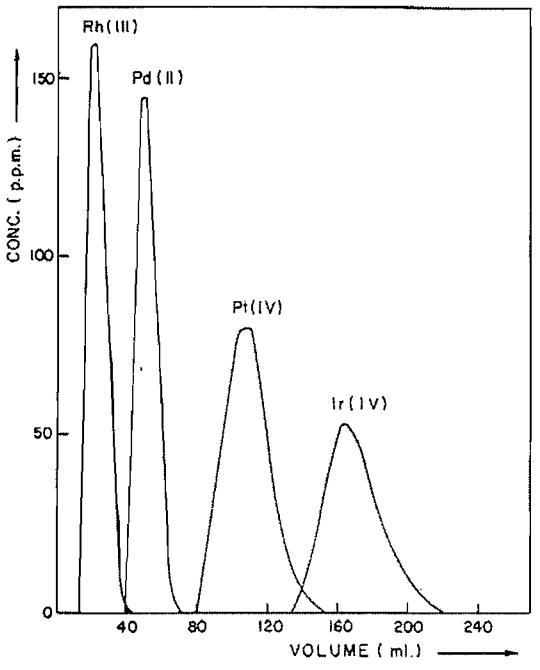

Figure 1.20: Chromatographic elution graph of a mixture of Rh, Pd, Pt and Ir on Sephadex G-10. Concentration of metals salts $5x10^{-3}$M. Column dimensions, 300x10 mm. Flow rate, 0.5 mL/min. Eluent, 1M NaCl.

Chelating ion exchange resins are polymers carrying functional groups which are able to form complexes with selected ions. In contrast to the conventional ion exchange resins described above, chelating resins combine with complexes through ion exchange and complexing reactions, and hence can exhibit high selectivity to some ions or groups of ions, providing a wide range of practical applications.

More recently Xiaopeng[63] et al. have been investigating a chelating resin containing isonicotinic acid hydrazone (P-NHZ) as the functional group in the separation and concentration of Pd and Pt in road dust (Figure 1.21).

Figure 1.21: Structure of polyacrolein-isonicotinic acid hydrazone chelating resin.

The results for the loading and elution of Pd and Pt under different conditions are summarized in Table 1.6. It shows that Pd and Pt can be selectively taken up by P-NHZ resin within a wide range of acidity and in the presence of different acid media, such as HCl, HNO_3, HF. The results reveal that P-NHZ resin is very effective for the concentration and separation of Pd and Pt.

Loading conditions	Element	Average recovery (%)
HCl, 0.1-1.0 M	Pd	96.2
	Pt	84.6
HNO_3, 0.3-0.8 M[(a)]	Pd	94.4
	Pt	84.2
HF, 0.45-1.2 M[(a)]	Pd	93.8
	Pt	93.6
H_3BO_3, 0.08-0.32 M[(a)]	Pd	99.7
	Pt	88.8

Table 1.6: [(a)]In the presence of 0.1 M HCl. Chromatographic column, 8 mm with 0.4g P-NHZ resin, resin bed height 2 cm, feed solution 100 mL, elution solution: 0.5% (w/v) thiourea in 0.1 M HCl 50 mL; flow rate 2 mL/min; room temperature.

The recovery of Pd throughout the experiments suggest that quantitative separation and elution can be achieved under the experimental conditions used, whilst recoveries for Pt remain somewhat incomplete, only about 85% of the initial sample was recovered.

1.8 The objectives of this thesis

The aim of this project is to find new strategies for binding MCl_6^{2-} anions to organic based receptors, and therefore the synthesis of these novel receptor molecules. Early results in this area of study led to the exploration of solid supported organic receptor molecules as a novel approach to the selective separation of MCl_6^{2-}.

A variety of solid supports bearing guanidinium, thiourea and isothiouronium groups have been synthesised and their performance as anion exchangers tested with various simple mono-anions such as Br^-, I^-, SCN^-, NO_3^-, $H_2PO_4^-$, di-anions such as $S_2O_3^{2-}$, SO_4^{2-}, HPO_4^{2-}, AMP^{2-}, ADP^{2-}, ATP^{2-} and the tri-anion PO_4^{3-}. In order to establish the possible effect of the interactions involves in the mechanism of the anion exchange.

The performance of the solid-supported resin as chromatographic media was evaluated by injecting samples of a reduced PGMs concentrate onto previously packed columns with the desired solid support.

Chapter 2

Strategies for binding $[MCl_6]^{2-}$ anions and the synthesis and characterisation of new polymer solid-supported guanidine resins

2.1 Consequences of proton transfer in guanidine

Guanidine was first obtained by oxidative degradation of an aromatic natural product, guanine, isolated from Peruvian guano[64]. The guanidine moiety is incorporated in many natural products and also in synthetic systems of biological importance. Guanidine is a substructure of many important molecules, such as already discussed arginine, creatine (muscular energy intermediate), guanine (the purine base of the nucleic acids DNA and RNA) and other biomolecules[65].

The guanidinium ions are special cases of n-π conjugated heteroallylic systems[66]. One imino and two amino nitrogens are linked to the same carbon atom, leading to a cross-conjugated system containing six π-electrons[67,68].

Guanidine and the guanidinium ion exhibit unusual thermodynamic stability (for acyclic systems), delocalization of six π-electrons and energetic barriers to rotation. The enhanced stability of the neutral and of the ionic species was considered in terms of resonance theory by Pauling[69,70]. According to this theory, the derived free base

structures, allows the change to be separated (Figure 2.1). Protonation of guanidine leads to a highly symmetric ion, for which three equivalent resonance structures are possible.

The remarkable stability of the guanidinium ion, similar to that observed for other Y-shaped delocalized systems containing six π-electrons, has lead to the proposition of a new type of aromaticity, the so called "Y-aromaticity"[67,68]. The aromaticity of the guanidinium ion leads to unique properties, especially with respect to physicochemical characteristics, in particular the basicity of guanidine in aqueous solution.

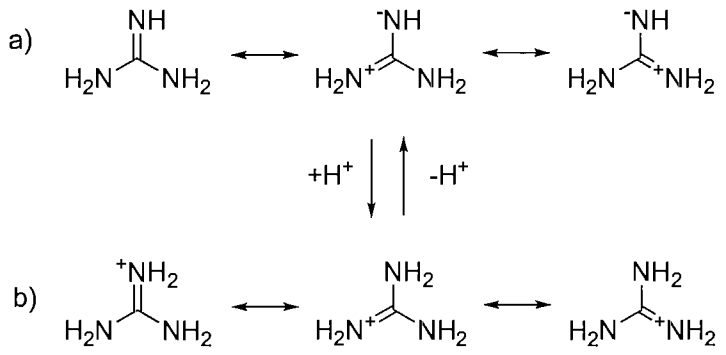

Figure 2.1: Resonance stabilization of a) guanidine and b) guanidinium ion.

Obtaining guanidine as a free base provided the opportunity to explain the difference between the basicities of guanidine in the gas phase and in solution. Comparison with other organic bases, exhibiting smaller or higher basicity than that of guanidine, indicated that all the factors, Y-delocalization, resonance and symmetry, play an important role in the stability of the protonated forms.

Guanidine possesses three nitrogen atoms, susceptible protonation. The n-π conjugation possible between the amino and imino nitrogen (Figure 2.1) increases the basicity of the *N*-imino centre and decreases the basicity of the *N*-amino atom. As a consequence of this conjugation effect, the *N*-imino atom is first protonated[71,72]. The basicity of the *N*-amino atom is relatively weak. Similar behaviour was observed in amidines[73,74]. In the neutral amidine molecule, the *N*-imino atom is much more susceptible to proton attachment than the *N*-amino atom.

Even in strong acids, such as H_2SO_4, CF_3SO_3H and FSO_3H in SO_2ClF, only monoprotonated guanidinium ion was observed[72,75,76]. A second protonation of guanidine (at the *N*-amino atom in the monocation) is possible in the so called "magic acid"[77] (the 1:1 molar FSO_3H/SbF_5 acid system) diluted in SO_2 or SO_2ClF[72,75]. Tri- and tetraprotonated guanidines (Figure 2.2) have not been identified.

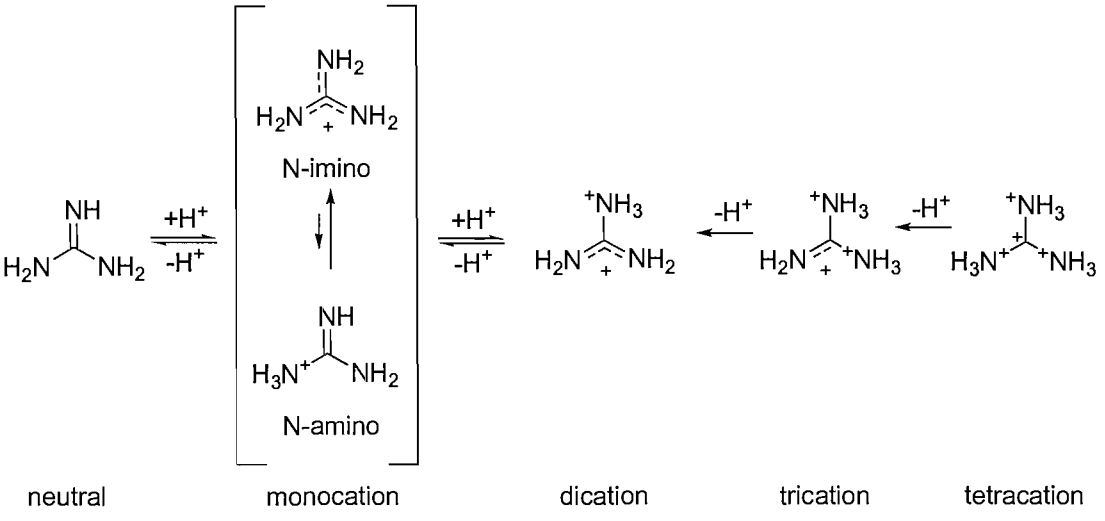

Figure 2.2: Protonated forms of guanidine.

The free species (guanidine, its conjugate acid and the proton) do not exist in solution, they are always solvated by one or more solvent molecules. Guanidine is an exceptionally strong base. The basicity of guanidine (pK_a= 13.6)[78] is close to the hydroxide ion. It reacts with water and CO_2 from air giving the corresponding guanidinium salts. In neutral aqueous solution, it exist mainly in the monoprotonated form.

Substitution of the nitrogen atoms in guanidine by electron-donating groups (alkyls) slightly increases its basicity, and substitution by electron-accepting groups (Ph, NH_2, OH, OMe, COMe, CN, NO_2) causes the reverse effect[79].

Guanidine is a stronger base than nitrogen compounds containing one potentially basic site (*N*-imino or *N*-amino) linked to a carbon atom, such as pyridines, amines and amidines. It is also stronger than compounds with two basic nitrogens, such as diamimes[80]. Other bidentate nitrogen ligands, such as proton sponges[81] and vinamidines[82], have an even higher basicity than guanidine. More basic still are

phosphazene[83] containing a potentially basic *N*-imino atom bonded to a phosphorus (V) atom.

2.2 Hydrogen bonded complexes of $PtCl_6^{2-}$

Currently few literature precedents have been reported relating to receptors binding hexchloroplatinate (IV) it was therefore decided to employ various simple compounds such as, amidinium derivatives, guanidinium derivatives, urea and pyrazine, in an attempt to obtain hydrogen bonded complexes of this anion to study the structure and conformation between the hydrogen bond donor and guest.

2.2.1 (Benzamidinium)$_2$ $PtCl_6$

X-ray quality single crystals of benzamidinium-$PtCl_6$ were obtained by slow evaporation of a mixture of benzamidine and H_2PtCl_6 in isopropanol /nitromethane (1/1 v/v) solution. The compound crystallises as orange block in the space group $P2_1/c$. The crystal structure is shown in Figures 2.3 and 2.4.

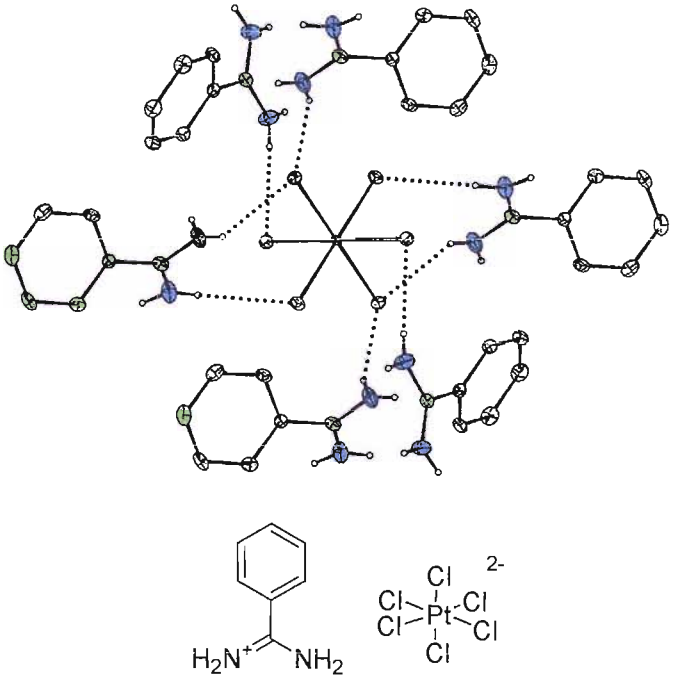

Figure 2.3: X-ray crystal structure of benzamidinium-$PtCl_6$ displaying the hydrogen bonding.

As shown in Figure 2.3, the anion $[PtCl_6]^{2-}$, is coordinated to six benzamidinium cations via N-H···Cl hydrogen bonds in a range of 2.52 - 2.99 Å. Four benzamidinium show monodentate coordination and the other two show bidentate coordination. The Pt atom sits on a crystallographic inversion centre (the packing is shown in Figure 2.4). The distance between the benzyl rings was found to be 3.51 Å. Over distances of this lengh, π-π stacking interactions are likely to be occurring between the benzyl groups.

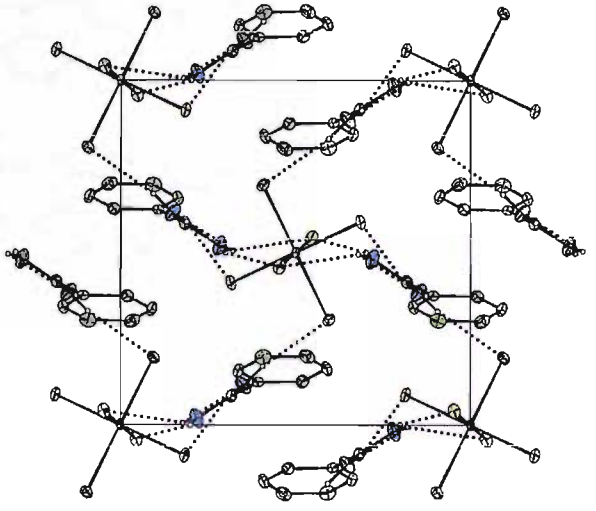

Figure 2.4: X-ray crystal structure of benzamidinium $[PtCl_6]^{2-}$ viewed down the *a* axis displaying the hydrogen-bonding network in solid state and π stacking interactions.

2.2.2 (4-Guanidinium benzoic acid)$_2$ - $PtCl_6$

X-ray quality single crystals of 4-guanidinium benzoic acid-$PtCl_6$ have been obtained by slow evaporation from H_2O/ isopropanol (1/1 v/v) solution. The crystal structure reveals the presence of dimers in the solid state. These subunits comprise two molecules of guanidinium benzoic acid are bound together via the formation of hydrogen bonds between the carbonyl group and the guanidinium NH_2 with the distances between the N-H and the O carbonyl being 2.17 Å (Figure 2.5). As a result of the dimer formation, $[PtCl_6]^{2-}$is bound by six molecules of guanidinium benzoic acid. Four of them via N-H···Cl contacts with a range of distance between 2.47 and 2.90 Å. The other two via OH···Cl contacts (not shown in diagram) with a distance of

2.17 Å. The OH···Cl contacts cross-link the 2D sheets into 3D network. The Pt atom sits on an inversion centre (see Appendix for structure information). The distance between the benzyl rings was found to be 4.27 Å. This distance is too long for π- π stacking interactions to occur between the benzyl groups.

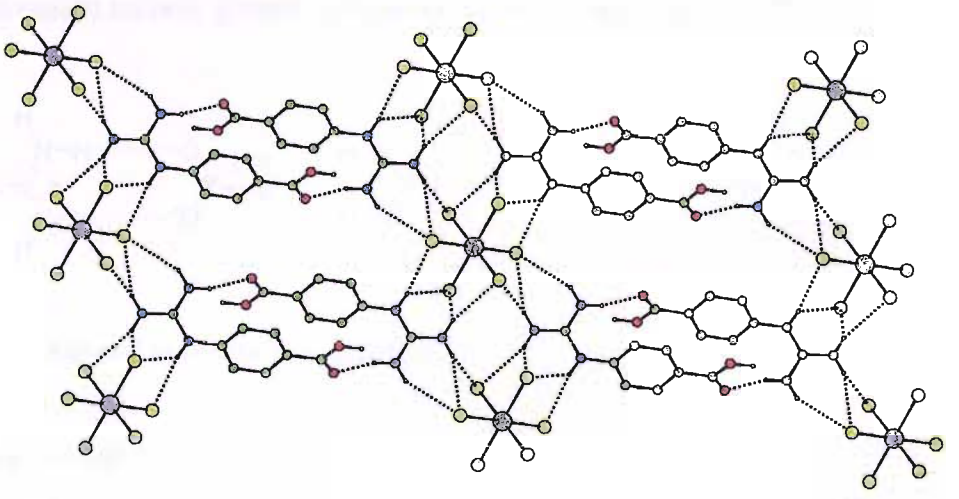

Figure 2.5: X-ray crystal structure of complex (guanidinium benzoic acid)$_2$-$[PtCl_6]^{2-}$ showing the hydrogen bonded network in the solid state, OH···Cl hydrogen bonds above and below the plane of the page are omitted for clarity.

The X-ray crystal structures which have been obtained with hexachloroplatinate (IV) and charged receptors such as guanidinium and amidinium motifs confirm that our desired anion can be bound via hydrogen bonds and electrostatic interactions. These results permit us to investigate the design of new receptors based on the guanidinium group.

2.3 Anion receptors based on guanidinium group

The guanidinium functional group (pK_a ca. 13.5) is part of the side chain of the essential amino acid arginine. It contains three amines in a plane, and it remains protonated over a wide pH range. It presents the possibility of forming five hydrogen bonds. These structural features make it a versatile moiety for molecular

recognition[84]. The positively charged guanidinium moiety constitutes a good binding group for oxo anions such as carboxylate[85,86] or phosphate[87]. The combination of hydrogen bonding and electrostatic interactions leads to the formation of strong complexes. In general there are three different hydrogen bonding arrangements from guanidinium to phosphate (Figure 2.6). In fact, nature uses guanidinium moieties to coordinate to anionic groups, such as in the previously reported HIV-1 Tat protein[13].

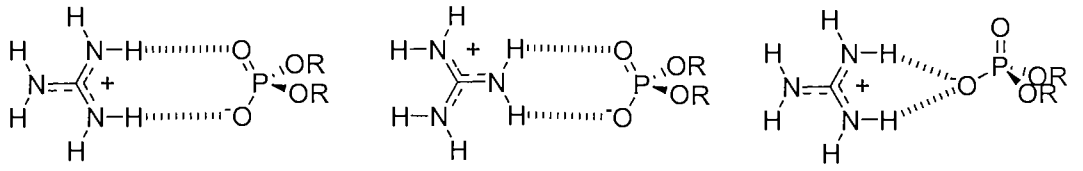

Figure 2.6: General hydrogen-bonding patterns from guanidinium to phosphates.

As a result of the exceptional properties to bind anions, many research groups in the field of molecular recognition have designed receptors containing the guanidinium motif. de Mendoza[88] and co-workers reported the complexation of *p*-nitrobenzoate by receptor 13 and extraction of this anion from water.

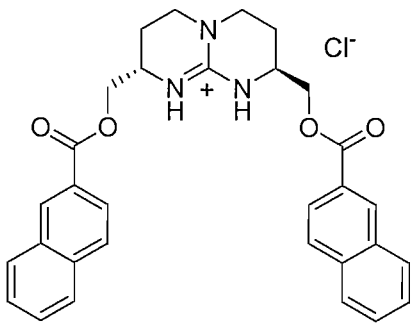

13

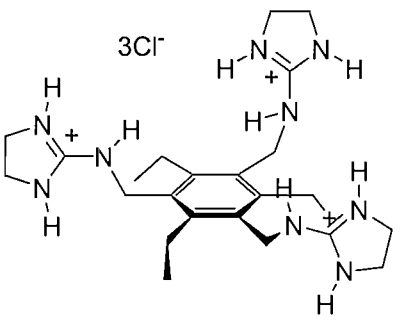

14

An excellent example of strong coordination between guanidinium group and carboxylates was reported by Anslyn[89] et al. They found that compound **14** can interact very strongly with citrate, displaying a binding constant of 6900 M^{-1} in D_2O. They also proved that receptor **14** is capable of binding citrate in a crude extract of orange juice at pH 7.4 with a stability constant of 4600 M^{-1} in D_2O.

2.3.1 Synthesis of bifunctional guanidinium receptor

Bis-guanidinium isophthalamide **16** has been prepared in accordance with literature procedure[90]. Isophthaloyl dichloride was previously reacted with methanol to afford compound **15** (Scheme 2.1). This compound was reacted with guanidinium hydrochloride in sodium methoxide solution, prepared *in situ* from MeOH and Na (s) in order to obtain the chloride salt of the isophthalamide guanidinium derivative **16**. Anion metathesis was achieved by reacting this compound with $AgBF_4$ followed by filtration, in order to obtain compound **17**. Tetrafluoroborate has been chosen as counteranion since it does not bind to the anion binding sites of the receptor.

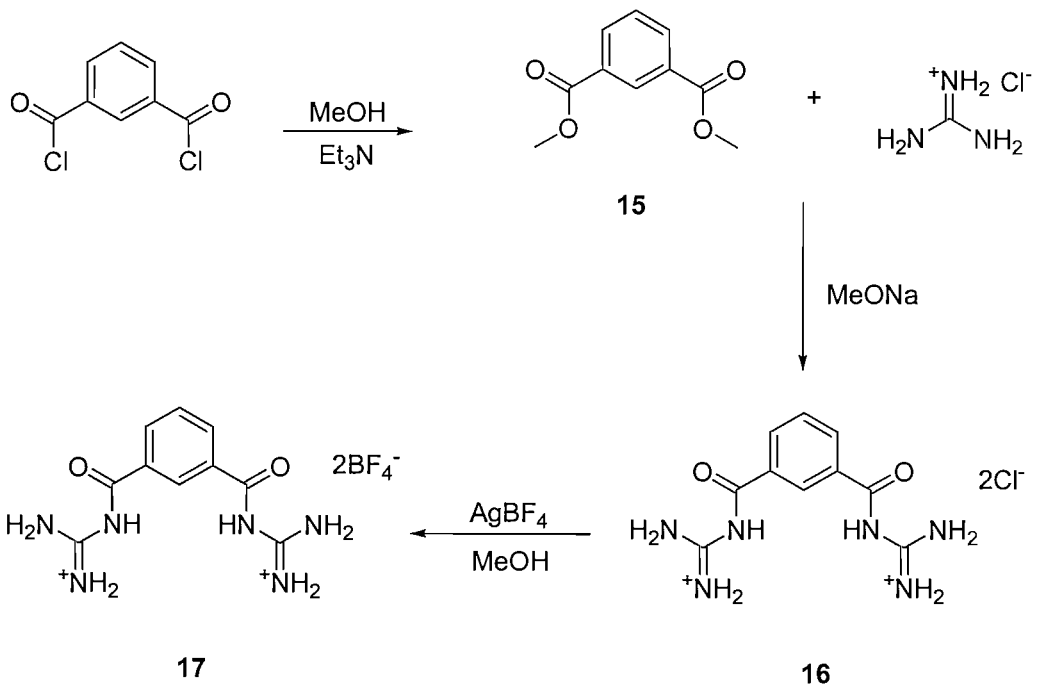

Scheme 2.1

Slow crystallization of compound **16** and hexachloroplatinate (IV) from H_2O/ isopropanol solution led to the formation of single crystals suitable for X-ray crystallographic analysis (Figure 2.7). The water molecule and one *bis*(acylguanidinium) are disordered. The interactions between the six $PtCl_6^{2-}$ and compound **16** can be split into three groups N-H_2···2Cl, N-H···2Cl and 2N-H···Cl. The hydrogen bond interactions N-H···Cl have a range of distance between 2.39 and 2.93 Å.

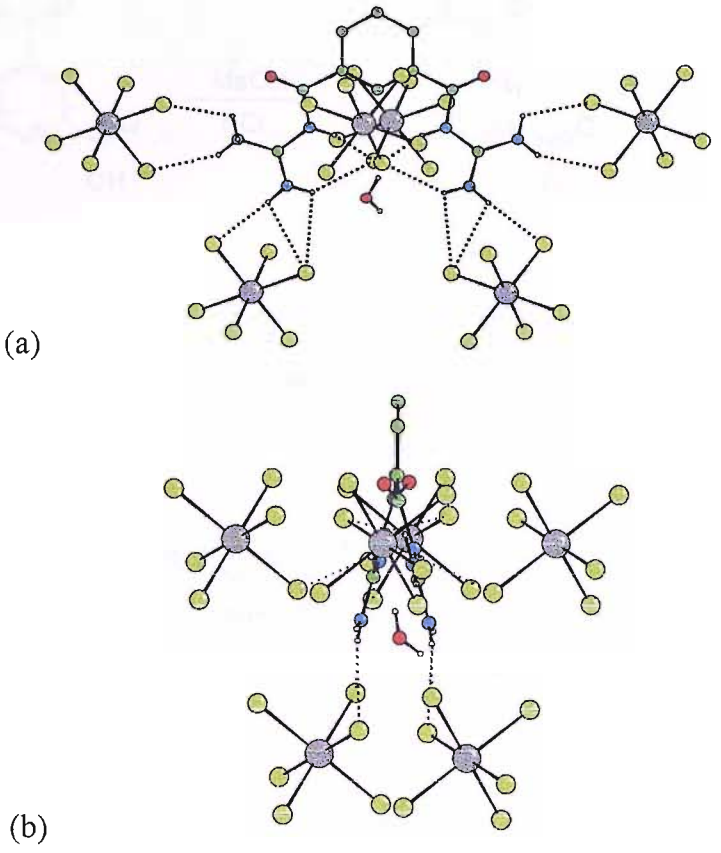

Figure 2.7: X-ray crystal structure of **16** (a) top and (b) side views displaying the hydrogen bonding motif.

The anion coordination properties of compound **17** have been investigated using ^{1}H NMR titration techniques in acetonitrile-d_3, however the fit could not be obtained due to multiple equilibria in solution. As shown in figure 2.5 compound **17** can form multiple hydrogen bonds with a number of guests.

2.3.2 Synthesis of trifunctional guanidinium receptor

Tris-guanidinium derivative **19**, has prepared according to Scheme 2.2. Benzene-1,3,5-tricarboxylic acid was dissolved in MeOH in the presence of HCl to afford compound **18**. This compound was reacted with guanidinium hydrochloride in a sodium methoxide solution, prepared *in situ* from MeOH and Na(s) in order to obtain the chloride salt of the *tris*-guanidinium derivative **19**.

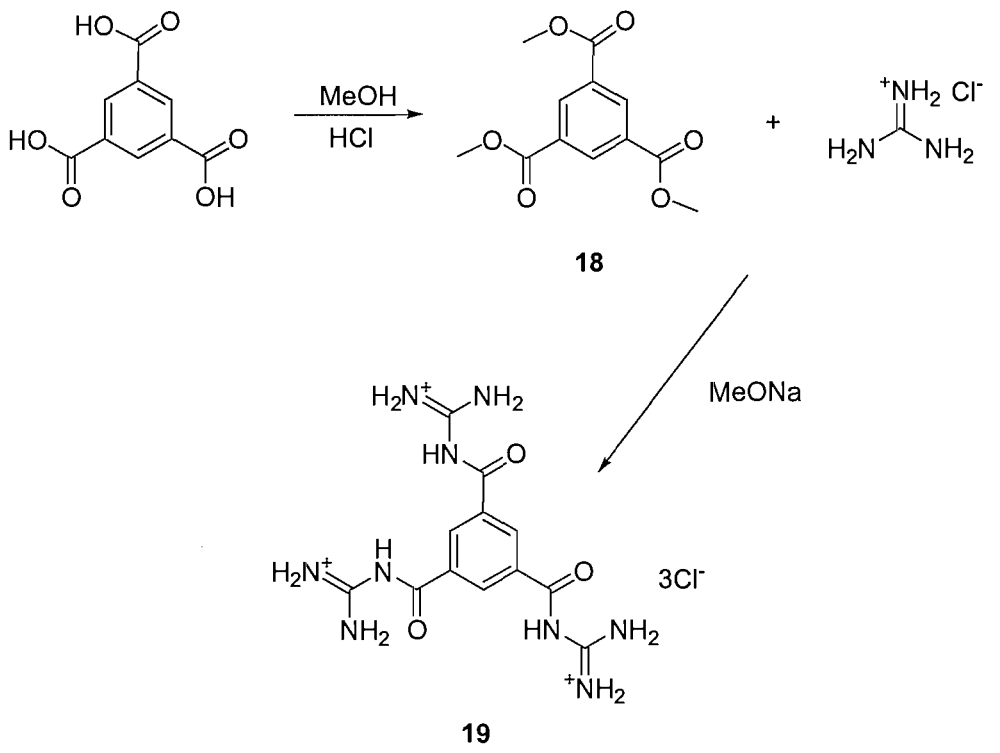

Scheme 2.2

X-ray quality single crystals of **19** and hexachloroplatinate (IV) have been obtained by slow evaporation of H_2O/ isopropanol (1/1 v/v) solution. Moreover, the X-ray structure shows that there are several molecules of water acting as a link between host and guest. The interactions on compound **19** with $PtCl_6^{2-}$ can be described hydrogen bond interactions, the shortest distances between guanidinium NH to O water is 1.95 Å and to OH water to the $PtCl_6^{2-}$ is 2.45 Å. As shown in Figure 2.8 compound **19** can form multiple hydrogen bonds with the guest (multiple equilibria in solution). As a result of this, its complexation properties with hexachloroplatinate (IV) could not be investigated.

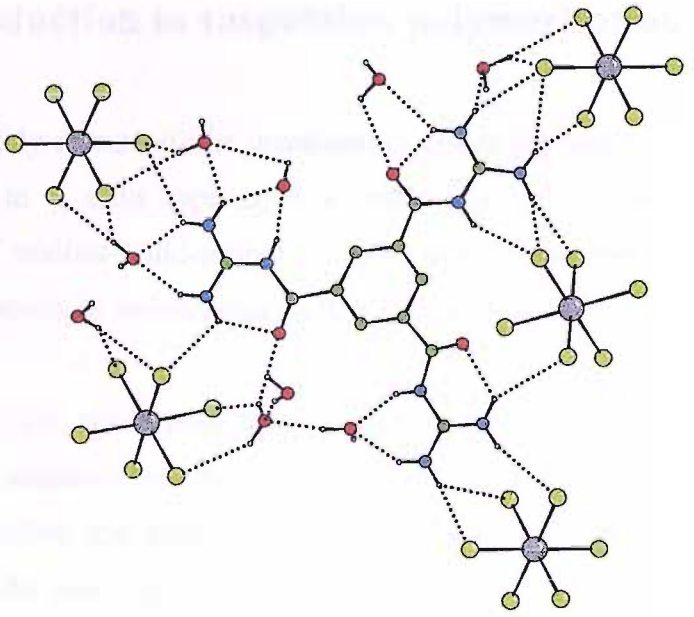

Figure 2.8: The X-ray crystal structure of **19** displaying the 1st shell of the 3D hydrogen bonded network.

Figure 2.9 shows the packing diagram viewed down *a*. Hydrogen bond interactions have been omitted for clarity. This clearly shows the location of the water between the host and the guest.

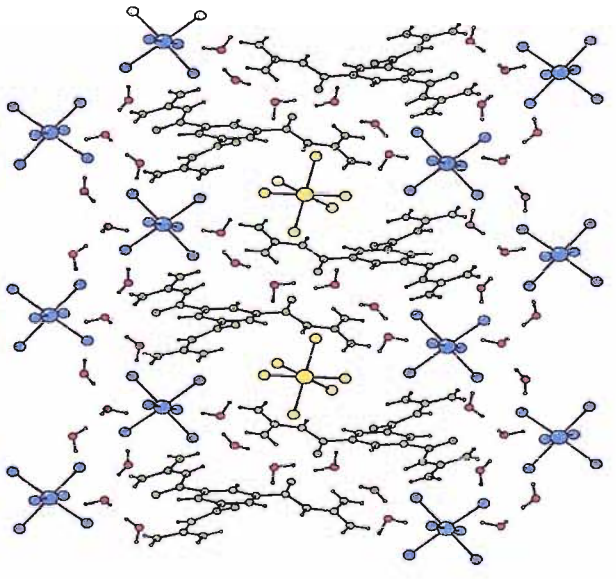

Figure 2.9: Packing diagram of cation **19** with $PtCl_6^{2-}$. The different colours represent cyrstallographically independent molecules, with the exception of the five water molecules which are all in the same colour.

2.4 Introduction to suspension polymerisation

As previously discussed, the guanidinium group has been chosen as the desired group to fix to a solid support. The next stage of this project describes the preparation of various solid-supports, which uses suspension polymerisation (SP) and inverse suspension polymerisation (ISP) techniques.

Suspension (or bead) polymerisation is one of the most efficient techniques employed to achieve free radical polymerisation in industry[91]. As the term suspension implies, the main feature of the technique is the maintenance of a suspension of the monomer in an immiscible solvent throughout the polymerisation process. The suspension medium is an effective heat transfer agent and as a result high rates of polymerisation can be maintained to achieve complete polymerisation in relatively short periods of time. In practice the size, shape, and often the uniformity of the crosslinked polymer particles is vital in most applications.

The technique of suspension polymerisation allows such particles to be produced fairly readily and with high reproducibly. The methodology is used widely at laboratory scale. Typically a styrene and divinyl benzene (DVB) liquid mixture is dispersed as spherical liquid droplets (the dispersed or non-continuous phase) in an excess of an immiscible water phase (continuous phase). The styrene-DVB mixture also contains a source of free radicals, the polymerisation initiator, and the aqueous phase generally contains a low level of a "suspension stabiliser", often a water soluble polymer, which helps to maintain the organic monomer droplets separated from each other. The suspension[92] is maintained as stable and uniform by continuous stirring and the reaction is typically heated to ~80 °C for 16 h. During this period the spherical liquid monomer droplets are converted into hard glassy polymer particles, still retaining the spherical symmetry of the original liquid droplets (Figure 2.10).

Inverse suspension polymerisation (ISP) is based on the same principles as suspension polymerisation, only the polarity of the dispersed and continuous phase has been reversed. In ISP an aqueous or highly polar monomer phase is dispersed in a non polar continuous phase. As in conventional suspension polymerisation, the

reaction is induced by free radical initiators present in the dispersed phase. Figure 2.11 shows the type of suspension polymerisation reactor used[93].

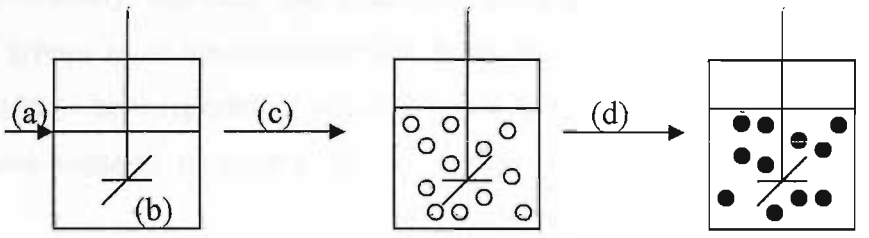

Figure 2.10: Schematic representation of suspension polymerisation: (a) organic co-monomer mixture containing dissolved initiator; (b) aqueous continuous phase containing dissolved polymeric suspension stabiliser; (c) shearing to form co-monomer liquid droplets; (d) thermal polymerisation to form solid polymer resin beads.

Typical radical initiators are azobisisobutyronitrile **20** and benzoyl peroxide **21**, both of which cleave readily on heating or irradiation with ultraviolet light, the former being the most commonly employed. Both are readily soluble in a wide range of monomers and organic solvents. For polymerisation carried out in aqueous solutions, water soluble inorganic persulfates make useful initiators.

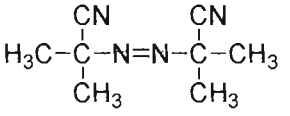

20

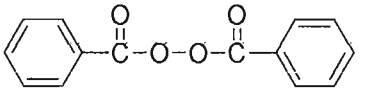

21

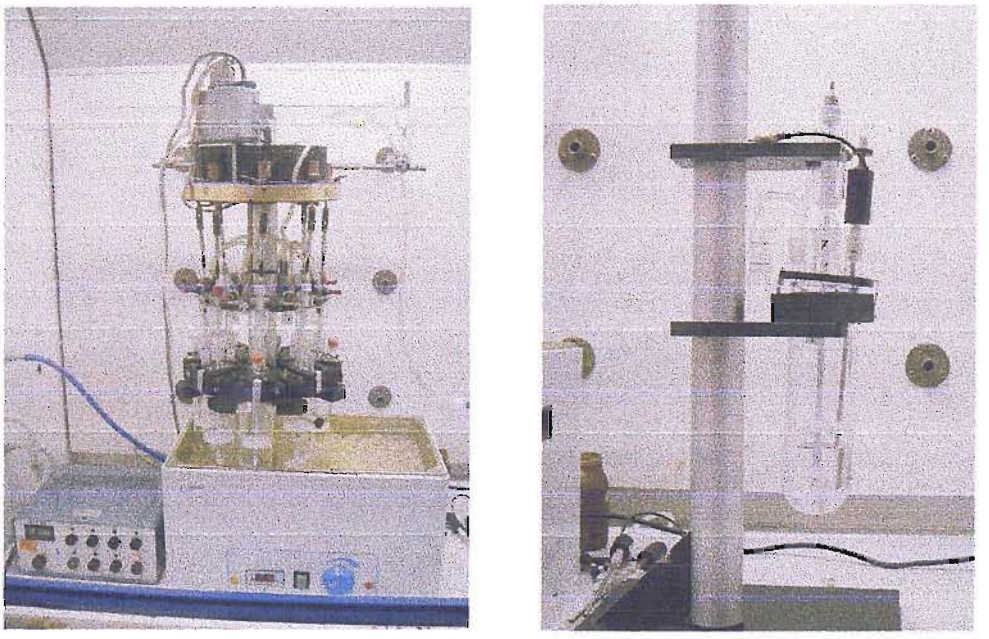

Figure 2.11: Suspension polymerisation reactor, internal volume 500 mL.

2.5 Polymer-supported guanidine

As previously reported, the guanidine motif has been employed by several research groups as an ion exchanger for its ability to bind metals. To date few cited examples have been reported in which this moiety has been used in conjunction with solid phase supports in order to produce chromatographical method of separation anions.

Polymeric ion exchange and chelating resins for gold recovery has been studied by Kolarz[94] and co-workers. They investigated the sorption of $[Au(CN)_2]^-$ (dicyanaoaurate) and $[AuCl_4]^-$ (tetrachloroaurate) anions on several anion exchangers with substituted guanidyl groups (Figure 2.12).

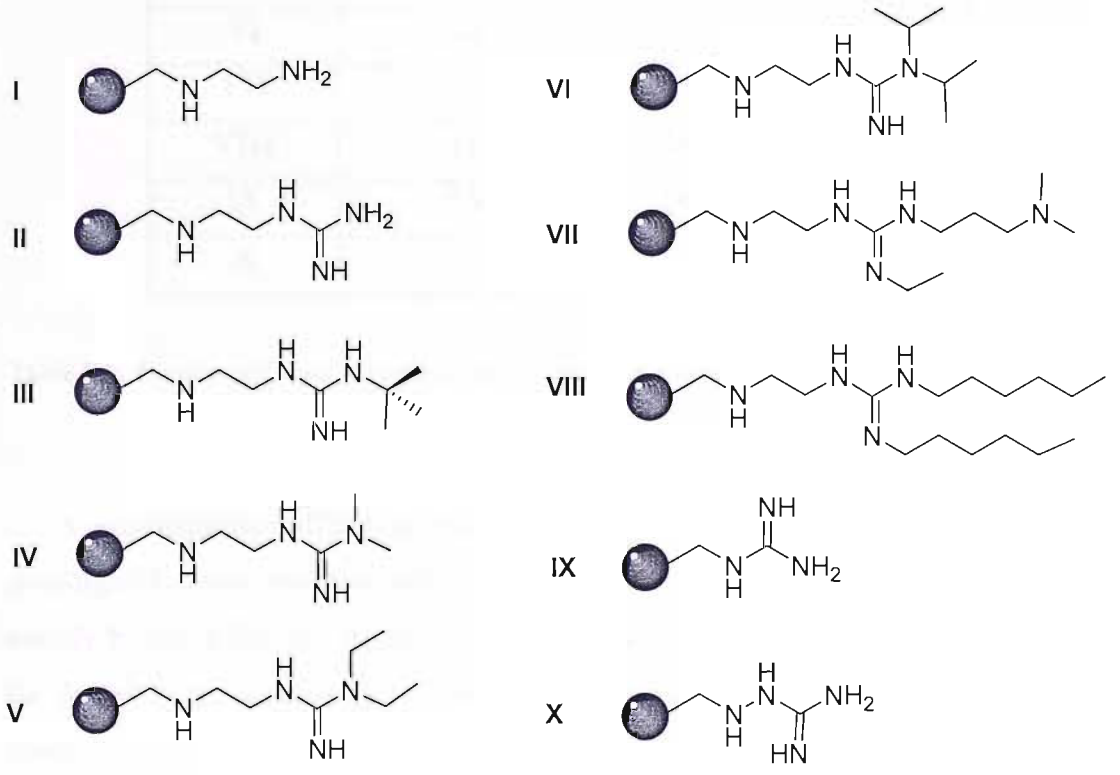

Figure 2.12: Anion exchangers. Matrix derived from vinylbenzyl chloride (VBC) and divinylbenzene (DVB) 2% copolymer.

The results of the sorption of gold dicyanoaurate from a cyanide solution of very low concentration (2 ppm) at pH 9.6 are presented in Table 2.1. They found a very high sorption of gold anions on to supports **VII** and **VIII**. This sorption is greater than on the anion exchangers with guanidine and aminoguanidine ligands, **IX** and **X** respectively.

The order of resin sorption ability for $[Au(CN)_2]^-$ is:

VII > VIII > II ~ IV > X > IX >> III > VI > V > I

The sorption ability increases according to the following order for $[AuCl_4]^-$:

VIII > I > III > IV > IV > VII > V > II > X > XI

Symbol resin	Ligand conc. mmol/g	$Au[CN]_2^{-(a)}$ mg/g	$Au[Cl_4]^{-(b)}$ mg/g
I	2.4	3.2	99.6
II	1.5	20.2	57.7
III	2.3	12.5	95.4
IV	2.0	20.2	74.0
V	1.5	8.8	62.0
VI	2.2	10.4	87.2
VII	1.7	*35.9*	68.9
VIII	2.0	28.7	*117.1*
IX	1.4	14.9	24.9
X	1.3	16.5	30.9

Table 2.1: Sorption of dicyanoaurate and tetrachloroaurate anions. (a) $Au[CN]_2^-$ concentration 2 ppm, pH 9.6. (b) $[AuCl_4]^-$ 50 ppm, pH 2.6.

A considerable difference was found between the sorption capacity of the investigated anion resin towards $AuCl_4^-$ and $Au(CN)_2^-$. It is throught to be induced mainly by the difference in pH of the solutions containing these anions. At low pH the degree of protonation of the nitrogen atoms provided by the guanidyl ligands is much greater. The opposite tendency, to increase efficiency of coordination of metal cation is seen upon a pH increase.

Previous studies on sulfaguanidine as ligand for square planar complexes[95,96] have shown that it reacts very well with palladium but does not interact with platinum. Following this discovery Schmuckler[97] et al. decided to incorporate the sulfonyl-guanidine ligand into a styrene divinylbenzene copolymer in order to see whether separation could be achieved on such resin. They too, found that the guanidine group is present in its imine[96] form, in which the N of amine is the most basic donor and serves as a good nucleophile for the bonding of $PdCl_2$ (Figure 2.13).

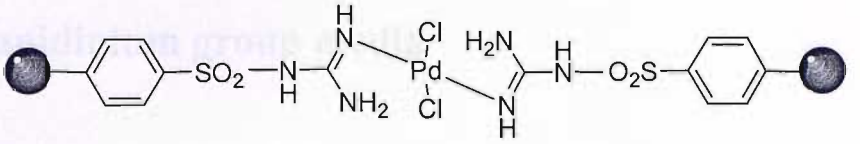

Figure 2.13: Mechanism of the interaction of the resin with palladium chloride.

The results (Table 2.2) indicated that when palladium-platinum mixtures of varying ratios were passed through a column of the guanidine resin, good separation between the two metals was achieved. Palladium was completely adsorbed, while platinum passed through the column unaffected. The palladium could be almost quantitatively eluted from the resin with 3-4M hydrochloric acid.

No	Initial conc. in 10 mL (mg)		Effluent conc. in 25 mL (mg)		Eluate conc. in 25 mL HCl[a] (mg)	
	Pd	Pt	Pd	Pt	Pd	Pt
1	10	1.0	Traces	0.875	9.050	0.050
2	1.0	1.0	None	0.900	0.712	0.038
3	1.0	10	None	9.825	0.725	0.050
4	10	50	Traces	48.38	9.650	0.925
5	10	10	Traces	9.375	9.675	0.375
6	1.0	50	None	48.750	0.887	0.625

Table 2.2: Separation of mixtures containing palladium and platinum by the guanidine resin at pH 2. [a] Elution in experiments 1-3 was carried out with 3M HCl, and experiment 4-6 with 4M HCl.

2.6 Synthesis and characterisation of solid-supported guanidinium group media

In order to establish differences between different supports bearing the guanidinium group and its behaviour as ion exchangers, polystyrene, silica gel and methacrylate resin derivatives have been prepared.

2.6.1 Styrene based resins

Two potential guanidine support resins, **23** and **27**, were synthesised. Resin **23** was prepared by reacting the guanylating agent[98] **22** with aminomethylated polystyrene resin. The reaction mixture was shaken overnight, to give a colourless resin (Scheme 2.3).

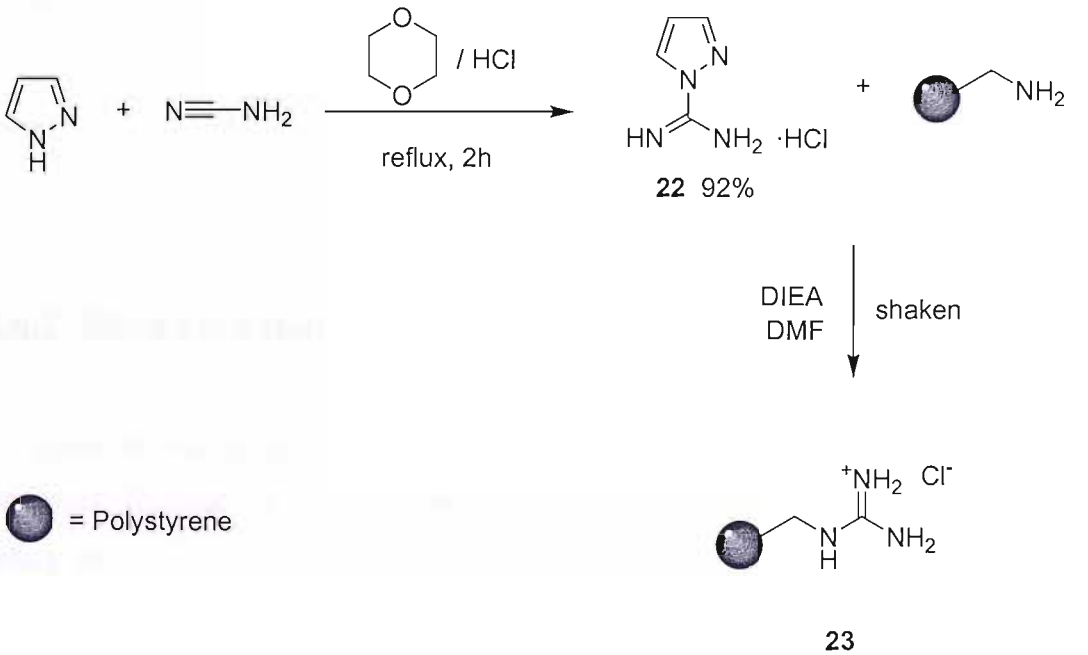

Scheme 2.3

Resin beads **24** were synthesised by suspension polymerisation (SP) of a solution of vinyl benzyl chloride (VBC) (90 vol.%) and divinyl benzene (DVB) (10 vol.%) following the literature method[93]. Reacting the guanylating agent **22** with the aminomethylated polystyrene **26**, previously synthesised according to literature

methods[99], resin **27** was produced and characterised by elemental analysis and FTIR spectroscopy (Scheme 2.4).

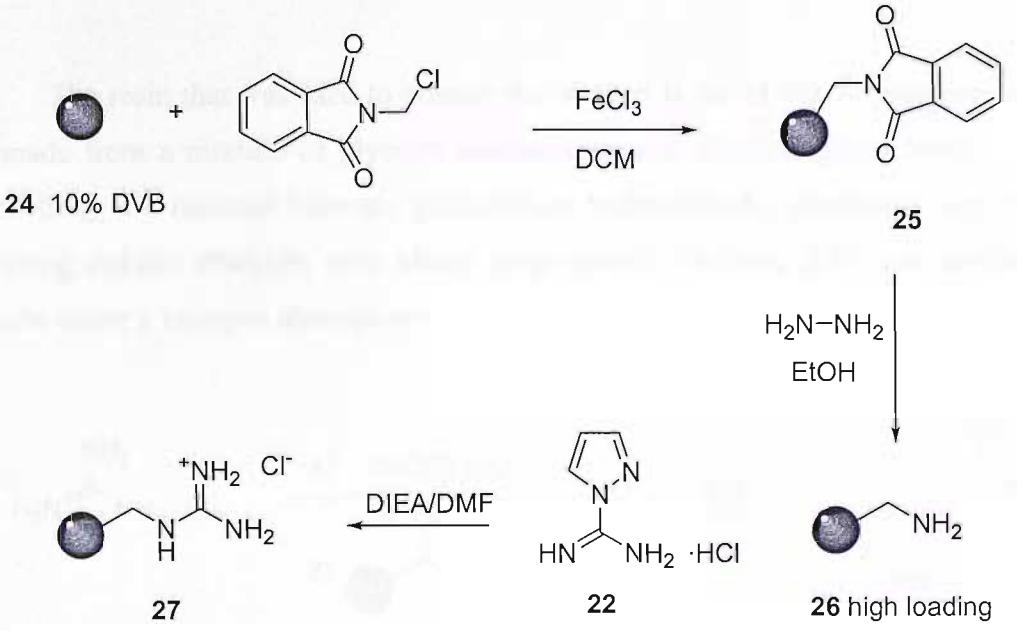

Scheme 2.4

2.6.2 Silica gel based

Silica **28** was prepared by reacting the guanylating agent **22** with aminopropyl silica gel. The reaction mixture was refluxed overnight, giving a colourless material. Silica **28** was characterised by elemental analysis and FTIR spectroscopy (Scheme 2.5).

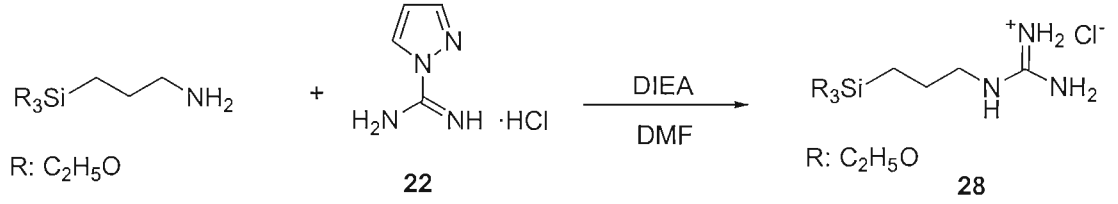

Scheme 2.5

2.6.3 Methacrylate based resins

2.6.3.1 Glycidyl methacrylate resin

The resin that was used to prepare the product is called Macro prep epoxide. It is made from a mixture of glycidyl methacrylate and ethylene glycol dimethacrylate. Initially the reaction between guanidinium hydrochloride, previously deprotonated using sodium ethoxide, with Macro prep epoxide (Scheme 2.6) was carried out *in situ* under a nitrogen atmosphere.

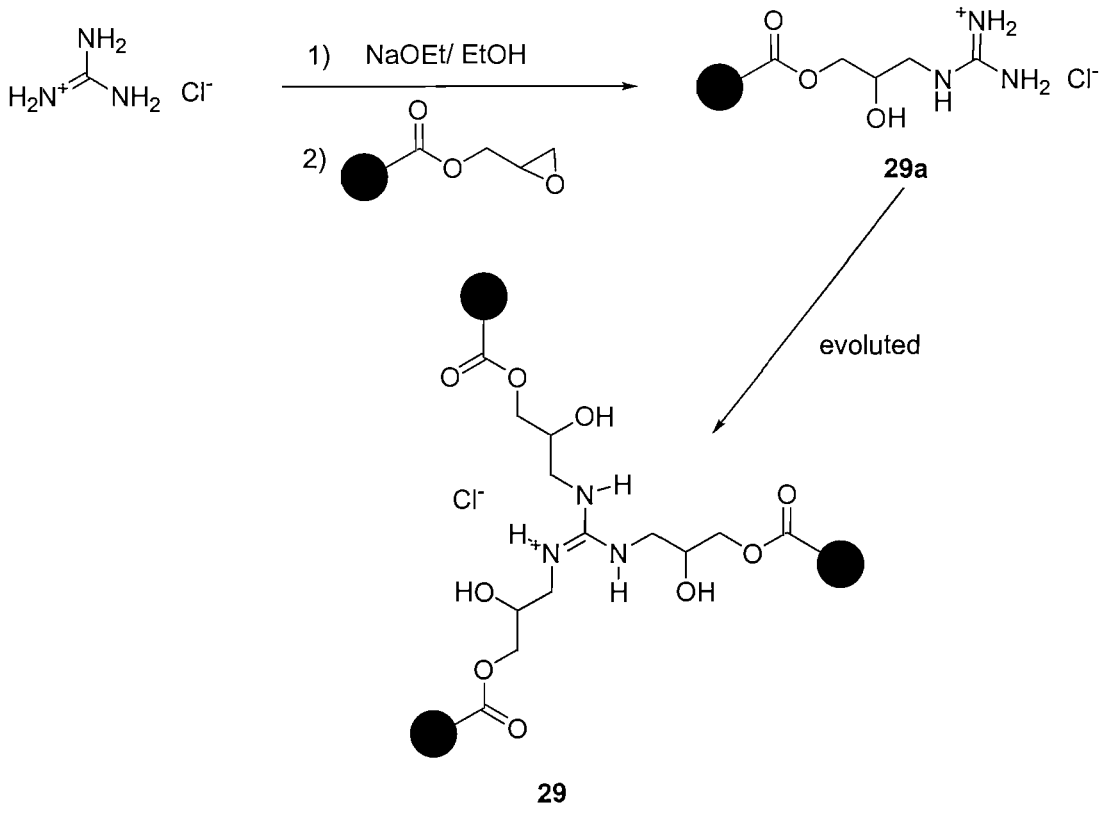

Scheme 2.6

The microanalysis of resin **29a** showed that the percentage conversion of the epoxide group was 35%, suggesting incomplete reaction with the epoxide group. However the FTIR showed that there was no stretch at 907 cm^{-1} (due to epoxide) and suggest complete conversion of the epoxide. One possible explanation is that after the first alkylation the guanidine rearranged so that the alkylated imino group became the amino group and then the new imino group could attack again (scheme

2.7). As a result of this, the polymer would be expected to be highly cross-linked and this would explain the 35% conversion grade. Alternativaly epoxide may be reacting with solvent.

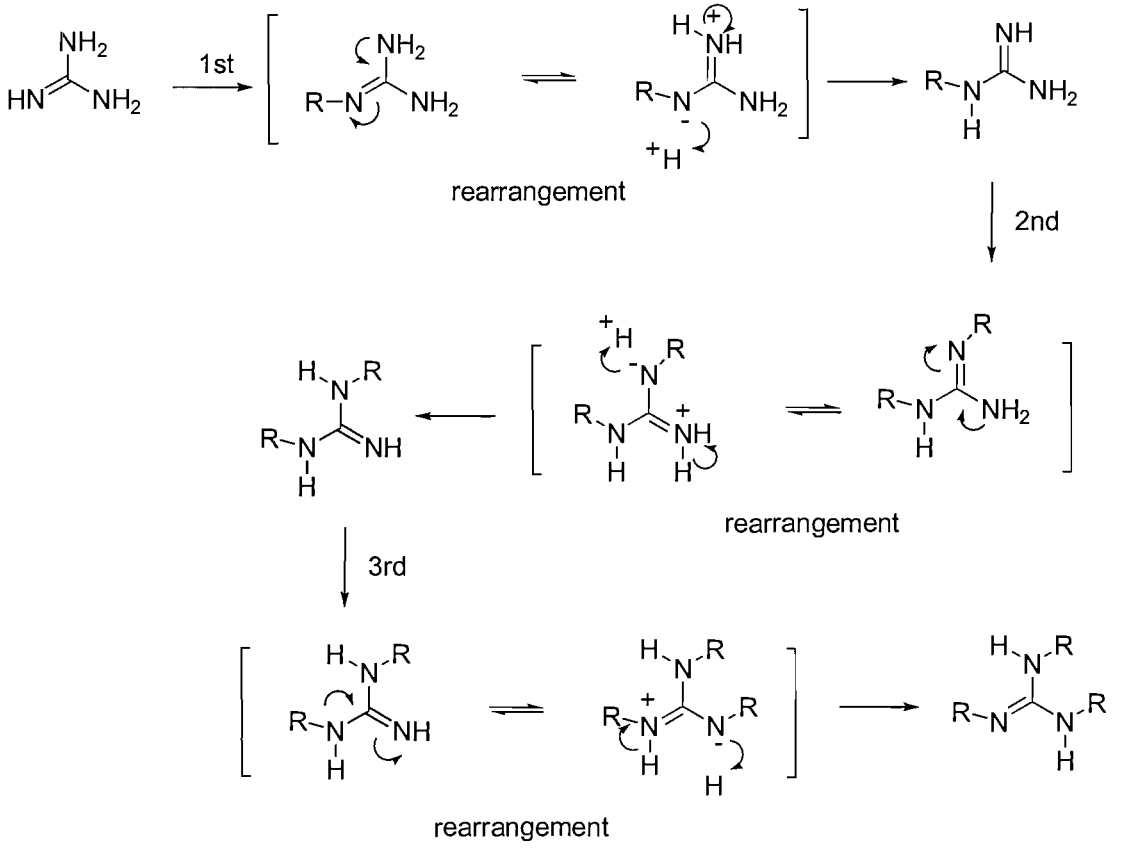

Scheme 2.7. Proposed mechanism for the alkylation of guanidine with Macro prep epoxide.

2.6.3.2 Inverse suspension polymerisation (ISP) using 2-amino ethyl methacrylate (AEM)

The cross-linker used in the copolymerisation of the AEM was the commercially available polyethylene glycol dimethacrylate (PEGDM) (Figure 2.14). It was found that PEGDM is insoluble in liquid paraffin/cyclohexene but is soluble in water.

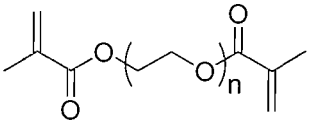

Figure 2.14: Structure of PEGDM

2.6.3.2.1 Optimisation of conditions for the ISP

Initially the ISP of AEM and PEGDM was carried out using an arbitrary 2% mol of cross-linker and 10% water (w/w). Varying amounts of the cross-linker PEGDM were added in the monomer phase to achieve the synthesis of polymers **30a** to **30g**. The reactions were carried out using a system for the multiparallel synthesis of the polymer[93]. The reaction mixture was stirred for 16 h.

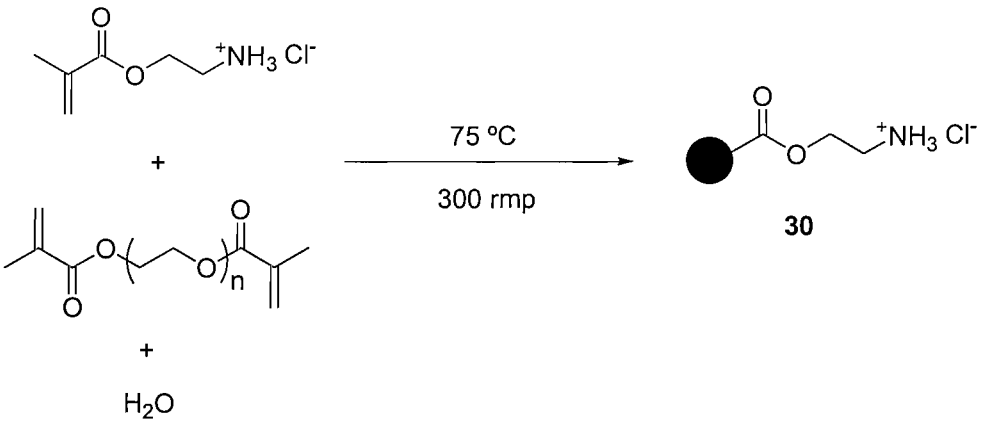

Scheme 2.8: ISP of PEGDM and AEM.

The stabiliser used in the continuous phase was sorbitan monoleate (Span80®) which has a relatively low molecular weight and is a surfactant type molecule. The inverse polymerisation resulted in the formation of solid polymer particles in good yield. Hexane, cyclohexane and volume ratios of 1:1 and 2:1 of liquid paraffin:cyclohexane were employed as the continuous phase. Table 2.3 shows the conditions used during the optimisation of the ISP of AEM and PEGDM.

Resin code	Cross-linker (mol %)	Water (Wt %)	Continuous phase	Initiator (Weight %)	Resin appearance
30a	2	10	Hexane	$K_2S_2O_8$ (0.1)	Sticky brown gel
30b	2	10	(a)	$K_2S_2O_8$ (0.1)	Yellow liquid gel
30c	2	10	(a)	V-50 (0.1)	Yellow gel
30d	5	12.5	Cyclohexane	V-50 (0.1)	Yellow solid gel
30e	10	11	(b)	V-50 (0.1)	Pale yellow solid
30f	20	11	(b)	V-50 (0.1)	Colourless solid
30g	40	11	(b)	V-50 (0.1)	Colourless solid

Table 2.3: Conditions for the ISP of PEGDM and AEM. (a) Liquid paraffin:cyclohexane (1:1). (b) Liquid paraffin:cyclohexane (2:1). Stirrer speed 300 rpm. Temperature 75 °C. Stabiliser, Span80®.

2.6.3.3 Guanidine group functionalisation

The functionalisation of resins **31** and **32** to guanidine-containing moieties was achieved by reacting reagent **22** with resins **30f** and **30g** in the presence of DIEA in dimethylformamide. The reaction mixture was spin-shaken for 3 days at room temperature to give resins **31** and **32**. These resins were characterised by elemental analysis and FTIR spectroscopy (Scheme 2.9)

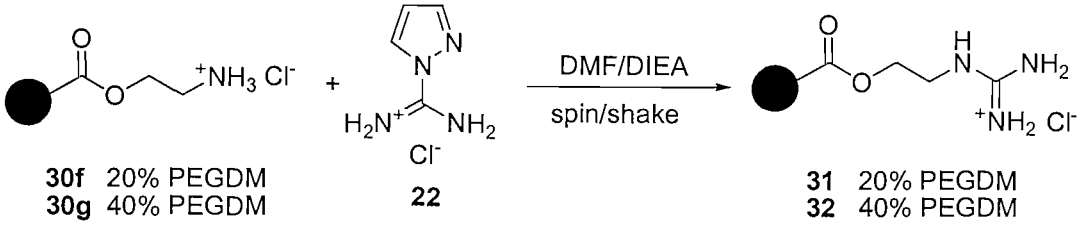

Scheme 2.9

2.7 Synthesis and characterisation of solid-supported double-arm guanidinium group resins

A new solid support bearing an extra guanidinium group arm has been synthesised and investigated, to see if the bifunctional guanidinium polymer could improve the ion-exchange properties with the simple anions and the PGMs.

2.7.1 Styrene based resins

2.7.1.1 Vinyl benzyl diamino synthesis (VBDA)

Monomers **34** and **35** were prepared in accordance with the literature[100,101] (Figure 2.15). ISP of VBDA$^+$ **34** was carried out using similar conditions to those used previously to obtain polymer **30**, however in this case no resins were obtained. Therefore monomer **35** was selected as a similar alternative and using suspension polymerisation the desired polymer was obtained.

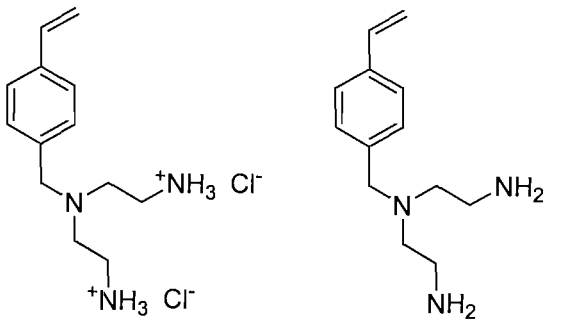

34 **35**

Figure 2.15: Vinyl benzyl diamino (VBDA) monomers.

2.7.1.2 *Suspension polymerisation using VBDA*

The cross-linker used in the copolymerisation of vinyl benzyl diamino (VBDA) was the commercially available divinyl benzene (DVB). VBDA **35** was found to have desirable properties; be insoluble in water and good solubility in toluene, essential in the suspension polymerisation techniques.

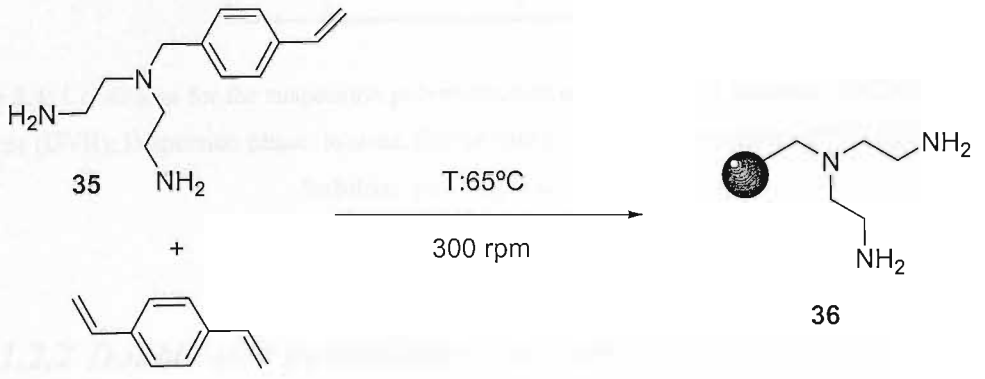

Scheme 2.10: Suspension polymerisation of vinyl benzyl diaminoethyl (VBDA) and divinyl benzene (DVB).

2.7.1.2.1 *Optimisation of conditions for the suspension polymerisation (SP) using vinyl benzyl diamino (VBDA)*

Suspension polymerisation of vinyl benzyl diamino (VBDA) and divinyl benzene (DVB) was carried out using an arbitrary 10% mol of cross-linker. Different amounts of the cross-linker DVB were added in the monomer phase (toluene) to achieve the synthesis of polymers **36a-36c**. The reactions were carried out using a system for the multiparallel synthesis of the polymer[93] which required the reaction mixture to be stirred for 16 h.

The stabiliser used in the continuous phase was poly(vinyl alcohol) 87-89% hydrolysed (PVA) and Na_2HPO_4 to bring the pH of the solution to 7.2. Water was employed as the continuous phase. Table 2.4 shows the conditions used during the

optimisation of the suspension polymerisation of vinyl benzyl diamino (VBDA) and divinyl benzene (DVB).

Resin code	Cross-linker (mol %)	Resin appearance
36a	10	Light yellow, solid
36b	20	Cream, solid
36c	30	Dark cream, solid

Table 2.4: Conditions for the suspension polymerisation of vinyl benzyl diamino (VBDA) and divinyl benzene (DVB). Dispersion phase, toluene. Stirrer speed 300 rpm. Temperature 65°C. Initiator, AIBN. Stabiliser, polyvinyl alcohol (PVA).

2.7.1.2.2 Double arm guanidinium functionalised polymer

Resin **36** was functionalised with a guanidinium group to produce resin **37**. This was achieved by reacting reagent **22** with resin **36b**, previously prepared by suspension polymerisation techniques, in the presence of DIEA in dimethylformamide. The reaction mixture was refluxed for 48h with an overhead mechanical stirrer to give resins **37**. (Scheme 2.11)

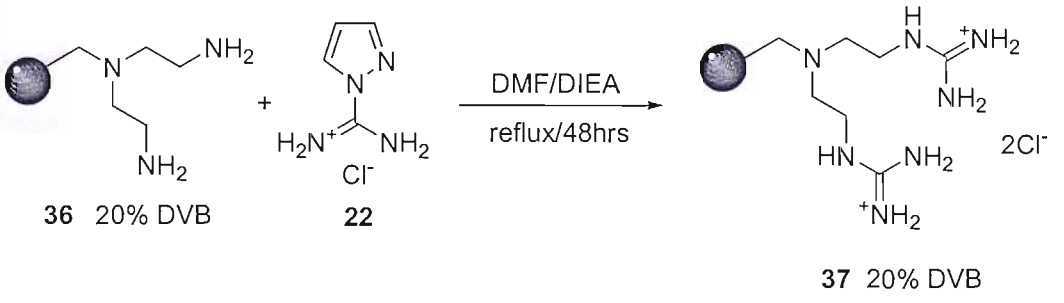

36 20% DVB **22** **37** 20% DVB

Scheme 2.11

2.7.1.3 *Suspension polymerisation using vinyl benzyl chloride (VBC)*

An alternative synthetic route has been developed to achieve a double arm guanidinium functionalised polymer in high loading. This new route involves the suspension polymerisation of vinyl benzyl chloride (VBC) with divinyl benzene (DVB) and styrene (Scheme 2.12), and its functionalisation (Scheme 2.13).

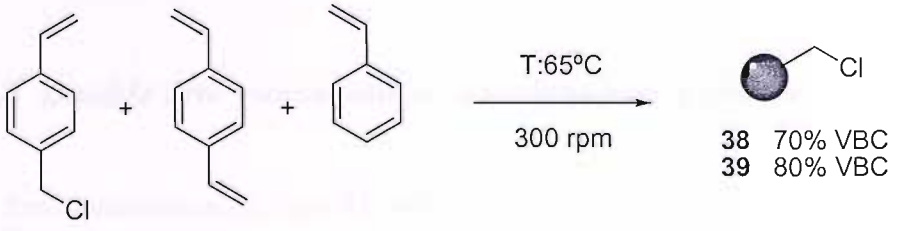

Scheme 2.12

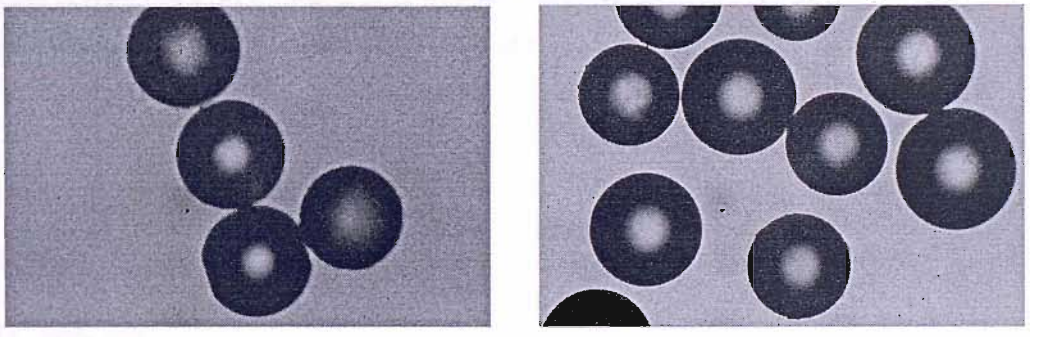

Figure 2.16: Left beads from SP of 70% vinyl benzyl chloride (VBC). Right beads from SP of 80%

Suspension polymerisation of vinyl benzyl chloride (VBC), divinyl benzene (DVB) and styrene was carried out using an arbitrary 80 (mol %) and 70 (mol %) of functionalised monomer. The cross-linker, DVB, concentration was fixed at 5 (mol %). The reactions were carried out using a system for the multiparallel synthesis of the polymer[93], again stirring for 16 hrs. Table 2.5 shows the conditions used during the SP of VBC, DVB and styrene.

Resin code	VBC (mol %)	Styrene (mol %)	Dispersion phase	Initiator (Weight %)	Resin appearance
38	70	25	Toluene	AIBN (1.0)	White beads
39	80	15	Toluene	AIBN (1.0)	White beads

Table 2.5: Conditions for the suspension polymerisation of vinyl benzene chloride (VBC), DVB and styrene. Continuous phase, water. Stirrer speed 300 rpm. Temperature 65°C. Stabiliser, polyvinyl alcohol (PVA).

2.7.1.3.1 Double arm guanidinium functionalised polymer

The functionalisation of resin **43** with guanidine group was achieved by reacting reagent **40** with resin **39**, previously prepared by SP techniques, with the presence of NaI in N-methyl pyrrolidinone (NMP). The reaction mixture was refluxed for 48hrs with overhead mechanical stirrering to give the pale yellow resin[102,103] **41**. Deprotection with hydrazine to yield a colourless resin **42**. Reaction of **42** with guanidyl agent **22** afforded resin **43** (Scheme 2.13).

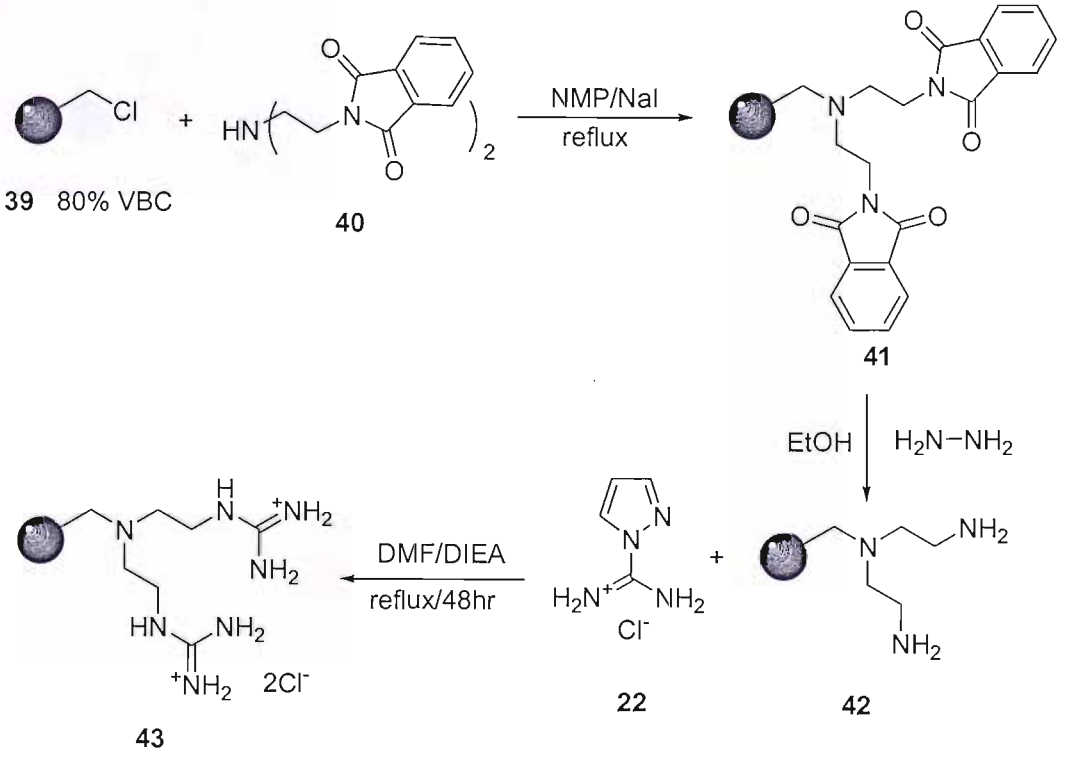

Scheme 2.13

2.7.2 Macro-prep based resins

Macro-prep epoxide resin was functionalised in to a double arm alcohol resin **45** by reacting diethanolamine **44** with Macro-prep epoxide in the presence of dioxane, resin **45** was prepared via the literature method[104].

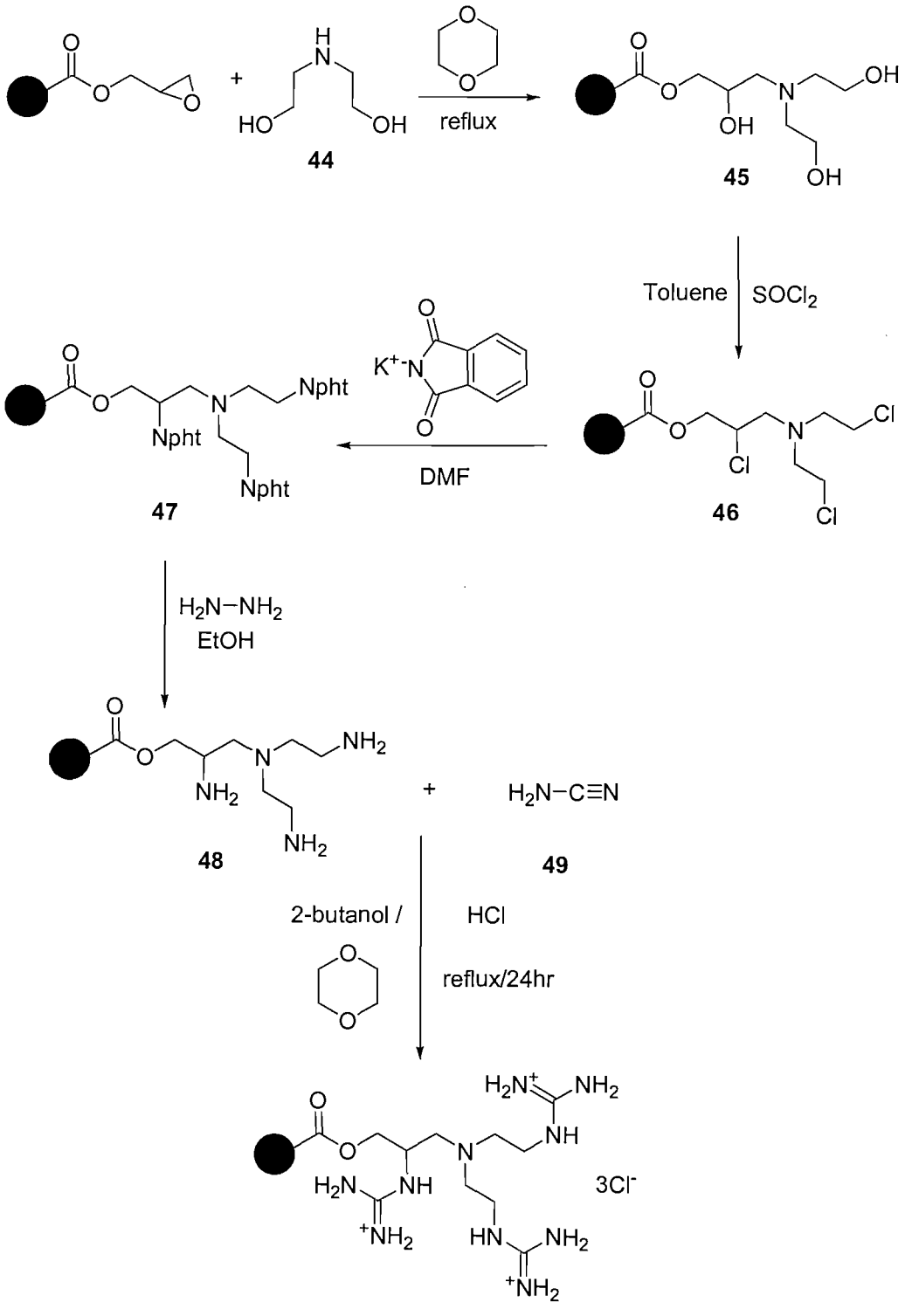

Scheme 2.14

Then this polymer was reacted with thionyl chloride in toluene in order to obtain the chlorinated polymer **46**[105].This white pale resin was reacted with potassium phthalamide in the presence of DMF affording resin **47**. Deprotection with hydrazine produced the colourless resin **48**. This was then reacted with cyanamide[94] **49** in order to obtain the macroprep guanidinium derivative **50** (Scheme 2.14).

2.8 Evaluation of the solid-supports in ion chromatography

In order to establish the possible effects of the interactions involved in the anion exchange mechanism, solid supports bearing electrostatic and multiple hydrogen bond interaction sites, have been investigated as anion exchange resins. Moreover, resins bearing moieties capable of producing single hydrogen bond interactions only and electrostatic interactions have been also investigated. Furthermore, the effect of higher eluent concentration and the differences displayed by various solid supports have also been investigated.

The performance of the polymer-supported resins as ion exchangers was evaluated by injecting a solution of each anion (150 μL) onto 60mm x 5mm columns packed in aqueous HCl. The samples were eluted with 0.05M $NaClO_4$ at a flow rate of 0.40 mL/min and a fraction of the eluent continuously analysed by a refractive index analyser (Figure 2.17). Prior to the analysis, the column was thoroughly washed with sodium perchlorate solution to stabilize the system.

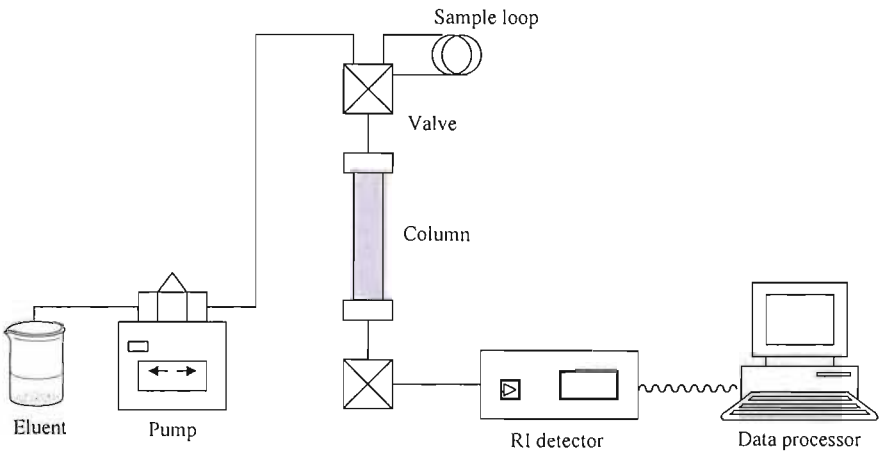

Figure 2.17: Schematic representation of chromatographic rig

The chromatograms produced show a large peak at t_R=1.3. This peak corresponds to the elution of $NaClO_4$. The proposed mechanism is shown in Figure 2.18. The following peaks are the corresponding anions NaX. The chromatograms were obtained by injection of solutions with the desired anion in $NaClO_4$ at 0.05 M and 0.5M respectively. The graphs produced were then overlaid to give a better understanding of their separation relative to each other.

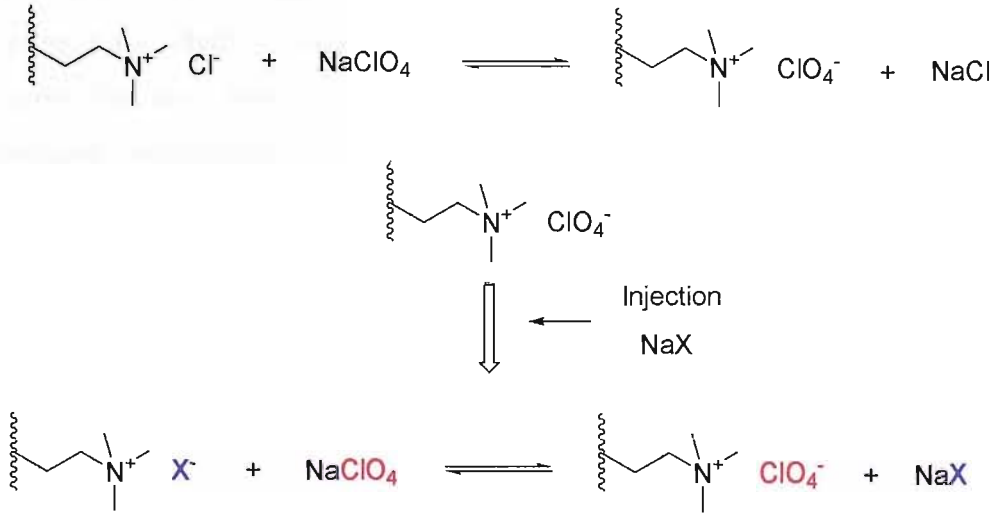

Figure 2.18: Proposed ion-exchange mechanism.

To compare the separation of simple anions revealed in the chromatograms produced by the various solid supports, the parameter of bed volume has been introduced. This parameter relates three different variables: depth and diameter of the column, flow rate and time. This allows comparisons between solid supports to be drawn, even while some of the conditions used were not the same. H is the depth of the column in cm, r is radius of the column in cm and fw is the flow rate in mL/min.

$$BV = (H \times r^2 \times \pi)/fw$$

Perchlorate has been used in the investigations because it has beneficial properties: perchlorate is a strongly competing anion, more so than chloride. For this reason is more strongly retained on anion exchange columns than most other mono-anions[106]. It therefore makes a good eluent because it does not require high eluent concentrations to allow the anions to move down the column.

2.8.1 The effects of hydrogen bond interactions

2.8.1.1 Comparison of guanidinium with ammonium salt resin

Resins **28**, **31** and **61** were tested as anion exchangers with the mono charged anions Br^-, I^-, SCN^-, NO_3^- and the dianion $S_2O_3^{2-}$. In order to establish a comparison of how the anions exchange in the resin they were tested first with aminopropyl silica gel support **61** which is functionalised as a quaternary ammonium chloride salt. Therefore the only interactions expected between the resin and the anions are electrostatic interactions and the possibility to form three hydrogen bond intereactions. With resins **28** and **31** more interactions would be expected, such as electrostatic interactions together with hydrogen bonds. Because of these increased interactions increases in retention times for resins **28** and **31** can be predicted.

Chromatograms for the ion chromatography by resins **28**, **31** and **61** are depicted in Figures 2.19 to Figure 2.21.

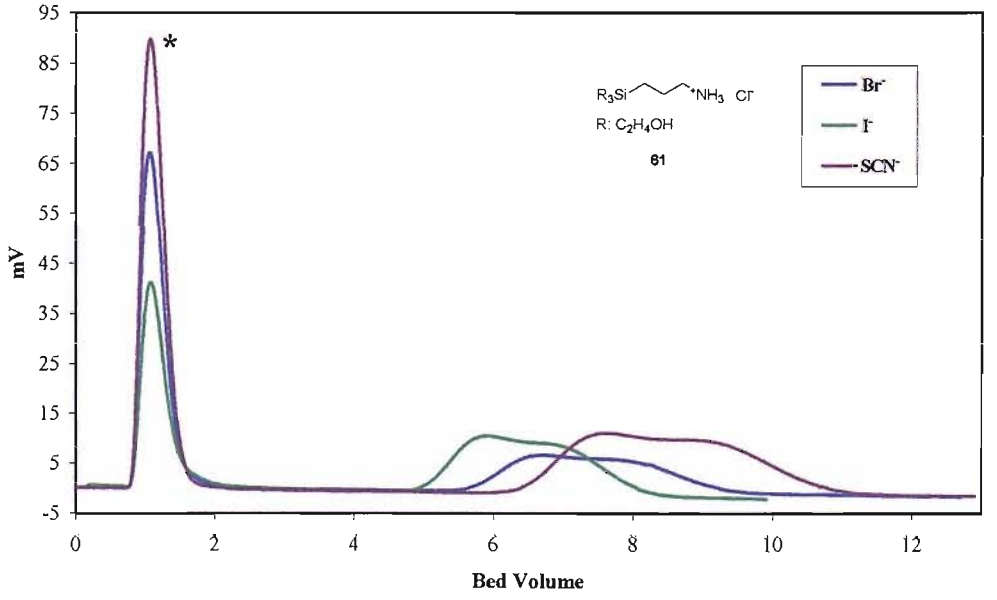

Figure 2.19: Ion chromatography of Br^-, I^-, NO_3^-, SCN^-, $S_2O_3^{2-}$ on resin **61** using 0.05M $NaClO_4$. To give a clearer diagram the anions which were retained (NO_3^-, $S_2O_3^{2-}$) in the column are not shown in the chromatogram. $^*ClO_4^-$ elution.

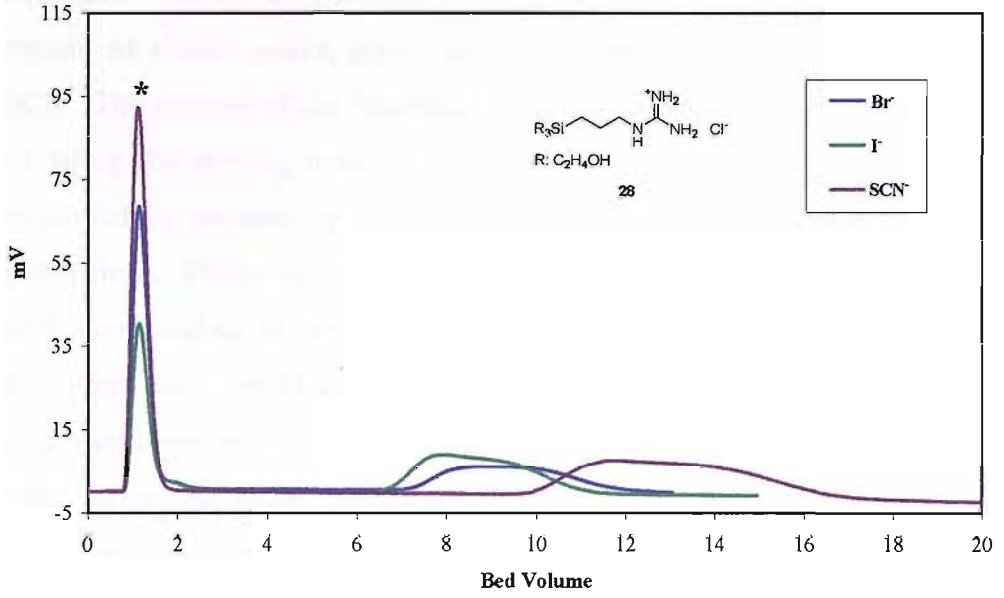

Figure 2.20.: Ion chromatography of Br^-, I^-, NO_3^-, SCN^-, $S_2O_3^{2-}$ on resin **28** using 0.05M $NaClO_4$. To give a clearer diagram the anions which were retained (NO_3^-, $S_2O_3^{2-}$) in the column are not shown in the chromatogram. $^*ClO_4^-$ elution.

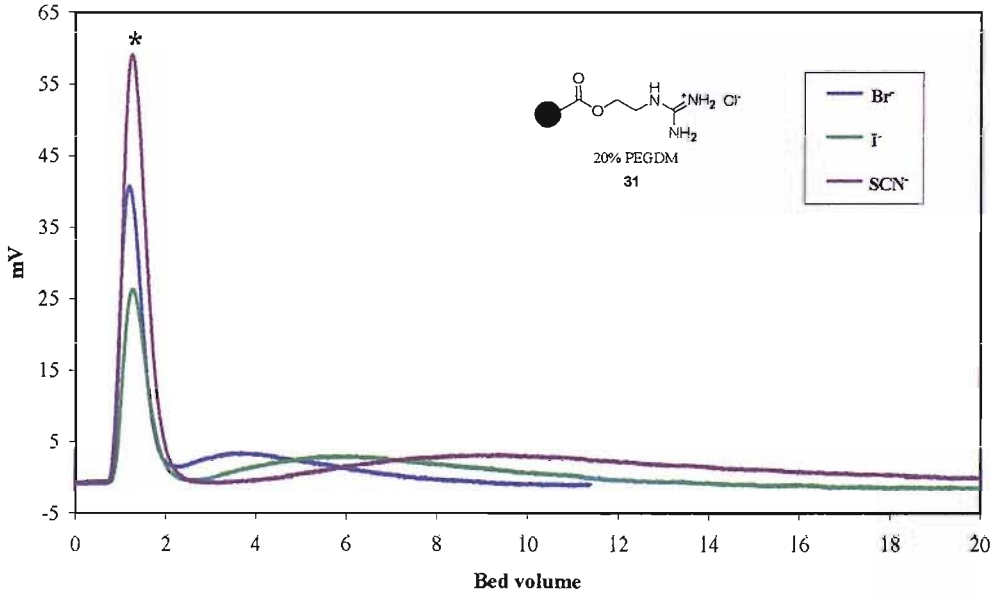

Figure 2.21.: Ion chromatography of Br^-, I^-, NO_3^-, SCN^-, $S_2O_3^{2-}$ on resin **31** using 0.05M $NaClO_4$. To give a clearer diagram the anions which were retained (NO_3^-, $S_2O_3^{2-}$) in the column are not shown in the chromatogram. $^*ClO_4^-$ elution.

As previously predicted the retention time for resin **28** is increased when compared with the aminopropyl silica gel **61**. Both solid supports shown the same pattern of elution peaks, giving the elution order I^- followed by Br^- followed by SCN^-. The loading of the functional groups are comparable due to aminopropyl gel **61** being the starting material for resin **28**. The increased retention time can be explained by considering that solid support **28** produces coplanar hydrogen bond interactions. This arrangement allows several strong hydrogen bonds to be formed to each anion, and so the anions are strongly retained. The aminopropyl silica gel **61** on the other hand produces a tetragonal hydrogen bonding array, allowing fewer hydrogen bond interactions to form between support and the anion, thus the anions elute earlier. As shown in the chromatograms, aminopropyl silica gel **61** support shows less retention time with all the anions that were screened compared to support **28**. The $S_2O_3^{2-}$ anion was not eluted from either column **28** or **61**.

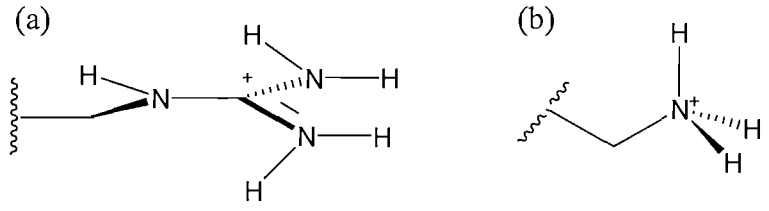

Figure 2.22: Geometry of the hydrogen donor in (a) guanidinium and (b) ammonium.

In the chromatogram relating to support **31**, the retention times have been decreased in comparison with both the aminopropyl silica **61** and **28**. However, the elution peaks shown in the chromatogram are much broader than those obtained from the previously screened supports **28** and **61**. This is maybe caused by the strong interaction between the support and the anions, also it maybe caused by the loading which has been increased three fold. The elution order was found to be different for resin **31**, Br^- was eluted first, then I^- and SCN^-, probably caused by hydrophobic nature of the solid support. It is probable that the methacrylate based resin, being greater than the silica based resin, and that this causes the hydrophobic anions to be more stable in this hydrophobic environment so they are retained for a longer time in the column. With none of the three support were the oxo-anions eluted.

2.8.1.2 Comparison of resins with the capacity to form multiple hydrogen bonds with single hydrogen bond donors

To establish a comparison of how hydrogen bond interactions can affect the anion exchange mechanism several different solid support systems were investigated. First solid supports **33** and **63**, which possess only one hydrogen bond donor, were tested with the mono charged anions Br^-, I^-, SCN^-, NO_3^- and the dianion $S_2O_3^{2-}$. Support **33** is functionalised with an alkylated guanidinium group while support **63** exists as a trimethylammonium chloride salt, so the only interactions expected between these solid supports and the anions are the electrostatic interactions and a single hydrogen bond **33**. With solid supports **28** and **31** further interactions could be expected, for they possess the possibility of forming multiple hydrogen bonds. Due to these extra interactions it is possible to predict an increase in retention times for supports **28** and **31** compared to the retention times of **33** and **63**.

The chromatograms for the ion chromatography experiments by resins **28**, **31**, **33** and **63** are depicted in Figures 2.23 to 2.26.

The chromatograms were obtained by injection of solutions with the desired anion in $NaClO_4$ at 0.05 M. The results were then overlaid to give a better understanding of the separation relative to each other.

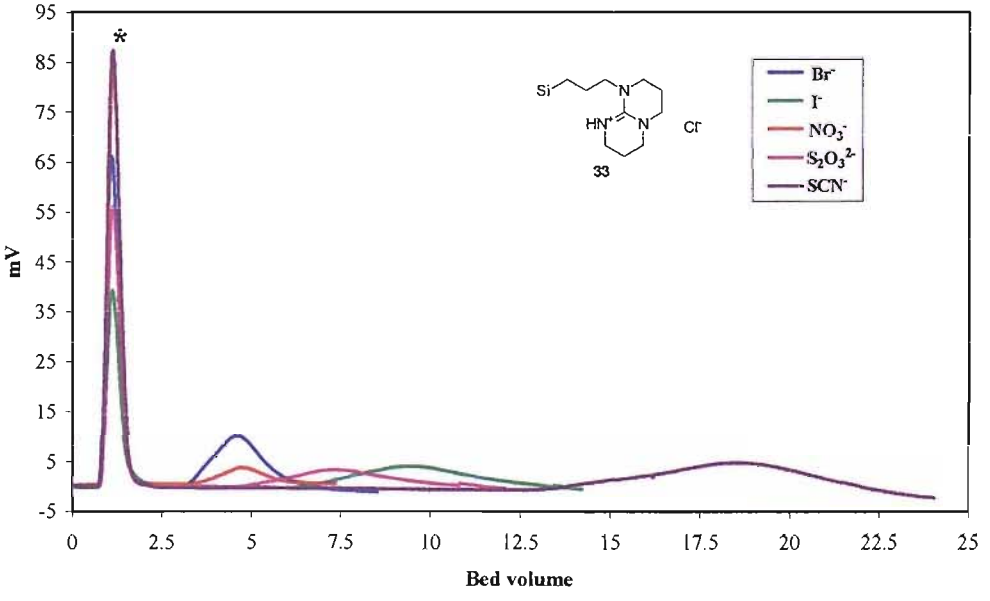

Figure 2.23.: Ion chromatography of Br^-, I^-, NO_3^-, SCN^-, $S_2O_3^{2-}$ on resin **33** using 0.05M $NaClO_4$. $^*ClO_4^-$ elution.

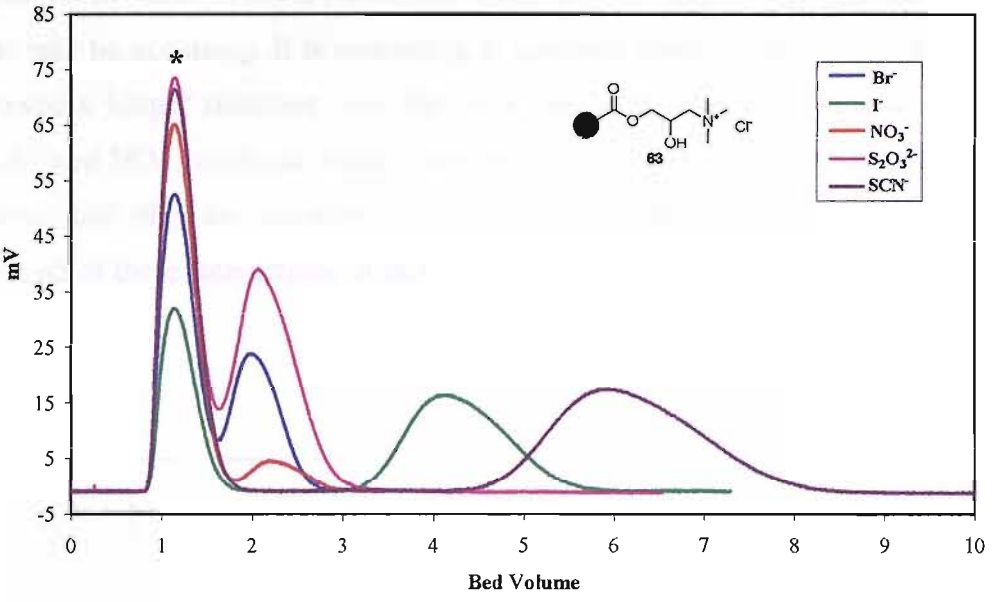

Figure 2.24: Ion chromatography of Br^-, I^-, NO_3^-, SCN^-, $S_2O_3^{2-}$ on resin **63** using 0.05M $NaClO_4$. *ClO_4^- elution.

Macroprep High Q **63** support showed lower retention time for all the screened than **33**. Its retention times were also lower than those seen with both guanidinium supports, **28** and **31**.

The behaviour of $S_2O_3^{2-}$ was expected to follow a different pattern to that seen for the mono charged anions. Mono charged anions behave according to the classical Hofmeister selectivity sequence[17]. It was expected that the retention time of $S_2O_3^{2-}$ would be much longer as it possesses two negative charges and so would be retained in the column for a longer period. However it shows a retention time even shorter than that seen for I^- and SCN^-. The reason for this behaviour is likely to be due to the $S_2O_3^{2-}$ anion being more hydrophilic than I^- and SCN^- and this, combined with the hydrophobic nature of the support (methacrylate **63**) causes the elution of $S_2O_3^{2-}$ from the column while the hydrophobic anions such as I^- and SCN^- are more stable in this environment, so are retained for a longer time in the column.

The chromatograms obtained for resin Si-TBD **33** display some interesting behaviour. Shorter retention times are seen with all the anions when compared to **28** and **31**. Surprisingly, the SCN^- anion showed the longest retention time, t_R=19.

The guanidinium based solid supports **28** and **31** showed much longer retention times for Br^- and I^-. This is potentially due to the multiple hydrogen bond interactions that may be occurring. It is interesting to compare these results to support **33**, which showed a longer retention time for SCN^-, not with I^- or Br^-. Oxo-anions, such as $S_2O_3^{2-}$ and NO_3^-, were not eluted from the column. This suggests that hydrogen bond interactions play an important role in the ion exchange mechanism, and that the strength of these interactions in this case is preventing the elution of these anions.

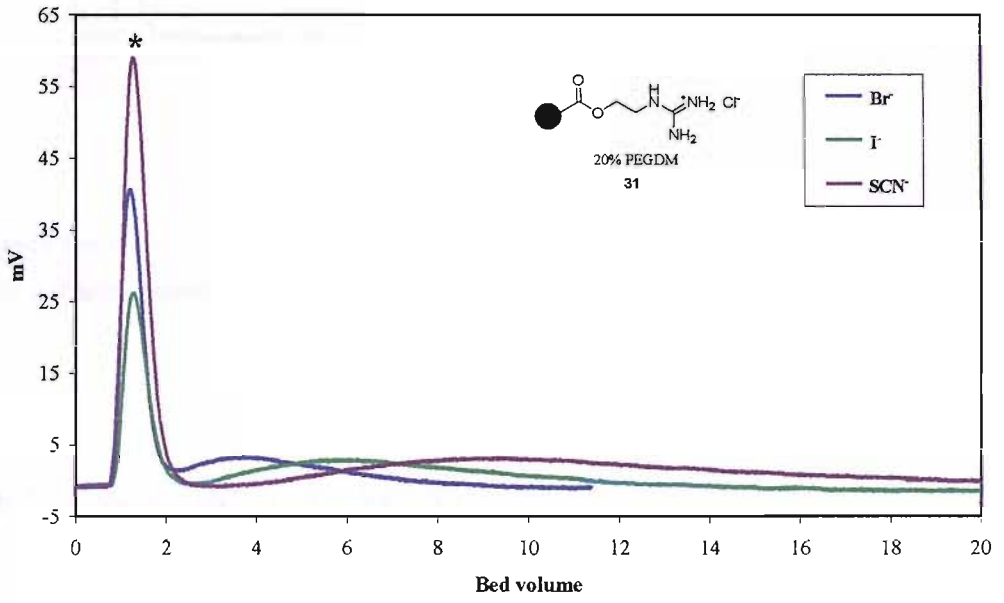

Figure 2.25.: Ion chromatography of Br^-, I^-, NO_3^-, SCN^-, $S_2O_3^{2-}$ on resin **31** using 0.05M $NaClO_4$. To give a clearer diagram the anions which were retained (NO_3^-, $S_2O_3^{2-}$) in the column are not shown in the chromatogram. $^*ClO_4^-$ elution.

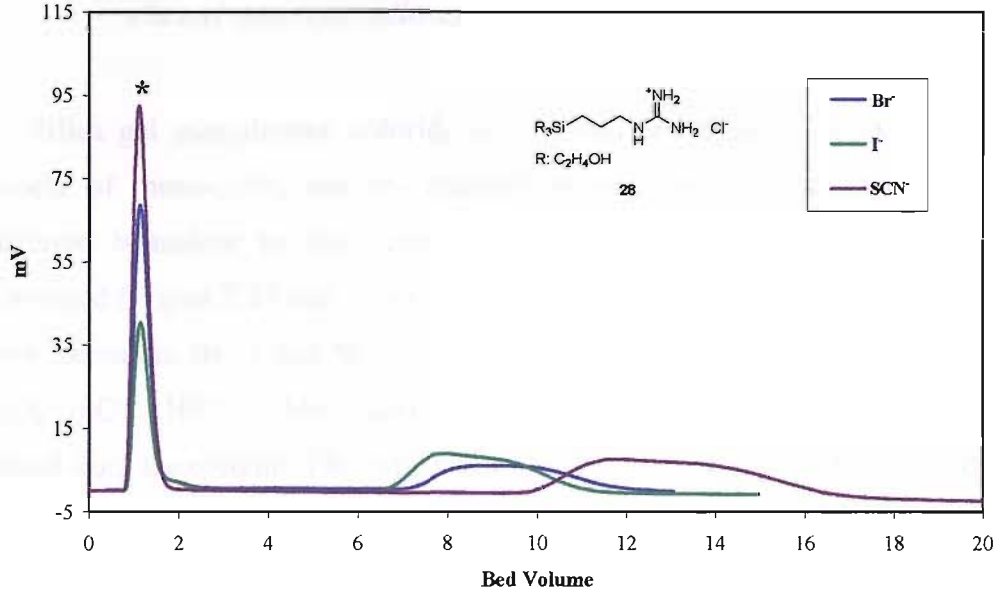

Figure 2.26.: Ion chromatography of Br^-, I^-, NO_3^-, SCN^-, $S_2O_3^{2-}$ on resin **28** using 0.05M $NaClO_4$. To give a clearer diagram the anions which were retained (NO_3^-, $S_2O_3^{2-}$) in the column are not shown in the chromatogram. $^*ClO_4^-$ elution.

2.8.2 Consideration of the effect of higher eluent strength

It was decided that the strength of the eluent could have an effect on the behaviour of these systems, and so this possibility was investigated. The concentration of the eluent was increased by ten fold to 0.5M $NaClO_4$.

The performance of the polymer-supported resins as ion exchangers was evaluated by injecting a solution of each anion (150 μL) onto 60mm x 5mm columns packed in aqueous HCl. The samples were eluted with 0.5M $NaClO_4$ at a flow rate of 0.40 mL/min and a fraction of the eluate continuously analysed by a refractive index analyser. Prior to the analysis, the column was thoroughly washed with sodium perchlorate solution to stabilize the system.

As a result of the increase in eluent concentration the chromatograms produced display a negative peak at t_R=1.3. This negative peak is produced when the anion is injected: the concentration of the anion being analysed is lower than the reference solution in the cuvette, which was used previously to calibrate the system.

2.8.2.1 Comparison of guanidinium based supports at different eluent concentrations

Silica gel guanidinium chloride salt **28** was tested as anion exchanger with a variety of mono-, di-, and tri- charged anions. The result produced show very different behaviour to that seen previously when the lower concentration was employed (Figure 2.27 and 2.28). The retention time of support **28** shows a decrease with the anions Br^-, I^- and SCN^-. The mono-charged NO_3^- and $H_2PO_4^-$, the di-anions $S_2O_3^{2-}$, SO_4^{2-}, HPO_4^{2-}, AMP^{2-} and ADP^{2-}, and the tri-anion PO_4^{3-} were all successfully eluted from the column. The explanation for this behaviour is that due the increase in the concentration of the eluent the competition between eluent and anions has also been increased, and this causes the elution of the above anions. ATP^{2-} was not eluted from the column, due to the high selectively its guanidinium group for phosphate[13,87]. To better represent the data, two chromatograms have been produced.

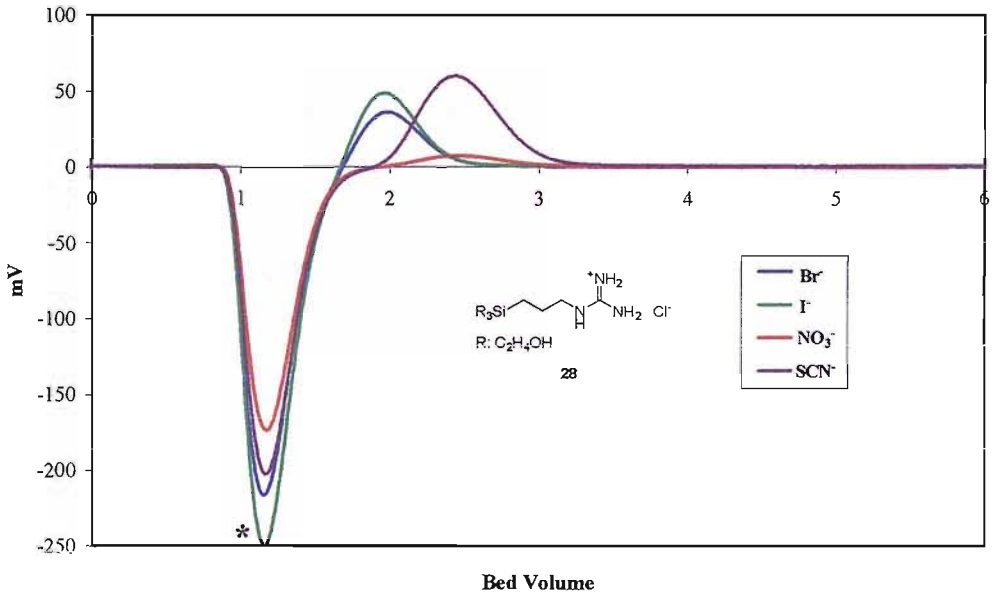

Figure 2.27.: Ion chromatography of Br^-, I^-, NO_3^-, SCN^-, on resin **28** using 0.5M $NaClO_4$. $^*ClO_4^-$ elution.

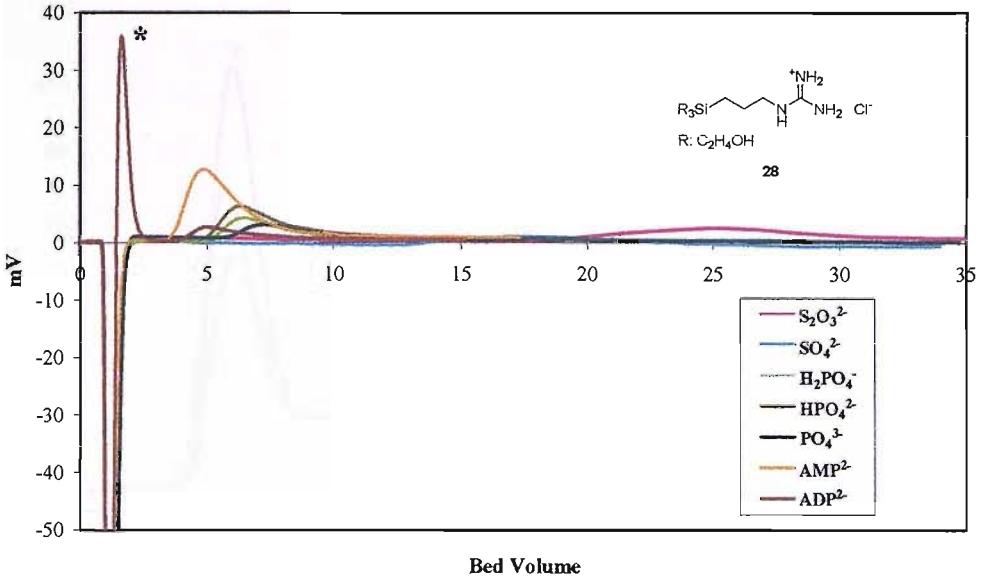

Figure 2.28.: Ion chromatography of $S_2O_3^{2-}$, SO_4^{2-}, $H_2PO_4^-$, HPO_4^{2-}, PO_4^{3-}, AMP and ADP on resin **28** using 0.5M $NaClO_4$. $^*ClO_4^-$ elution.

In the case of the guanidinium silica support **28** the retention times for all varieties of phosphates, even the tri-anion PO_4^{3-}, were shorter than those seen for the sulfates $S_2O_3^{2-}$ and SO_4^{2-}, t_R=25 and t_R=17 respectively. This was irrespective of the charge of the anions.

In contrast to the silica guanidinium support **28**, the methacrylate guanidinium derivative **31**, produced a very different chromatogram (Figure 2.29). Only the mono-charged species such as Br^-, I^- and SCN^- were eluted from the column, and they were eluted with shorter retention times than previously when using lower concentration eluent. Neither of the oxo-anions was eluted from the column.

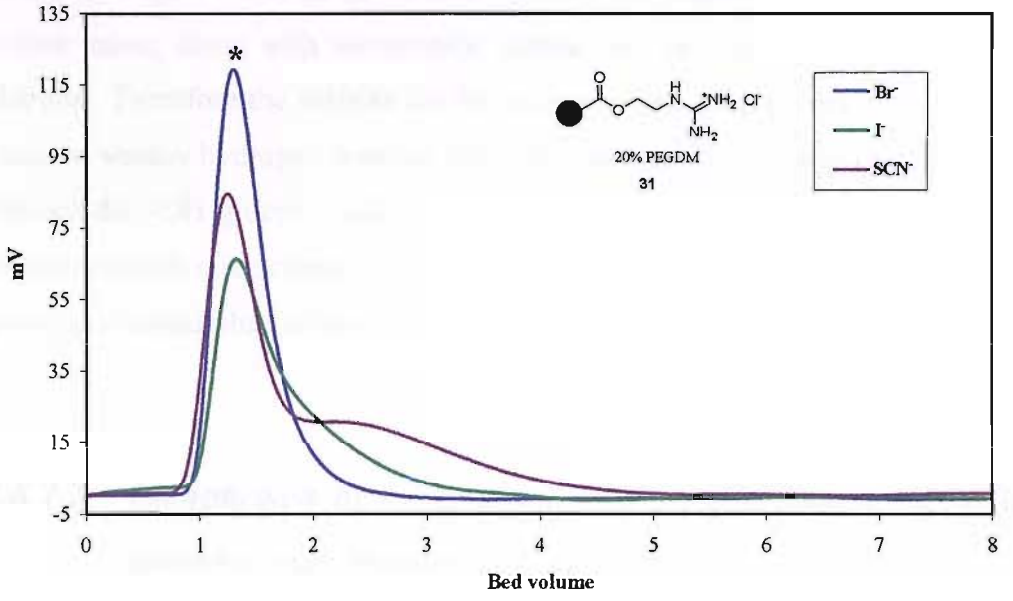

Figure 2.29: Ion chromatography of Br^-, I^-, NO_3^-, SCN^-, on resin **31** using 0.5M $NaClO_4$. To give a clearer diagram the anions which were retained (NO_3^-, $S_2O_3^{2-}$, SO_4^{2-}, $H_2PO_4^-$, HPO_4^{2-}, PO_4^{3-}, AMP, ADP and ATP) in the column are not shown in the chromatogram. $^*ClO_4^-$ elution.

An explanation for the strong retention of the oxo-anions in the column could be the formation of very strong multiple hydrogen bonds between the anions and solid support **31** (Figure 2.30).

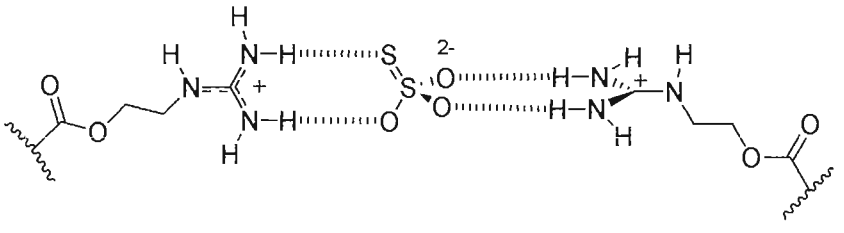

Figure 2.30: Proposed hydrogen bond interactions between $S_2O_3^{2-}$ and support **31**.

In all the chromatograms the retention times for sulfates were longer than for phosphates. This increased retention time can be explained by considering that at the working p*H* of around 7, phosphates exist in two different species, $H_2PO_4^-$ and HPO_4^{2-}. The majority of the anion exists as $H_2PO_4^-$, which is obviously singly

charged. Sulfate exists almost exclusively as the dianion species SO_4^{2-}. This allows strong hydrogen bonds to be formed between the support and the oxygens on the sulfate anion, along with electrostatic interactions resulting from the two negative charges. Therefore the sulfates are strongly retained. Phosphates on the other hand produce weaker hydrogen bonding with the solid support as some of these will form through the –OH groups. Additionally, having only a single negative charge means the electrostatic interactions will be lower than those seen with sulfate. Therefore the phosphate anions elute earlier.

2.8.2.2 Comparison of ammonium chloride salt support at different eluent concentrations

As previously reported during the discussion of guanidinium silica support **28**, silica gel ammonium chloride salt **61** shows the same characteristic pattern as **28**. Only three anions (Br^-, I^-, SCN^-) were eluted from the column when 0.05M $NaClO_4$ was used. When 0.5M $NaClO_4$ was used as the eluent, very different results were seen compared to (Figure 2.31 and 2.32) 0.05M $NaClO_4$. The retention time for Br^-, I^- and SCN^- decreased. The mono-charged anions NO_3^- and $H_2PO_4^-$, and the di-anions $S_2O_3^{2-}$, SO_4^{2-}, HPO_4^{2-} and AMP^{2-} were all successfully eluted from the column. Both the sulfates anions $S_2O_3^{2-}$ and SO_4^{2-} produced longer retention times t_R=14, than all varieties of phosphates.

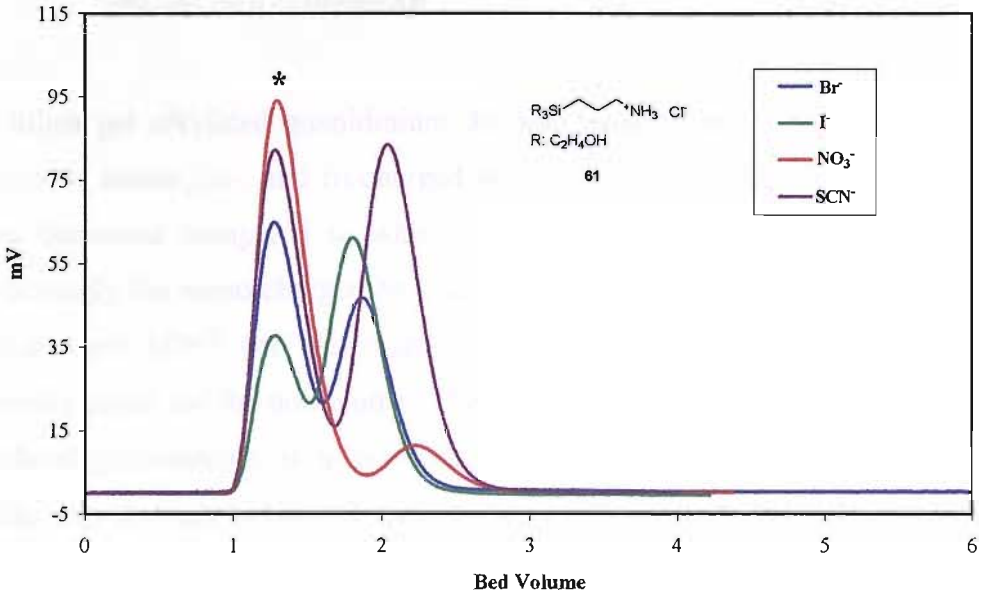

Figure 2.31: Ion chromatography of Br^-, I^-, NO_3^-, SCN^-, on resin **61** using 0.5M $NaClO_4$. $^*ClO_4^-$ elution.

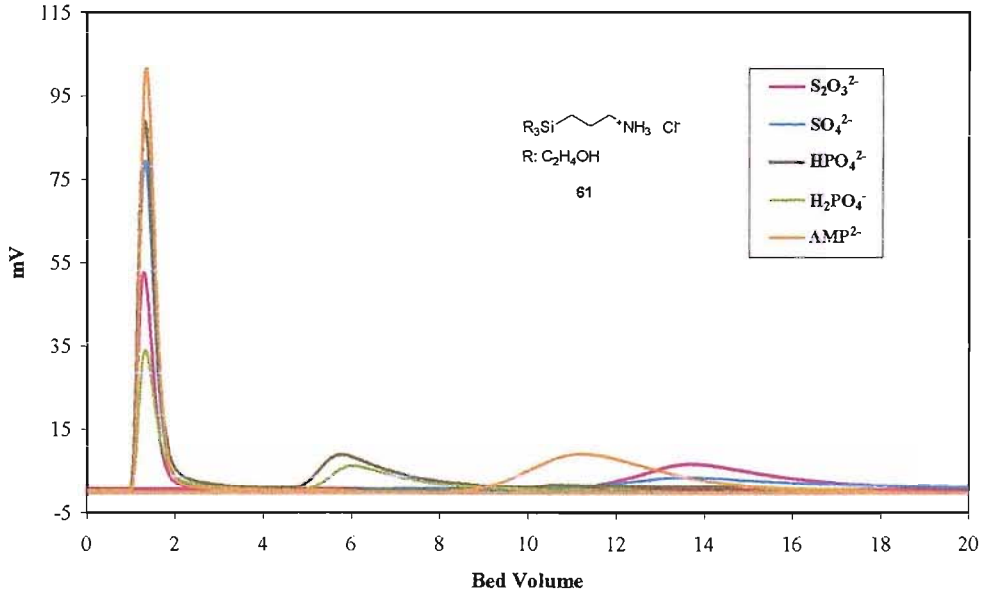

Figure 2.32: Ion chromatography of $S_2O_3^{2-}$, SO_4^{2-}, $H_2PO_4^-$, $HPO_4^{2-}$and AMP on resin **61** using 0.5M $NaClO_4$. $^*ClO_4^-$ elution.

2.8.2.3 *Comparison of alkylated guanidinium support at different eluent concentration*

Silica gel alkylated guanidinium **33** was tested as an anion exchanger with a variety of mono-, di-, and tri-charged anions. Retention times for Br^-, I^- and SCN^- have decreased compared to when lower concentration was used (Figure 2.33). Surprisingly the mono-charged NO_3^- and $H_2PO_4^-$, the di-anions $S_2O_3^{2-}$, SO_4^{2-}, HPO_4^{2-}, AMP^{2-} and ADP^{2-}, and the tri-anion PO_4^{3-} were not eluted from the column. The probable cause for the non-elution of all oxo-anions is the nature of the ligand, the alkylated guanidinium is a very strong base and so interacts with these anion sufficiently strongly to prevent their movement through the column.

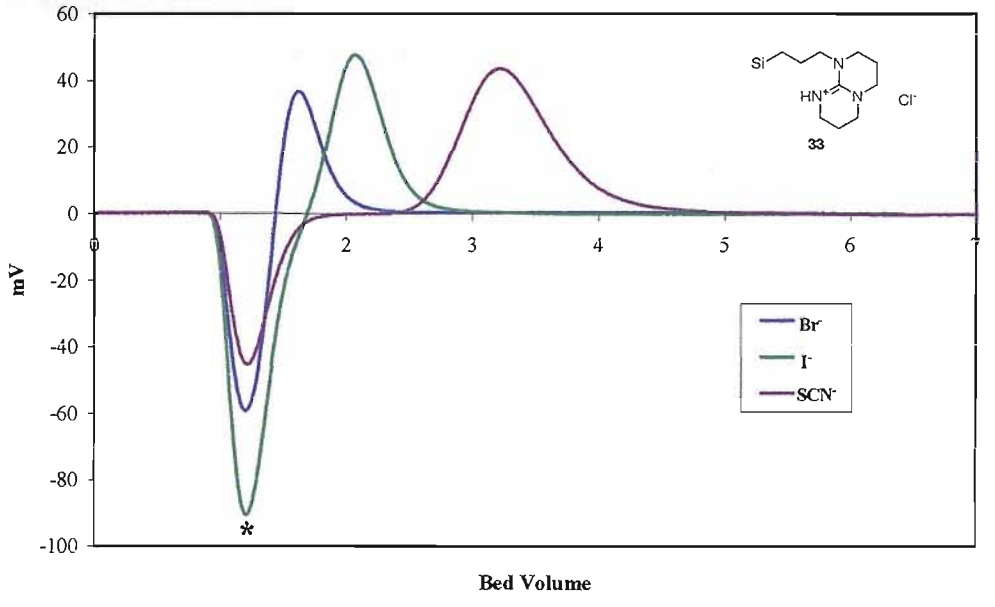

Figure 2.33: Ion chromatography of Br^-, I^-, SCN^-, on resin **33** using 0.5M $NaClO_4$. $^*ClO_4^-$ elution.

2.8.3 Discussion of retention times and elution order

2.8.3.1 Consideration of the interaction mechanism with the silica gel derivatives

Silica gel is a slightly acidic, hydrophilic solid support. Comparison of various based support containing different functionalisation reveals differing the effects of the substituent groups. Solid supports were tested using the same conditions; samples were eluted with 0.05M $NaClO_4$ at a flow rate of 0.40 mL/min in a 60x5 mm column. Silica gel based resin **61** contains a single aminopropyl group, which due to its charged nature can create hydrogen bond interactions and electrostatic interactions. The silica based resin **28** also incorporates a charged moiety a single guanidinium group. Once again the charged nature of this group allows it to form hydrogen bond interaction and electrostatic interactions. Both **61** and **28** displayed the same behaviour, giving the elution order of $I^- \sim Br^- > SCN^-$ while retaining the oxo-anions in the column.

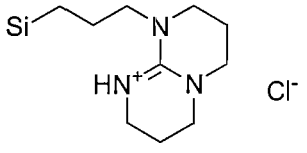

33

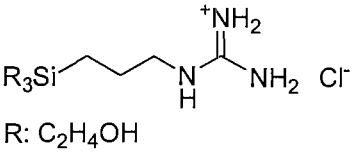

28

$Br^-, NO_3^- > S_2O_3^{2-} > I^- > SCN^-$

$I^- \sim Br^- > SCN^-$

The behaviour of **33** is significantly different from that of **61** and **28**. The elution order is Br^- and NO_3^- followed by $S_2O_3^{2-}$ then I^- and finally SCN^-. This elution order is not according the Hofmeister[17] sequence. It would be expected that I^- elutes first followed by Br^-, NO_3^- and SCN^- and finally the dianion $S_2O_3^{2-}$. It is probable that this behaviour can be due to the nature of the ligand that is a very strong base.

2.8.3.2 Consideration of the interaction mechanism with the methacrylate derivatives

Methacrylate-based solid supports are less hydrophilic than the silica gel supports. Once again, the comparison of two different methacrylate based resin reveals information about the exchange mechanism. Macroprep High Q resin **63** contains a quaternary ammonium group, capable of forming electrostatic interactions, with the possibility of a hydrogen bond interaction. This can be compared to **31**, which incorporates a guanidinium group. This is capable of producing electrostatic interaction and multiple hydrogen bond interactions. Both solid supports have been tested as ion exchangers using the same conditions; samples were eluted with 0.05M $NaClO_4$ at a flow rate of 0.40 mL/min in a 60x5 mm column.

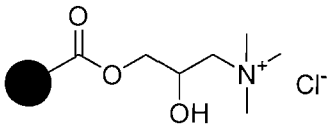

63

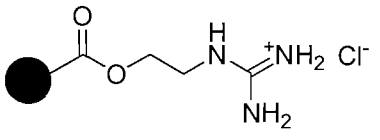

20% PEGDM

31

$Br^-, NO_3^- > S_2O_3^{2-} > I^- > SCN^-$

$Br^- > I^- > SCN^-$

A comparison of the methacrylate and silica backbones reveals that the methacrylate guanidinium **31** support has a different elution order to the analogous silica guanidinium support **28**, the order of Br^- and I^- elution is reversed. This elution order of **31** is not in accordance with the Hofmeister[17] sequence. Another comparison that can be drawn is to Macroprep High Q **63** support with alkylated guanidinium silica support **33**. Both these resins demonstrated the same elution order of Br^-, $NO_3^- > S_2O_3^{2-} > I^- > SCN^-$, showing a no Hofmeister sequence. The retention times for Macroprep derivative **63** were found to be shorter than those of the aklylated guanidinium silica **33**. It is probable that the hydrophobicity of the methacrylate based resin, being greater than the silica based resin, and that this causes the hydrophobic anions to be more stable in this hydrophobic environment so they are retained for a longer time in the column.

2.8.3.3 *Consideration of the differences displayed by the two different solid supports used*

Two different solid support backbones have been used, the silica gel and the methacrylate derivatives. The performance of these two supports relative to each other has been explored. Silica gel guanidinium **28** and methacrylate guanidinium **31** have been tested as anion exchangers with a variety of anions. As previously discussed none of the oxo-anions were eluted from either of them. Only the mono charged anions such as I^-, Br^- and SCN^- were eluted from the columns.

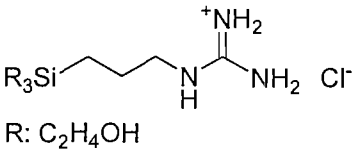

28

$I^- > Br^- > SCN^-$

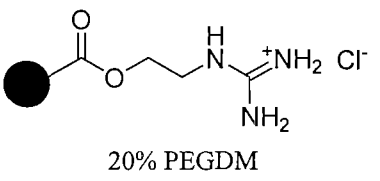

31

$Br^- > I^- > SCN^-$

The retention times on silica **28** are longer, t_R=8 for I^-, t_R=9 for Br^- and t_R=13 for SCN^-, compared to methacrylate **31** where t_R=6, t_R=4 and t_R=10 respectively. Considering the elution order reveals a significant difference. For the silica **28**, the elution order was: $I^- > Br^- > SCN^-$ behaving according to the Hofmeister[17] sequence, while with methacrylate **31** the sequence $Br^- > I^- > SCN^-$ was observed.

An explanation for this behaviour could be the hydrophobicity of the matrix supports. Silica gel is more hydrophilic than to the methacrylate support. As previously discussed, I^- is a more hydrophobic anion than Br^-, so it follows that when hydrophilic supports are employed in the analysis I^- should elute before Br^-. In the case of silica **28** a hydrophilic support, I^- was eluted first followed closely by the Br^- as expected. However, when a hydrophobic support was used such as methacrylate **31** the opposite effect was found, Br^- eluting first, followed by I^-.

2.8.4 The effects of incorporating an extra guanidinium arm

An extra guanidinium group has been incorporated into the structure of a resin in order to establish the affect on the anion exchange mechanism. The double arm guanidinium solid support **43** is based on a polystyrene matrix. Solid support **43** was tested (Figure 2.34) as an anion exchanger with a variety of mono-, di-, and tri-charged anions. Apart from the mono charged anions I^-, Br^- and SCN^- no anion exchange was found to occur. The rest of the anions eluted at the same time that perchlorate eluted. This could be due to the strong hydrophobic effects existing in the column between the solid support and the anion solutions. Comparing this solid support with the methacrylate support **31** which contains only one guanidinium group, the same characteristic elution order of $Br^- > I^- > SCN^-$ is seen. The retention times for support **43** were increased compared to **31** which correlate to the increased level of hydrogen bonding and electrostatic interaction occurring during the elution process. On support **43** the retention times were Br^- t_R=2, I^- t_R=3 and SCN^- t_R=4.5 while previously for support **31** they were Br^- t_R=1.5, I^- t_R=1.7 and SCN^- t_R=2.5.

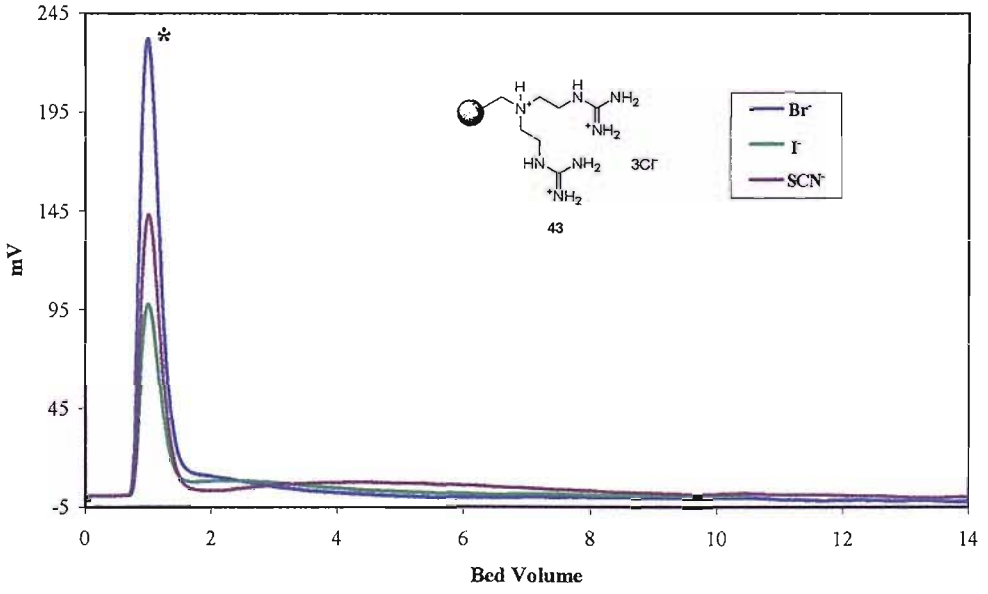

Figure 2.34: Ion chromatography of Br^-, I^-, SCN^-, on resin **43** using 0.5M $NaClO_4$. $^*ClO_4^-$ elution.

2.9 Conclusions

A variety of solid supports bearing mono guanidinium (**23**, **27-29** and **31**), bifunctional guanidinium (**37** and **43**) and a trifunctional guanidinium (**50**) resins have been synthesised and their performance as chromatographic media has been evaluated.

As previously discussed solid supports capable of producing multiple hydrogen bonds interactions with the anions displayed longer retention times compared with those solid supports which can not produce them, or can only produce fewer interactions. This suggests that hydrogen bond interactions play an important role in the ion exchange mechanism.

Chapter 3

Synthesis and characterisation of new polymer solid-supported thiourea resins

3.1 Proton transfer in the thiourea moiety

Thiourea is the thiocarbonyl analogue of urea. It has been known since the middle of the 19th century that thiourea forms 1:1 compounds[107] with strong acids such as HCl and H_2SO_4. There are two possible structures for the monoprotonated thiourea, the sulfonium form **I** and the ammonium form **II**.

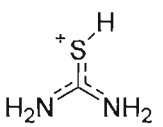

I

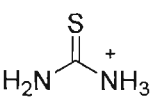

II

The preferred site of protonation has been studied extensively by various experimental and theoretical techniques such as the semiempirical SCF calculations which have been used to demonstrate that S-protonation is energetically favoured

over N-protonation[108]. Conductivity studies of thiourea in $ClSO_3H$ were also interpreted in terms of monoprotonation on the sulphur atom[109].

In the presence of strong acids, such as FSO_3H in SO_2ClF, only the sulfur-monoprotonated[110] thiourea **I** was observed. A second protonation of thiourea (at the *N*-amino atom in the monocation) is possible when more acidic FSO_3H/SbF_5 is used in place of FSO_3H with SO_2ClF as the solvent. In theory protonation of the thiouronium ion **I** can yield three different dicatanions (Figure 3.1) the N,S-diprotonated structure **III**, the S,S-diprotonated structure **IV**, or the N,N-diprotonated structure **V**.

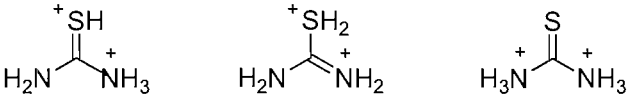

III **IV** **V**

Figure 3.1: Dications form for the thiourea.

Further protonation of diprotonated thiourea **III** is theoretically possible and can occur either on sulfur or on nitrogen leading to structures **VI** and **VII**, respectively (Figure 3.2). However triprotonated thiourea has not been observed experimentally, only calculated as being a kinetically stable species at the B3LYP/6-31G* level. The N,S,S-triprotonated structure form **VI** was found to be the minimum energy structure.

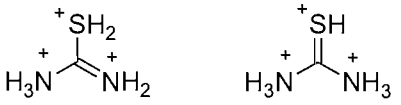

VI **VII**

Figure 3.2: Trication form for the thiourea.

Thiourea is soluble in water and insoluble in organic solvents. It presents basic properties due to the electron lone pairs of the sulphur and nitrogen atoms. These lone pairs give to thiourea a complexation power especially towards heavy metals. According to the Lewis structure, the coordination can be affected from the nitrogen or sulphur atoms.

Hence, thiourea is potentially capable of forming coordinate bonds through both sulphur and nitrogen atoms. In an acidic medium, thiourea is protonated and the proton will be bonded to the sulfur atom, so favouring the bonding of the metal ions to nitrogen atoms.

3.2 Polymer-supported thiourea

The recovery and separation of PGMs from primary and secondary sources is considered a strategic solution to the high demand for these metals in industrial applications and the increasing scarcity of such metals.

Sulfur containing reagents are important extractants of PGMs with respect to selectivity and extraction efficiency. A number of investigations with various types of these reagents have been performed to investigate the solvent extraction properties of platinum from chloride media.

The coordinating resins are polymers with covalently bound functional groups containing one or more atoms that are capable of forming complexes directly with metal ions or their complexes. Over the past few years a number of coordinating and chelating resins have been synthesised and tested for the separation and recovery of precious metals and platinum group metals.

Several studies with thiourea derivatives containing sulphur and nitrogen donor atoms have been conducted to explore the extraction of PGMs from chloride media. In these studies, Pt(IV) was reduced to Pt(II) by the addition of $SnCl_2$. It has been found that with extractants such as diphenylthiourea (DPTU)[111,112] and di-o-tolylthiourea (DOTTU)[113,114], Pt(II) was extracted as $PtCl_2(2R)$ species, where R is the reagent. In another study, heating of the Pt(IV) solutions to at least 100°C was essential for the extraction of Pt(II) with DPTU, in which Pt(II) is extracted as $PtCl_2(DPTU)_4$ complex.

A chelating resin containing thiosemicarbazide as the functional group and based on macroreticular polystyrene-divinylbenzene was prepared by Siddhanta[115] and co-workers.

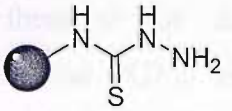

Figure 3.3: Chelating agent containing thiosemicarbazide.

They investigated the sorption behaviour of Pd(II), Pt(IV), Rh(III) and Ru(III) on the thiosemicarbazide resin in 1-2M hydrochloric acid media. The results show that the resin did not absorb Ir(III) at pH 0, which makes its separation from the other PGMs easy.

More recently, several thiourea derivatives have been studied for the extraction of Pt(II) from chloride solutions after the reduction of Pt(IV). However, there is insufficient information on the determination of the composition of the extracted Pt(IV) complexes and their respective extraction constants. In a previous study, Uheida[116,117] and co-workers studied the selective extraction of Pd(II) from other PGMs by nonylthiourea (NTH). The results shown that NTH can be used for the extraction of Pt(IV) from chloride solutions containing low concentrations of these metals. They also report that the extraction of Pt(IV) with NTH takes place through the formation of $PtCl_4(NTH)$ and $PtCl_4(NTH)_4$ species in the organic phase.

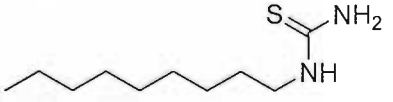

Figure 3.4: The extractant nonylthiourea (NTH).

In 1956, Parrish[118] prepared polystyryl isothiourea (PITU) by the reaction of chloromethylated polystyrene and thiourea. He did not, however characterise this resin. Later, Koster and Schmuckler[119] took interest in the chelating properties of the PITU resin and they discovered its ability to bind PGMs ions by chelation. This work led to the development of a commercial resin known as "Srafion MMRR".

In subsequent investigations on PITU resins Warshawsky[120] and co-workers found difficulties in eluting the PGMs ions from this gel-type resin. They showed

that the binding mechanism of PGMs ions by isothiourea resins is dependant on the polymer matrix. This led to them to the development of "Movimex", a macroreticular resin, which binds the PGMs as ionic and therefore elutable complexes. The behaviour of PITU resins at different acidities is attributed to the weak base properties of the functional isothiourea groups which are subject to the following acid-base equilibrium:

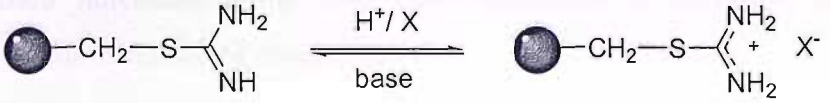

PITU-isothiourea (free base form) **a**

PITU-isothiouronium (acid conjugate form) **b**

The PITU resins in the isothiourea form (**a**) will bind metal cations by coordination, but when converted to the isothiouronium form (**b**) will bind anions by an anion exchange mechanism. Theoretically, the number of cation ligating sites (NH, NH_2, S) in the isothiourea form (**a**) is three times higher than the anion binding sites in the isothiouronium form (**b**). Further investigation of both PITU resins, led Warshawsky[121-123] et al. to provide a comparison on the metal binding capacity between resins "Srafion MMRR" and "Movimex". The results show that both resins have similar loading capacities from dilute acids (0.05M HCl) this drops drastically for Srafion in 6M HCl, while for Movimex the long plateau remains.

The previously reported development of thiourea and isothiourea derived anion exchangers by Warshawsky, Siddhanta and more recently by Uheida has encouraged us to design new solid supports based upon this thiourea and isothiourea motif. A series of resins have been synthesised using a variety of functional groups and their behaviour as anion exchange resins studied using chromatographic separation techniques.

3.3 Synthesis and characterisation of solid-supported thiourea group

In order to investigate differences between various supports bearing the guanidine and thiourea as ion exchanger groups, several supports containing the thiourea motif have been synthesised. Also anion exchangers incorporating the isothiouronium functional group have been developed to provide a comparison between the various modes of attachment.

3.3.1 Silica gel based

Silica **51** was prepared by reacting the butyl isothiocyanate with aminopropyl silica gel. The reaction mixture was refluxed overnight, giving a colourless resin. Silica **51** was characterised by elemental analysis and FTIR spectroscopy (Scheme 3.1).

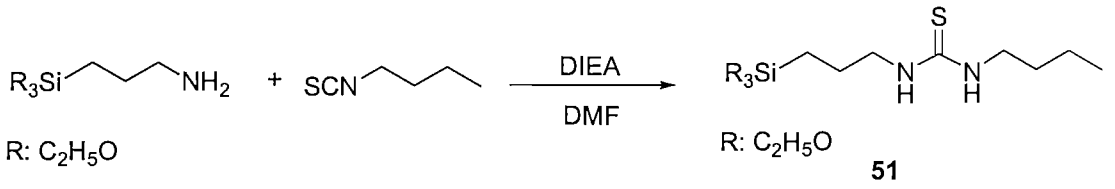

Scheme 3.1

3.3.2 Methacrylate-based resin

The functionalisation of resin **52** to a thiourea group was achieved by reacting butyl isothiocyanate with resin **30f**, previously prepared by ISP techniques in the presence of DIEA in dimethylformamide. The reaction mixture was spin-shaken for

48 h to give resin **52**. Solid support was then characterised by elemental analysis and FTIR spectroscopy (Scheme 3.2)

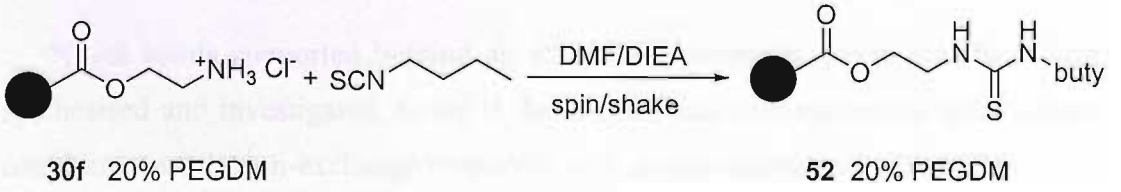

30f 20% PEGDM **52** 20% PEGDM

Scheme 3.2

3.3.3 Isothiouronium resin derivative

As previously mentioned, the good properties that this kind of support have and the remarkable affinity for PGM ions encouraged us to synthesise a support bearing the isothiouronium as a functionalised group. Resin **53**[124] was prepared by reacting thiourea with the Merrifield resin (1% DVB) in methanol, affording a colourless resin. Resin **53** was characterised by elemental analysis and FTIR spectroscopy (Scheme 3.3).

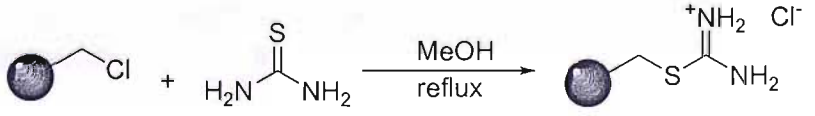

53

Scheme 3.3

3.4 Synthesis and characterisation of solid-supported double-arm thiourea group resins

Novel solids supported bearing an extra isothiouronium group arm have been synthesised and investigated, to see if the bifunctional isothiouronium solid support could improve the ion-exchange properties with simple anions and with PGMs.

3.4.1 Polystyrene-based resin

The functionalised double arm isothiouronium resin **57** was achieved by reacting[125] diethanolamine **54** with polymer **39**, previously prepared by SP techniques. The reaction mixture was refluxed for 24h with overhead mechanical stirring to give the pale yellow resin **55**. This was followed by chlorination with thionyl chloride to yield a dark yellow resin **56**[105], which was then reacted with thiourea[124] in the presence of methanol affording resin **57** (Scheme 3.4).

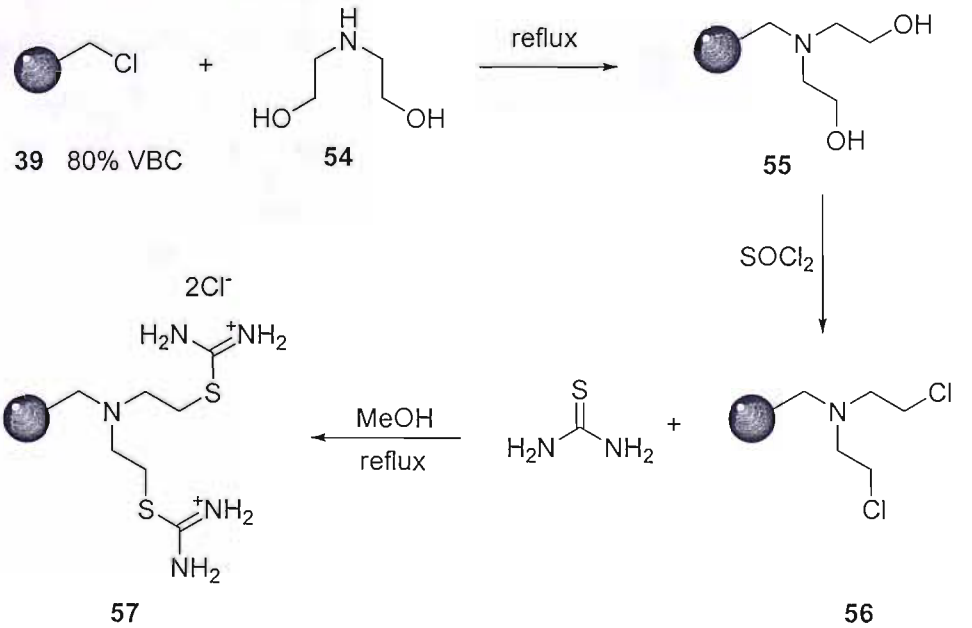

Scheme 3.4

3.4.2 Glycidyl methacrylate-based resin

Macro-prep epoxide resin was functionalised into a double arm isothiouronium resin **60** by reacting diethanolamine **54** with macro-prep epoxide in the presence of dioxane. This was converted to resin **58** via literature procedure[104]. Polymer **58** was reacted[105] with thionyl chloride in toluene in order to obtain the chlorinated polymer **59**. This pale white resin was reacted with thiourea in the presence of methanol affording resin **60**[124]. This resin characterised by elemental analysis and FTIR spectroscopy (Scheme 3.5).

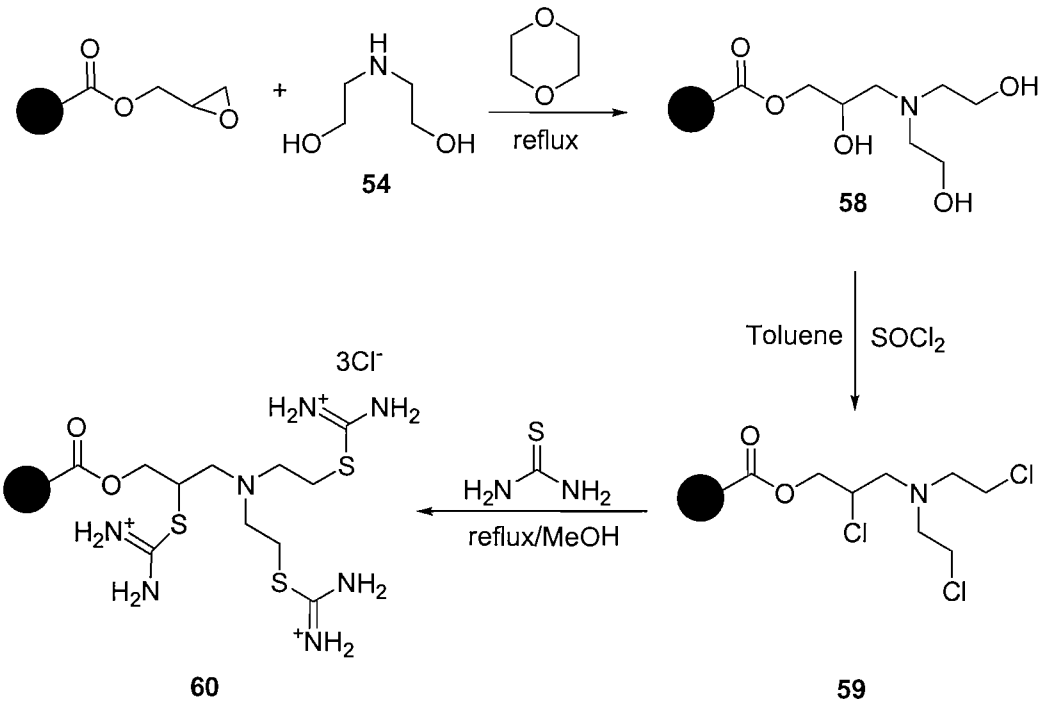

Scheme 3.5

3.5 Evaluation of the solid-supports in ion chromatographs

The performance of the polymer-supported resins as ion exchangers was evaluated by injecting a solution of each anion (150 μL) onto 60mm x 5mm columns packed in aqueous HCl. The samples were eluted with 0.5M $NaClO_4$ at a flow rate of 0.40 mL/min and a fraction of the eluent continuously analysed by a refractive index analyser (Figure 3.5). Prior to the analysis, the column was thoroughly washed with sodium perchlorate solution in order to stabilize the system.

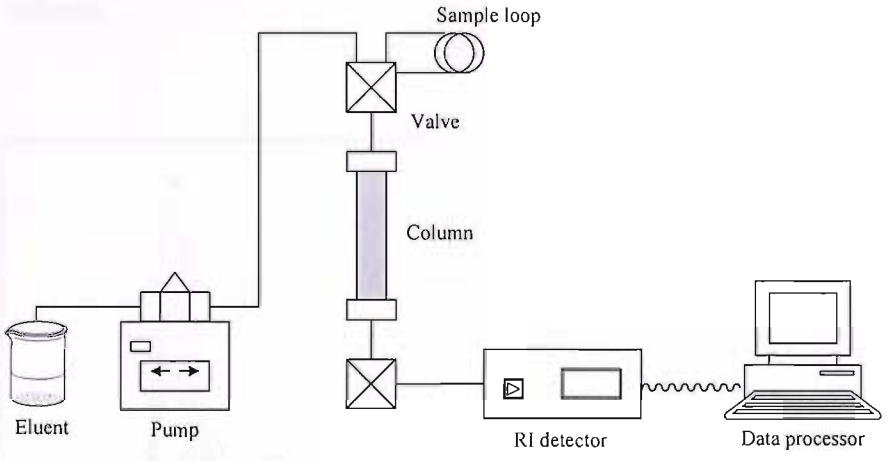

Figure 3.5: Schematic representation of chromatographic rig

3.5.1 Effects of incorporating thiourea in to the resin

As previously discussed, solid-supports bearing guanidinium groups have been analysed by ion chromatography. The results showed that hydrogen bond interactions can play an important role in ion exchange chromatography. As a result of this, several solid-supports bearing thiourea as the only functionality have been synthesised. These supports have been designed with the intention of producing just one kind of interaction: the hydrogen bonds. In order to establish the possible differences between guanidinium and thiourea groups, thiourea containing solid-supports have been tested as anion exchange resins.

3.5.1.1 Comparison of thiourea with guanidinium resin

Silica gel thiourea **51** was tested (Figure 3.6 and 3.7 respectively) as an anion exchanger with a variety of mono-anions such as Br^-, I^-, SCN^-, NO_3^-, $H_2PO_4^-$, di-anions such as $S_2O_3^{2-}$, SO_4^{2-}, HPO_4^{2-}, AMP^{2-}, ADP^{2-} and the tri-anion PO_4^{3-}. The expected reduction in retention time for all the anions on support **51** is seen. This is probably caused by the strength of the interactions involved. In this particular case the only interactions are hydrogen bond interactions, which are much weaker than electrostatic interactions. Furthermore, all the anions without exception were eluted from the column.

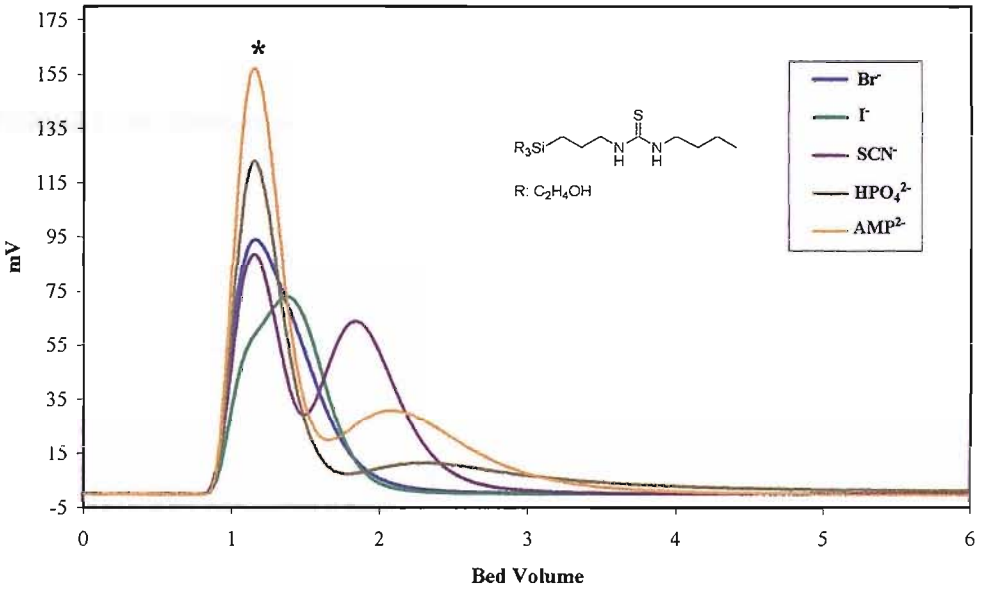

Figure 3.6: Ion chromatography of Br^-, I^-, SCN^-, HPO_4^{2-}, AMP^{2-} on resin **51** using 0.5M $NaClO_4$. *ClO_4^- elution.

The results show a drastically decreased retention times when compared with guanidinium containing solid support. This is especially true for the oxo-anions, for example t_R=25 with guanidinium based support to t_R=4 with support **51** for $S_2O_3^{2-}$. The same characteristic pattern of elution as with silica gel guanidinium **28** was found, Br^-, I^-, SCN^- eluted first, followed by oxo-anions.

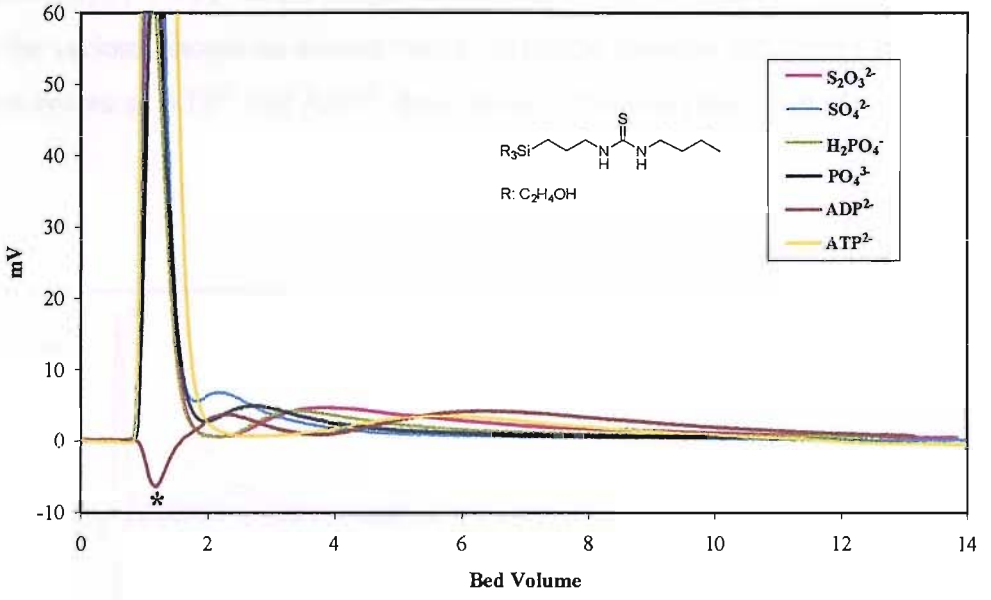

Figure 3.7: Ion chromatography of $S_2O_3^{2-}$, SO_4^{2-}, $H_2PO_4^-$, PO_4^{3-}, ADP^{2-} and ATP^{2-} on resin **51** using 0.5M $NaClO_4$. $^*ClO_4^-$ elution.

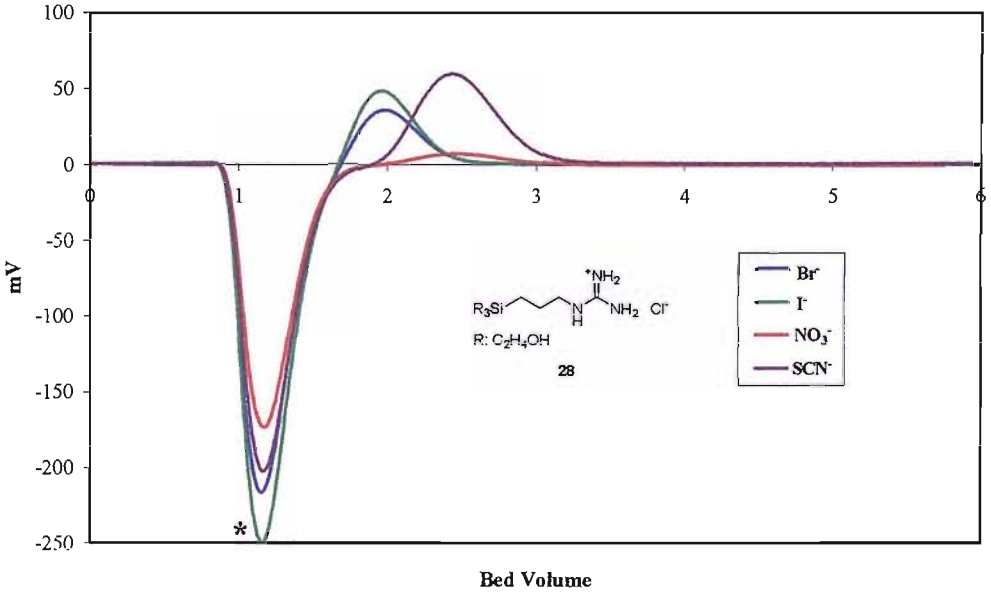

Figure 3.8: Ion chromatography of Br^-, I^-, NO_3^-, SCN^-, on resin **28** using 0.5M $NaClO_4$. $^*ClO_4^-$ elution.

Another important result, is that with the guanidinium support **28** (Figure 3.9) the sulfates $S_2O_3^{2-}$, SO_4^{2-} show longer retention times, t_R=25 and t_R=17 respectively, than all the various phosphate anions tested. With the thiourea support **51** this pattern has been reversed, ATP^{2-} and ADP^{2-} show longer retention times than the sulfate anions.

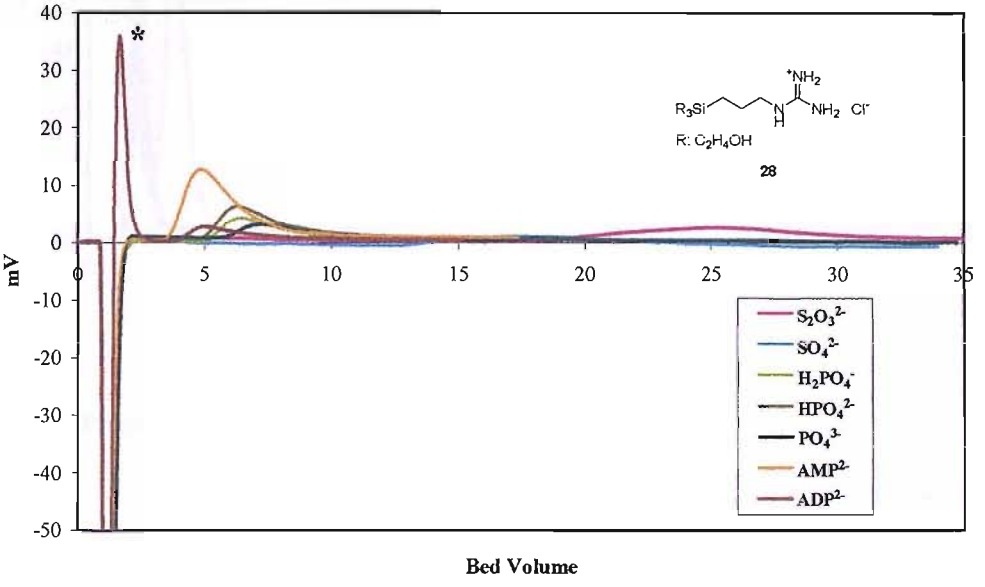

Figure 3.9: Ion chromatography of $S_2O_3^{2-}$, SO_4^{2-}, $H_2PO_4^-$, HPO_4^{2-}, PO_4^{3-}, AMP^{2-} and ADP^{2-} on resin **28** using 0.5M $NaClO_4$. $^*ClO_4^-$ elution.

3.5.1.2 Methacrylate thiourea derivative 52

Methacrylate thiourea **52** was tested (Figure 3.10) as an anion exchanger with a variety of mono-anions such as Br^-, I^-, SCN^-, $H_2PO_4^-$, di-anions such as $S_2O_3^{2-}$, SO_4^{2-}, HPO_4^{2-}, AMP^{2-}, ADP^{2-} and the tri-anion PO_4^{3-}. The results show no anion exchange occuring between the support and the anions. All the anions were eluted at the same time as the reference peak (t_R=1.5). This behaviour could be explained by considering the matrix. The methacrylate matrix is more hydrophobic than the silica gel **51**, and so no anion exchange has been found.

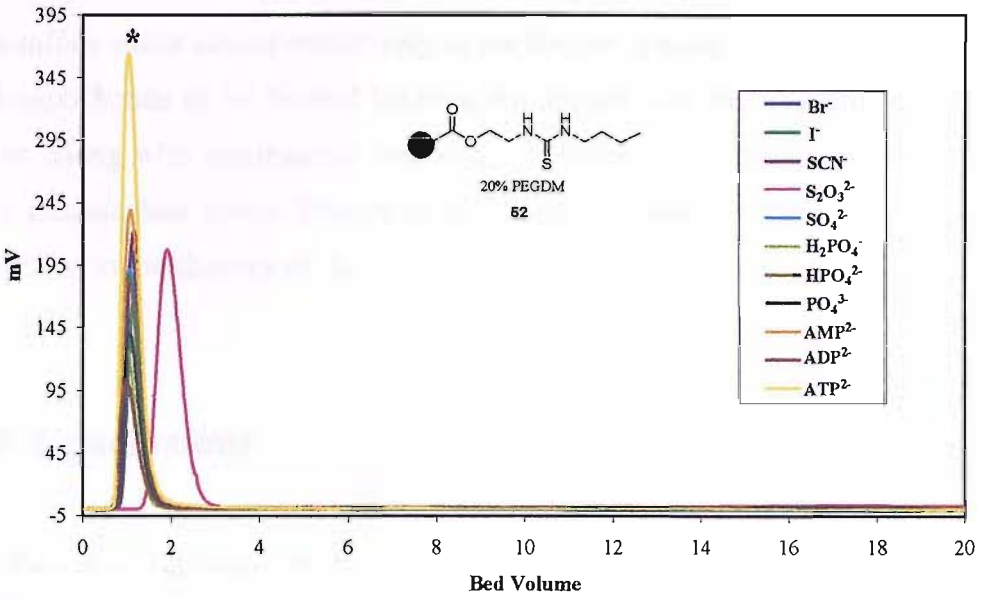

Figure 3.10: Ion chromatography of Br^-, I^-, SCN^-, $S_2O_3^{2-}$, SO_4^{2-}, $H_2PO_4^-$, HPO_4^{2-}, PO_4^{3-}, AMP^{2-}, ADP^{2-} and ATP^{2-} on resin **52** using 0.5M $NaClO_4$. $^*ClO_4^-$ elution.

3.5.2 Discussion of retention times and elution order

As previously reported, retention times are much longer in supports that combine hydrogen bond and electrostatic interactions (**28**) than supports in which just hydrogen bond interactions are used (**51**). The retention times for simple anions such as Br^-, I^-, SCN^- were reduced by half with the thiourea support **51** when compared with the guanidinium support **28**. The phosphate anions showed the same pattern as before, retention times were reduced by half (t_R=5 to 7 for **28**, t_R=2 to 3.5 for **51**). For $S_2O_3^{2-}$ and SO_4^{2-} different behaviour was seen. Not only were the retention times for both reduced by a factor of four with the thiourea support **51** when compared to **28**, but also the elution order was found be different.

In the guanidinium solid support **28** the retention times for SO_4^{2-} is very similar to $S_2O_3^{2-}$, t_R=17.5 and t_R=25 respectively. With **28** and **51** supports the same elution order of SO_4^{2-} then $S_2O_3^{2-}$ was found. Surprisingly the thiourea support displayed a different elution order in that SO_4^{2-} eluted before the phosphates. The reverse was

seen previously with the guanidinium support **28**; it was found that phosphates were eluted before SO_4^{2-}. This behaviour can be explained by considering the possibility that sulfate exists almost exclusively as the dianion species SO_4^{2-} . This allows strong hydrogen bonds to be formed between the support and the oxygens on the sulfate anion, along with electrostatic interactions resulting from the two negative charges with guanidinium group. Despite in the thiourea support **51** this interaction can not occur due to the absence of the electrostatic interactions.

3.6 Conclusions

Two new solid supports bearing thiourea moieties (**51** and **52**) one bearing mono isothiouronium (**53**) and two bifunctional isothiouronium resins (**57** and **60**) have been synthesised. Their performance as chromatographic media has been evaluated.

The thiourea motif showed different behaviour when compared to guanidinium based resins. All the retention times of all the anions were decreased when thiourea was employed as an anion exchanger.

It has been identified that hydrophobic effects can play an important role. This is shown with thiourea silica gel **51**, which can only utilise hydrogen bond interactions, and so the anions were continuously eluted. However, methacrylate thiourea support **52** showed no anion exchange.

Chapter 4

Separation of PGM anions feed by new solid-support media

4.1 Background

As previously discussed, due their low natural abundance, the complex processes required for their extraction and refining and the isolation techniques of the PGMs are of great importance. The important properties which they possess and the wide use of palladium and platinum not only in automotive catalytic converters but as a drug (Pt) and in food production (Pd)[59] has led to more uncontrolled release of these metals in the environment, which further increases the importance of such isolation techniques.

The PGMs sample was a treated precious metal feed liquor from a South African refinery, its composition is shown in Table 4.1. The redox potential of 680 mV suggests that the Pd will be present in its 2+ oxidation state[126] while the Ir and Rh species will be present in their 3+ oxidation states. Ru will be present in both its 3+

and 4+ oxidation states. Pt will be present in its 4+ oxidation state. In general, at around 6 M HCl Pt(IV) will be present as $[PtCl_6]^{2-}$, Pd(II) as $[PdCl_4]^{2-}$, Rh(III) largely as $[RhCl_6]^{3-}$, Ir(III) largely as $[IrCl_6]^{3-}$ and Ru(III) largely as $[RuCl_6]^{3-}$.

Acidity H+ (M)	5.81
Redox (mV)	680
Element	**mgL^{-1}**
Ag	647.56
Al	298.93
As	1003.82
Au	0.00
Bi	1634.34
Ca	154.62
Co	424.62
Cr	61.45
Cu	10804.10
Fe	1.30
Ir	3585.05
Mg	138.22
Mn	13.55
Mo	0.48
Na	1797.11
Ni	28222.30
Os	55.67
Pb	2152.40
Pd	40431.70
Pt	92577.65
Rh	9433.65
Ru	15342.90
S	13054.50
Sb	25.00
Se	10.68
Sn	12.71
Te	0.77
Zn	104.66

Table 4.1: PGMs feed composition.

A variety of new solid-supports bearing guanidinium, thiourea and isothiouronium groups (Figure 4.1) have been synthesised and evaluated by injecting a reduced PGM feed has been investigated.

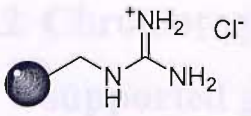

23

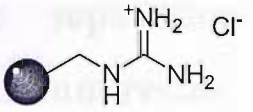

27 high loading

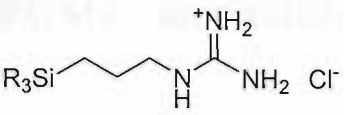

R: C_2H_4OH

28

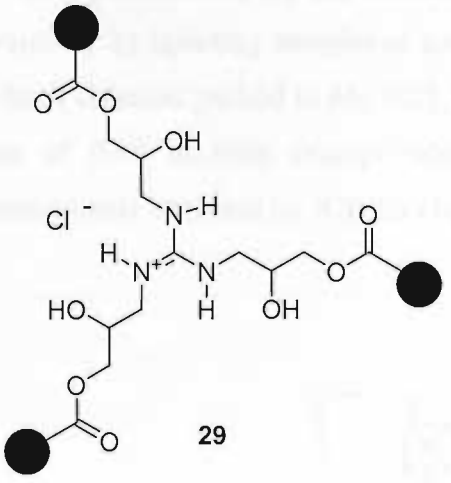

29

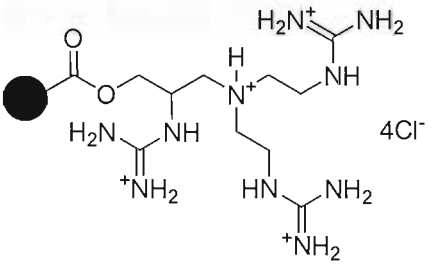

50

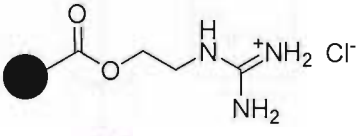

20% PEGDM

31

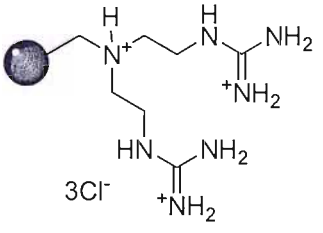

37

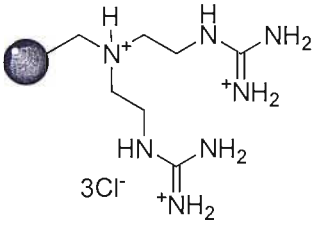

43 gel type

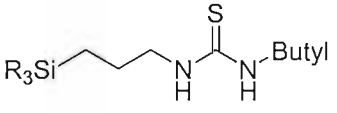

R: C_2H_4OH

51

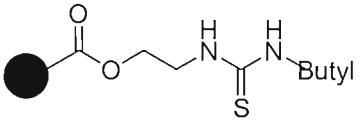

20% PEGDM

52

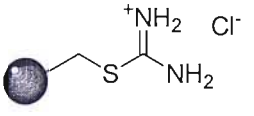

53

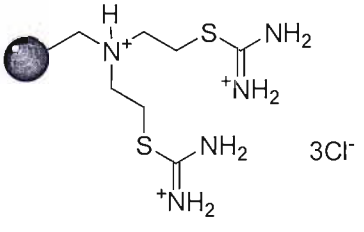

57

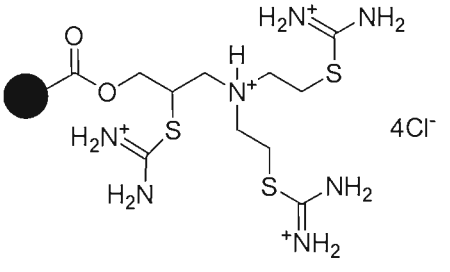

60

Figure 4.1: Novel guanidinium and thiourea/isothiouronium solid-supports.

4.2 Chromatographic separation of PGMs on solid-supported guanidinium resins

The performance of the solid-supported resin as chromatographic media was evaluated by injecting samples of a reduced PGM concentrate (150 μL) onto 200mm x 5mm columns packed in 6M HCl. The samples were eluted with 6M HCl at a flow rate of 0.40 mL/min (except where noted) and a fraction of the eluate was continuously analysed by ICP-ES (Figure 4.2).

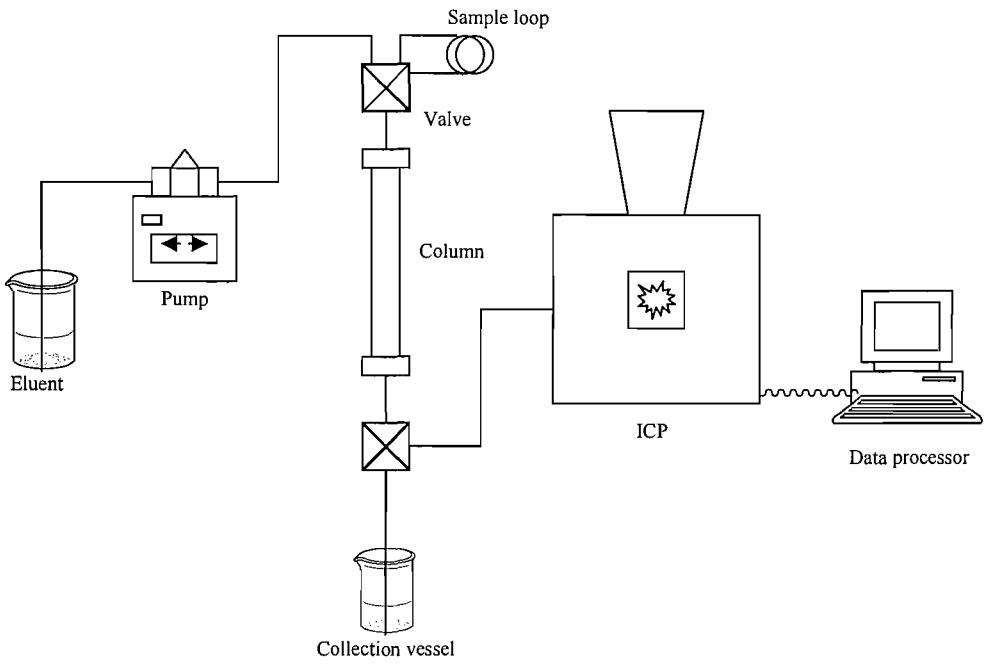

Figure 4.2: Schematic representation of chromatographic rig.

The chromatograms for the separation of the PGMs by resin **27**, **27** to **29** and **31** are depicted in Figure 4.4 to Figure 4.10 respectively.

Polystyrene **23** (Figure 4.4) showed no retention of any metals. This could be caused by the high hydrophobicity of the media giving it poorly compatibility with the aqueous media. Polystyrene **27** (Figure 4.5) was prepared to establish if the hydrophobic effects which were found in support **23**, could be reduced by increasing the loading of functionalised guanidinium four fold, however the desired effect was

not observed. No retention of any metals was demonstrated, apart from on **27** in which case there is some interaction producing tailing.

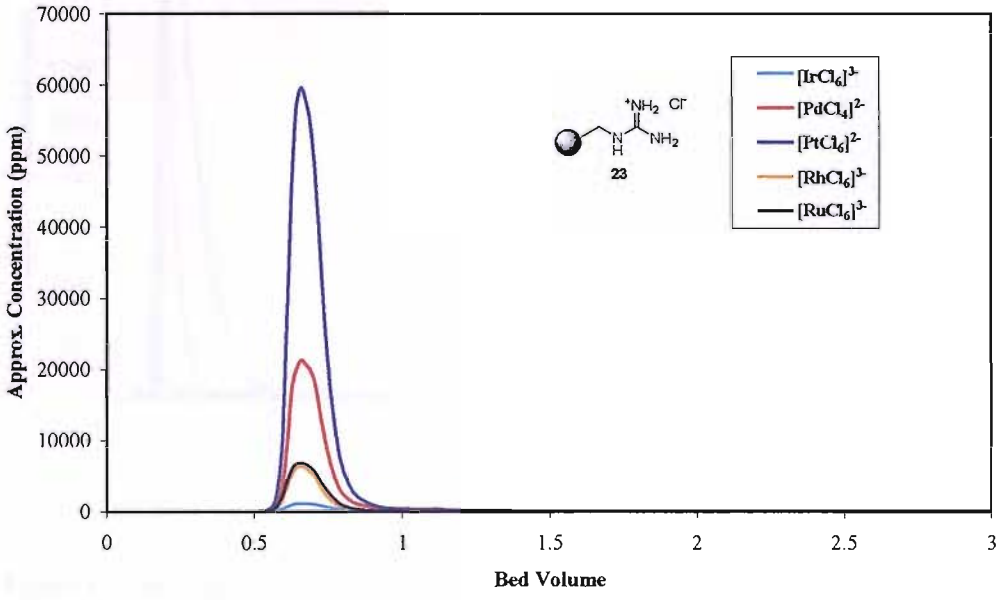

Figure 4.4: Separation of a reduced PGM feed on resin **23** using 6M HCl.

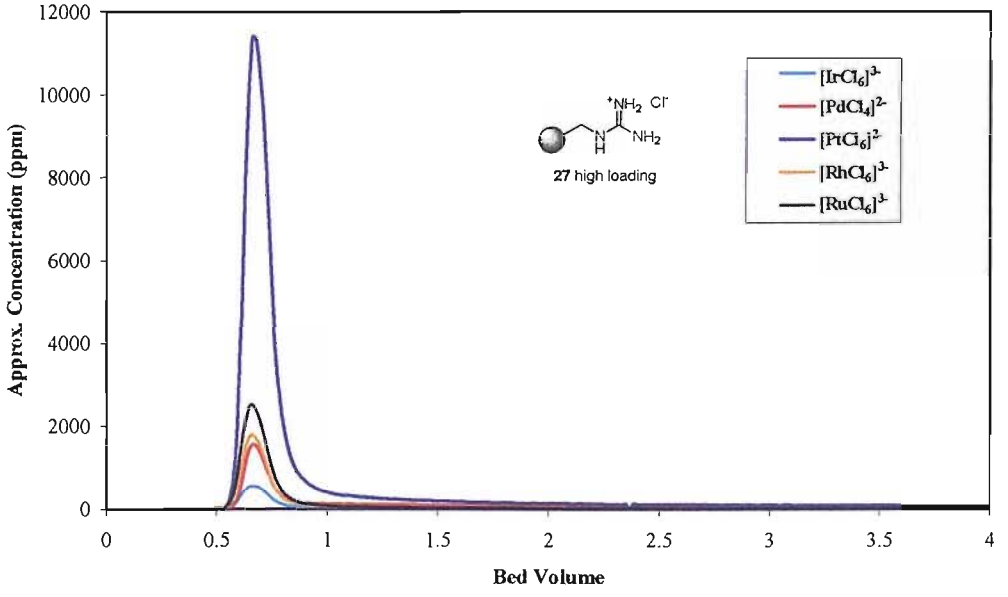

Figure 4.5: Separation of a reduced PGM feed on resin **27** using 6M HCl.

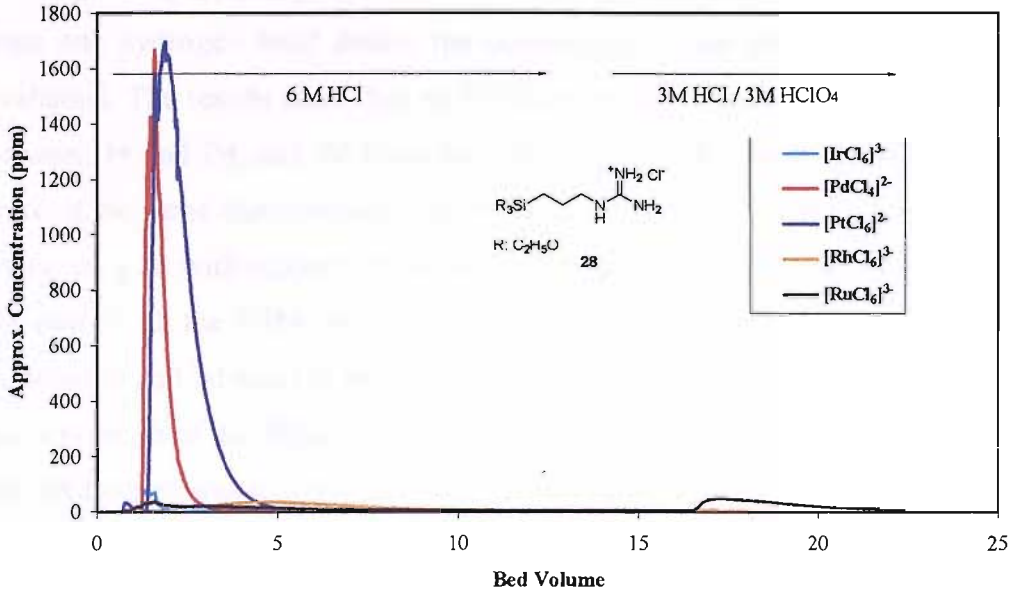

Figure 4.6: Separation of a reduced PGM feed on silica **28** using 6M HCl and 3M HCl/3M $HClO_4$.

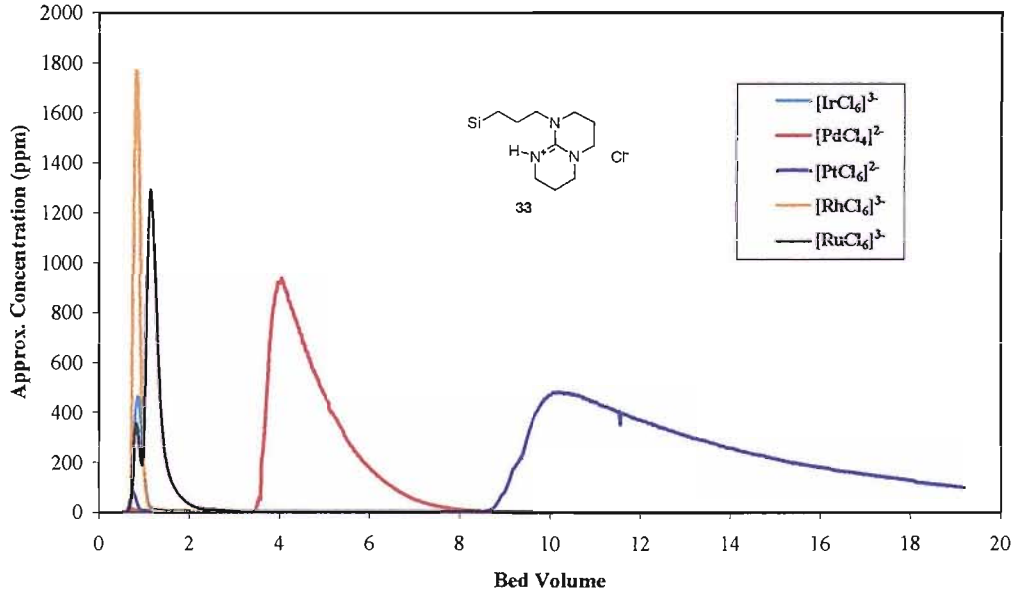

Figure 4.7: Separation of a reduced PGM feed on Silica **33** using 6M HCl.

In order to provide a comparison between resins bearing groups capable of forming multiple hydrogen bonds and resins bearing groups capable of producing at least one hydrogen bond donor, the commercially available solid support **33** was evaluated. The results show that all PGMs were eluted from the column. Separation between Pt and Pd, and Pd from the rest of the PGMs was achieved. This support showed the same characteristic elution order pattern as the theoretical elution order. Comparing **33** with support **28** shows they produce very different chromatograms. In the case of **28** the PGMs were very strongly retained in the column, and separation between Pt and Pd was not obtained. Hydrogen bond interactions drastically affected the separation of the PGMs. **28** was also found to have a significant affinity for Ru in 6M HCl which was strongly retained in the column. This behaviour can be explained by considering the possibility that ruthenium is present in its dimer species, which possesses four negative charges. The result is that it is able to form multiple strong hydrogen bonds with the support, as well as having a significant electrostatic contribution to the interaction from the negative charges, and so the ruthenium is strongly retained.

A comparison of methacrylate resin derivative **31** (Figure 4.10) and silica **28** (Figure 4.6) shows they produced very different chromatograms. Silica **28** showed practically no-retention of any metals apart from ruthenium which was strongly retained in the column. The eluting solvent was then changed to a mixture of 3M HCl and 3M $HClO_4$, increasing the competition between eluent and sample and so liberating the ruthenium species. This can be explain by Ru (III) elutes at the first stage of the elution process, and the last peak was found to correspond to the ruthenium dimer species $[Ru_2OCl_{10}]^{4-}$.

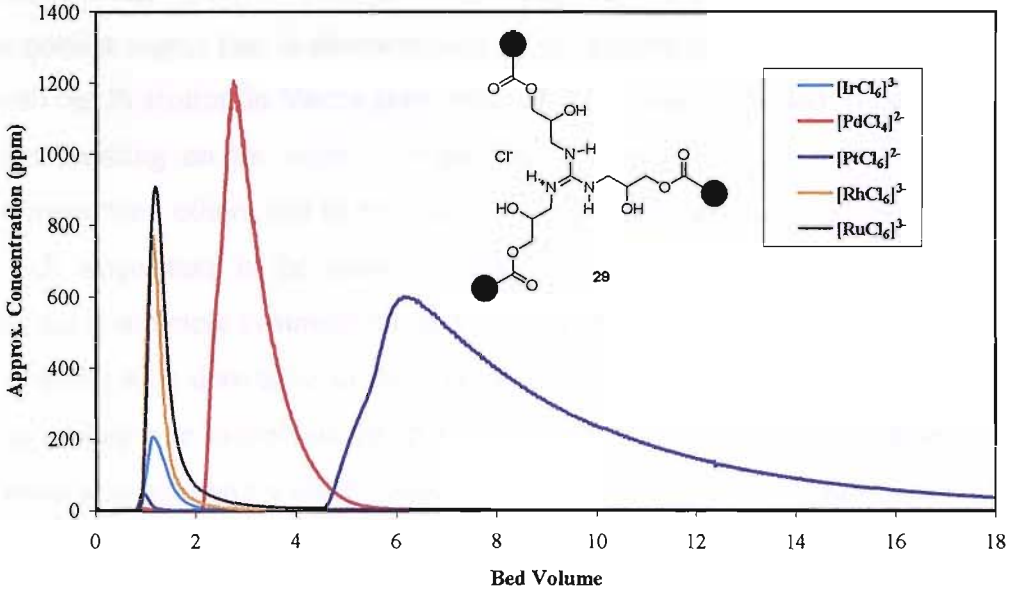

Figure 4.8: Separation of a reduced PGM feed on resin **29** using 6M HCl.

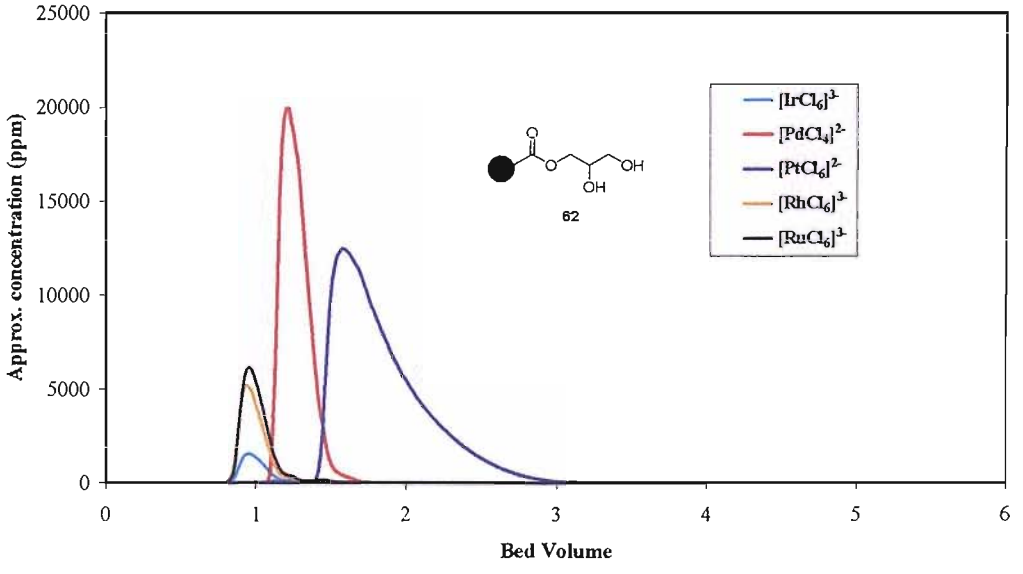

Figure 4.9: Separation of reduced PGM feed on resin **62** using 6M HCl.

Macro prep resin **29** demonstrates separation of Pt from Pd, and Pd from Ru, Rh and Ir peaks with the latter metals essentially not being retained (Figure 4.8). In addition to this, the separation of the PGMs by this support showed the same

characteristic elution order pattern that the theoretical elution order: $[MCl_6]^{3-}$ (Ir, Rh); $[MCl_4]^{2-}$ (Pd); and longer retention times for $[MCl_6]^{2-}$ species (Pt). Another important aspect that is demonstrated by the chromatogram is the tail that appeared with the Pt elution in Macro prep resin **29**. This may be caused by different binding sites existing on the resin. Not all these binding sites are equivalent, some are stronger than others and in the more active binding sites the retention time of Pt is much longer than in the weaker binding sites. As a result the chromatogram peaks are not completely symmetrical, and produce the tail.

Resin **62** a derivative of the commercially available Macro prep epoxide, which has undergonne hydrolysis, has been evaluated as chromatographic media in order to create a comparison with **29**. Separations on Macro prep **29** and **62** show the same characteristic pattern and the same elution order. In the absence of guanidinium groups the retention of the PGMs is much shorter than when this group is present in the column.

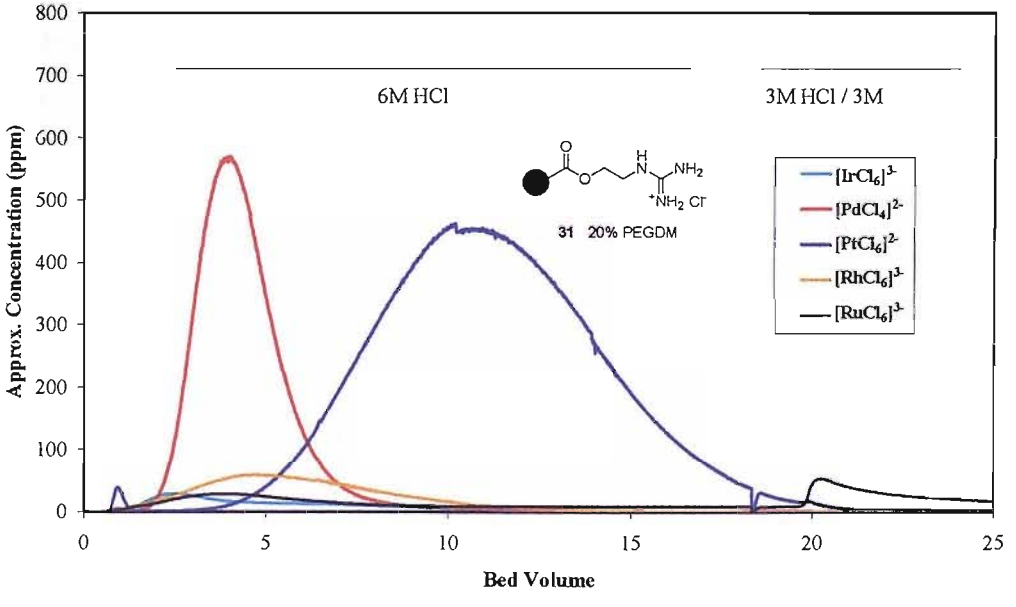

Figure 4.10: Separation of a reduced PGM feed on resin **31** using 6M HCl and 3M HCl/3M $HClO_4$.

Methacrylate **31** shows selectivity for Pd and Pt, separating these while the remaining metals were retained. Again the ruthenium present showed the same

characteristic pattern: at the beginning of the screen it was strongly retained and when the eluting solvent was changed it eluted producing the same shape of peak as before with silica **28**. The theoretical elution order for the PGMs is $[MCl_6]^{3-}$ (Ir, Rh); $[MCl_4]^{2-}$ (Pd); and $[MCl_6]^{2-}$ species (Pt). Separation of the PGMs feed by **31** a new elution order was observed: Ir, Pd, Rh, and Pt.

Some interesting behaviour was found when the 6M HCl eluent was change to 3M HCl/3M $HClO_4$ during the separation of the PGMs on silica **28** and methacrylate resin **31** with ruthenium. A short and broad peak is seen in both chromatograms suggesting the possibility of a Ru dimer species. To confirm our suspicions Johnson Matthey provided some Ru dimer species produced[127] by oxidation of ruthenium chloride to screen silica **28** to see if the same behaviour as previously seen was repeated. The conditions that were employed were the same as previously used. The chromatograms were overlaid to give a better understanding of the relative separation. The line in blue (Figure 4.11) belongs to the previously screened silica **28**, where the presence of the Ru dimer species was identified. The first peak (blue) corresponds to "Ru (III)" species followed by $[Ru_2OCl_{10}]^{4-}$ from the real feed. The pink line corresponds to the synthetic Ru dimer species $[Ru_2OCl_{10}]^{4-}$. The difference of 2 bed volumes between both samples of $[Ru_2OCl_{10}]^{4-}$ is due to the period when the eluent was changed.

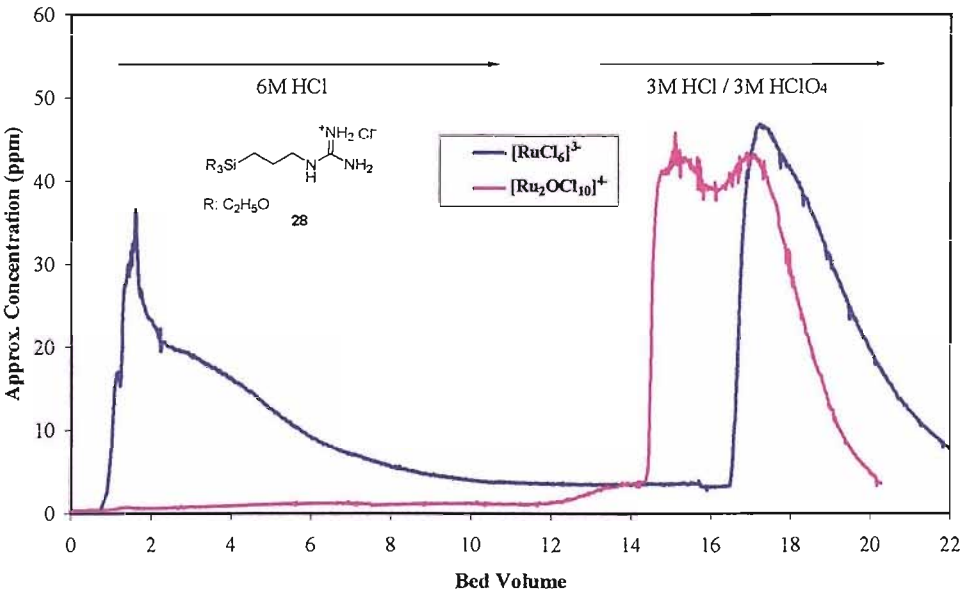

Figure 4.11: Separation of a Ru-dimer species and $[RuCl_6]^{3-}$ on Silica **28** using 6M HCl.

As previously discussed, the ruthenium dimer species was strongly retained on the column by both the silica **28** and methacrylate **31** supports. In order to obtain more information about ruthenium's behaviour with the guanidinium supports, X-ray quality single crystals of the guanidinium chloride salt with a sample of ruthenium dimer species provided by Johnson Matthey have been obtained by slow evaporation from H_2O/ EtOH (1/1 v/v) in HCl solution. However, the desired crystal structure was not obtained. Instead a new structure of the guanidinium salt of $[RuCl_6]^{3-}$ was obtained. The structure adopts a complex 3D hydrogen bonded network. Shown below is the immediate environment around one of the $[RuCl_6]^{3-}$. Half of each $[RuCl_6]^{3-}$ has been generated by symmetry (both Ru sit on an inversion centre), so there is only one $[RuCl_6]^{3-}$ per three guanidiniums. The X-ray crystal structure also shows that water is acting as a link between guanidinium and $[RuCl_6]^{3-}$ as well as bridging between two guanidiniums. The shortest distances between guanidinium and water are 2.09 Å for N-H···O and between the ruthenium and water the distances are 2.52 Å for OH···Cl (Figure 4.12).

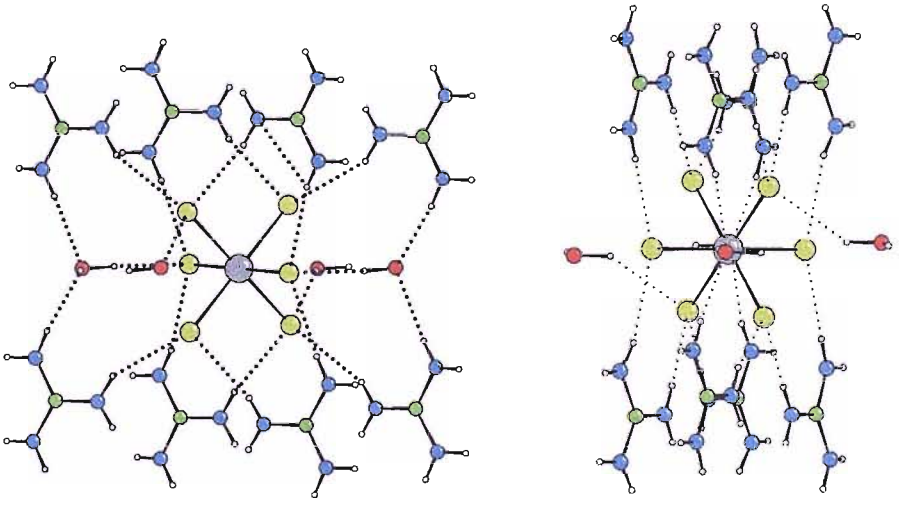

Figure 4.12: X-ray crystal structure of $RuCl_6^{3-}$ with guanidinium, showing the first hydrogen bonding coordination shell.

After several attempts to obtain a crystal structure of the Ruthenium dimer species with various guanidinium compounds were unsuccessful it was decided to employ various simple compounds such as amidium derivatives in anattempt to elucidate the solid state behaviour. X-ray quality single crystals of the benzamidinium chloride salt with the ruthenium dimer species (provided by Johnson Matthey) (Figure 4.13) were obtained by slow evaporation from H_2O/ isopropanol

(1/1 v/v) in HCl solution. It shows hydrogen bond interactions between the Ru dimer species and the amidinium group, with a range of distances from 2.39 to 2.86 Å.

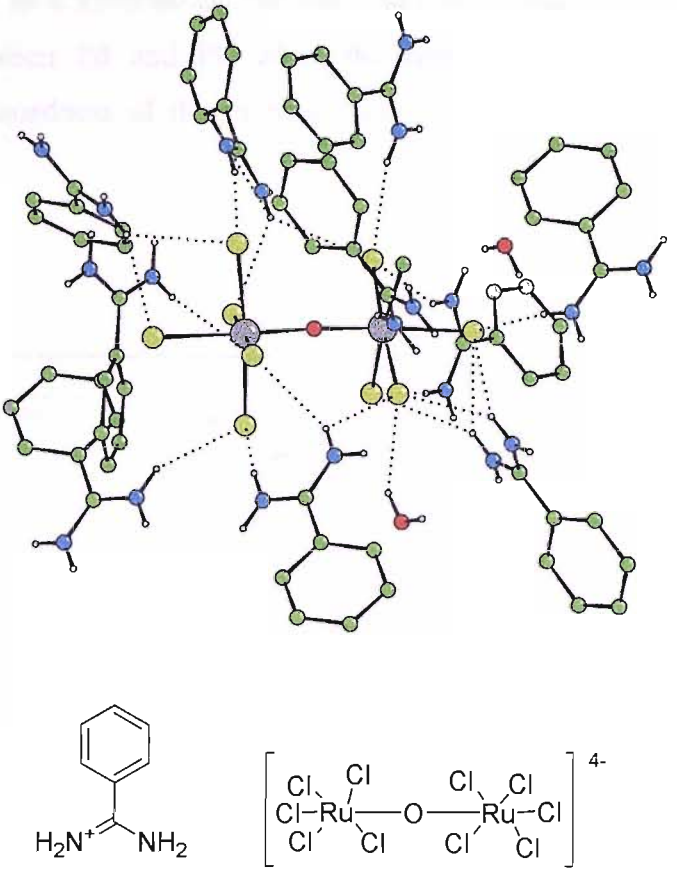

Figure 4.13: X-ray crystal structure of $Ru_2OCl_{10}^{4-}$ with benzamidinium.

4.3 Chromatographic separation of PGMs on solid-supported double-arm guanidinium group resins

The performance of the polymer-supported resin as chromatographic media was evaluated by injecting samples of a reduced PGM concentrate (150 µL) onto 200mm x 5mm columns packed in 6M HCl. The samples were eluted with 6M HCl (except where noted) at a flow rate of 0.40 mL/min and a fraction of the eluate continuously analysed by ICP-ES.

The chromatographic separation of the PGMs by **37** is presented in Figure 4.14. Resin **37** is a macro-reticular polymer due to its high cross-link ratio (30% DVB). PGMs were completely immobilised on the top on the column. Changing the eluent from 6M HCl to a mixture of 3M HCl/3M $HClO_4$ did result in a slight peak separation between Pd and Pt, while the remaining metals were significantly retained. The broadness of the Pt peak may be due to the relatively slow kinetic uptake.

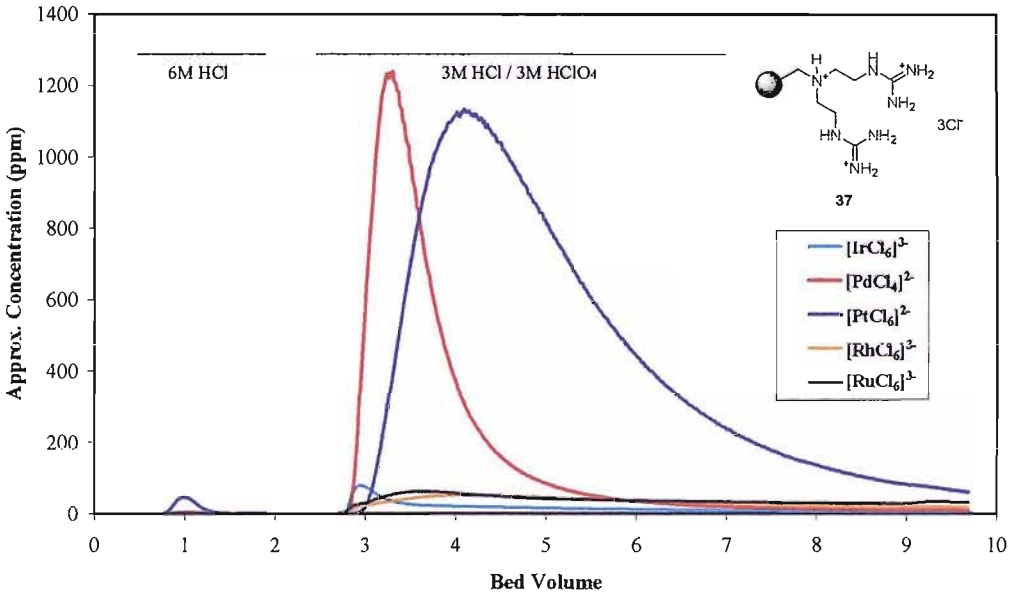

Figure 4.14: Separation of a reduced PGM feed on resin **37** using 6M HCl and mixed 3M HCl/3M $HClO_4$.

Figure 4.15 shows the chromatographic separation of the PGMs by gel type resin **43**. While the copper and nickel metals were as usual, not retained, the PGMs were completely immobilised on the top 50% of the column. Changing the eluent to 3M HCl/ 3M $HClO_4$ resulted in a reduction in the bed volume of the column (nearly 10%). Once the eluent had been changed all the PGMs began to elute from the column. Due to the initially observed immobilisation of the feed over 50% of the column, the resulting chromatogram shows long tails for Pd and Pt. While with macro-reticular resin **37** separation between Pd and Pt was achieved, in gel type resin **43** this was not observed.

In the case of gel-type styrene resins **43** the hydrophilicity of the guanidinium groups was not strong enough, even when the functionality loading of the resin was increased by four fold. The hydrophobic interactions caused by the matrix of the resin were very important in determining the interaction of the resin with hydrochloric media and no retention of PGMs was observed.

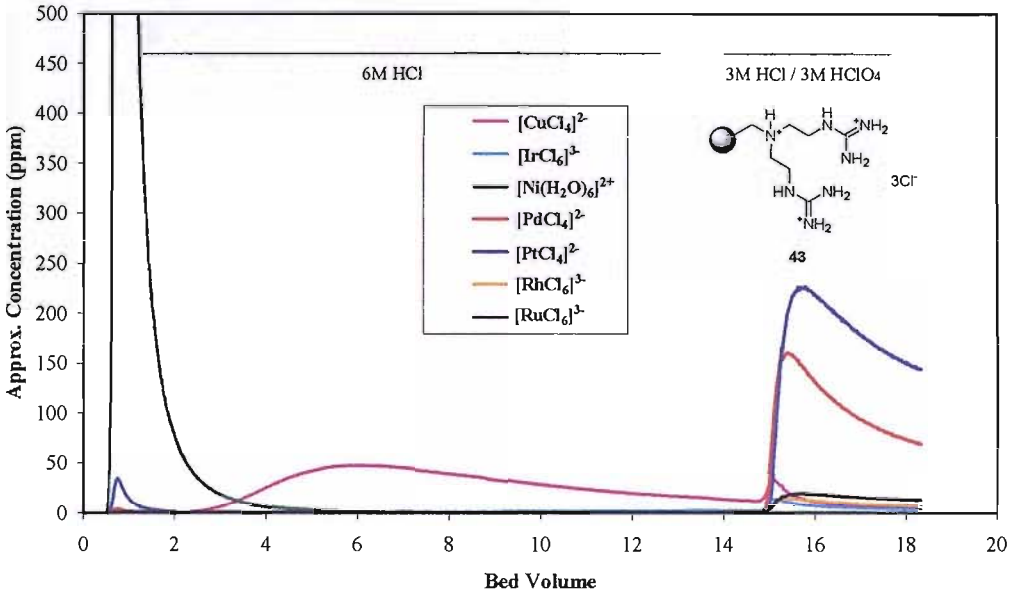

Figure 4.15: Separation of a reduced PGM feed on resin **43** using 6M HCl and mixed 3M HCl/3M $HClO_4$.

The chromatographic separation of PGMs by **50** is depicted in Figure 4.16. Resin **50** showed good separation between Pd and Pt. As soon as the feed was injected four bands were observed, first a yellow band corresponding to the copper, the second band was bright orange and belonged to palladium, the third one was the dark pink rhodium and the last one (dark orange) was retained over the top of the column. Slight bed volume change was observed when the eluent was changed to 3M HCl/ 3M $HClO_4$. The theoretical elution order for the PGMs is $[MCl_6]^{3-}$ (Ir, Rh); $[MCl_4]^{2-}$ (Pd); and longer retention times for $[MCl_6]^{2-}$ species (Pt). However, in the separation of the PGMs feed by **50** a new elution order was seen: Pd, Rh and Ir, and Pt.

Subsequent studies (Figure 4.17) on support **50** with the synthetic solution containing Ir(III), Rh (III) and Ru (III) showed that all the metals were eluted near each other. This suggests that the first Ir peak seen previously (Figure 4.16) must correspond to a different Ir (III) species.

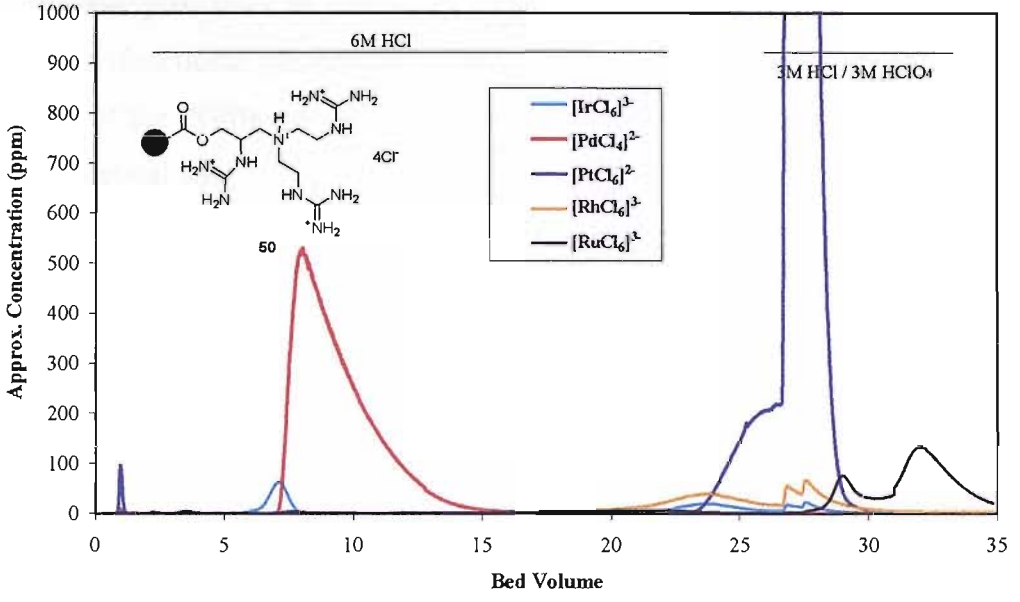

Figure 4.16: Separation of a reduced PGM feed on resin **50** using 6M HCl and mixed 3M HCl/3M $HClO_4$.

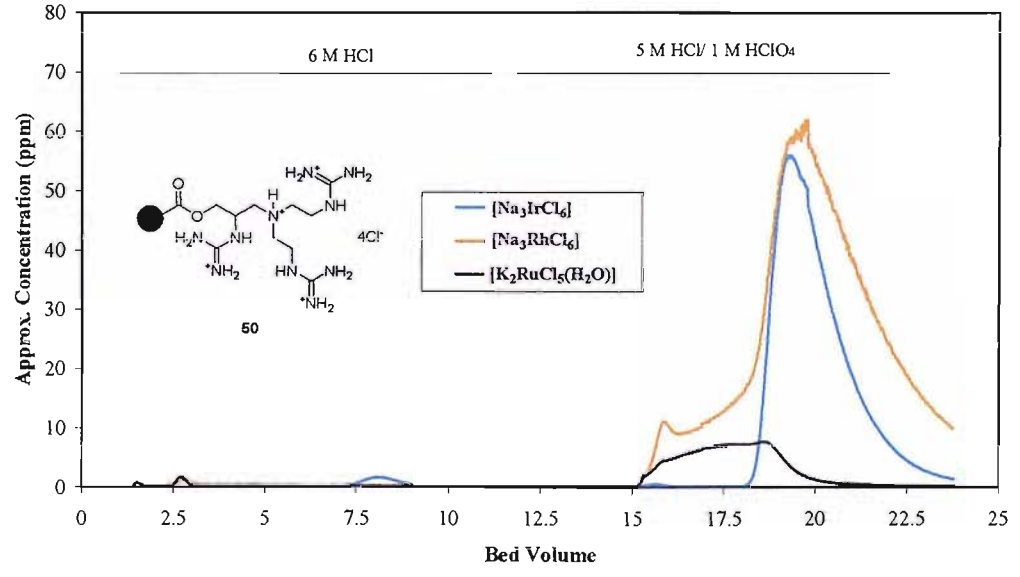

Figure 4.17: Separation of synthetic of Na_3IrCl_6, Na_3RhCl_6 and $K_2RuCl_5(H_2O)$ on resin **50** using 6M HCl and 5M HCl/1M $HClO_4$.

4.4 Conclusions

Silica supported guanidinium was found to have a significant affinity for Ru in 6M HCl, and was strongly retained in the column. However, very little retention of the other PGMs was found.

Methacrylate resin **31** shows separation of Pt from the rest of the PGMs.

For trifunctional guanidinium support **50** it was found that separation of Pd from the rest of the PGMs was achieved, but with a new elution order when compared to the theoretical one.

4.5 Chromatographic separation of PGMs by solid-supported thiourea resin.

The performance of the polymer-supported resin as chromatographic media was evaluated by injecting samples of a reduced PGM concentrate (150 µL) onto 200mm x 5mm columns packed in 6M HCl. The samples were eluted with 6M HCl (except where noted) at a flow rate of 0.40 mL/min and a fraction of the eluate was continuously analysed by ICP-ES.

The chromatograms for the separation of the PGMs by resins **51-53** are depicted in Figures 4.18 to 4.20 respectively.

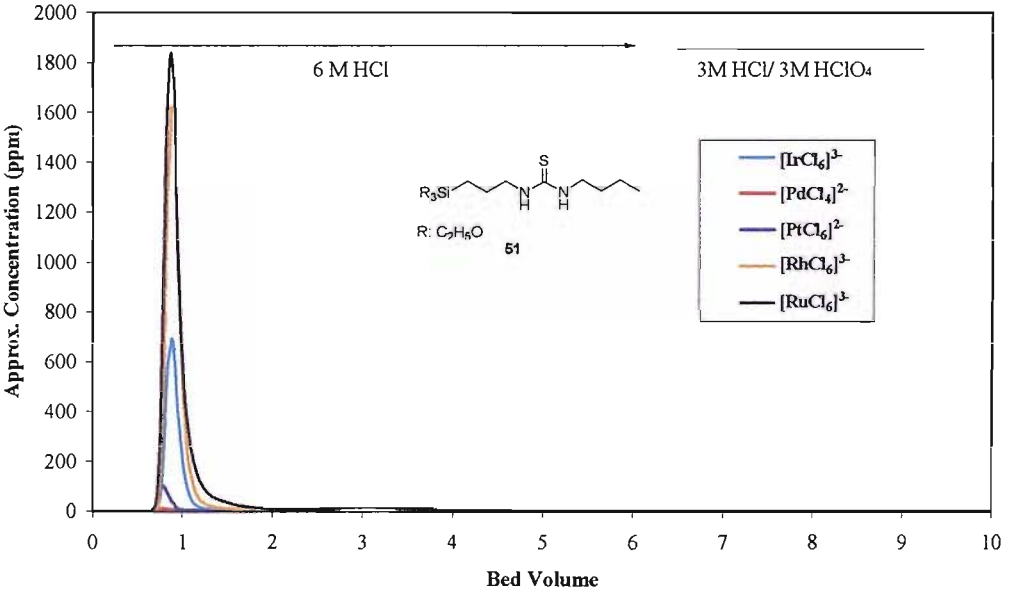

Figure 4.18: Separation of a reduced PGM feed on resin **51** using 6M HCl and 3M HCl/3M $HClO_4$.

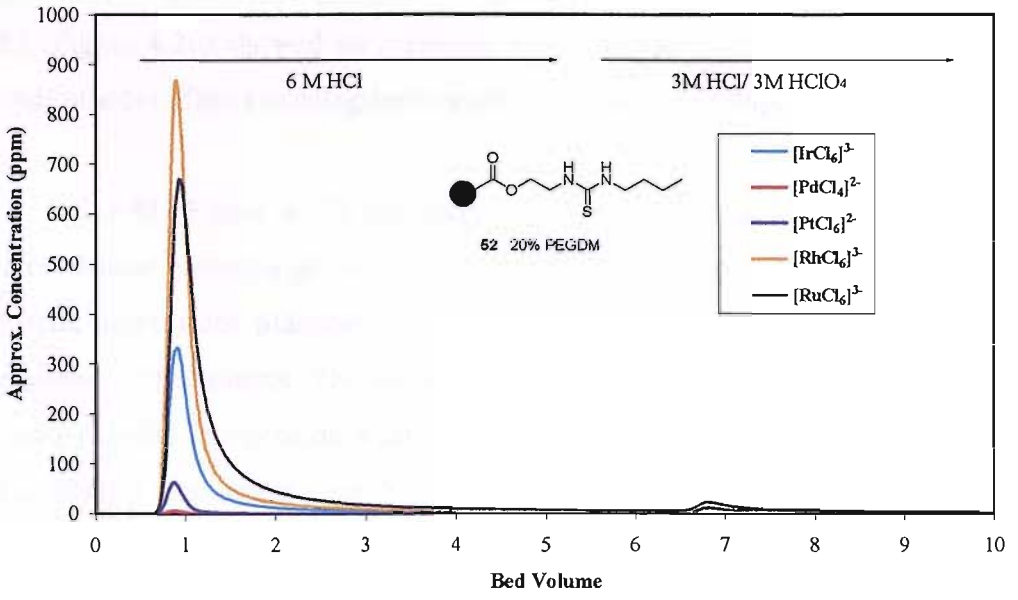

Figure 4.19: Separation of a reduced PGM feed on resin **52** using 6M HCl and mixed 3M HCl/3M $HClO_4$.

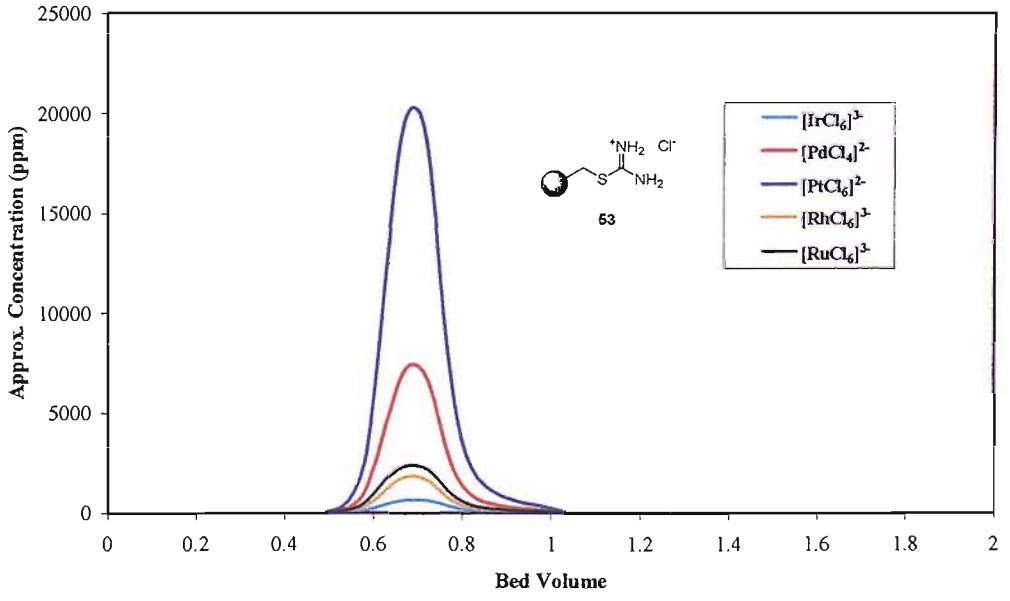

Figure 4.20: Separation of a reduced PGM feed on resin **53** using 6M HCl.

Again the gel-type resin showed the same characteristic pattern as the analogous guanidinium polystyrene **23**, no retention of any PGMs. Isothiouronium polystyrene **53** (Figure 4.20) showed no retention of any metals. This could be caused by high hydrophobic effects existing between the resin and the sample.

Silica **51** (Figure 4.18) and methacrylate resin derivative **52** (Figure 4.19) gave very similar chromatograms. Both supports showed practically no-retention of any metals apart from platinum and palladium which were conversely very strongly retained in the column. The eluting solvent was changed to 3M HCl and 3M $HClO_4$ increasing the competition with the $HClO_4$. However neither Pt nor Pd were eluted. To explore the interaction between the solid support and the $[PtCl_6]^{2-}$ further crystallisations were set up using the same conditions that would be found inside the solid support (6M HCl). X-ray quality single crystals of thiourea with a $PtCl_6^{2-}$ have been obtained by slow evaporation from 6M HCl solution, 6M HCl/isopropanol solution and 6M HCl/MeOH solution. All the crops of crystal were analysed and in all of them the same X-ray structure were obtained (Figure 4.21). This crystal structure has already been reported by Arpalahti[128].

The X-ray structure shows that $PtCl_6^{2-}$ as being coordinated by four thiourea through the sulfur atoms. The thio-amidinium groups are disordered over two orientations. The interactions between platinum-thiourea complex and Cl^- can be described as hydrogen bond interactions with a range of distance between 2.12 and 2.84 Å. Furthermore $[PtCl_6]^{2-}$ has been reduced to Pt(II). This strong coordination between thiourea groups and $[PtCl_6]^{2-}$ could explain why $[PtCl_6]^{2-}$ was not able to be eluted from the column.

The chloride is coordinated by six Pt thio-amidinium molecules. The sulfur coordinated to Pt forms chains in the [301] direction by double N-H···S hydrogen bonds of 2.54Å. These chains are linked in the other two directions via N-H···Cl hydrogen bonds (in the range 2.12 – 2.84Å) to form a 3D network.

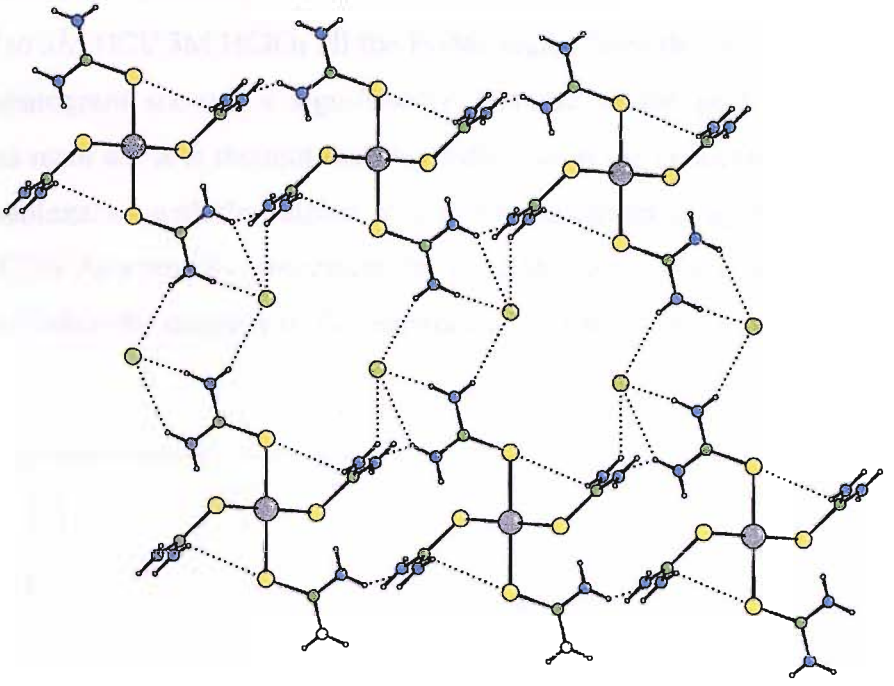

Figure 4.21: X-ray structure of Pt-4(SCN_2H_4) with chloride. A slice through part the structure of Pt-4(SCN_2H_4) showing both the N-H···Cl and N-H···S interactions. The six fold coordination of the Cl is completed by units above and below the plane of the page.

4.6 Chromatographic separation of PGMs by solid-supported double-arm isothiouronium group

The performance of the polymer-supported resin as chromatographic media was evaluated by injecting samples of a reduced PGM concentrate (150 μL) onto 200mm x 5mm columns packed in 6M HCl. The samples were eluted with 6M HCl (except where noted) at a flow rate of 0.40 mL/min and a fraction of the eluate continuously analysed by ICP-ES.

The chromatograms of the separation of the PGMs by resins **57** and **60** are depicted in Figure 4.22 and Figure 4.24 respectively.

The chromatographic separation of PGMs by **57** (Figure 4.22) showed the same characteristic pattern as its analogous guanidininium resin **43**: the copper and nickel metals were unretained while the PGMs were completely immobilised in the top 50% of the column. Changing the eluent to 3M HCl/ 3M $HClO_4$ produced in a

reduction in the bed volume of the column (nearly 10%). Once the eluent had been changed to 3M HCl/ 3M $HClO_4$ all the PGMs eluted from the column. However, the Pd chromatogram showed a significantly decrease of the peak compared to the analogous resin **43**. It is thought that this reduction of the concentration of Pd is due to its complexation with the sulphur of the isothiouronium group present in the resin (Figure 4.23). As a result of increasing the ionic strength of the eluent some of the Pd was eluted while the majority of Pd remained co-ordinated to the resin.

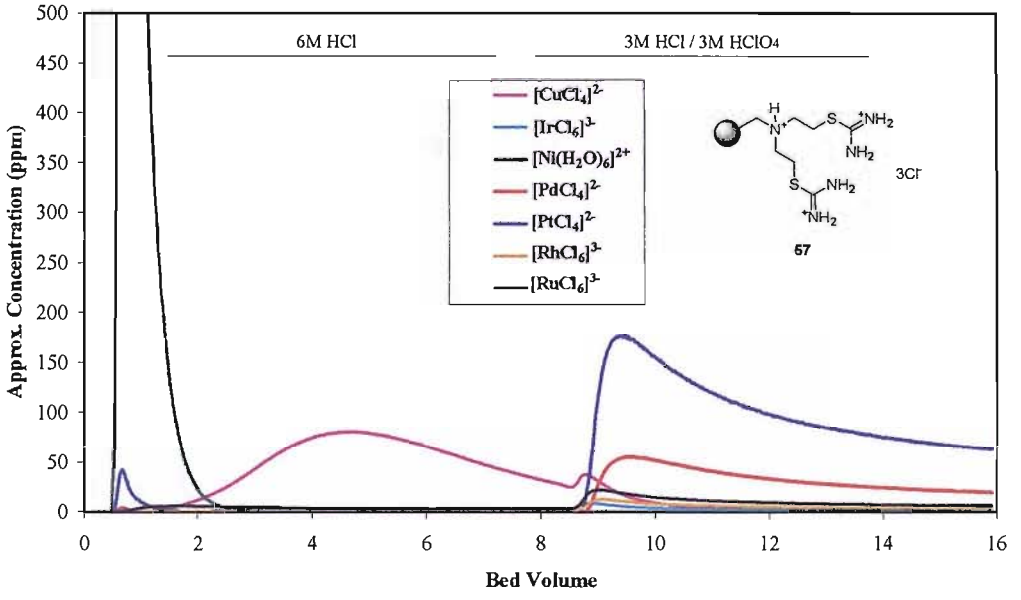

Figure 4.22: Separation of a reduced PGM feed on resin **57** using 6M HCl and mixed 3M HCl/3M $HClO_4$.

Figure 4.23 demonstrates the proposed co-ordinating moieties of $[PdCl_4]^{2-}$ with the isothiouronium groups of resins **57** and **60**. Complexation is achieved through the sulfur atoms as seen in previous work[129].

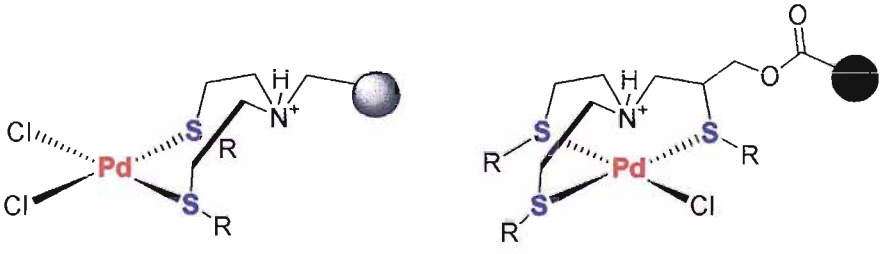

Figure 4.23: Schematic representation of the co-ordination between $[PdCl_4]^{2-}$ with resin **57** (left) and resin **60** (right), R= amidinium group.

Previous studies on support **60** using 6M HCl as the eluent revealed a strong retention for all PGMs. As a result of this the separation of PGMs by **60** was performed with the high ionic strength solution, of 3M HCl/ 3M $HClO_4$ (Figure 4.24). Results showed that Pt eluted well from the column, while the remaining metals were strongly retained, eluted exceptionally slowly. The only exception was Pd which was co-ordinated to the sulphur atom in the resin as proposed above (Figure 4.23).

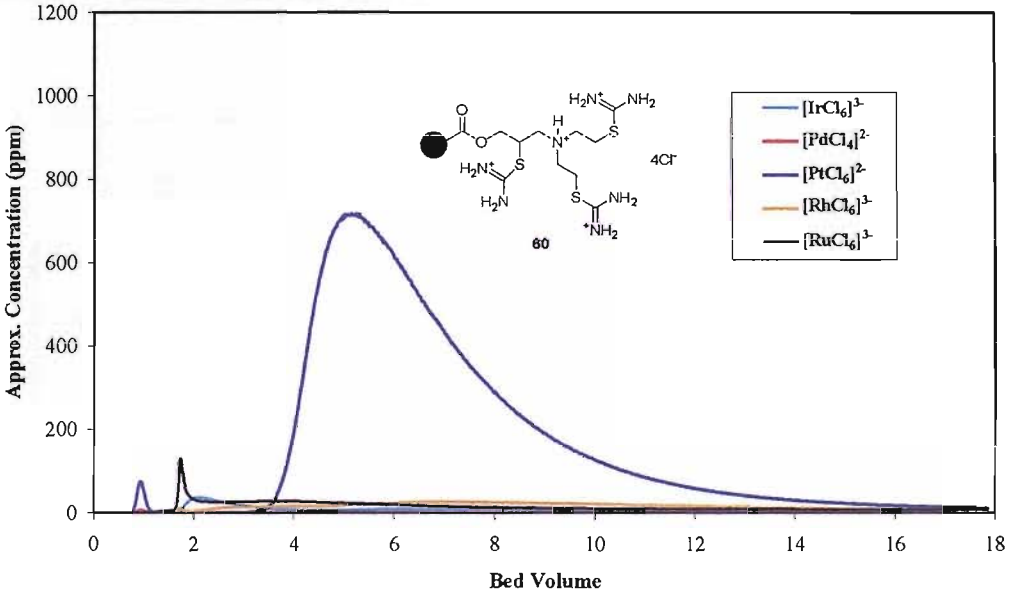

Figure 4.24: Separation of a reduced PGM feed on resin **60** using mixed 3M HCl/3M $HClO_4$.

By contrast with the analogous guanidinium resin **50** that showed short retention of Pd, Pd was immobilised on the resin **60** through coordination.

A comparison of Pd retention times on different solid supports is shown in Figure 4.25. Resin **48**, bearing the guanidinium groups, showed no co-ordination with the Pd and so the Pd was eluted from the column (over 150 ppm). With the analogous resin **57**, which contains two chelating sites, the co-ordination was found to be strong increasing the competitivity of the solution, released part of the Pd that was co-ordinated on to the resin (over 50 ppm). The Macroprep resin **60** derivative, with three potential chelating sites, did not release Pd, even when eluted with 3M HCl/ 3M $HClO_4$, remained completely co-ordinated to the resin.

The explanation for this effect is called the chelate effect[130]. It is dependant on the number of arms, which contain chelating groups that are present in the resin. The more of these there are, the more stable the interaction will be, so the stronger interaction. In this particular example, resin **60** contains three potential chelating arms, as a result of which the co-ordination between Pd and isothiouronium is very strong. Two chelating arms are present in resin **57**, so a strong interaction was expected but not as strong as with resin **60**. In fact, the interaction is much weaker, shown by the fact that some Pd was eluted. Resins containing no chelating groups, such as **43** demonstrated no co-ordination.

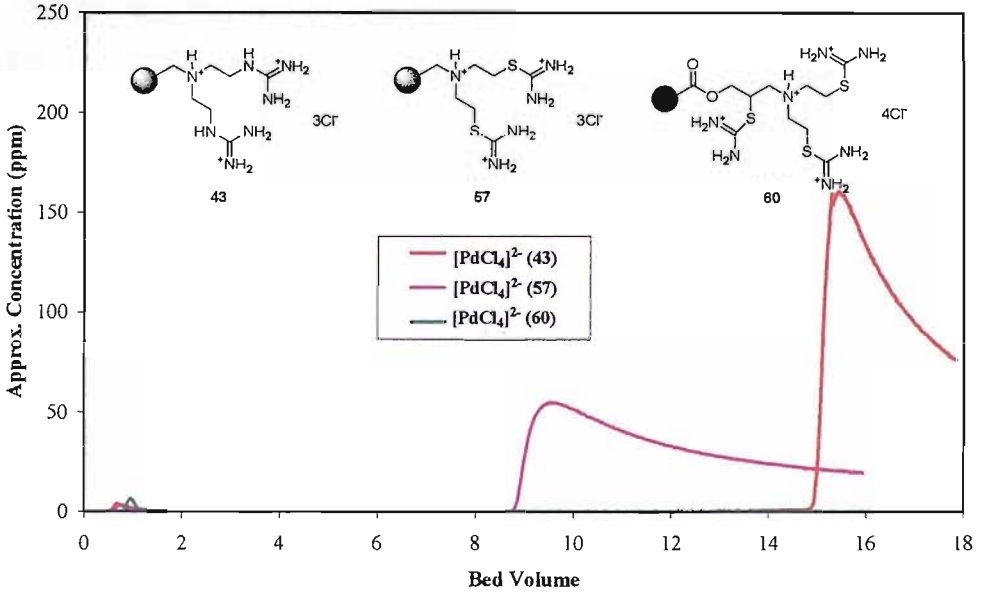

Figure 4.25: Comparison of Pd retention in different solid support resins.

4.7 Conclusions

During the chromatographic separation of the PGMs on the resins supporting the thiourea motif, in general non retention of PGMs was found. The exception to this was Pd which was co-ordinated to the resin, proposed as going through the sulfur atom of the thiourea.

Like the gel-type guanidinium polystyrene **23** investigated previously, the mono isothiouronium gel-type resin did not exhibit any ion exchange properties with the PGMs in hydrochloric solution media. This may have been caused by the hydrophobic interactions between the resin matrix.

The bifunctional isothiouronium resins both showed strong co-ordination with the Pd.

Chapter 5

Selective receptors for hexachloroplatinate (IV)

5.1 Isophthalic acid derivatives

5.1.1 Isophthalic acid derivatives as anion receptors

A number of research groups have employed isophthalic acid derivatives to produce anion receptors. In particular, Crabtree and co-workers[131] reported that simple receptors (Figure 5.1) formed very strong complexes with chloride and bromide through hydrogen bonding interactions.

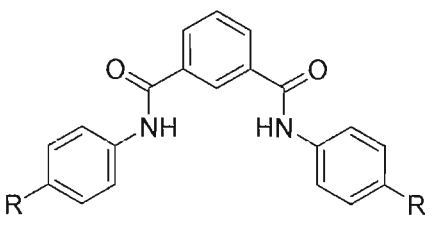

Figure 5.1: Isophthalic acid derivatives, **64a** R=H; **64b** R=*n*-Bu.

They found that receptor **64b** forms complexes exclusively is a 1:1 host:anion stoichiometry. Stability constants were determined in dichloromethane-d_2, 6.1×10^4 M^{-1} for chloride and 7.1×10^3 M^{-1} for bromide.

The interest in anion-directed self assembly[132,133] inspired Gale and co-workers[134] to use the isophthalamide skeleton to study the assembly properties of neutral isophthalamides containing electron withdrawing groups designed to enhance the ligand-anion interaction. They reported that very simple ligands can form anion-directed structures such as double helices in the solid state (Figure 5.2).

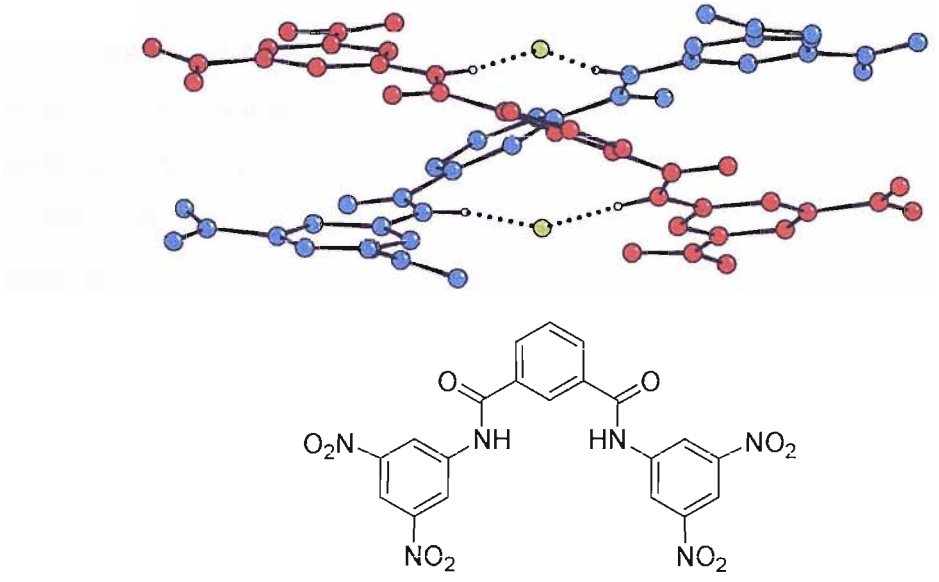

Figure 5.2: The hydrogen bonding network present in the fluoride complex.

Hamilton[135] et al. have designed more complex receptors focusing on the structural opportunities that barbituric acid and its derivatives present (Figure 5.3). Their approach for the recognition of barbiturates exploits the triple hydrogen bond complementarity between 2,6-diamidopyridines and imides[136,137].

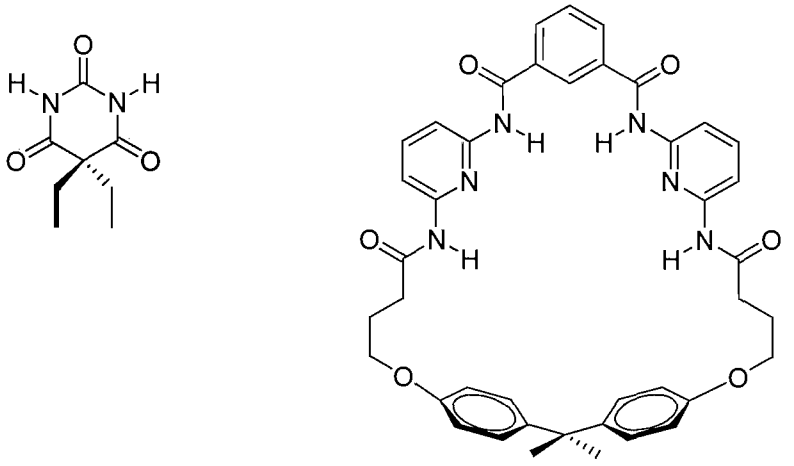

65

Figure 5.3: Macrocyclic receptor and barbital.

Hamilton and co-workers have shown that the complementary positioning of H-bonding groups within a cavity can lead to strong complexation between uncharged molecules. As a result of this complementary between barbital and the macrocyclic receptor **65**, the high association constant of, 1.3×10^6 M^{-1} in chloroform-d_3 was obtained.

Another example that also deserves our attention are the mixed isophthaliamide/ amine macrocycles **66a** and **66b** synthesised by Bowman-James and co-workers[138,139] (Figure 5.4). They report that macrocycle **66a** exhibits a significant selectivity for phosphate and sulfate demonstrating binding constants of 831 and 776 M^{-1} respectively in dimethyl sulfoxide-d_6. The reasons for this selectivity are revealed as a) complementary between the receptor and oxo-anions b) the presence of the tertiary amines which can facilitate the deprotonation of the anion, so providing an electrostatic component to binding. In later studies on macrocycle **66b** the results indicated that it shows higher affinities for phosphate and sulfate with stability constants of 9.3×10^4 and 1.4×10^3 M^{-1} respectively in dimethyl sulfoxide-d_6.

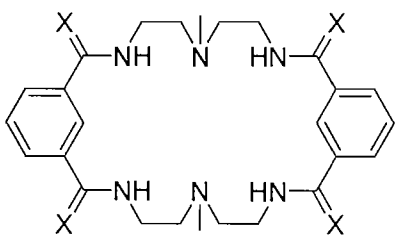

66a X = O
66b X = S

Figure 5.4: Mixed isophthaliamide/ amine macrocycle.

5.1.2 Synthesis and characterization

The successful development of isophthalic acid derived anion receptors has encouraged us to design new receptors based upon this isophthalic motif. A series of compounds have been synthesised, using a variety of functional groups, and their behaviour as anion receptors studied using ^{1}H NMR titration techniques.

Three novel isophthalic acid derivatives **67**, **68** and **69** have been synthesised by functionalizing isophthaloyl dichloride (Scheme 5.1). N,N'-bis (3-amino-phenyl) isopthalamide **67** was prepared by reacting isophthaloyl dichloride with 1,3 phenylenediamine. Upon reaction of **67** with 3 equivalents of either acetyl chloride or octanoyl chloride in the presence of triethylamine and DMAP, compounds **68** and **69** have been obtained in 41% yield respectively. Compound **69** was synthesised to see if the solubility of the receptor could be improved.

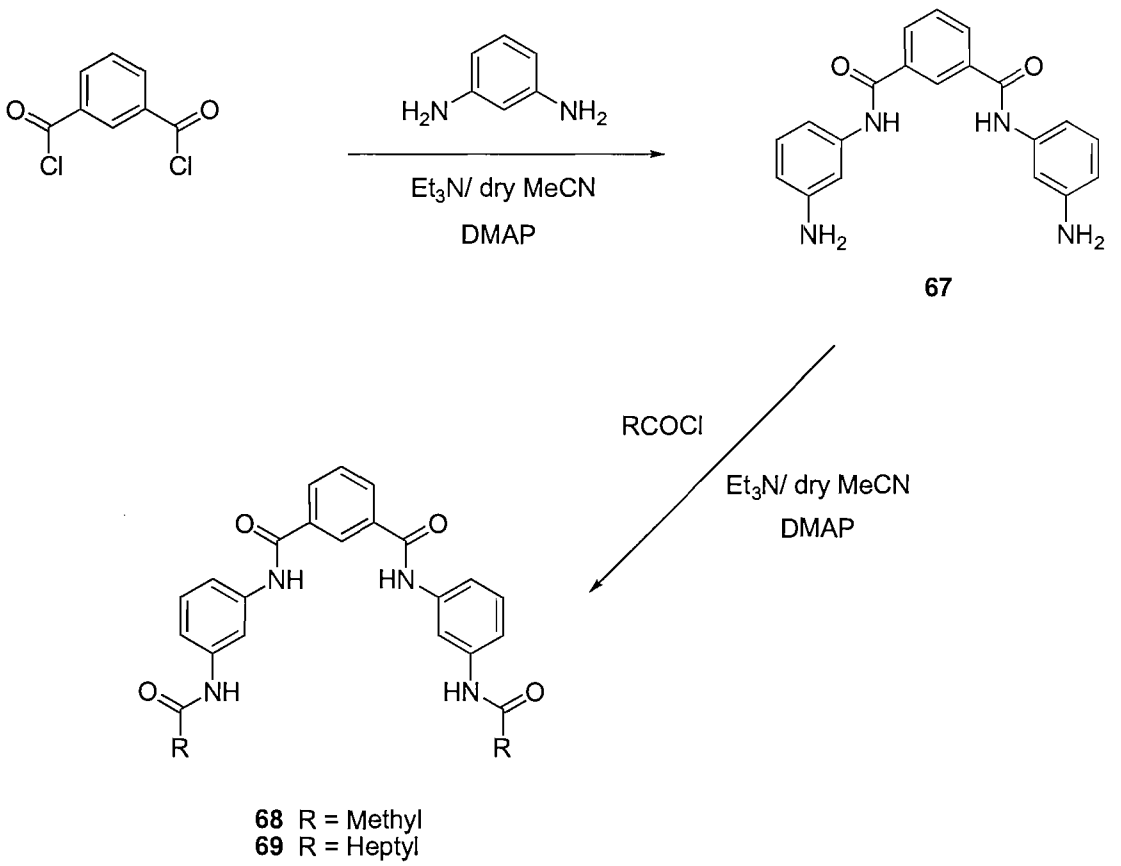

Scheme 5.1

X-ray quality single crystals of **67** have been obtained by slow evaporation of acetonitrile solution of this receptor (Figure 5.5).

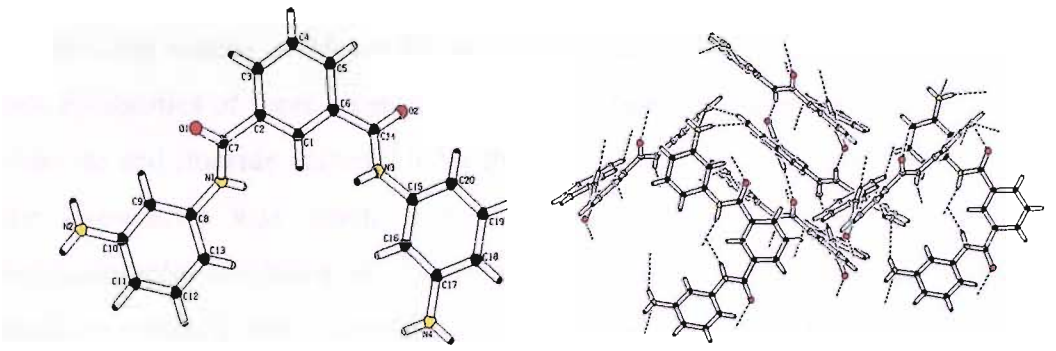

a **b**

Figure 5.5: X-ray crystal structure of receptor **67**, **a)** showing the structure and **b)** displaying the hydrogen bonding network in the solid state.

5.1.3 Coordination studies

^{1}H NMR titration techniques have been used in order to investigate the complexation properties of receptors **67**, **68** and **69**. Anions were added as their tetrabutylammonium salts, because this cation does not compete with the anion binding site. Specific aliquots of the anions were injected into a solution of known concentration of the host, and the shift of the amide proton peak recorded. Association constants have been elucidated using EQNMR software[140].

5.1.3.1 Binding studies results

The anion complexation properties of receptor **67** were investigated in acetonitrile-d_3 solution. Dimethyl sulfoxide-d_6 was used for solubility reasons for receptors **68** and **69.**

NMR titration experiments revealed the interesting anion complexation properties of receptor **67**. It shows high selectivity for small anions such as chloride and fluoride. Despite the fact that receptor **67** does not show strong coordination with the oxo-anions it has been found that benzoate is bound by receptor **67** with a

stability constant of 237 M^{-1} in acetonitrile (0.5% water) solution. Unfortunately precipitation and crystallization processes during the titration experiment on receptor **67** with $PtCl_6^{2-}$ did not allow the association constant to be calculated.

Binding studies of **68** and **69** were conduced in dimethyl sulfoxide-d_6 due to the low solubilities of these receptors. They were found to have a weak interaction with chloride and fluoride anions. Under these same conditions the stability constants for the oxo-anions was much higher. The interaction between receptor **68** and hexachloroplatinate has been also reported. Further investigation revealed that $PtCl_6^{2-}$ interacts strongly with dimethyl sulfoxide, and so this stability constant are not reliable. For this reason receptor **69** was not titrated with hexachloroplatinate. The results of the anion complexation properties are summarized in Table 5.1.

Anion	Receptor 67[(a)]	Receptor 68[(b)]	Receptor 69[(b)]
Fluoride	413	< 10	(c)
Chloride	480	< 10	< 10
Bromide	87	-	-
Dihydrogen phosphate	73	144	37
Benzoate	236	17	17.5
Hexachloroplatinate	ppt	< 10*	-

Table 5.1: Association constant of receptors **67**, **68** and **69** (M^{-1}) with various anionic guest at 25 °C. The errors were estimated to be < 15%. (a) NMR titration were carried out in acetonitrile (0.5% water). (b) NMR experiments carried out in DMSO (0.5% water). (c) No binding observed. *Not reliable – it was subsequently found that $PtCl_6^{2-}$ can react with DMSO.

5.2 Pyridine dicarboxylic acid derivatives

5.2.1 Pyridine dicarboxylic acid derivatives as anion receptors

Substitution of pyridine functionality in the place of the phenyl group of the original isophthalic amide cleft allows an analogous receptor to be synthesised that possesses a more pre-organised binding cleft motif (Figure 5.6). This pre-organization of the pyridine dicarboxy amide has been used by many research groups in order to synthesis more selective receptors.

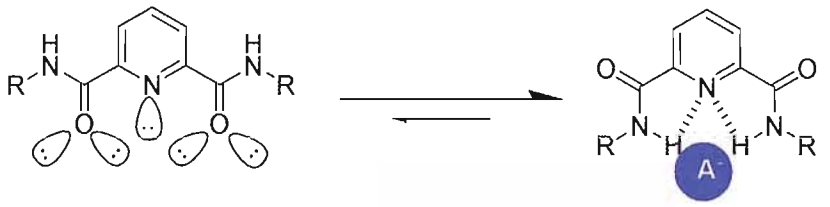

Figure 5.6: Pyridine dicarboxy amide equilibrium.

Bowman-James and co-workers[139] synthesised both amide and thioamide derived clefts that contained a pyridine substituent in place of the phenyl group as previously observed (Figure 5.4). Their findings reported that monocycle **70a** is superior in binding dihydrogen phosphate compared to the isophthalamide based receptor **66a** by a factor of 13 times greater. Receptor **70b**, the thioamide ligand, shows higher affinities for hydrogen sulphate than its analogous isophthalamide derivative **66b** (Figure 5.7).

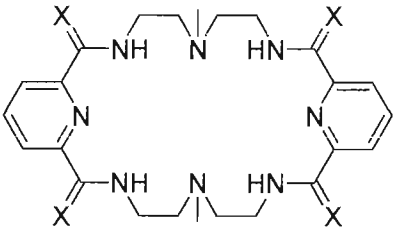

70a X = O
70b X = S

Figure 5.7: Pyridine amide/ amine cleft.

Szumna and Jurczak[141] have linked two pyridine clefts together to form an acetate selective macrocyclic receptor (Figure 5.8). Surprisingly, it was found that the crystal structure of tetrabutylammonium acetate complex with **71** is in a 2:1 receptor:anion ratio in the solid state. However 1:1 receptor:anion complexes were identified as existing in solution with an association constant of 2640 M^{-1} in dimethyl sulfoxide-d_6.

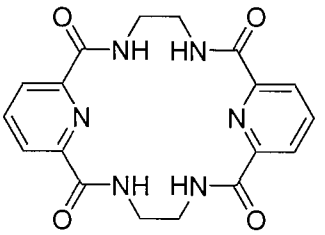

71

Figure 5.8: Dipyridine derivative macrocyclic.

Another interesting receptor is **72**, synthesised by Anslyn[142] and co-workers. They studied its binding properties using planar anions such as carboxylates and nitrates. In this case the interesting feature of the new host is the geometry: the configuration in a trigonal prismatic array which gives the receptor the possibility of coordinating to the π-electron system of the anions. In further studies on receptor **72** reveals that acetate is bound within the cavity of the box with a stability constant 770 M^{-1} in acetonitrile-d_3: dichloromethane-d_2 3:1 (v/v).

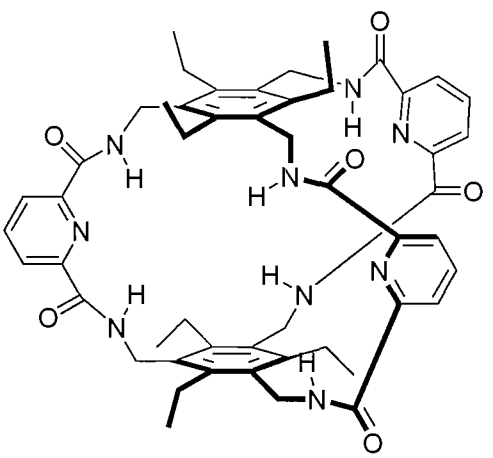

72

Figure 5.9: Bicyclic cyclophane.

5.2.2 Synthesis and characterization

As previously discussed, pyridine dicarboxy amides have been employed to produce a wide range of receptors capable of coordinating different anions. Our receptors were synthesized with the possibility that later on they could be fixed to a solid support through the nitrogen of the pyridine. This explains why pyridine 3,5-dicarboxylic acid is used in place of pyridine 2,6-dicarboxylic acid.

Two novel receptors **74** and **75**, based on the pyridine dicarboxylic acid derivatives have been synthesised according to Scheme 5.2. Pyridine-3,5-dicarboyl dichloride **73** was prepared by refluxing with an excess of thionyl chloride overnight. Upon reaction of **73** with an excess of 1,3-phenyldiamine (ca. 10 equiv.) in the presence of triethylamine and DMAP, compound **74** was obtained in 55% yield.

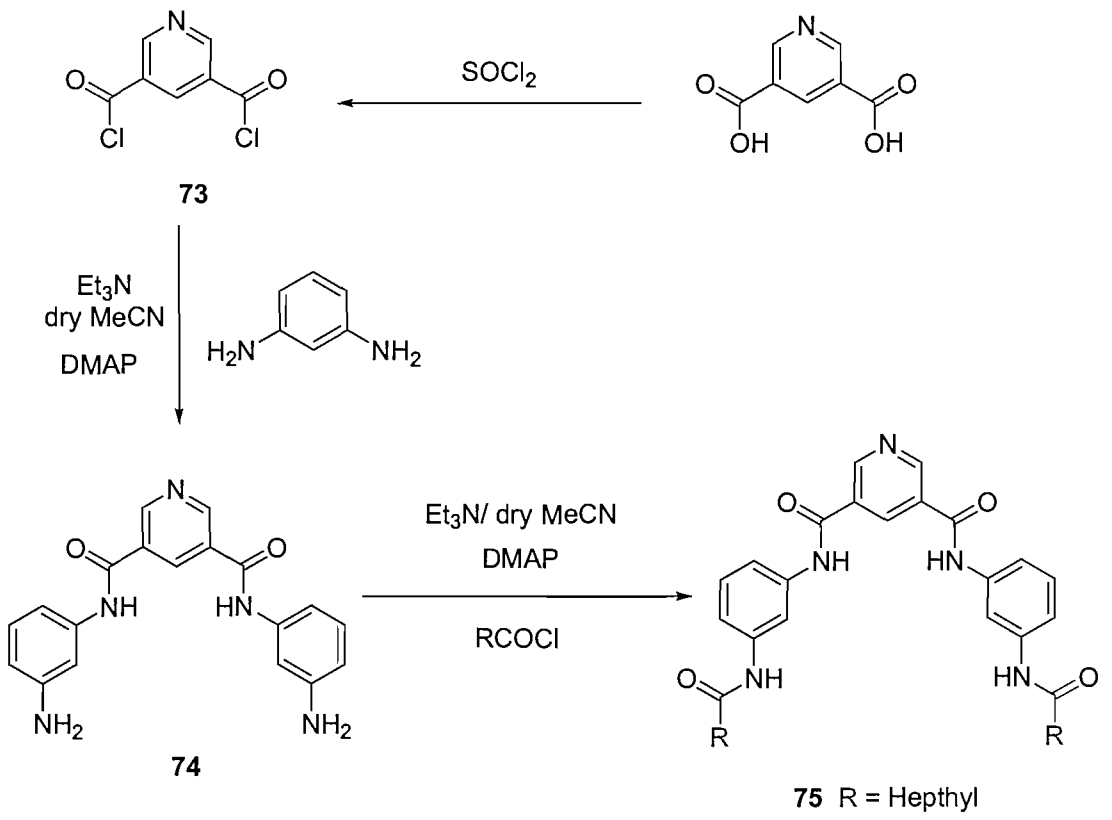

73 **74** **75** R = Heptyl

Scheme 5.2

Compound **75** was prepared by refluxing an acetonitrile solution of **74** with 3 equivalents of octanoyl chloride in the presence of triethylamine and a catalytic amount of DMAP, and was isolated in 21% yield.

5.2.3 Coordination studies

^{1}H NMR titration experiments in DMSO-d_6 (0.5% water) have been performed in order to investigate the anion coordination properties of receptors **74** and **75**. Anions were added as their tetrabutylammonium salts, as this cation does not compete with anion binding site. Association constants have being elucidated using EQNMR software[140].

5.2.3.1 Binding studies results

Binding studies of **74** and **75** were conduced in dimethyl sulfoxide-d_6 (0.5% water) due to the low solubilities of these receptors. Receptors **74** and **75** were found to have a weak interaction with chloride and fluoride under these conditions. Receptor **75** was found to demonstrate a slightly higher stability constant with benzoate (Table 5.2).

Anion	Receptor 74[(a)]	Receptor 75[(a)]
Fluoride	(c)	< 10
Chloride	< 10	< 10
Dihydrogen phosphate	< 10	-
Benzoate	< 10	33
Hydrogen sulphate	(c)	(c)
Hexachloroplatinate	-	< 10*

Table 5.2: Association constant of receptors **74** and **75** (M^{-1}) with various anionic guest at 25 °C. The errors were estimated to be < 15%. (a) NMR experiments carried out in DMSO (0.5% water). (c) No binding observed. *Not reliable – it was subsequently found that $PtCl_6^{2-}$ can react with DMSO.

The interaction between **75** and dihydrogen phosphate requires special attention. The studies were conduced once again in dimethyl sulfoxide-d_6 (0.5% water). The results are depicted in table 5.3. The titration curves were obtained for both 1:1 and 2:1 binding models, however a satisfactory fit could not be obtained. It is possible that the anion is protonating the receptor, causing multiple equilibria in solution.

Guest:Host	K_1	*Error*	K_2	*Error*
2:1	93	*36*	426	*2.6*
2:1	707	*59*	173	*30*
1:1	36	*26*	-	-

Table 5.3: Association constants of receptor **75** (M^{-1}) with hydrogen phosphate at 25 °C.

5.3 *3,4*-Diphenyl pyrrole amide clefts

5.3.1 Pyrrole as anion receptor

The anion coordination ability of receptors containing pyrrole groups has been an area of increasing interest. Gale[143-147] et al. have been investigating the anion complexation properties of different receptors based on the pyrrole motif for the last few years. They report the introduction of electron withdrawing chlorine substituents to the 3- and 4- positions of the pyrrole ring, enhanced the affinity of receptor **76b** for anions such as chloride[132].

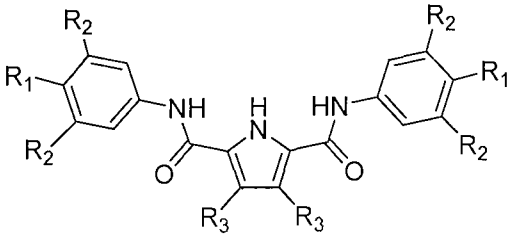

76a $R_1 = R_2 = H$. $R_3 = Ph$
76b $R_1 = R_2 = H$. $R_3 = Cl$
77 $R_1 = NO_2$. $R_2 = H$. $R_3 = Ph$
78 $R_1 = H$. $R_2 = NO_2$. $R_3 = Ph$

Figure 5.10: General extructure of amidopyrrole cleft.

They decided to introduce electron withdrawing groups on to the amide positions in an attempt to enhance the affinity of the receptor without increasing the acidity of the pyrrole proton, in receptors **77** and **78**. Enhanced anion affinity was found just for the benzoate increasing from 560 M^{-1} for receptor **76a** to 4150 M^{-1} for receptor **77** and 4200 M^{-1} for receptor **78**. In previous experiments on **76b** it had been found that dihydrogen phosphate and benzoate were deprotonated by the receptor[132], however in the case of receptor **78** just the addition of fluoride shows the deprotonation process.

In a more recent investigation Gale[144] and co-workers found that pendant arm pyrrolic amido cleft receptors **79**, **80** and **81** have high affinities for oxoanions such as dihydrogen phosphate: 2050 M^{-1} with receptor **79**, and extremely strongly with hydrogen sulphate 10000 M^{-1} in DMSO-d_6 (0.5% water). However, the association constants with **80** and **81** were lower for dihydrogen phosphate and hydrogen sulphate respectively.

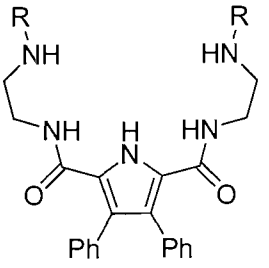

79 R = H
80 R = H_2^+/ $2PF_6^-$
81 R = $COCH_3$

Figure 5.11: 3,4-Diphenyl amido derivatives.

In following work, Gale[148] and co-workers decided to combine 2-amido- and 2,5-diamidopyrrole anion binding sites with crown ether moieties and explore the coordination properties of these new receptors.

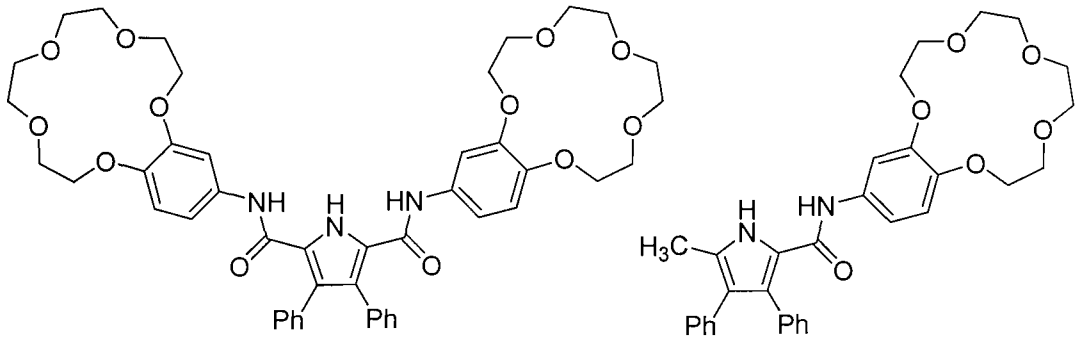

82 **83**

Figure 5.12: Crown ether appended amidopyrrole clets.

The results reported that metal cations can sequester anions from "ion-pair receptors". Also in one case an increase of the fluoride affinity for receptor **82** was observed upon addition of caesium cations.

5.3.2 Synthesis and characterization

As previously discussed, amidopyrrole clefts have been employed to produce a wide range of selective receptors capable of coordinating different anions. In previous work on analogous compound **81** showed interesting complexation properties with hexachloroplatinate and as a result of this one novel pyrrole amide-crown ether has been synthesised **86** to see if the coordination properties could be improved.

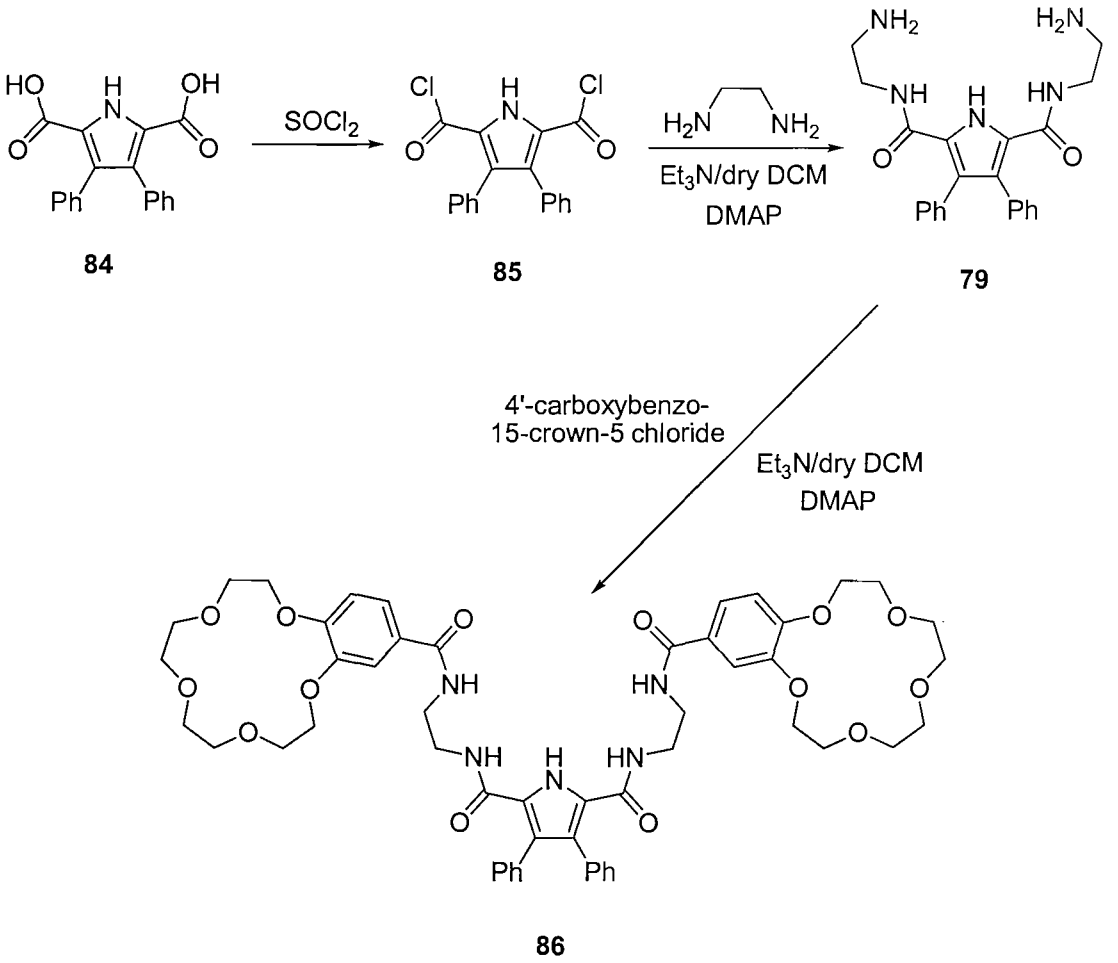

84 **85** **79**

86

Scheme 5.3

The pyrrole diamide crown-ether has been prepared according to Scheme 5.3. Dicarboxy-3,4-diphenyl pyrrole **84** was prepared following literature procedures[149] and was refluxed with an excess of thionyl chloride overnight in order to obtain the bis-acid chloride **85**. Upon reaction of **85** with ethylenediamine in dichloromethane in presence of a catalytic amount of DMAP and compound **79** was obtained[144]. Receptor **86**, was synthesised by reaction of compound **79** with 2 equivalents of 4'-carboxybenzo-15-crown-5 chloride in dry dichloromethane in the presence of triethylamine and a catalytic amount of DMAP and was isolated in 64% yield. Previously the 4'-carboxybenzo-15-crown-5 had been converted into 4'-carboxybenzo-15-crown-5 chloride by refluxing with thionyl chloride.

5.3.3 Coordination studies

The coordination ability of receptor **86** has been studied in the absence and presence of stoichiometric quantities of sodium, potassium and caesium cations and determined by ^{1}H NMR titration techniques. Anions were added as their tetrabutylammonium salts.

5.3.3.1 Binding studies results

The complexation properties between compounds **79** and **86** with TBA hexachloroplatinate were studied initially. Binding studies were conducted in dimethyl sulfoxide-d_6 (0.5% water) and acetonitrile-d_3 due to the precipitation and crystallization processes during the titration experiments.

In previous work on compound **79** a large shift was observed between 6.00 to 8.00 ppm for one amide proton and 6.35 to 9.15 ppm for the second one. However, when the complexation properties were studied it was found that the stability constant could not be calculated (correctly) due to the amide peaks being obscured by benzylic protons (Table 5.4).

Solvent (0.5% water)	Receptor 79*
DMSO-d_6	(a)
MeCN-d_3	ppt
MeCN-d_3/DMSO-d_6 (9/1)	13[(b),(c)]

Table 5.4: Associaation constant of receptor **79** (M^{-1}) with TBA hexachloroplatinate (IV) as guest at 25 °C. The errors were estimated to be < 15%. (a) No binding was observed. (b) Only 7 points have been used to calculate the stability constant. (c) Error 21%. *Not reliable – it was subsequently found that $PtCl_6^{2-}$ can react with DMSO.

Several cations such as potassium, sodium and caesium were used to study the complexation properties of receptor **86**. Interestingly the presence of the cation did not enhance the anion coordination strength at all. Instead a decrease of the association constant values was observed (Table 5.5). Only hexachloroplatinate (IV) was bound to receptor more strongly in the presence of potassium in acetonitrile-d_3 dimethyl sulfoxide-d_6 (9:1) solution.

Cation	Solvent (0.5% water)	Receptor 86*
-	MeCN-d_3/DMSO-d_6 (9/1)	39
2 eq. of K^{+} [(a)]	MeCN-d_3/DMSO-d_6 (9/1)	52
2 eq. of Cs^{+} [(b)]	DMSO-d_6	31
2 eq. of Cs^{+} [(b)]	MeCN-d_3/DMSO-d_6 (9/1)	ppt
2 eq. of Cs^{+} [(b)]	MeCN-d_3/DMSO-d_6 (1/1)	ppt
2 eq. of Na^{+} [(b)]	DMSO-d_6	36.5
2 eq. of Na^{+} [(b)]	MeCN-d_3/DMSO-d_6 (9/1)	ppt
2 eq. of Na^{+} [(b)]	MeCN-d_3/DMSO-d_6 (1/1)	29.4

Table 5.5: Association constant of receptor **86** (M^{-1}) with hexachloroplatinate (IV) as guest at 25 °C. The errors were estimated to be < 15%. (a) Cation added as hexafluorophosphate salt. (b) Cation added as tetraphenylborate salt. *Not reliable – it was subsequently found that $PtCl_6^{2-}$ can react with DMSO.

NMR titration experiments have been carried out on receptor **86** in order to see an increase of the stability constant values compared to its analogous receptors **79**, **80**

and **81**. The coordination studies have been performed in dichloromethane-d_2 solution (Table 5.6). Surprisingly crown free receptor **86** showed high selectivity for bromide.

Anion	Receptor 35
Fluoride	(a)
Chloride	787[b]
Bromide	1249
Dihydrogen phosphate	(a)
Hydrogen sulphate	495

Table 5.6: Association constant of receptor **86** (M^{-1}) with various anionic guest at 25 °C. The errors were estimated to be < 15%. (a) The fit could not be obtained. (b) Error 17 %.

5.4 Dimethyl sulphoxide effect in the complexation properties with $PtCl_6^{2-}$

As previously reported, it is possible that the TBA hexachloroplatinate (IV) is interacting strongly with the solvent (dimethyl sulphoxide), causing the formation of complexes between $PtCl_6^{2-}$ and DMSO, Figure 5.13 and 5.14. X-ray quality single crystals of $PtCl_6^{2-}$ and DMSO were obtanied by slow evaporation of an acetonitrile:dimethyl sulphoxide (9:1 v/v) solution.

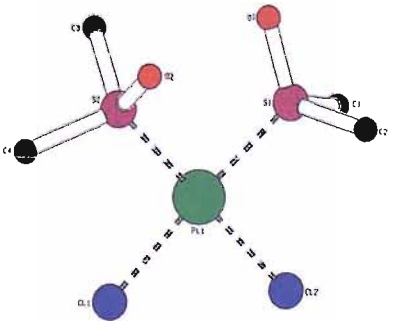

Figure 5.13: The X-ray crystal structure of $PtCl_2$-2DMSO.

Due to these interactions between $PtCl_6^{2-}$ and the solvent, the coordination studies that have been performed in dimethyl sulphoxide solution are not reliable. The low association constants could be due to the formation of complexes between $PtCl_6^{2-}$ and DMSO which interfere with our studies.

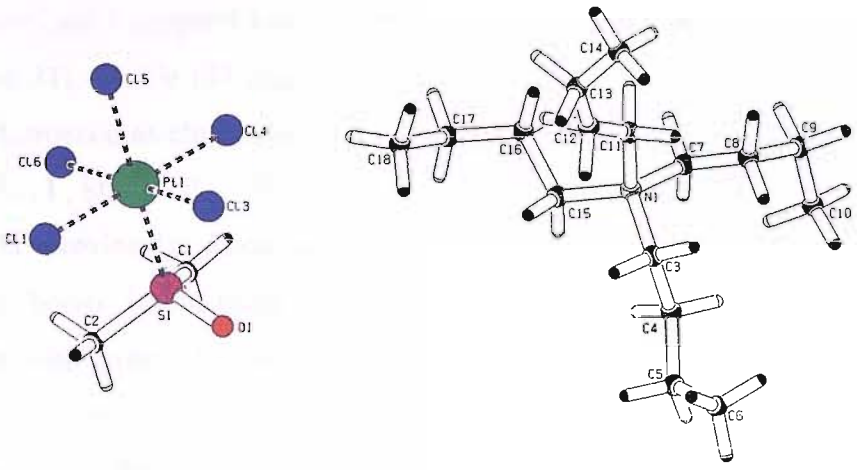

Figure 5.13: The X-ray crystal structure of TBA $PtCl_5$-DMSO.

5.5 Conclusions

Anion complexation studies have been carried out on isophthalamides (e.g. **67-68-69**), amidopyridines (e.g. **74-75**) and amidopyrroles (e.g. **79-86**), in order to investigate whether these compounds could behave as efficient receptors of hexachloroplatinate (IV) anions. However solubility problems have affected our results. Moreover, we showed that DMSO can complete with the guest substrate by occupying the binding sites.

Overall summary

This thesis concerns the synthesis of new solid supports for anion separation. X-ray crystallographic studies of hexachloroplatinate(VI) show that hydrogen bond donor groups such as guanidinium and amidinium complex this anion in the solid state. Novel solid supports bearing the guanidinium group, with either a single (**23**, **27-29** and **31**), double (**37** and **43**) or triple arm (**50**) motif have been prepared and their performance as chromatographic media has been evaluated with simple anions such as Br^-, I^-, SCN^-, NO_3^-, $H_2PO_4^-$, $S_2O_3^{2-}$, SO_4^{2-}, HPO_4^{2-}, AMP^{2-}, ADP^{2-}, ATP^{2-}, and PO_4^{3-}. As previously discussed solid supports capable of producing multiple hydrogen bonds interactions with the anions displayed longer retention times compared with those solid supports which can not produce them, or can only produce fewer interactions. This suggests that hydrogen bond interactions play an important role in the ion exchange mechanism.

Also several solid supports bearing thiourea moieties (**51** and **52**) one bearing mono isothiouronium (**53**) and two bifunctional isothiouronium resins (**57** and **60**) have been synthesised. Their performance as chromatographic media has been evaluated with simple anions such as Br^-, I^-, SCN^-, NO_3^-, $H_2PO_4^-$, $S_2O_3^{2-}$, SO_4^{2-}, HPO_4^{2-}, AMP^{2-}, ADP^{2-}, ATP^{2-}, and PO_4^{3-}. The thiourea motif showed different behaviour when compared to guanidinium based resins. All the retention times of all the anions were decreased when thiourea was employed as an anion exchanger.

It has been identified that hydrophobic effects can play an important role. This is shown with thiourea silica gel **51**, which can only utilise hydrogen bond interactions, and so the anions were continuously eluted. However, methacrylate thiourea support **52** showed no anion exchange.

Solid supports bearing thiourea moieties (**51** and **52**) bearing mono isothiouronium (**53**) and two bifunctional isothiouronium resins (**57** and **60**) have been synthesised and their performance as chromatographic media has been evaluated by injecting a reduced platinum group metal (PGM) feed. Chromatographic separation of PGM feed on the resins containing thiourea showed no retention for any PGMs.

During the chromatographic separation of the PGMs on the resins supporting the thiourea motif, in general non retention of PGMs was found. Like the gel-type guanidinium polystyrene **23** investigated previously, the mono isothiouronium gel-type resin did not exhibit any ion exchange properties with the PGMs in hydrochloric solution media. This may have been caused by the hydrophobic interactions between the resin matrix. The bifunctional isothiouronium resins both showed strong co-ordination with the Pd. The exception was Pd which was very strongly co-ordinated to the resin through the sulfur atom.

Novel solid supports bearing the guanidinium group, with either a single (**23**, **27-29** and **31**), double (**37** and **43**) or triple arm (**50**) motif have been prepared and their performance as chromatographic media has been evaluated by injecting a reduced PGM feed. Single guanidinium arm functionalised silica gel strongly retained ruthenium on the column in 6M HCl. Methacrylate guanidinium single arm resin showed separation of Pt from the rest of the PGMs. The triple arm guanidinium support was capable of separating Pd from the rest of the PGMs. New elution orders for the PGMs were also found when triple arm guanidinium support was used.

Finally, anion complexation studies have been carried out on isophthalamides (**67-68-69**), amidopyridines (**74-75**) and 3,4-diphenylamidopyrrole clefts (**79-86**), in order to investigate whether these compounds could behave as efficient receptors of MCl_6^{2-} anions. However solubility problems have affected our results. Moreover, we showed that DMSO can complete with the guest substrate by occupying the binding sites.

Chapter 6

Experimental

6.1 Solvent and reagent pre-treatment

Where necessary the solvents were purified prior to use. Dichloromethane was distilled over calcium hydride. Diethyl-ether was distilled from sodium using benzophenone as an indicator. Acetonitrile was distilled over calcium hydride. Anhydrous methanol was purchased from Aldrich (99.8%). Thionyl chloride was distilled from 10% (w/w) triphenyl phosphate and stored under nitrogen. The thin layer chromatography (TLC) was perfomed on PET-backed plates Fluka silica gel 60. Fluka silica gel 60, 220-440 mesh, was used for column chromatography. Commercial grade reagents have been used without further purification. Reagents prepared in accordance with literature are so referenced. All the syntheses have been performed under an inert atmosphere of nitrogen. Tetrabutylammonium salts of the anions used during ^{1}H NMR titrations have been thoroughly dried overnight under high vacuum.

6.2 Instrumental methods

NMR data were recorded on Bruker AM300, AC300, AV300 and DPX400 spectrometers. The spectra were referenced internally using the residual protio-solvent (^1H) or the signal of the solvent (^{13}C) and chemical shifts reported in ppm. Low resolution mass spectra were recorded on a Micromass Platform single quadrupole mass spectrometer, whereas high resolution mass spectra were recorded on a VG 70-250-SE normal geometry double focusing mass spectrometer by the mass spectrometry service at the University of Southampton. Elemental analyses were carried out at the University of Strathclyde and by Medac Ltd. Melting points were recorded in open capillaries on a Gallenkamp melting point apparatus and are uncorrected. Infrared spectroscopy (FTIR) was carried out using a MKII Golden Gate single reflexion ATR system from Specac and Satallite FTIR™ from Thermo Mattson. A VISTA-PRO simultaneous ICP-OES (Varian) was used in the analysis of the eluent in all the chromatographic separations of the PGMs carried out. Ion chromatographs were obtained via an ion chromatographic system consisting of a refractive index detector, Spectra System RI 150 by Thermo Separation Products and using Gilson Miniplus 3 pump.

6.3 Synthesis

6.3.1 Synthesis included in chapter 2

6.3.1.1 Preparation of bis(acylguanidinium) tetrafluoroborate 17

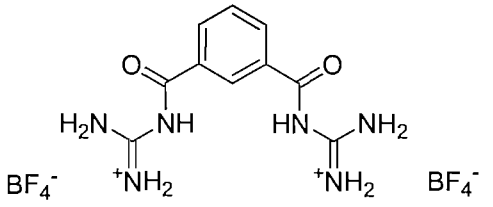

Bis(acylguanidinium)[87] dihydrochloric acid **16** (100 mg, 0.31 mmol) was dissolved in hot MeOH then $AgBF_4$ (121 mg, 0.62 mmol) was added. A white precipitate was formed, the solvent was decanted off, and the organic layer was removed under reduced pressure. A white solid was produced. (130 mg, 98%). δ_H

(300 MHz; DMSO-d_6; Me_4Si): 7.85 (t, 1H, J= 8.2 Hz, ArH), 8.30-8.39 (br. s, 8H, guanidinium NH_2 and 2H, ArH), 8.56 (s, 1H, ArH), 11.69 (s, 2H, CONH). δ_C (75 MHz; DMSO-d_6; Me_4Si): 128.7, 130.1, 133.0, 133.4, 155.8, 167.3. MS ES^-: m/z, 423.2 (M-H), 459.2 (M+Cl). m.p (decomp.): 248-254 °C.

6.3.1.2 *Preparation of tri(acylguanidinium) hydrochloric acid* ***19***

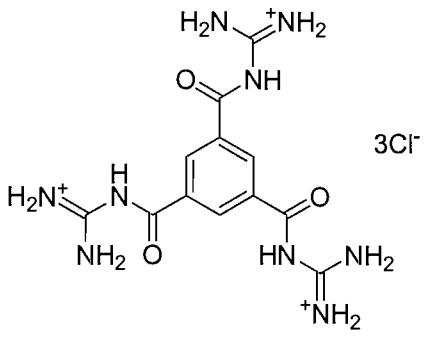

Benzene-1,3,5-tricarboxylic acid trimethyl ester **18** (7 g, 28 mmol) previously synthesised by reacting benzenetricarboxylic acid with HCl conc. in MeOH. Was reacted with guanidinium hydrochloride (16 g, 166 mmol) were added in a previously prepared sodium methoxide (5 g, 194 mmol) solution. The reaction mixture was refluxed 24 h under N_2 atmosphere. After cooling the crude was filtered off. The filtrate was removed in *vacuo* and the resulting solution was added H_2O (100 mL) and then acidified with conc. HCl. The white precipitate was filtered and washed with MeOH. Yield (2g, 16%). δ_H (300 MHz; DMSO-d_6; Me_4Si): 8.95 (s, 3H, ArH), 8.56-8.74 (br. s, 12H, guanidinium NH_2), 12.29 (s, 3H, CONH). δ_C (75 MHz; DMSO-d_6; Me_4Si): 132.6, 132.8, 155.1, 165.6. MS ES^-: m/z, 440.2 ($M\text{-}H^+$). Elemental analysis **19** Calcd: C, 32.56; H, 4.18; N, 28.46. Obs. C, 32.42; H, 4.33; N, 27.60. m.p (decomp.) $\geq$ 320°C.

6.3.1.3 *Preparation of guanidinium-methylated polystyrene resin 23*

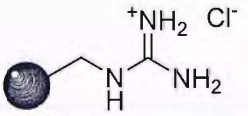

1H-Pyrazole-1-carboxamidine hydrochloride[98] **22** (2 g, 13 mmol) and DIEA (1 mL) were dissolved in DMF (20 mL), and then added to the aminomethylated polystyrene resin (2.5 g, 2.8 mmol) previously pre-swollen in DMF (10 mL) for 40 min and subsequently drained. The reaction mixture was then shaken/spin 24 h. The resin was filtered off, and washed with DMF (3x10 mL), DCM (3x10 mL), MeOH (3x10 mL), Et_2O (3x10 mL). The resin was then dried under high vacuum overnight affording a colourless resin. Results for **23** are presented in Table 6.1.

Resin code	Conversion (%)	Yield isolated g ; %
23	72	2.5 ; 92

Table 6.1: Results for resin **23**.

Microanalysis; Resin **23** Calcd: C, 83.87; H, 7.62; N, 4,53. Obs. C, 83.45; H, 7.54; N, 4.53. FTIR cm^{-1} 3328 (NH_2 guanidine), 2921 (-CH_2-), 1662 (C=N).

6.3.1.4 *Preparation of guanidinium-methylated polystyrene high loading resin 27*

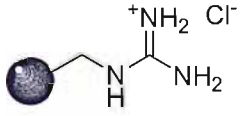

high loading

To the aminomethylated polystyrene **26** (4.5 g, 18 mmol) was added the 1H-pyrazole-1-carboxamidine hydrochloride[98] **22** (10.3 g, 71 mmol) and DIEA (3 mL) previously dissolved in DMF (80 mL). The resulting mixture was then refluxed for

48 h. The resin was filtered off, washed with DMF (3x50 mL), DCM (3x50 mL), MeOH (3x50 mL), Et_2O (3x50 mL) and dried under high vacuum overnight. Results for **27** are presented in Table 6.2.

Resin code	Conversion (%)	Yield isolated g ; %
27	63	5.10 ; 96

Table 6.2: Results for resin **27**.

Microanalysis; Resin **27** Calcd: C, 73.25; H, 7.57; N, 10.42. Obs. C, 72.19; H, 7.28; N, 10.42. FTIR cm^{-1} 3329 (NH_2 guanidine), 2925 (-CH_2-), 1646 (C=N, guanidine), 1451 (phenyl).

*6.3.1.5 Preparation of guanidinium supported silica **28***

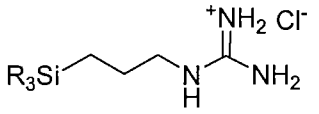

R: C_2H_5O

1H-Pyrazole-1-carboxamidine hydrochloride[98] **22** (1.2 g, 8 mmol) and DIEA (1 mL) were dissolved in DMF (50 mL), followed by the addition of 2-aminopropyl silica gel (2 g, 2 mmol). The resulting mixture was then refluxed overnight under an N_2 atmosphere. The resin was filtered off, washed with DMF (3x10 mL), DCM (3x10 mL), MeOH (3x10 mL), Et_2O (3x10 mL). The resin was dried under high vacuum overnight yielded a colourless resin. Results for **28** are presented in table 6.3.

Resin code	Conversion (%)	Yield isolated g ; %
28	86	2.0 ; 93

Table 6.3: Results for resin **28**.

Microanalysis; Silica **28** Calcd: C, 6.19; H, 1.94; N, 4.01. Obs. C, 6.77; H, 1.63; N, 4.02. FTIR cm^{-1} 3324 (NH_2 guanidine), 1659 (C=N, guanidine), 1040 (silica).

*6.3.1.6 Preparation of guanidine supported Macro prep **29***

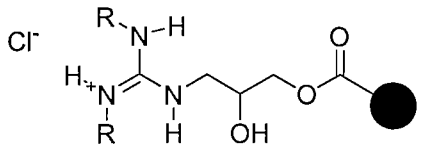

Macroprep Epoxide is supplied by Bio-rad Laboratories with a particle size of 50μm (1.5 g, 6 mmol) was added to a solution of guanidinium hydrochloride (1 g, 10 mmol) previously deprotonated using sodium ethoxide (0.2 g, 9 mmol). The reaction mixture was refluxed overnight under an N_2 atmosphere. After cooling the reaction mixture was filtered off, then the resin was washed with HCl/H_2O followed with EtOH. The resin was dried under high vacuum overnight. Results for **29** are presented in Table 6.4.

Resin code	Conversion (%)	Yield isolated g ; %
29	35	1.8 ; 87

Table 6.4: Results for resin **29**.

Microanalysis; Compound **29** Calcd: C, 52.72; H, 7.19; N, 5.21. Obs. C, 51.29; H, 7.41; N, 5.21. FTIR cm^{-1} 3352 (NH guanidine), 2949 ($-CH_2-$), 1716 (C=O, carbonyl), 1643 (C=N, guanidine).

*6.3.1.7 Preparation of 2-aminoethyl methacrylate polymer **30***

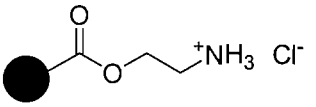

A continuous phase was prepared by mixing 1mL of sorbitan monooleate (Span®80) in liquid paraffin (40 mL) and cyclohexane (20 mL). The continuous

phases were degassed inside sealed cylindrical reaction vessels equipped with mechanical stirring bars connected to a central stirring motor. The vessels were purged with N_2 through the solutions. The monomer phases were kept under N_2 before addition to the continuous phases at 35 °C. Droplets were formed by stirring the two phases at 300 rpm for 30 min, then the temperature was increased to 75°C, with continuous stirring for 16 h. The resins were then filtered, washed with cyclohexane (3x50 mL), MeOH (3x50 mL), and extracted in a soxhlet with MeOH for 24 h. Finally the resins were washed with Et_2O (3x50 mL) and dried under high vacuum overnight. The monomer phase compositional data, inverse suspension polymerisation conditions for **30f** and **30g** are presented in Tables 6.5 and 6.6.

Resin code	Mass (g) AEM	Mass (g) PEGDM	Mass (g) V-50	Mass (g) H_2O
30f	5.05	4.18	0.050	7
30g	3.78	8.36	0.037	7

Table 6.5: Monomer phase composition data for **30f** and **30g**.

Resin code	Stirrer speed (rmp)	Yield isolated (%)	Loading* (mmolN/g rs)
30f	300	80	3.15
30g	300	89	1.46

*Calculations based on the microanalytical data.

Table 6.6: Conditions used in the ISP of **30f** and **30g**.

Microanalysis; Resin **30f** Calcd: C, 46.15; H, 7.52; N, 6.76. Obs. C, 49.03; H, 8.15; N, 4.40. FTIR cm^{-1} 3392 (NH_2), 2922 ($-CH_2-$), 1722 (C=O, carbonyl).

Microanalysis; Resin **30g** Calcd: C, 48.79; H, 7.74; N, 5.07. Obs. C, 56.20; H, 8.97; N, 2.05. FTIR cm^{-1} 3421 (NH_2), 2922 ($-CH_2-$), 1723 (C=O, carbonyl).

6.3.1.8 *Preparation of guanidinium support methacrylate polymers 31 and 32*

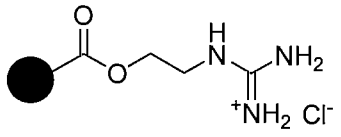

DMF was added to the resin, allowing it to swell for 15 min, then it was removed. 1H-Pyrazole-1-carboxamidine hydrochloride[98] **22** and DIEA, previously dissolved in DMF were then added to the resin. The resulting reaction mixture was spin-shaken for 48 h. The resin was filtered off, and washed with DMF (3x20 mL), DCM (3x20 mL), MeOH (3x20 mL) and Et_2O (3x20 mL). The resin was dried under high vacuum overnight. The conditions of reaction and results for **31** and **32** are presented in Tables 6.7 and 6.8 respectively.

Resin code	Mass (g) resin	Mmol of resin	Mass (g) reagent 43	Mmol of reagent 43	Vol (mL) DMF	Vol (mL) DIEA
31	11	34.7	12.7	87	110	10
32	2	2.97	1.1	7.3	15	2

Table 6.7: Conditions of reaction data for **31** and **32**.

Resin code	Conversion (%)	Yield isolated g ; %
31	63	9.48 ; 75
32	98	1.8 ; 80

Table 6.8: Results for resins **31** and **32**.

Microanalysis; Resin **31** Calcd: C, 45.91; H, 7.84; N, 8.07. Obs. C, 46.04; H, 7.53; N, 8.06. FTIR cm^{-1} 3342 (NH_2 guanidine), 2950 ($-CH_2-$), 1724 (C=O, carbonyl), 1652 (C=N, guanidine), 1145 (N-C, secondary amine).

Microanalysis; Resin **32** Calcd: C, 51.19; H, 8.49; N, 6.10. Obs. C, 49.90; H, 7.80; N, 6.10. FTIR cm^{-1} 3318-3129 (NH_2 guanidine), 2870 (-CH_2-), 1723 (C=O, carbonyl), 1650 (C=N, guanidine), 1108 (N-C, secondary amine).

*6.3.1.9 Preparation of polymer **36** using VBDA monomer*

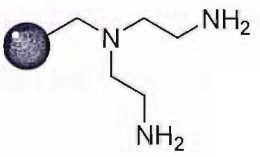

Premixed organic phases (Table 6.9) were added to the aqueous phases (1g of PVA ((poly(vinyl alcohol), 87-89% hydrolyzed), 2g of Na_2HPO_4, 200 mL of H_2O) while stirring in 500 mL cylindrical reaction vessels equipped with mechanical stirring bars connected to a central stirring motor and having been purged with N_2. The suspensions were allowed to equilibrate for 30 min, the temperature was then raised to 65°C for 16h. The crude polymers were collected and washed with DMF (3x100 mL), DCM (3x100 mL), MeOH (3x100 mL), Et_2O (300 mL). The resins were dried in *vacuo* and bright yellow resins were obtained.

Resin code	VBDA mmol ; g	% VBDA	DVB mmol ; g	% DVB	Toluene[(a)] (mL)
36a	32 ; 7	90	3.5 ; 0.5	10	31
36b	32 ; 7	80	7.9 ; 1	20	31
36c	25 ; 5.4	70	10.6 ; 1.4	30	31

Table 6.9: Stoichiometry of the premixed organic phase. (a) Initiator AIBN (1.0% w/w) was added to the organic phase. Speed stirrer 300 rpm.

Resin code	Yield isolated g g ; %	Loading* (mmolN/g rs)
36a	0.7 ; 9	8.17
36b	4.24 ; 53	6.76
36c	1.1 ; 16	4.38

*Calculations based on the microanalytical data.

Table 6.10: Results for resins **36a**, **36b** and **36c**.

Microanalysis; Resin **36a** Calcd: C, 73.29; H, 9.45; N, 17.24. Obs. C, 69.65; H, 8.22; N, 11.45. FTIR cm^{-1} 3355 (NH_2, broad), 2921-2852 ($-CH_2-$).

Microanalysis; Resin **36b** Calcd: C, 75.40; H, 9.26; N, 15.32. Obs. C, 70.05; H, 7.86; N, 9.48. FTIR cm^{-1} 3285 (NH_2, broad), 2924 ($-CH_2-$).

Microanalysis; Resin **36c** Calcd: C, 77.51; H, 9.07; N, 13.41. Obs. C, 79.39; H, 8.00; N, 6.14. FTIR cm^{-1} 3460 (NH_2), 3015-2946 ($-CH_2-$).

6.3.1.10 Preparation of double arm guanidinium polymer 37

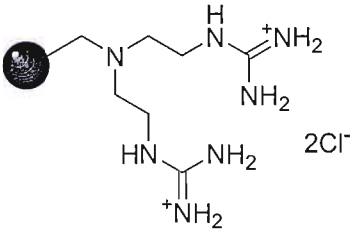

20% DVB

DMF was added to the resin **36b** (3 g, 20.3 mmol). It was allowed to swell for 15 min, then drained. 1H-Pyrazole-1-carboxamidine hydrochloride[98] **22** (6 g, 40.6 mmol) and DIEA (2 mL) previously dissolved in DMF (200 mL) were then added to the resin. The resulting mixture was refluxed and stirred with an overhead mechanical stirrer for 48 h at 100°C. The resin was filtered off, washed with DMF (3x50 mL), DCM (3x50 mL), MeOH (3x50 mL), Et_2O (3x50 mL). The resin was dried under high vacuum overnight. The results for **37** are presented in Table 6.11.

Resin code	Conversion (%)	Yield isolated g ; %
37	43	3.40 ; 73

Table 6.11: Results for resin **37**.

Microanalysis; Resin **37** Calcd: C, 59.72; H, 7.33; N, 14.31. Obs. C, 60.92; H, 7.18; N, 14.30. FTIR cm^{-1} 3226 (NH_2 guanidine, broad), 2927 (-CH_2-), 1649 (C=N, guanidine).

*6.3.1.11 Preparation of polymers **38** and **39** by SP technique*

38 70% VBC
39 80% VBC

Premixed organic phases (Table 6.12) were added to the aqueous phases (1g of PVA ((poly(vinyl alcochol), 87-89% hydrolyzed), 2g of Na_2HPO_4, 200 mL of H_2O) while stirring the mixture in 500 mL cylindrical reaction vessels equipped with mechanical stirring bars connected to a central stirring motor and having been purged with N_2. The suspensions were allowed to equilibrate for 30 min, the temperature was then raised to 65°C for 16 h. The crude polymers were collected and washed with H_2O (300 mL), H_2O/THF (1:1) (300 mL), THF (150 mL), THF/MeOH (1:1) (300 mL) and MeOH (100 mL). The beads were dried in *vacuo* and white beads were obtained.

Resin code	DVB[(a)] mmol ; g	% Styrene	Styrene mmol ; g	% VBC	VBC mmol ; g	Toluene[(b)] (mL)
38	3.5 ; 0.45	25	17.5 ; 1.8	70	49 ; 7.47	10
39	3.5 ; 0.45	15	10.5 ; 1.1	80	56 ; 8.54	10

Table 6.12: Stoichiometry of the premixed organic phase. (a) 5% cross-linking. (b) Initiator AIBN (1.0% w/w) was added to the organic phase.

Resin code	Yield isolated g ; %
38	7.77 ; 77
39	7.55 ; 78

Table 6.13: Results for resins **38** and **39**.

Microanalysis; Resin **38** Calcd: C, 77.25; H, 6.48; Cl, 16.26. Obs. C, 75.38; H, 6.45; Cl, 16.31. FTIR cm^{-1} 2919 ($-CH_2-$), 1446 (CH=CH, phenyl), 701 (C-Cl).

Microanalysis; Resin **39** Calcd: C, 75.11; H, 6.30; Cl, 18.58. Obs. C, 73.90; H, 6.29; Cl, 17.50. FTIR cm^{-1} 2919 ($-CH_2-$), 1446 (CH=CH, phenyl), 706 (C-Cl).

6.3.1.12 Preparation of double arm amine resin 42

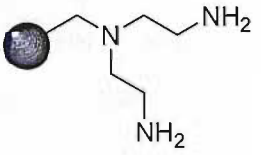

Resin **38** (6.5g, 30.3 mmol) was dissolved in N-methyl pyrrolidinone (NMP) (250 mL) and to this was added sodium iodide (4.53g, 30.3 mmol), followed by **40**, previously synthesised via the literature procedure[100]. The reaction mixture was heated to 110°C with gentle stirring for 24 h. The resin was rewarded from the solution by filtration and then was cross washed with MeOH (3x100 mL), H_2O (3x100 mL), NMP (10% in DCM, 3x100 mL), DCM (3x100 mL) and Et_2O (100 mL). The resin was dried in *vacuo*, yielding the yellow-orange resin **41**. Without further purification resin **41** (13.5 g, 125 mmol) was suspended in EtOH (300 mL). After allowing the resin to swell, hydrazine monohydrate (20 mL, 410 mmol) was added and the resulting mixture was refluxed for 2 h. The resin was removed from the solution by filtration, and was then cross washed with hot H_2O (400 mL), hot EtOH (150 mL), DMF (150 mL), DMF:H_2O (1:1, 150 mL), H_2O (150 mL), EtOH (150 mL), MeOH (150 mL) and Et_2O (150 mL). The resin was dried under high vacuum overnight, yielding a colourless resin. The results for **42** are presented in Table 6.14.

Resin code	Conversion (%)	Yield isolated g ; %
42	87	8.84 ; 92

Table 6.14: Results for resin **42**.

Microanalysis; Resin **42** Calcd: C, 75.30; H, 8.98; N, 14.05. Obs. C, 72.59; H, 8.32; N, 12.65. FTIR cm^{-1} 3241 (NH_2 amine, broad), 2917 (-CH_2-), 1441-1363 (CH=CH, phenyl).

6.3.1.13 Preparation of double arm guanidinium resin 43

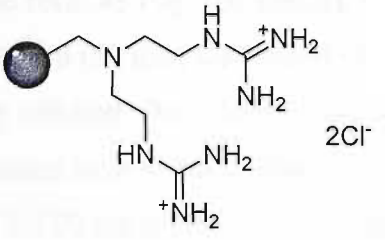

DMF was added to the resin **42** (7.5g, 67.5 mmol) it was allowed to swell for 15 min, then drained. 1H-Pyrazole-1-carboxamidine hydrochloride[98] **22** (26.50g, 180 mmol) and DMAP (catalytic amount) previously dissolved in DMF (200 mL) were then added to the resin. The resulting reaction mixture was refluxed and stirred with an over head mechanical stirrer for 48 h at 100°C. The resin was filtered off, and washed with DMF (3x50 mL), DCM (3x50 mL), MeOH (3x50 mL) and Et_2O (3x50 mL). The resin was dried under high vacuum overnight. The results for **43** are presented in Table 6.15.

Resin code	Conversion (%)	Yield isolated g ; %
43	53	7.99 ; 63

Table 6.15: Results for resin **43**.

Microanalysis; Resin **43** Calcd: C, 60.10; H, 7.03; N, 15.54. Obs. C, 60.35; H, 7.36; N, 15.54. FTIR cm^{-1} 3300 (NH_2 guanidine), 2927 (-CH_2-), 1658 (C=N, guanidine), 1450 (CH=CH, phenyl).

6.3.1.14 Preparation of trifunctional chloride resin **46**

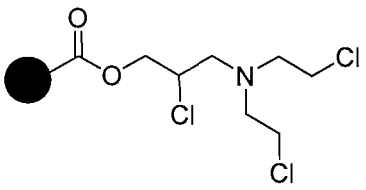

Toluene was added to the resin **45** (9g, 108 mmol), the resin allowed to swell for 15 min. Thionyl chloride solution (50 mL) was added via syringe over 5 min at room temperature. After complete addition, the reaction was heated to 60-65°C for 16 h. The reaction mixture was cooled to ambient temperature, filtered, and the resin then cross washed with toluene (3x100 mL), EtOH (3x100 mL) and MeOH (3x100 mL). The resin was dried under high vacuum overnight, yielding a colourless resin. The results for **46** are presented in Table 6.16.

Resin code	Conversion (%)	Yield isolated g ; %	Loading* (mmol Cl/g rs)
46	100	10.21 ; 67	7.2

*Calculations based on the microanalytical data.

Table 6.16: Results for resin **46**.

Microanalysis; Resin **46** Calcd: C, 47.55; H, 6.40; N, 3.31; Cl, 25.23 Obs. C, 47.62; H, 6.39; N, 3.24; Cl, 25.52. FTIR cm^{-1} (no –OH strecht), 2960 (-CH_2-), 1723 (C=O, carbonyl).

6.3.1.15 Preparation of trifunctional amine resin 48

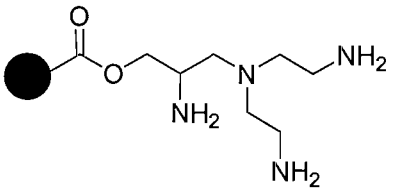

DMF (200 mL) was added to the resin **46** (23g, 165 mmol), the resin was allowed to swell for 15 min. Potassium phthalamide (40g, 215 mmol) was added, after complete addition, the mixture was heated to 120°C with gentle stirring for 24 h. The resin was removed from the solution by filtration and then cross washed with hot DMF (3x50 mL), hot DMF:H_2O (1:1, 3x50 mL), H_2O (3x50 mL), H_2O:dioxane (1:1, 3x50 mL), dioxane (3x50 mL), EtOH (3x50 mL) and MeOH (3x50 mL). The resin was dried under high vacuum overnight, yielding the colourless resin **47**. Without further purification resin **47** (32 g, 230 mmol) was suspended in EtOH (300 mL). After allowing the resin to swell, hydrazine monohydrate (20 mL, 410 mmol) was added, the resultant mixture was refluxed for 2 h. The resin was removed from the solution by filtration, and then was cross washed with hot H_2O (400 mL), hot EtOH (150 mL), DMF (150 mL), DMF:H_2O (1:1, 150 mL), H_2O (150 mL), EtOH (150 mL), MeOH (150 mL) and Et_2O (150 mL). The resin was dried under high vacuum overnight, yielding a colourless resin. The results for **48** are presented in Table 6.17.

Resin code	Conversion (%)	Yield isolated g ; %	Loading* (mmol N/g rs)
48	85	10.1 ; 74	9.6

*Calculations based on the microanalytical data.

Table 6.17: Results for resin **48**.

Microanalysis; Resin **48** Calcd: C, 54.25; H, 8.62; N, 13.10. Obs. C, 53.62; H, 7.80; N, 13.50. FTIR cm^{-1} 3249 (NH_2 amine, broad), 2944 (-CH_2-), 1723 (C=O, carbonyl).

6.3.1.16 Preparation of trifunctional guanidinium support resin ***50***

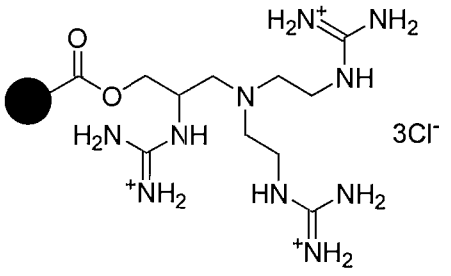

1,4-Dioxane (20 mL) to resin **48** (9g, 87 mmol) 1,4-dioxane (20 mL), the resin allowed to swell for 15 min. Cyanamide **49** (18g, 432 mmol) in 2-butanol (135 mL) in the presence of HCl (18 mL) were then added to the mixture. The resulting reaction mixture was refluxed for 24 h. The resin was filtered off, and washed with 2-butanol (3x100 mL), 1,4-dioxane (3x100 mL), MeOH (3x100 mL) and Et_2O (3x100 mL). The resin was dried under high vacuum overnight. The results for **50** are presented in Table 6.18.

Resin code	Conversion (%)	Yield isolated g ; %
50	53	3.40 ; 73

Table 6.18: Results for resin **50**.

Microanalysis; Resin **50** Calcd: C, 42.61; H, 6.76; N, 15.62. Obs. C, 43.07; H, 6.85; N, 15.62. FTIR cm^{-1} 3327-3190 (NH_2 guanidine, broad), 2956 (-CH_2-), 1719 (C=O, carbonyl), 1656 (C=N, guanidine),

6.3.1.17 Preparation of 0.05 M solution

The eluent was prepared by dissolving sodium perchlorate (3.06 g, 25 mmol) in deionized water (500 mL) to achieve a 0.05 M concentration.

Stock standard solutions of 1000 ppm of the various anions were prepared by dissolving the appropriate amount of each sodium salt in 0.05 M $NaClO_4$ (20mL) Table 6.25.

Anions	% of anion	Mass (mg)
Br^-	77	34.72
I^-	84	29.76
NO_3^-	72.9	34.29
SCN^-	71	35.21
$S_2O_3^{2-}$	71	35.21
SO_4^{2-}	67.6	36.97
$H_2PO_4^-$	80	30.92
HPO_4^{2-}	66.81	37.37
PO_4^{3-}	43.17	57.90
AMP^{2-}	88.2	28.32
ADP^{2-}	90.2	27.70
ATP^{2-}	91.6	27.27

Table 6.25: Composition of the anions.

6.3.1.18 Preparation of 0.5M solution

The eluent was prepared by dissolving sodium perchlorate (30.61 g, 250 mmol) in deionized water (500 mL) to achieve a 0.5 M concentration.

Stock standard solutions of 1000 ppm of the various anions were prepared by dissolving the appropriate amount of each sodium salt in 0.5 M $NaClO_4$ (20mL). Table 6.25.

6.3.2 *Synthesis included in chapter 3*

6.3.2.1 Preparation of silica gel supported thiourea **51**

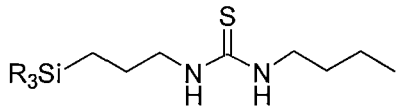

R: C_2H_5O

To the aminopropyl silica gel (4 g, 4.4 mmol) DMF (50 mL) was added. Butyl isothiocyanate (1.5 g, 13.2 mmol) and DIEA (2 mL) previously mixed in DMF (50 mL) were then added to the silica. The resulting reaction mixture was refluxed for 48 h. The silica was filtered off, washed with DMF (3x50 mL), DCM (3x50 mL), MeOH (3x50 mL) and Et_2O (3x50 mL). The product was dried under high vacuum overnight. The results for **51** are presented in Table 6.19.

Resin code	Conversion (%)	Yield isolated g ; %
51	95	4.3 ; 96

Table 6.19: Results for resin **51**.

Microanalysis; Resin **51** Calcd: C, 10.11; H, 2.41; N, 2.90. Obs. C, 11.02; H, 2.23; N, 2.91. FTIR cm^{-1}, stretch of silica is too strong that masked thiourea peaks.

6.3.2.2 Preparation of methacrylate supported thiourea **52**

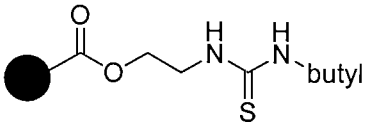

52 20% PEGDM

To resin **30f** (3 g, 8.7 mmol) DMF (15 mL) was added. The resin was allowed to swell for 15 min, and then drained. The butyl isothiocyanate (2.5 g, 22 mmol) and DIEA (3 mL) previously mixed in DMF (30 mL) were then added to the resin. The

resulting reaction mixture was spin-shaken for 48 h. The resin was filtered off, and washed with DMF (3x20 mL), DCM (3x20 mL), MeOH (3x20 mL) and Et_2O (3x20 mL). The resin was dried under high vacuum overnight. The results for **52** are presented in Table 6.20.

Resin code	Conversion (%)	Yield isolated g ; %
52	68	4.0 ; 77

Table 6.20: Results for resin **52**.

Microanalysis; Resin **52** Calcd: C, 50.67; H, 8.33; N, 5.67. Obs. C, 54.58; H, 8.24; N, 5.67. FTIR cm^{-1} 3304 (NH secondary amine), 2933 ($-CH_2-$), 1723 (C=O, carbonyl), 1145 (S=C, thiourea).

6.3.2.3 Preparation of Merrifield resin supported isothiouronium 53

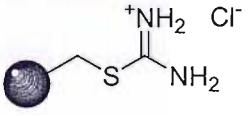

To the Merrifield resin (8 g, 18 mmol) MeOH (100 mL) was added. The resin was allowed to swell for 15 min. Thiourea (4.1 g, 54 mmol) was dissolved in MeOH (150 mL) and added. The resulting reaction mixture was gently refluxed for 48 h. The resin was filtered off, washed with MeOH (3x150 mL) and Et_2O (3x100 mL). The resin was dried under high vacuum overnight. The results for **53** are presented in Table 6.21.

Resin code	Conversion (%)	Yield isolated g ; %
53	98	8.8 ; 89

Table 6.21: Results for resin **53**.

Microanalysis; Resin **53** Calcd: C, 69.45; H, 6.39; N, 4.96. Obs. C, 73.41; H, 6.99; N, 4.96. FTIR cm^{-1} 3262 (NH_2 isothiouronium, broad), 3024-2923 (-CH_2-), 1645 (C=N, isothiouronium), 1449 (CH=CH, phenyl).

6.3.2.4 Preparation of polystyrene double arm chloride 56

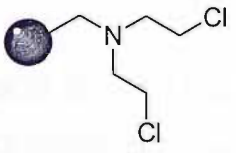

Resin **55** was prepared following literature procedures[125] by reacting polymer **39** with diethanolamine **54**. Thionyl chloride solution (60 mL, excess) was added via syringe over 5 min to resin **55** (diethanol polystyrene derivative) (8.5g, 88 mmol) at room temperature. After complete addition, the reaction was heated to 60-65°C for 16 h. The reaction mixture was cooled to ambient temperature, filtered and then the resin was cross washed with toluene (3x100 mL), EtOH (3x100 mL) and MeOH (3x100 mL). The resin was dried under vacuum overnight, yielding a colourless resin. The results for **56** are presented in Table 6.22.

Resin code	Conversion (%)	Yield isolated g ; %	Loading* (mmol Cl/g rs)
56	92	9.75 ; 83	8.3

*Calculations based on the microanalytical data.

Table 6.22: Results for resin **56**.

Microanalysis; Resin **56** Calcd: C, 58.28; H, 6.26; N, 4.24; Cl, 29.70. Obs. C, 55.10; H, 6.25; N, 3.79; Cl, 29.58. FTIR cm^{-1} (no OH stretch), 2930 (-CH_2-), 1448 (CH=CH, phenyl).

6.3.2.5 *Preparation of polystyrene double arm isothiouronium 57*

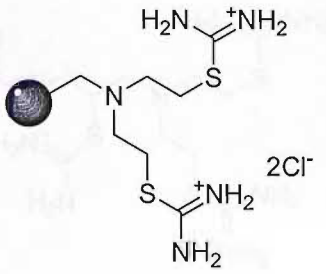

To resin **56** (9g, 75 mmol) MeOH (50 mL) was added, the resin allowed to swell for 15 min. Thiourea (17.1 g, 225 mmol) previously dissolved in MeOH (200 mL), was added to the resin. The resulting reaction mixture was gently refluxed for 48 h. The resin was filtered off, and washed with MeOH (3x150 mL) and Et_2O (3x100 mL). The resin was dried under high vacuum overnight, yielding a colourless resin. The results for **57** are presented in Table 6.23.

Resin code	Conversion (%)	Yield isolated g ; %
57	62	11.32 ; 77

Table 6.23: Results for resin **57**.

Microanalysis; Resin **57** Calcd: C, 44.04; H, 5.98; N, 13.09. Obs. C, 46.69; H, 6.50; N, 13.09. FTIR cm^{-1} 3237-3041 (NH_2 isothiouronium), 2837 (-CH_2-, masked), 1640 (C=N, isothiouronium), 1019 (C-S, thiourea).

6.3.2.6 *Prepration of Macroprep trifunctional isothiouronium derivative* **60**

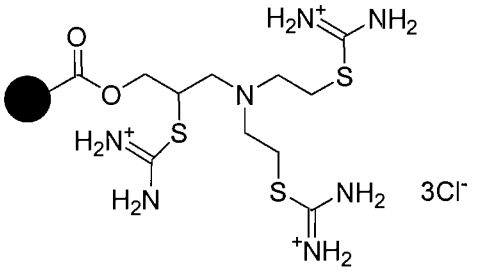

To resin **59** (9g, 65 mmol) MeOH (50 mL) was added, the resin was allowed to swell for 15 min. Thiourea (15.4 g, 202 mmol) previously dissolved in MeOH (200 mL) was added to the resin. The resulting reaction mixture was gentle refluxed for 48 h. The resin was filtered off, and washed with MeOH (3x150 mL) and Et_2O (3x100 mL). The resin was dried under high vacuum overnight, yielding a colourless resin. The results for **60** are presented in Table 6.24.

Resin code	Conversion (%)	Yield isolated g ; %
60	98	12.5 ; 53

Table 6.24: Results for resin **79**.

Microanalysis; Resin **60** Calcd: C, 36.46; H, 6.00; N, 14.98. Obs. C, 37.44; H, 6.15; N, 12.90. FTIR cm^{-1} 3225 (NH_2 isothiouronium), 2948 (-CH_2-), 1724 (C=O, carbonyl), 1648 (C=N, isothiouronium), 1017 (C-S, thiourea).

6.3.3 Synthesis included in chapter 5

6.3.3.1 Preparation of N, N-bis-(3-aminophenyl)isophthaldiamide **67**

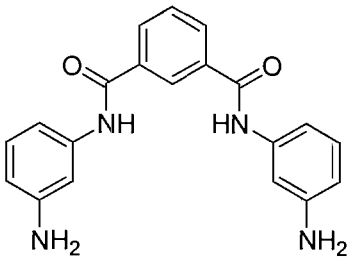

Isophthaloyl dichloride (1 g, 5 mmol) was dissolved in dry MeCN (280 mL). This solution was added with dropwise to a solution of 1,3 phenylendiamine (5.42 g, 50 mmol), triethylamine (3.54 g, 35 mmol) and catalytic amount of DMAP in dry MeCN (15 mL). The resulting solution was stirred overnight under a nitrogen atmosphere. The solvent was removed in *vacuo* and the crude product purified by column chromatography on SiO_2 eluting with dichloromethane/methanol, (94:6 v/v). A white compound was obtained (0.55 g, 32 %). δ_H (300 MHz; DMSO-d_6; Me_4Si): 5.21 (s, 4H, NH_2), 6.42 (d, 2H, *J*=7.3Hz, ArH), 6.98 (d, 2H, *J*= 8.2 Hz, ArH), 7.07 (t, 2H, *J*= 8.2 Hz, ArH), 7.22 (s, 2H, ArH), 7.74 (t, 1H, *J*= 7.3 Hz, ArH), 8.17 (d, 2H, *J*= 6.4 Hz, ArH), 8.55 (s, 1H, ArH), 10.22 (s, 2H, CONH). δ_C (75 MHz; DMSO-d_6; Me_4Si): 106.1, 108.3, 109.8, 126.8, 128.3, 128.7, 130.3, 135.4, 139.6, 148.9, 164.8. ES^+ mass spectrum, m/z, 347.1 ($M+H^+$), 693.2 ($2M+H^+$). Elemental analysis compound **67**·0.33CH_3CN· 0.33CH_2Cl_2. Anal. calcd: C, 64.94; H, 5.10; N, 15.63. Obs. C, 65.21; H, 4.84; N, 15.20. IR 3426(m), 3366(m), 3286(s), 1635(m), 1600(s), 1535(s), 1490(s), 1460(s), 1335(m), 1265(s), 1065(m). m.p (decomp.): 218-220°C

6.3.3.2 Preparation of N, N'-bis-(3 acetylaminophenyl)isophthaldiamide **68**

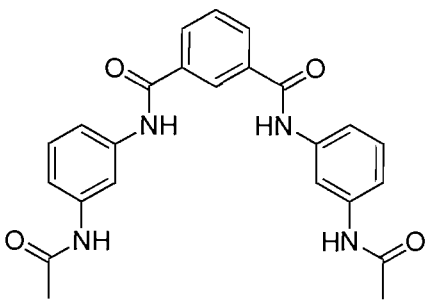

Compound **67** (0.5 g , 1.44 mmol) was dissolved in dry DCM (40 mL) and triethylamine (0.36 g , 3.6 mmol), acetyl chloride (0.34 g, 4.32 mmol) and a catalytic quantity of DMAP was added to the solution. The resulting solution was stirred overnight under a N_2 atmosphere. The solvent was then removed in *vacuo* and the product was obtained by crystallisation from MeCN, as a white compound (0.25 g, 41.4 %). δ_H (300 MHz; DMSO-d_6; Me_4Si): 2.15 (s, 6H, $COCH_3$), 7.36 (t, 2H, J =8.2 Hz, ArH), 7.44 (d, 2H, J= 8.2 Hz, ArH), 7.55 (d, 2H, J = 2.3 Hz, ArH), 7.77 (t, 1H, J = 8.2 Hz, ArH), 8.21 (s, 4H, ArH), 8.60 (s, 1H, Ar), 10.09 (s, 2H, CONH), 10.53 (s, 2H, CONH). δ_C (75 MHz; DMSO-d_6; Me_4Si): 24.6, 112.0, 115.4, 116.0, 127.7, 129.1, 129.3, 131.3, 135.8, 139.9, 140.2, 165.7, 168.9. MS ES$^+$: m/z, 453.1 $(M + Na)^+$, 883 $(2M+Na)^+$. Elemental analysis compound **68**·$1CH_2Cl_2$·$1H_2O$. Anal. Calcd: C, 56.29; H, 4.91; N, 10.50. Obs. C, 56.44; H, 4.75; N, 10.75. IR 3300(m), 3072(w), 1738(m), 1645(s), 1529(s), 1431(s), 1365(m), 1020(m). m.p (decomp.): >300°C.

6.3.3.3 Preparation of N,N'-bis-(3-octanoylaminophenyl)isopthaldiamide **69**

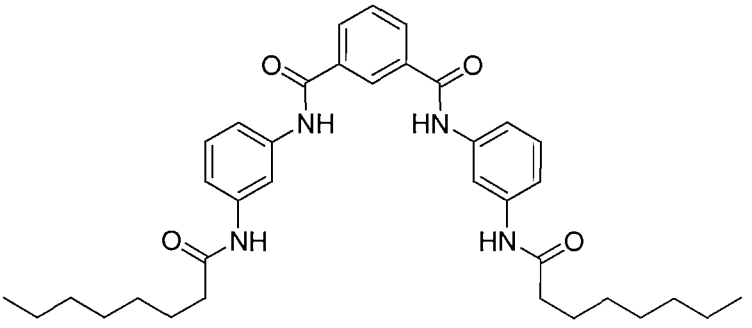

N,N-bis-(3-amino-phenyl) isophthalamide **67** (0.5 g , 1.44 mmol) was dissolved in dry MeCN (150 mL) and triethylamine (0.36 g , 3.6 mmol), octanoyl chloride (4.3 mmol) and a catalytic amount of DMAP were added to the solution. It was then stirred overnight under a N_2 atmosphere. The solvent was removed in *vacuo* and the residue was dissolved in DCM/MeOH and left for three days to crystallise, however a precipitate was formed. The precipitate was filtered off affording the amide **69**, (0.35 g, 41 %). δ_H (300 MHz; DMSO-d_6; Me_4Si): 0.96 (s, 5H, CH_2), 1.36 (s, 20H, CH_2), 1.68 (s, 5H,CH_2), 7.36(t, 2H, J = 7.3 Hz, ArH), 7.44 (d, 2H, J = 8.2 Hz, ArH), 7.55 (d, 2H, J =8.2 Hz ArH), 7.77 (t, 1H, J =8.2 ArH), 8.22 (d, 2H, J =9.1, ArH),

8.61 (s, 1H, ArH , 10.03 (s, 2H, CONH), 10.52 (s, 2H, CONH). δ_C (75 MHz; DMSO-d_6; Me_4Si): 13.91, 22.04, 25.15, 28.45, 28.62, 31.16, 36.36, 111.43, 114.76, 115.22, 127.02, 128.48, 128.65, 130.61, 135.09, 139.23, 139.55, 165.01, 171.27. MS ES^+: m/z, 599.4 $(M + H)^+$, 621.3 (M+Na), 1197.4 (2M), 1219.4 (2M+Na). Elemental analysis Compound **69**·1.5·H_2O. Anal. Calcd: C, 69.10; H, 7.89; N, 8.95. Obs. C, 69.43; H, 7.71; N, 8.95. IR 3306(s), 3066(w), 2926(s), 2921(s), 2856(m), 2606(w), 1645(s), 1540(s), 1415(s), 1310(m), 1255(s). m.p (decomp.): 284-286°C.

*6.3.3.4 Preparation of pyridine-3,5-dicarboxylic acid bis-[(3-aminophenyl)amide] **74***

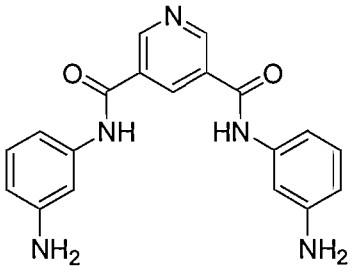

Pyridine-3,5-dicarbonyl dichloride **73** (5.98 mmol) was reacted with 1,3 phenylendiamine (6.46 g, 59.8 mmol), triethylamine (4.23 g, 41.86 mmol) and a catalytic quantity of DMAP in dry MeCN (30 mL) was added dropwise. The reaction was stirred overnight under N_2. The solvent was removed in *vacuo* and the residue dissolved in DCM. A precipitate formed, which was filtered off and the filtrate purified by column chromatography on silica eluting with dichloromethane/methanol (90/10 v/v). A green-yellow compound was obtained (1.15 g, 55 %). δ_H (300 MHz; DMSO-d_6; Me_4Si): 5.24 (s, 4H,ArNH), 6.44 (d, 2H, J = 8.2 Hz, ArH), 7.00 (d, 2H, J = 8.2 Hz, ArH), 7.08 (t, 2H, J =8.2 Hz ArH), 7.22 (s, 2H, Ar), 8.88 (s, 1H, PyH), 9.29 (s, 2H, PyH), 10.44 (s, 2H, CONH). δ_C (75 MHz; DMSO-d_6; Me_4Si): 105.95, 110.79, 114.59, 120.20, 128.65, 128.77, 148.92, 150.86. MS ES^-: m/z, 382.2 ($M+Cl^-$). IR 3333(w), 2978(m), 2605(s), 2497(s), 1612(s), 1444(s), 1263(w), 1036(m). m.p (decomp.): 158-164°C.

6.3.3.5 *Preparation of pyridine-3,5-dicarboxylic acid bis-[(3-octanoylaminophenyl)amide* **75**

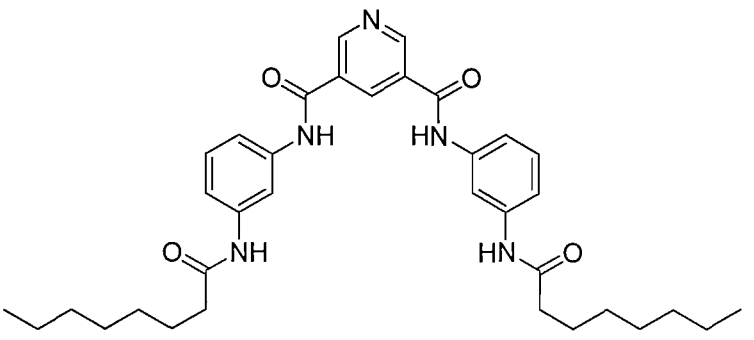

Pyridine-3,5-dicarboxylic acid bis-[(3-amino-phenyl)-amide] **74** (0.5g, 1.44 mmol) was dissolved in dry MeCN (250 mL) and triethylamine (0.36 g, 3.6 mmol), octanoyl chloride (4.3 mmol) and a catalytic quantity of DMAP were added to the solution which was then refluxed 24 h under a N_2 atmosphere. The solvent was removed in *vacuo* and the product obtained by precipitation from DCM/MeOH, as a white solid (0.18 g, 21%). δ_H (300 MHz; DMSO-d_6; Me_4Si): 0.96 (s, 5H, CH_2), 1.38 (s, 20H, CH_2), 1.69 (s, 5H,CH_2), 7.37(t, 2H, J = 7.1 Hz, ArH), 7.45 (d, 2H, J = 7.9 Hz, ArH), 7.57 (d, 2H, J =7.9 Hz ArH), 8.25 (s, 2H, Ar), 8.90 (s, 2H, PyH), 9.34 (s, 1H, PyH), 10.05 (s, 2H, CONH), 10.71 (s, 2H, CONH). δ_C (75 MHz; DMSO-d_6; Me_4Si): 13.91, 22.04, 25.13, 28.44, 28.60, 31.14, 36.37, 111.35, 114.99, 115.15, 128.76, 130.17, 134.68, 138.93, 139.64, 150.99, 163.44, 171.32. MS ES^+: m/z, 622.4 $(M+Na)^+$, 1221.6 (2M+Na) ,1822.1 (3M+Na). Elemental analysis: compound **75**·0.33CH_3CN·1CH_2OH·0.33CH_2Cl_2. Anal. Calcd: C, 65.95; H, 7.58; N, 11.09. Obs. C, 65.98; H, 7.58; N, 10.73. IR 3316(m), 3256(s), 3556(w), 2921(s), 2581(m), 1645(s), 1595(s), 1520(s), 1485(s), 1300(m), 1030(m). m.p (decomp.): 268-272°C

6.3.3.6 *Preparation of 3,4-diphenyl pyrrole amide clefts* **86**

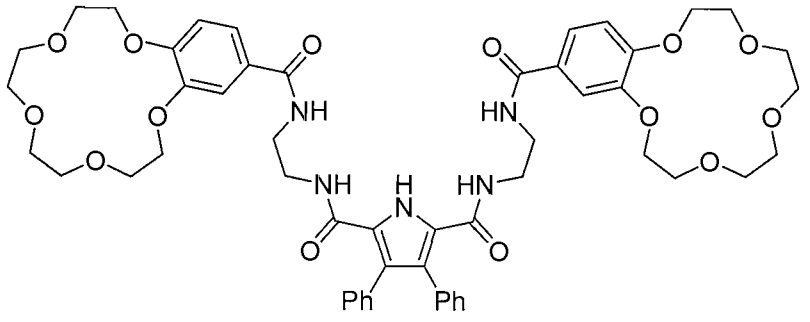

Compound **79** (0.31g, 0.8 mmol) was dissolved in dry DCM (25 mL), and this solution was added dropwise to a solution of 4'-carboxybenzo-15-crown-5 (1.6 mmol), triethylamine (0.20 g, 2 mmol), and a catalytic amount of DMAP. The resulting solution was stirred for 48 hrs under an N_2 atmosphere. The solvent was removed in *vacuo* and the product was purified by column chromatography on SiO_2 eluting with DCM/MeOH (9/1 v/v). Compound **86** was obtained as a pale white solid (0.5g, 63.7%). δ_H (300 MHz; $CDCl_3$-*d*; Me_4Si): 1.41 (m, 4H, CH_2NHCO), 3.11 (m, 4H, NHCO CH_2), 3.44 (m, 8H,CH_2OAr), 3.76(m, 8H OCH_2R), 3.92 (m, 8H RCH_2O), 4.19 (m, 8H RCH_2O), 6.02 (s, 2H, CONH), 6.86-7.42 (m, 16H, ArH)+ obscured amide CON*H*, 2H), 10.36 (s, 1H, NHPy). δ_C (75 MHz; $CDCl_3$-*d*; Me_4Si): 38.09, 39.76, 44.91, 67.81, 68.25, 69.23, 69.93, 111.37, 111.91, 119.60, 122.62, 126.78, 127.48, 129.55, 132.04, 147.54, 150.62, 160.64, 166.17. MS ES^+: m/z, 1002.2 $(M+Na)^+$. IR 3409(w), 3266(m), 2980(m), 2605(m), 2501(m), 1638(m), 1505(m), 1273(m), 1125(m), 1031(m). m.p (decomp.): 188-192°C.

Appendix

Crystal data

A.1 Introduction

The crystal structures presented in this thesis were solved by the EPSRC Crystallographic Service (Dr. S. Coles, Dr. M. E. Light, Prof. M. B. Hursthouse) at the University of Southampton. The refinement of the structures and the fractional co-ordinates are reported here for the sake of completeness and so that the structures may be regenerated from the text of this thesis if necessary.

A.2 Crystal data

Benzamidinium – $PtCl_6^{2-}$

Identification code	**03MEL001**
Empirical formula	$C_{14}H_{18}Cl_6N_4Pt$
Formula weight	650.11
Temperature	120(2) K
Wavelength	0.71073 Å
Crystal system	Monoclinic
Space group	$P2_1/c$
Unit cell dimensions	a = 8.76170(10) Å
	b = 10.6219(2) Å β = 108.7530(10)°
	c = 11.5677(2) Å
Volume	1019.41(3) Å^3
Z	2
Density (calculated)	2.118 Mg / m^3
Absorption coefficient	7.675 mm^{-1}
F(000)	620
Crystal	Orange Block
Crystal size	0.20 × 0.10 × 0.10 mm^3
θ range for data collection	3.12 – 25.03°
Index ranges	$-10 \le h \le 10$, $-12 \le k \le 12$, $-13 \le l \le 13$
Reflections collected	3503
Independent reflections	1804 [R_{int} = 0.0160]
Completeness to θ = 25.03°	99.8 %
Absorption correction	Semi–empirical from equivalents
Max. and min. transmission	0.5141 and 0.3090
Refinement method	Full-matrix least-squares on F^2
Data / restraints / parameters	1804 / 0 / 152
Goodness-of-fit on F^2	1.085
Final R indices [$F^2 > 2\sigma(F^2)$]	$R1$ = 0.0177, $wR2$ = 0.0451
R indices (all data)	$R1$ = 0.0184, $wR2$ = 0.0455
Extinction coefficient	0.0088(4)
Largest diff. peak and hole	0.994 and –1.788 e Å^{-3}

Table A.1: Crystal data and structure refinement.

Atom	*x*	*y*	*z*	U_{eq}	*S.o.f.*
C1	8847(3)	−1242(2)	6066(2)	13(1)	1
C2	10452(3)	−1581(3)	6632(3)	17(1)	1
C3	11384(4)	−1968(3)	5932(3)	22(1)	1
C4	10727(4)	−1991(3)	4676(3)	22(1)	1
C5	9145(4)	−1634(3)	4109(3)	20(1)	1
C6	8187(3)	−1266(3)	4803(3)	16(1)	1
C7	7855(3)	−845(3)	6821(2)	16(1)	1
N1	6324(3)	−1148(3)	6484(3)	23(1)	1
N2	8522(4)	−192(3)	7815(3)	23(1)	1
Pt1	5000	0	0	9(1)	1
Cl1	5549(1)	1959(1)	941(1)	16(1)	1
Cl2	7733(1)	−413(1)	461(1)	16(1)	1
Cl3	5046(1)	−880(1)	1847(1)	16(1)	1

Table A.2: Atomic coordinates [$\times 10^4$], equivalent isotropic displacement parameters [$Å^2 \times 10^3$] and site occupancy factors. U_{eq} is defined as one third of the trace of the orthogonalized U^{ij} tensor.

Guanidinium benzoic acid – $PtCl_6^{2-}$

Identification code	**03SOT019**
Empirical formula	$C_{16}H_{20}Cl_6N_6O_4Pt$
Formula weight	768.17
Temperature	120(2) K
Wavelength	0.71073 Å
Crystal system	Triclinic
Space group	P-1
Unit cell dimensions	$a = 6.9369(2)$ Å $\alpha = 75.0020(10)°$ $b = 7.5303(2)$ Å $\beta = 79.250(2)°$ $c = 13.3955(4)$ Å $\gamma = 64.374(2)°$
Volume	607.18(3) $Å^3$
Z	1
Density (calculated)	2.101 Mg / m^3
Absorption coefficient	6.475 mm^{-1}
F(000)	370
Crystal	Orange Block
Crystal size	0.30 × 0.20 × 0.10 mm^3
θ range for data collection	3.06 – 25.03°
Index ranges	$-7 \le h \le 8, -8 \le k \le 8, -15 \le l \le 15$
Reflections collected	4028
Independent reflections	2115 [$R_{int} = 0.0183$]
Completeness to $\theta = 25.03°$	99.0 %
Absorption correction	Semi–empirical from equivalents
Max. and min. transmission	0.5637 and 0.2469
Refinement method	Full-matrix least-squares on F^2
Data / restraints / parameters	2115 / 9 / 156
Goodness-of-fit on F^2	1.060
Final R indices [$F^2 > 2\sigma(F^2)$]	$R1 = 0.0253$, $wR2 = 0.0674$
R indices (all data)	$R1 = 0.0253$, $wR2 = 0.0674$
Extinction coefficient	0.0135(15)
Largest diff. peak and hole	1.488 and –1.850 e $Å^{-3}$

Table A.3: Crystal data and structure refinement.

Atom	*x*	*y*	*z*	U_{eq}	*S.o.f.*
Pt1	5000	0	0	10(1)	1
Cl1	3769(2)	3256(2)	−958(1)	17(1)	1
Cl2	5786(2)	1058(2)	1296(1)	17(1)	1
Cl3	1550(2)	609(2)	787(1)	15(1)	1
O1	3823(6)	2037(6)	5955(3)	27(1)	1
N1	11897(6)	5779(6)	1062(3)	20(1)	1
N2	9901(6)	6967(6)	2495(3)	19(1)	1
N3	10571(6)	3771(6)	2304(3)	17(1)	1
C1	10789(7)	5514(6)	1951(3)	14(1)	1
C2	9361(7)	3302(6)	3238(3)	15(1)	1
C3	7658(8)	2855(7)	3170(4)	18(1)	1
C4	6455(8)	2409(7)	4064(4)	19(1)	1
C5	6961(7)	2382(6)	5032(4)	18(1)	1
C6	8733(8)	2764(7)	5081(4)	20(1)	1
C7	9938(8)	3216(7)	4193(4)	20(1)	1
C8	5595(8)	1988(7)	5965(4)	22(1)	1
O2	6482(7)	1595(6)	6845(3)	39(1)	1

Table A.4: Atomic coordinates [$\times 10^4$], equivalent isotropic displacement parameters [$Å^2 \times 10^3$] and site occupancy factors. U_{eq} is defined as one third of the trace of the orthogonalized U^{ij} tensor.

Bis-acylguanidinium 16 – $PtCl_6^{2-}$

Identification code	**16**
Empirical formula	$C_{10}H_{17}Cl_6N_6O_3Pt$†
Formula weight	677.09
Temperature	120(2) K
Wavelength	0.71073 Å
Crystal system	Monoclinic
Space group	*C*2/*c*
Unit cell dimensions	$a = 10.4182(4)$ Å
	$b = 12.1527(5)$ Å $\beta = 94.729(3)°$
	$c = 15.7044(7)$ Å
Volume	1981.55(14) Å^3
Z	4
Density (calculated)	2.270 Mg / m^3
Absorption coefficient	7.915 mm^{-1}
F(000)	1292
Crystal	Orange needle
Crystal size	0.25 × 0.03 × 0.03 mm^3
θ range for data collection	2.96 – 25.03°
Index ranges	$-12 \le h \le 12$, $-14 \le k \le 14$, $-18 \le l \le 18$
Reflections collected	3303
Independent reflections	1750 [$R_{int} = 0.0313$]
Completeness to $\theta = 25.03°$	99.4 %
Absorption correction	Semi–empirical from equivalents
Max. and min. transmission	0.7972 and 0.2423
Refinement method	Full-matrix least-squares on F^2
Data / restraints / parameters	1750 / 51 / 138
Goodness-of-fit on F^2	1.054
Final *R* indices [$F^2 > 2\sigma(F^2)$]	*R1* = 0.0246, *wR2* = 0.0532
R indices (all data)	*R1* = 0.0318, *wR2* = 0.0557
Largest diff. peak and hole	0.982 and –1.139 e Å^{-3}

Table A.5: Crystal data and structure refinement. † Empirical formula doubled due to one Pt on special position.

Atom	*x*	*y*	*z*	U_{eq}	*S.o.f.*
C3	4043(4)	5971(4)	2870(3)	17(1)	1
C4	4032(5)	4818(4)	2860(3)	24(1)	1
C5	5000	4256(6)	2500	22(2)	1
C6	5000	6531(5)	2500	20(2)	1
C1A	2560(20)	8221(17)	4153(8)	15(3)	0.50
C2A	2996(5)	6536(4)	3292(3)	21(1)	0.50
O1A	1933(3)	6150(3)	3368(2)	25(1)	0.50
N1A	1408(4)	7994(4)	4185(3)	30(1)	0.50
N2A	3127(10)	9134(8)	4449(6)	29(2)	0.50
N3A	3293(19)	7493(15)	3733(8)	13(2)	0.50
C1B	2570(20)	8356(17)	3881(8)	15(3)	0.50
C2B	2996(5)	6536(4)	3292(3)	21(1)	0.50
O1B	1933(3)	6150(3)	3368(2)	25(1)	0.50
N1B	1408(4)	7994(4)	4185(3)	30(1)	0.50
N2B	2966(9)	9365(8)	3978(5)	29(2)	0.50
N3B	3383(19)	7650(16)	3487(8)	13(2)	0.50
Pt1	2500	2500	5000	13(1)	1
Cl1	3469(1)	1932(1)	3795(1)	36(1)	1
Cl2	1001(1)	1081(1)	4798(1)	19(1)	1
Cl3	1189(1)	3659(1)	4151(1)	36(1)	1
O1W	4738(8)	9738(5)	2702(5)	25(2)	0.50

Table A.6: Atomic coordinates [$\times 10^4$], equivalent isotropic displacement parameters [$Å^2 \times 10^3$] and site occupancy factors. U_{eq} is defined as one third of the trace of the orthogonalized U^{ij} tensor.

Tris-acylguanidinium 19 – $PtCl_6^{2-}$

Identification code	**19**
Empirical formula	$C_{24}H_{60}Cl_{18}N_{18}O_{18}Pt_3$
Formula weight	2112.27
Temperature	120(2) K
Wavelength	0.71073 Å
Crystal system	Monoclinic
Space group	$P2_1/n$
Unit cell dimensions	a = 8.2386(2) Å
	b = 10.4670(3) Å β = 94.5730(10)°
	c = 36.7498(12) Å
Volume	3158.97(16) Å^3
Z	2
Density (calculated)	2.221 Mg / m^3
Absorption coefficient	7.462 mm^{-1}
F(000)	2028
Crystal	Yellow Plate
Crystal size	0.15 × 0.10 × 0.03 mm^3
θ range for data collection	2.96 – 25.02°
Index ranges	$-9 \le h \le 9, -12 \le k \le 9, -43 \le l \le 43$
Reflections collected	9391
Independent reflections	5443 [R_{int} = 0.0438]
Completeness to θ = 25.02°	97.5 %
Absorption correction	Semi–empirical from equivalents
Max. and min. transmission	0.8071 and 0.4007
Refinement method	Full-matrix least-squares on F^2
Data / restraints / parameters	5443 / 24 / 415
Goodness-of-fit on F^2	1.055
Final R indices [$F^2 > 2\sigma(F^2)$]	$R1$ = 0.0395, $wR2$ = 0.0921
R indices (all data)	$R1$ = 0.0594, $wR2$ = 0.1019
Largest diff. peak and hole	1.528 and −1.811 e Å^{-3}

Table A.7: Crystal data and structure refinement.

Atom	*x*	*y*	*z*	U_{eq}	*S.o.f.*
N1	6596(6)	5339(5)	3511(2)	20(2)	1
N2	5050(7)	5617(6)	2953(2)	26(2)	1
N3	4016(7)	4534(6)	3430(2)	25(2)	1
N4	10186(7)	7194(6)	5032(2)	21(2)	1
N5	8515(8)	6793(6)	5501(2)	27(2)	1
N6	10667(8)	8175(6)	5581(2)	29(2)	1
N7	13771(7)	7986(5)	3577(2)	18(2)	1
N8	16397(7)	8756(6)	3725(2)	25(2)	1
N9	15224(7)	8910(6)	3143(2)	24(2)	1
O1	8086(6)	6498(5)	3128(2)	21(1)	1
O2	8215(6)	5768(5)	4836(2)	26(1)	1
O3	14687(6)	7172(4)	4130(2)	20(1)	1
C1	9139(8)	6317(6)	3749(2)	16(2)	1
C2	8758(8)	6240(6)	4104(2)	15(2)	1
C3	9902(8)	6539(6)	4393(2)	17(2)	1
C4	11449(8)	6901(6)	4311(2)	14(2)	1
C5	11854(9)	6978(6)	3956(2)	12(2)	1
C6	10712(8)	6696(6)	3667(2)	17(2)	1
C7	7933(8)	6071(6)	3432(2)	18(2)	1
C8	5215(9)	5180(7)	3285(3)	22(2)	1
C9	9333(9)	6445(7)	4764(2)	17(2)	1
C10	9745(9)	7382(7)	5377(2)	18(2)	1
C11	13562(8)	7377(6)	3902(2)	13(2)	1
C12	15177(8)	8567(6)	3482(3)	19(2)	1
Pt1	5630(1)	6674(1)	1787(1)	15(1)	1
Cl1	6423(2)	4982(2)	2170(1)	23(1)	1
Cl2	4920(2)	5218(2)	1322(1)	20(1)	1
Cl3	2989(2)	6554(2)	1965(1)	26(1)	1
Cl4	6337(2)	8068(2)	2262(1)	28(1)	1
Cl5	8260(2)	6814(2)	1607(1)	24(1)	1
Cl6	4871(2)	8380(2)	1409(1)	22(1)	1
Pt2	0	5000	0	18(1)	1
Cl7	−695(2)	7081(2)	137(1)	25(1)	1
Cl8	−2078(2)	4273(2)	342(1)	27(1)	1
Cl9	1864(2)	4913(2)	509(1)	30(1)	1
O1W	3040(7)	3320(5)	2079(2)	30(1)	1
O2W	560(7)	9(5)	374(2)	28(1)	1
O3W	9920(7)	6793(6)	2481(2)	33(2)	1
O4W	11827(7)	4870(6)	2780(2)	39(2)	1
O5W	6325(9)	3802(7)	4114(2)	49(2)	1
O6W	6360(8)	7838(6)	6059(2)	38(2)	1

Table A.8: Atomic coordinates [$\times 10^4$], equivalent isotropic displacement parameters [$Å^2 \times 10^3$] and site occupancy factors. U_{eq} is defined as one third of the trace of the orthogonalized U^{ij} tensor.

Guanidinium – $RuCl_6^{3-}$

Identification code	
Empirical formula	$C_3H_{20}Cl_6N_9ORu$
	$RuCl_6^{3-} \cdot 3(CN_3H_6^+) \cdot H_2O$
Formula weight	512.05
Temperature	120(2) K
Wavelength	0.71073 Å
Crystal system	Triclinic
Space group	*P*–1
Unit cell dimensions	$a = 7.4966(7)$ Å $\alpha = 93.828(10)°$
	$b = 8.6653(11)$ Å $\beta = 101.020(12)°$
	$c = 15.696(3)$ Å $\gamma = 113.327(7)°$
Volume	907.5(2) $Å^3$
Z	2
Density (calculated)	1.874 Mg / m^3
Absorption coefficient	1.755 mm^{-1}
F(000)	510
Crystal	Plate; Pale Red
Crystal size	0.5 × 0.2 × 0.05 mm^3
θ range for data collection	3.02 – 25.02°
Index ranges	$-8 \le h \le 8, -10 \le k \le 10, -18 \le l \le 18$
Reflections collected	13293
Independent reflections	3192 [$R_{int} = 0.0377$]
Completeness to $\theta = 25.02°$	99.7 %
Absorption correction	Semi–empirical from equivalents
Max. and min. transmission	0.9174 and 0.4740
Refinement method	Full-matrix least-squares on F^2
Data / restraints / parameters	3192 / 21 / 265
Goodness-of-fit on F^2	0.715
Final *R* indices [$F^2 > 2\sigma(F^2)$]	*R1* = 0.0250, *wR2* = 0.0594
R indices (all data)	*R1* = 0.0351, *wR2* = 0.0674
Extinction coefficient	0.0032(6)
Largest diff. peak and hole	0.561 and –0.666 e $Å^{-3}$

Table A.9: Crystal data and structure refinement.

Atom	x	y	z	U_{eq}	*S.o.f.*
Ru1	10000	0	0	14(1)	1
Cl1	11077(1)	460(1)	1555(1)	24(1)	1
Cl2	8937(1)	2218(1)	81(1)	20(1)	1
Cl3	6773(1)	−1938(1)	81(1)	21(1)	1
Ru2	0	5000	5000	13(1)	1
Cl4	2270(1)	5815(1)	4078(1)	18(1)	1
Cl5	−2094(1)	6078(1)	4153(1)	18(1)	1
Cl6	1754(1)	7670(1)	5922(1)	18(1)	1
N1	3563(4)	2452(4)	4023(2)	22(1)	1
N2	3682(5)	−144(4)	4005(2)	29(1)	1
N3	796(4)	82(4)	4088(2)	27(1)	1
C1	2682(5)	804(4)	4047(2)	17(1)	1
N4	9932(5)	6742(4)	2224(2)	24(1)	1
N5	7484(4)	5034(4)	1025(2)	22(1)	1
N6	8493(5)	3850(4)	2179(2)	24(1)	1
C2	8628(5)	5201(4)	1804(2)	18(1)	1
N7	2856(4)	5625(4)	1198(2)	23(1)	1
N8	4156(5)	4463(4)	2278(2)	24(1)	1
N9	5438(5)	7359(4)	2339(2)	28(1)	1
C3	4148(5)	5815(4)	1935(2)	19(1)	1
O1	5602(4)	10282(3)	1474(2)	25(1)	1

Table A.10: Atomic coordinates [$\times 10^4$], equivalent isotropic displacement parameters [$Å^2 \times 10^3$] and site occupancy factors. U_{eq} is defined as one third of the trace of the orthogonalized U^{ij} tensor.

Amidinium – $Ru_2OCl_{10}^{4-}$

Identification code	**2005sot0260**
Empirical formula	$C_{28}H_{38}Cl_{10}N_8O_2Ru_2$
Formula weight	1075.30
Temperature	120(2) K
Wavelength	0.71073 Å
Crystal system	Monoclinic
Space group	$P2_1/n$
Unit cell dimensions	a = 14.2896(18) Å
	b = 19.805(2) Å β = 92.810(14)°
	c = 14.3592(16) Å
Volume	4058.8(8) Å^3
Z	4
Density (calculated)	1.760 Mg / m^3
Absorption coefficient	1.442 mm^{-1}
F(000)	2144
Crystal	Block; Dark Red
Crystal size	0.06 × 0.05 × 0.03 mm^3
θ range for data collection	2.91 – 27.42°
Index ranges	$-18 \le h \le 18$, $-25 \le k \le 25$, $-18 \le l \le 13$
Reflections collected	42510
Independent reflections	9235 [R_{int} = 0.1018]
Completeness to θ = 27.42°	99.7 %
Absorption correction	Semi–empirical from equivalents
Max. and min. transmission	0.9580 and 0.9185
Refinement method	Full-matrix least-squares on F^2
Data / restraints / parameters	9235 / 3 / 458
Goodness-of-fit on F^2	1.043
Final R indices [$F^2 > 2\sigma(F^2)$]	$R1$ = 0.0529, $wR2$ = 0.1024
R indices (all data)	$R1$ = 0.0961, $wR2$ = 0.1203
Extinction coefficient	0.00124(14)
Largest diff. peak and hole	0.746 and –0.955 e Å^{-3}

Table A.11. Crystal data and structure refinement details.

Atom	*x*	*y*	*z*	U_{eq}	*S.o.f.*
Ru1	8293(1)	920(1)	7232(1)	16(1)	1
Ru2	6095(1)	84(1)	7279(1)	16(1)	1
Cl1	8628(1)	491(1)	8742(1)	21(1)	1
Cl2	8966(1)	–39(1)	6544(1)	22(1)	1
Cl3	8045(1)	1356(1)	5694(1)	21(1)	1
Cl4	7738(1)	1949(1)	7840(1)	22(1)	1
Cl5	9785(1)	1415(1)	7329(1)	22(1)	1
Cl6	6927(1)	–935(1)	7578(1)	23(1)	1
Cl7	6002(1)	282(1)	8909(1)	21(1)	1
Cl8	5136(1)	1037(1)	6946(1)	21(1)	1
Cl9	6104(1)	–131(1)	5669(1)	22(1)	1
Cl10	4726(1)	–593(1)	7349(1)	21(1)	1
O1	7164(2)	540(2)	7227(2)	17(1)	1
N1	7496(3)	2281(2)	46(3)	32(1)	1
N2	7448(3)	1170(2)	492(3)	34(1)	1
C1	7486(3)	1819(3)	701(4)	24(1)	1
C2	7521(4)	2024(3)	1690(4)	24(1)	1
C3	6989(4)	2567(3)	1981(4)	26(1)	1
C4	7024(4)	2752(3)	2915(4)	31(1)	1
C5	7606(4)	2411(3)	3554(4)	30(1)	1
C6	8148(4)	1879(3)	3264(4)	28(1)	1
C7	8114(4)	1685(3)	2344(4)	27(1)	1
N3	10262(3)	–3812(2)	4608(3)	26(1)	1
N4	11020(3)	–2937(2)	3923(3)	26(1)	1
C8	10454(3)	–3168(2)	4546(3)	19(1)	1
C9	10021(3)	–2694(2)	5201(3)	19(1)	1
C10	9844(3)	–2906(3)	6104(4)	23(1)	1
C11	9420(4)	–2460(3)	6699(4)	24(1)	1
C12	9179(4)	–1814(3)	6417(4)	28(1)	1
C13	9367(4)	–1601(3)	5519(4)	26(1)	1
C14	9802(3)	–2035(2)	4916(4)	24(1)	1
N5	4648(3)	2085(2)	3607(3)	33(1)	1
N6	5326(3)	1392(2)	4718(3)	23(1)	1
C15	5108(3)	2005(2)	4412(4)	20(1)	1
C16	5362(3)	2587(2)	4995(4)	20(1)	1
C17	4849(3)	3189(2)	4928(3)	20(1)	1
C18	5075(4)	3731(3)	5508(4)	24(1)	1
C19	5830(3)	3684(3)	6149(4)	22(1)	1
C20	6355(4)	3096(3)	6213(4)	23(1)	1
C21	6120(3)	2548(3)	5652(3)	21(1)	1
N7	12726(3)	–297(2)	6070(3)	28(1)	1
N8	11172(3)	–57(2)	5943(3)	32(1)	1
C22	11973(4)	–73(3)	6445(4)	24(1)	1
C23	12012(3)	165(3)	7420(4)	22(1)	1
C24	12860(4)	407(3)	7824(4)	25(1)	1
C25	12922(4)	594(3)	8747(4)	31(1)	1

C26	12143(4)	557(3)	9287(4)	29(1)	1
C27	11294(4)	328(3)	8886(4)	25(1)	1
C28	11225(4)	137(2)	7967(4)	21(1)	1
O2	8056(3)	3624(2)	520(3)	47(1)	1

Table A.12. Atomic coordinates [$\times 10^4$], equivalent isotropic displacement parameters [$Å^2 \times 10^3$] and site occupancy factors. U_{eq} is defined as one third of the trace of the orthogonalized U^{ij} tensor.

Thiourea – $PtCl_4^{2-}$

Identification code	
Empirical formula	$C_4H_{16}Cl_2N_8PtS_4$
Moiety formula	$Pt(SCN_2H_4)_4^{2+} . 2Cl^-$
Formula weight	570.48
Temperature	120(2) K
Wavelength	0.71073 Å
Crystal system	Monoclinic
Space group	*C*2/*c*
Unit cell dimensions	$a = 16.239(3)$ Å
	$b = 8.2985(17)$ Å $\beta = 113.49(3)°$
	$c = 12.824(3)$ Å
Volume	1584.9(6) $Å^3$
Z	4
Density (calculated)	2.391 Mg / m^3
Absorption coefficient	9.716 mm^{-1}
F(000)	1088
Crystal	Plate; Colourless
Crystal size	0.2 × 0.12 × 0.01 mm^3
θ range for data collection	3.45 – 27.48°
Index ranges	$-20 \leq h \leq 17, -10 \leq k \leq 10, -14 \leq l \leq 16$
Reflections collected	6163
Independent reflections	1817 [$R_{int} = 0.0382$]
Completeness to $\theta = 27.48°$	99.8 %
Absorption correction	Semi–empirical from equivalents
Max. and min. transmission	0.9091 and 0.2468
Refinement method	Full-matrix least-squares on F^2
Data / restraints / parameters	1817 / 18 / 88
Goodness-of-fit on F^2	1.038
Final *R* indices [$F^2 > 2\sigma(F^2)$]	*R1* = 0.0323, *wR2* = 0.0731
R indices (all data)	*R1* = 0.0447, *wR2* = 0.0810
Largest diff. peak and hole	2.674 and –2.076 e $Å^{-3}$

Table A.11: Crystal data and structure refinement details.

Atom	*x*	*y*	*z*	U_{eq}	*S.o.f.*
Pt1	2500	2500	0	12(1)	1
Cl1	4113(1)	−939(3)	705(2)	53(1)	1
S1A	1628(1)	295(3)	−19(2)	16(1)	0.72
C1A	527(5)	682(9)	−926(11)	17(1)	0.72
N1A	−17(5)	−558(9)	−1271(8)	22(1)	0.72
N2A	231(5)	2161(9)	−1238(7)	22(1)	0.72
S1B	1482(3)	588(7)	−1044(5)	16(1)	0.28
C1B	446(10)	1017(19)	−1020(30)	17(1)	0.28
N1B	−124(11)	−180(20)	−1160(20)	22(1)	0.28
N2B	216(12)	2484(19)	−846(19)	22(1)	0.28
S2A	3020(1)	2517(3)	1966(2)	16(1)	0.72
C2A	2127(5)	2866(10)	2339(6)	17(1)	0.72
N3A	1389(4)	3586(9)	1657(6)	22(1)	0.72
N4A	2203(6)	2373(9)	3356(6)	22(1)	0.72
S2B	1964(4)	2427(7)	1428(4)	16(1)	0.28
C2B	2826(15)	1940(30)	2691(19)	17(1)	0.28
N3B	3567(13)	1120(20)	2790(17)	22(1)	0.28
N4B	2713(15)	2400(20)	3642(19)	22(1)	0.28

Table A.12: Atomic coordinates [$\times 10^4$], equivalent isotropic displacement parameters [$Å^2 \times 10^3$] and site occupancy factors. U_{eq} is defined as one third of the trace of the orthogonalized U^{ij} tensor.

N,N-*bis*(3-aminophenyl)isophthalamide 67

Identification code	**67**	
Empirical formula	$C_{20}H_{18}N_4O_2$	
Formula weight	346.38	
Temperature	120(2) K	
Wavelength	0.71073 Å	
Crystal system	Rhombohedral	
Space group	*R*3*c*	
Unit cell dimensions	$a = 31.7794(7)$ Å	$\alpha = 90°$
	$b = 31.7794(7)$ Å	$\beta = 90°$
	$c = 8.5536(2)$ Å	$\gamma = 120°$
Volume	7481.2(3) Å^3	
Z	18	
Density (calculated)	1.384 Mg / m^3	
Absorption coefficient	0.093 mm^{-1}	
F(000)	3276	
Crystal	Needle; colourless	
Crystal size	0.20 × 0.05 × 0.05 mm^3	
θ range for data collection	3.08 – 27.46°	
Index ranges	$-38 \le h \le 41$, $-37 \le k \le 32$, $-11 \le l \le 8$	
Reflections collected	11269	
Independent reflections	3436 [$R_{int} = 0.0539$]	
Completeness to $\theta = 27.46°$	99.8 %	
Absorption correction	Semi–empirical from equivalents	
Max. and min. transmission	0.9954 and 0.9817	
Refinement method	Full-matrix least-squares on F^2	
Data / restraints / parameters	3436 / 1 / 244	
Goodness-of-fit on F^2	1.042	
Final *R* indices [$F^2 > 2\sigma(F^2)$]	*R1* = 0.0428, *wR2* = 0.0936	
R indices (all data)	*R1* = 0.0555, *wR2* = 0.0997	
Absolute structure parameter	0.9(14)	
Extinction coefficient	0.00079(11)	
Largest diff. peak and hole	0.246 and –0.276 e Å^{-3}	

Table A.13: Crystal data and structure refinement.

Atom	*x*	*y*	*z*	U_{eq}	*S.o.f.*
C1	8472(1)	890(1)	−3093(2)	17(1)	1
C2	8410(1)	518(1)	−4096(2)	17(1)	1
C3	7981(1)	74(1)	−4042(3)	20(1)	1
C4	7616(1)	2(1)	−3006(3)	24(1)	1
C5	7677(1)	372(1)	−2011(3)	22(1)	1
C6	8106(1)	819(1)	−2046(2)	18(1)	1
C7	8792(1)	595(1)	−5277(2)	17(1)	1
C8	9684(1)	1050(1)	−5693(3)	17(1)	1
C9	9728(1)	764(1)	−6823(2)	18(1)	1
C10	10158(1)	954(1)	−7703(3)	21(1)	1
C11	10541(1)	1414(1)	−7362(3)	26(1)	1
C12	10493(1)	1694(1)	−6200(3)	25(1)	1
C13	10067(1)	1515(1)	−5355(3)	22(1)	1
C14	8170(1)	1209(1)	−936(2)	19(1)	1
C15	8603(1)	2107(1)	−622(2)	18(1)	1
C16	9080(1)	2481(1)	−799(2)	19(1)	1
C17	9235(1)	2938(1)	−164(2)	19(1)	1
C18	8901(1)	3012(1)	671(3)	22(1)	1
C19	8431(1)	2633(1)	871(3)	25(1)	1
C20	8271(1)	2177(1)	223(3)	24(1)	1
N1	9255(1)	886(1)	−4785(2)	17(1)	1
N2	10205(1)	673(1)	−8873(2)	29(1)	1
N3	8466(1)	1668(1)	−1449(2)	20(1)	1
N4	9721(1)	3313(1)	−306(2)	21(1)	1
O1	8678(1)	409(1)	−6583(2)	22(1)	1
O2	7971(1)	1110(1)	370(2)	24(1)	1

Table A.14: Atomic coordinates [$\times 10^4$], equivalent isotropic displacement parameters [$Å^2 \times 10^3$] and site occupancy factors. U_{eq} is defined as one third of the trace of the orthogonalized U^{ij} tensor.

A.3 Graphics of ion chromatography

A.3.1 Macro prep High Q 63

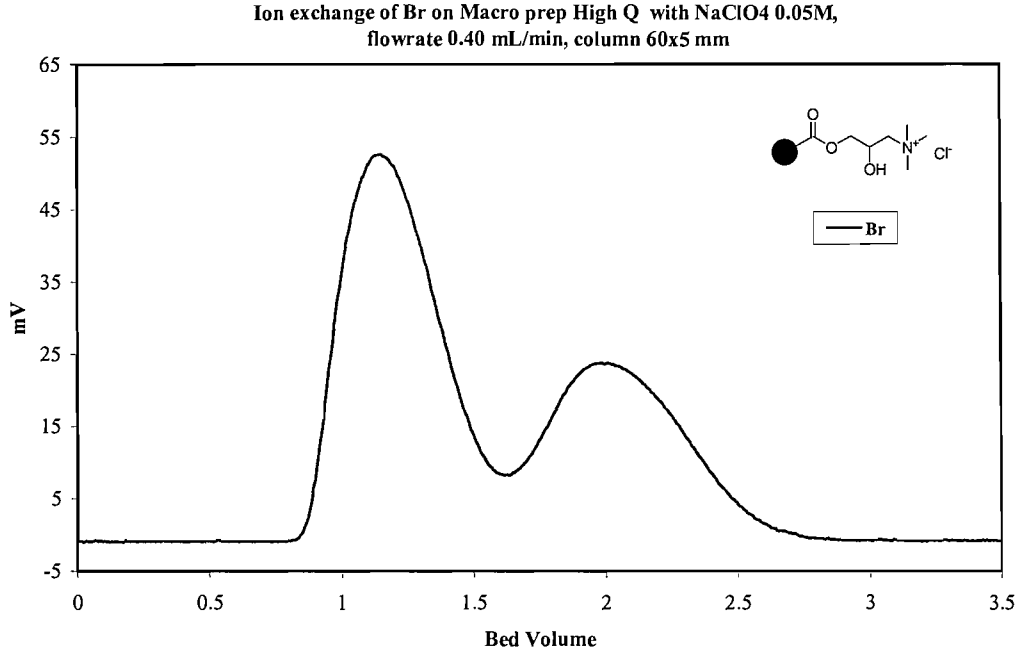

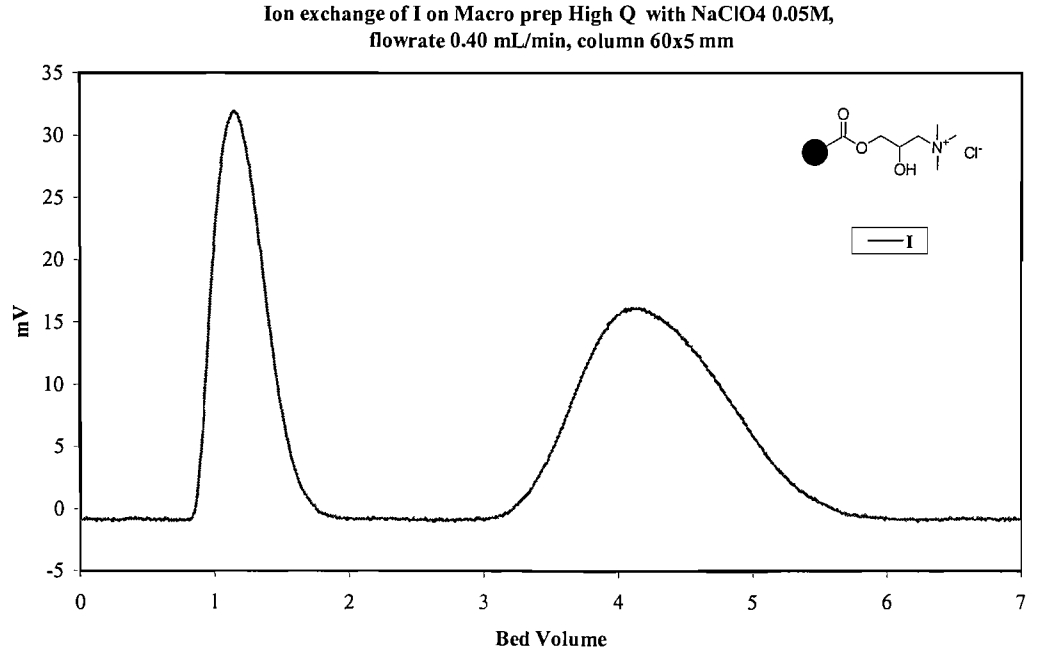

Ion exchange of NO3 on Macro prep High Q with NaClO4 0.05M, flowrate 0.40 mL/min, column 60x5 mm

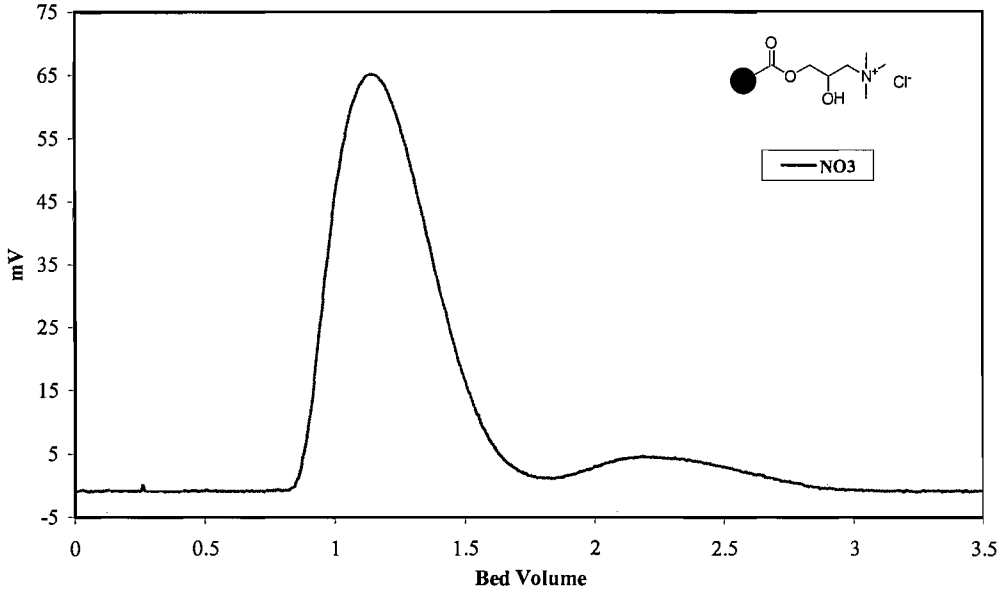

Ion exchange of S2O3 on Macro prep High Q with NaClO4 0.05M, flowrate 0.40 mL/min, column 60x5 mm

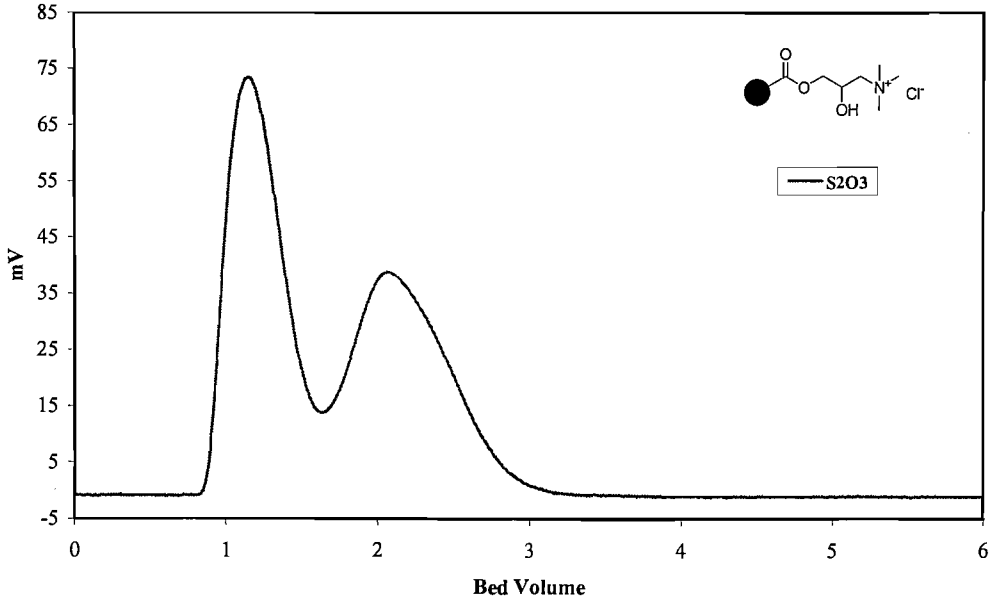

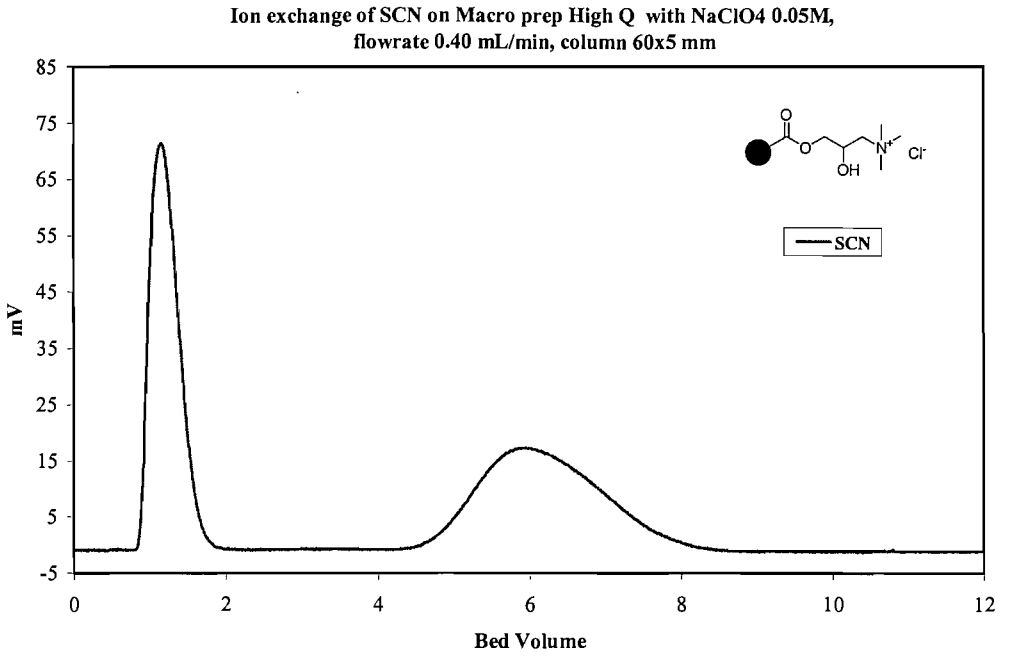

A.3.2 Methacrylate resin derivatives 31

A.3.2.1 Separation in 0.05M $NaClO_4$

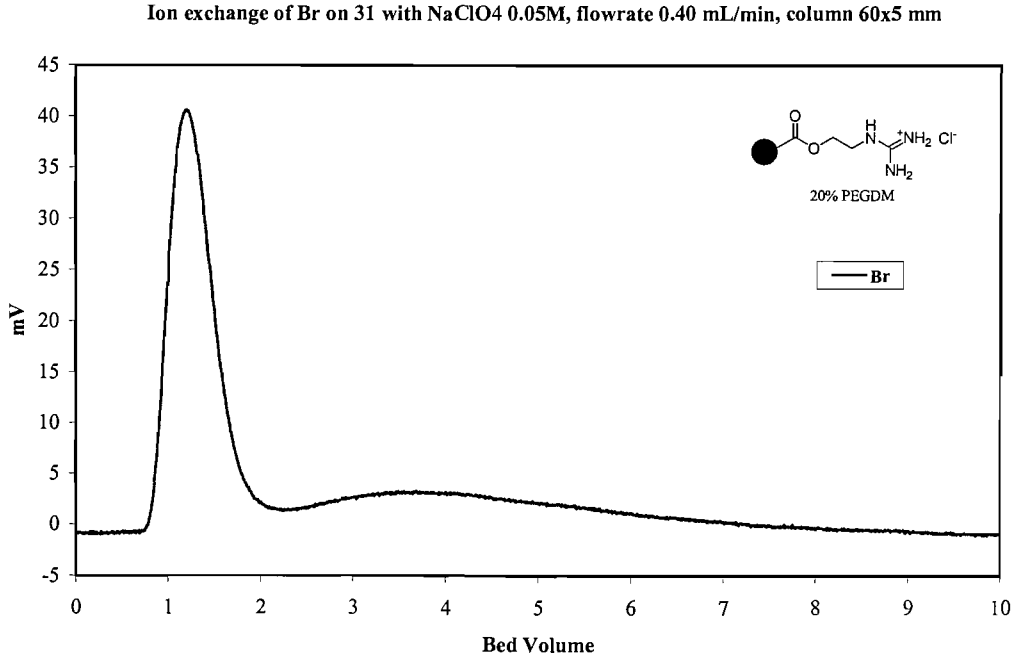

Ion exchange of I on 31 with NaClO4 0.05M, flowrate 0.40 mL/min, column 60x5 mm

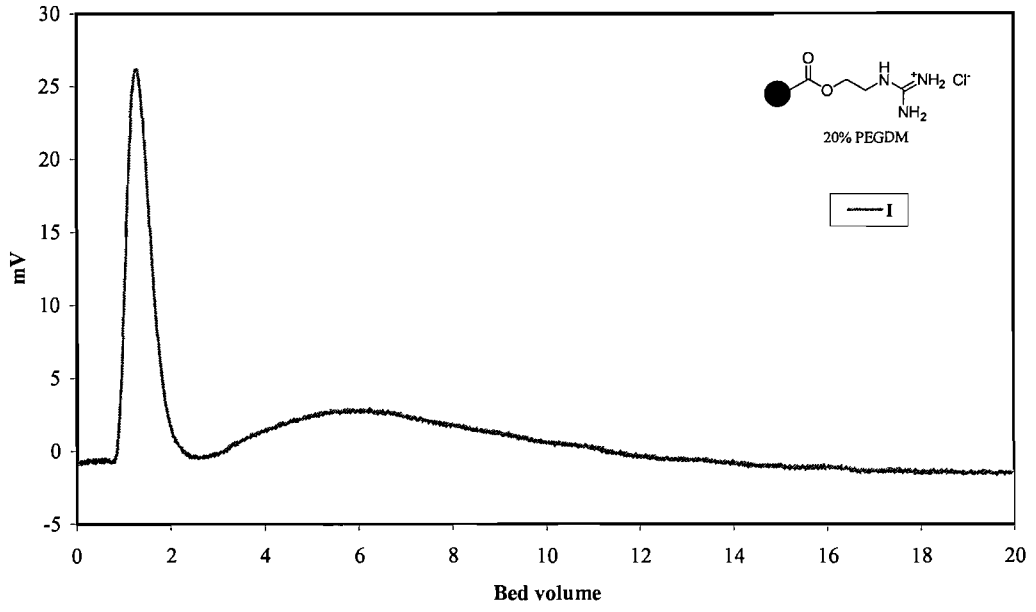

Ion exchange of NO3 on 31 with NaClO4 0.05M, flowrate 0.40 mL/min, column 60x5 mm

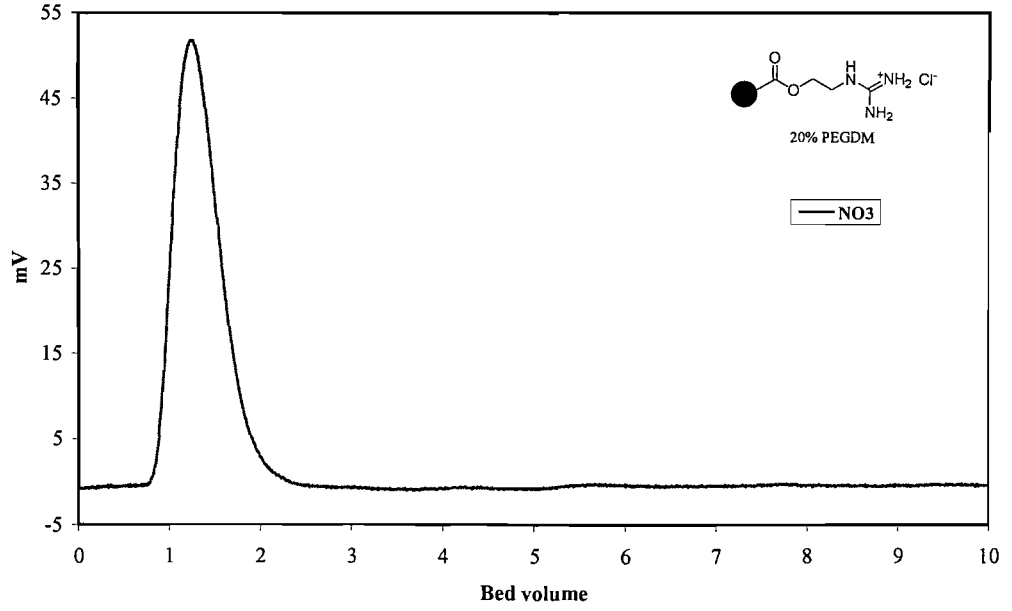

Ion exchange of S2O3 on 31 with NaClO4 0.05M, flowrate 0.40 mL/min, column 60x5 mm

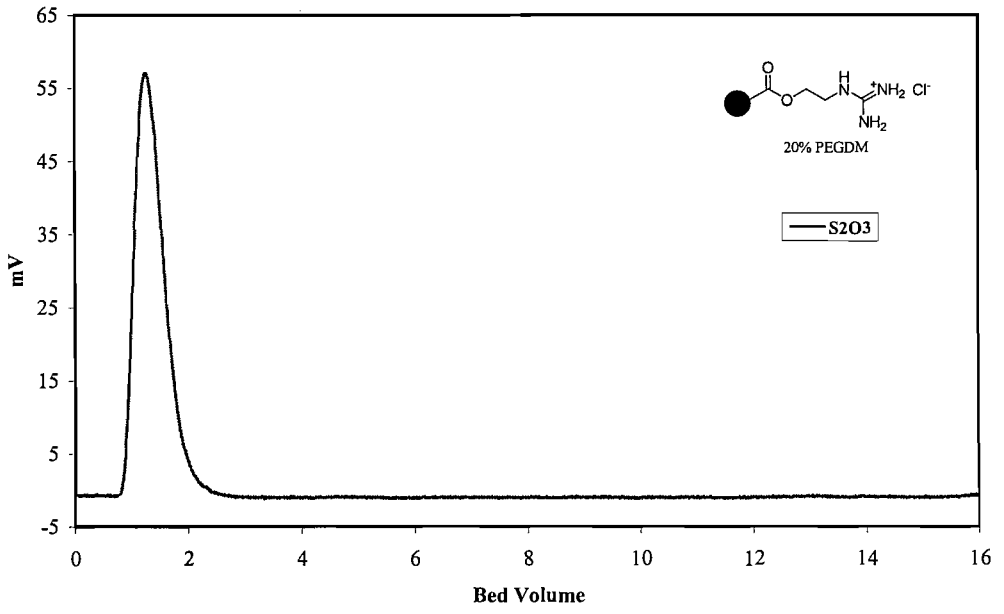

Ion exchange of SCN on 31 with NaClO4 0.05M, flowrate 0.40 mL/min, column 60x5 mm

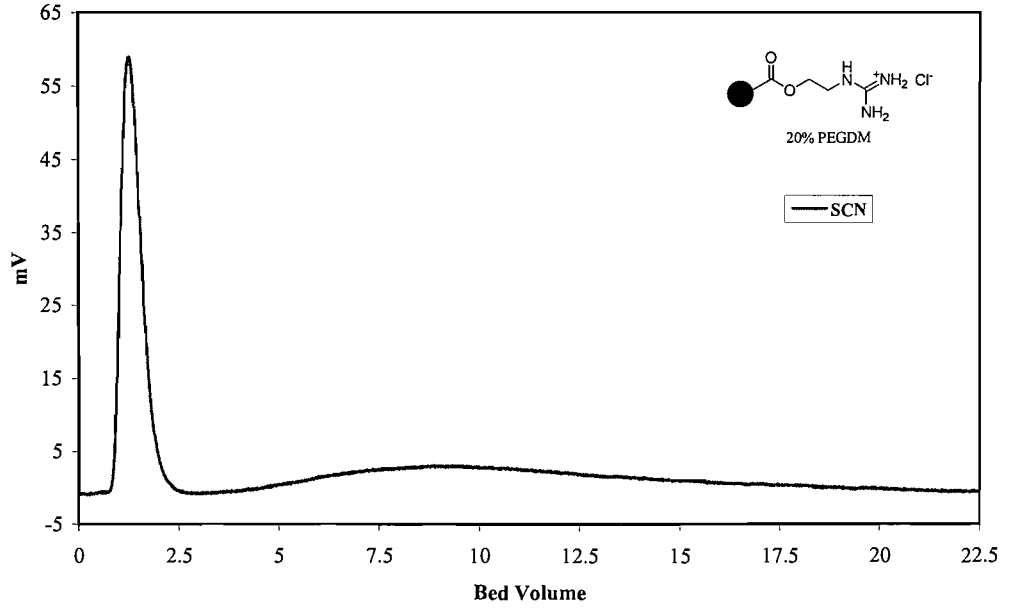

A.3.2.2 Separation in 0.5M $NaClO_4$

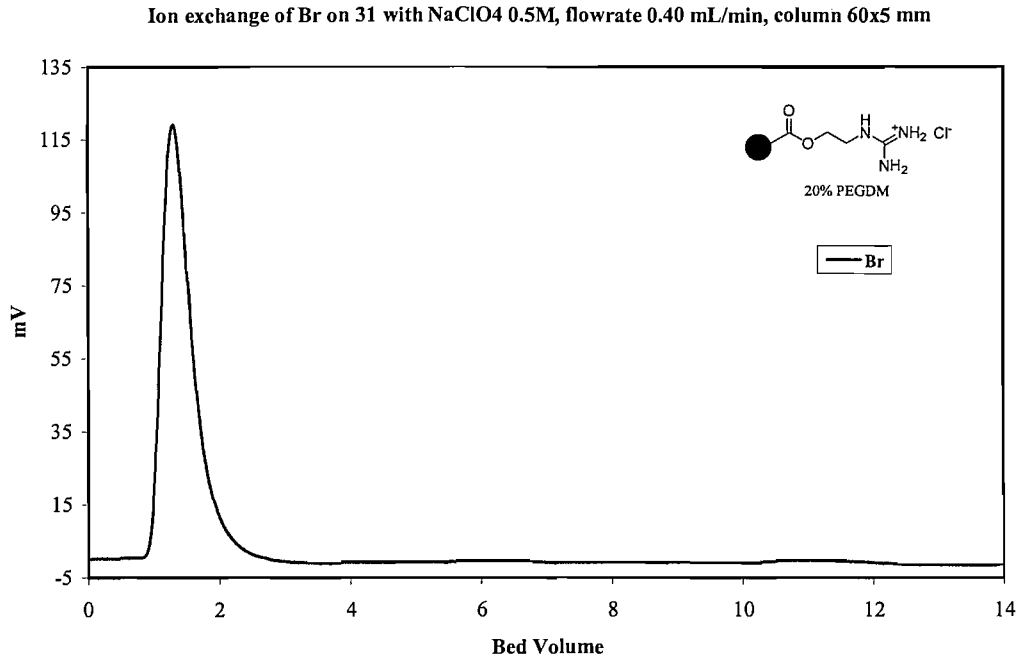

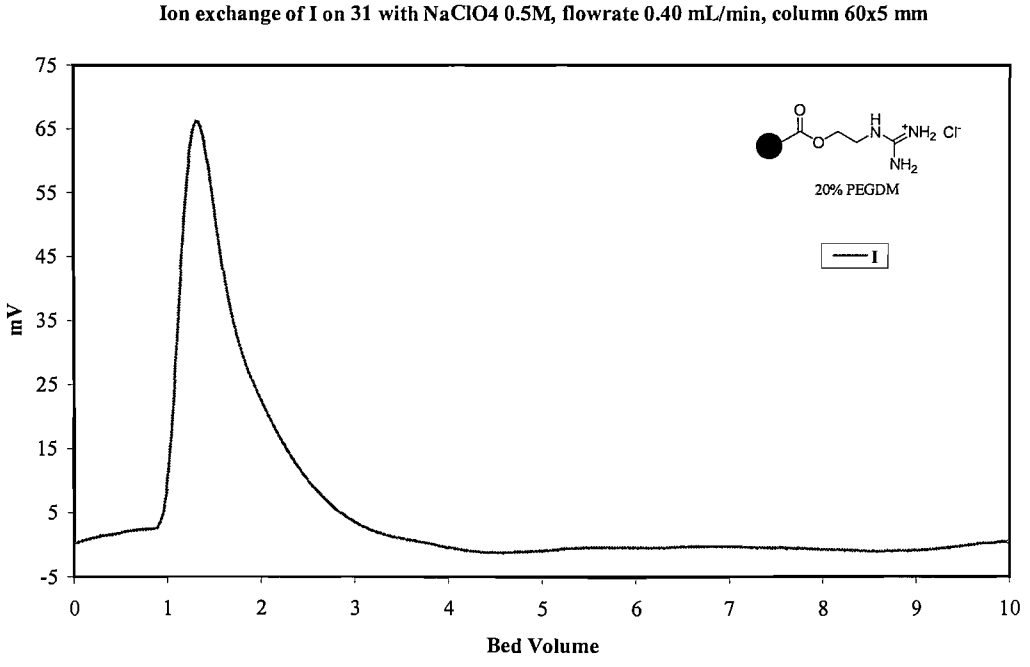

Ion exchange of NO3 on 31 with NaClO4 0.5M, flowrate 0.40 mL/min, column 60x5 mm

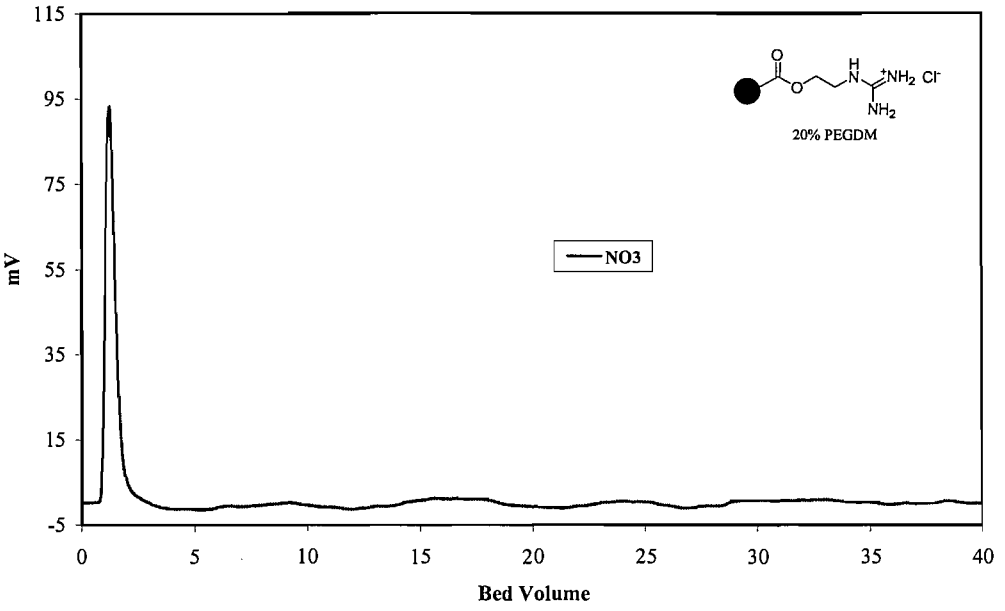

Ion exchange of S2O3 on 31 with NaClO4 0.5M, flowrate 0.40 mL/min, column 60x5 mm

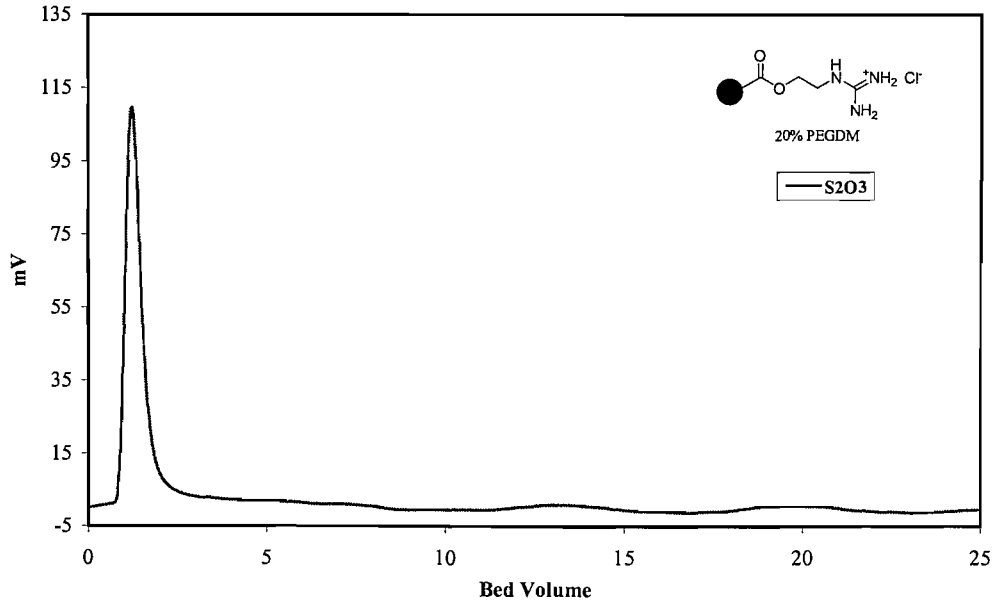

Ion exchange of SCN on 31 with NaClO4 0.5M, flowrate 0.40 mL/min, column 60x5 mm

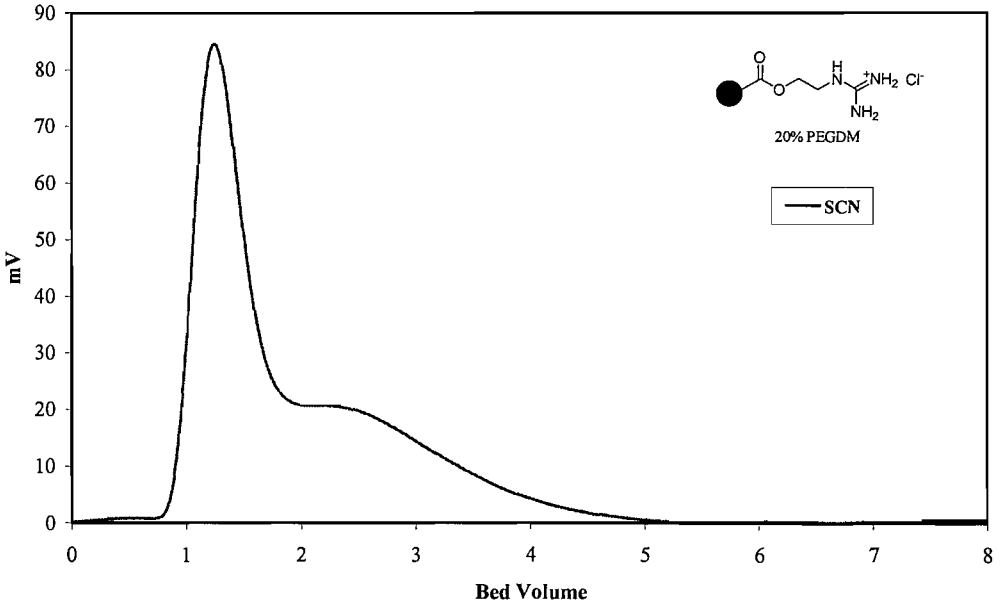

Ion exchange of SO4 on 31 with NaClO4 0.5M, flowrate 0.40 mL/min, column 60x5 mm

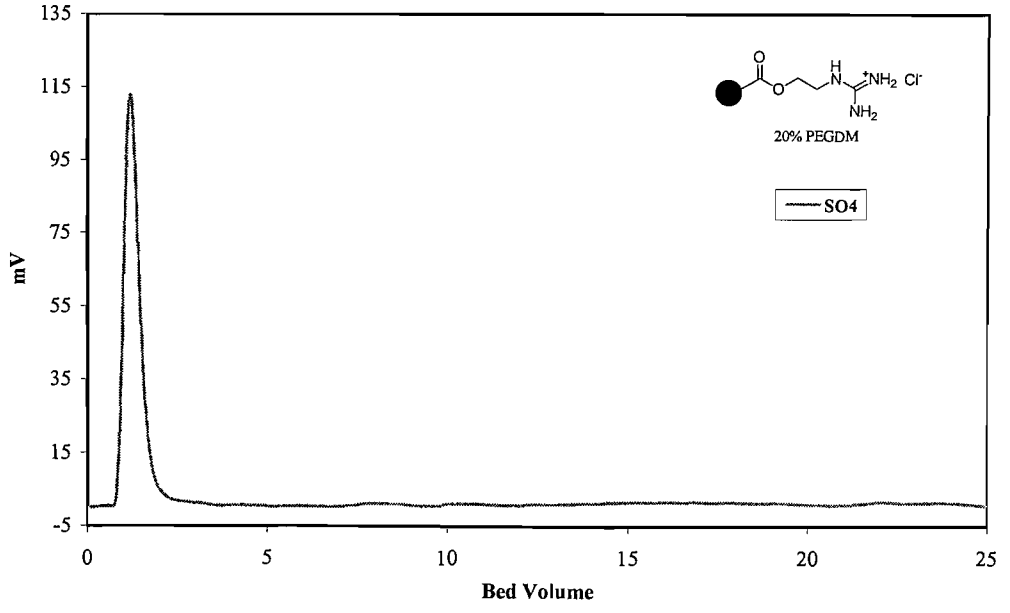

Ion exchange of H2PO4 on 31 with NaClO4 0.5M, flowrate 0.40 mL/min, column 60x5 mm

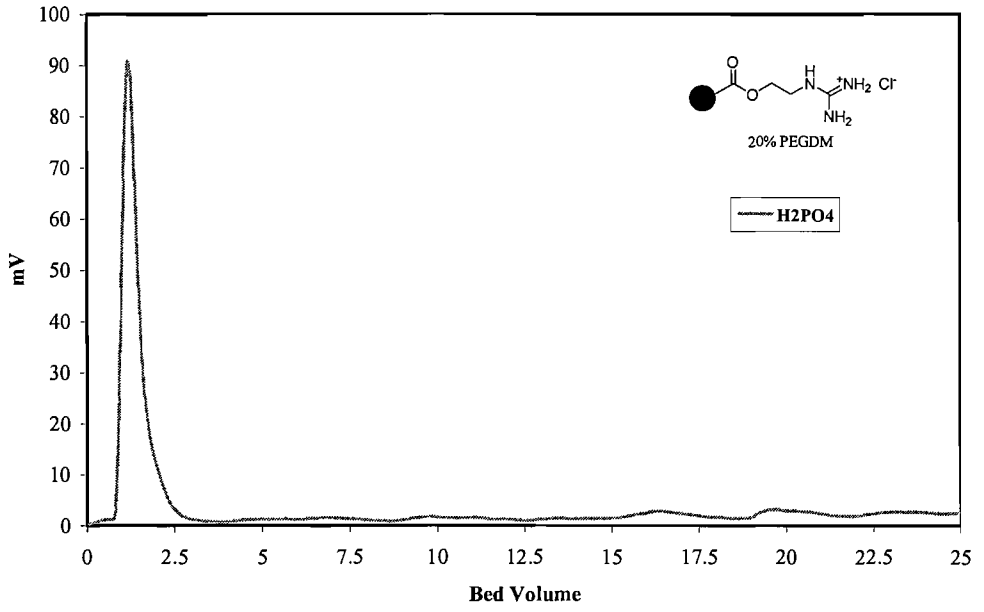

Ion exchange of HPO4 on 31 with NaClO4 0.5M, flowrate 0.40 mL/min, column 60x5 mm

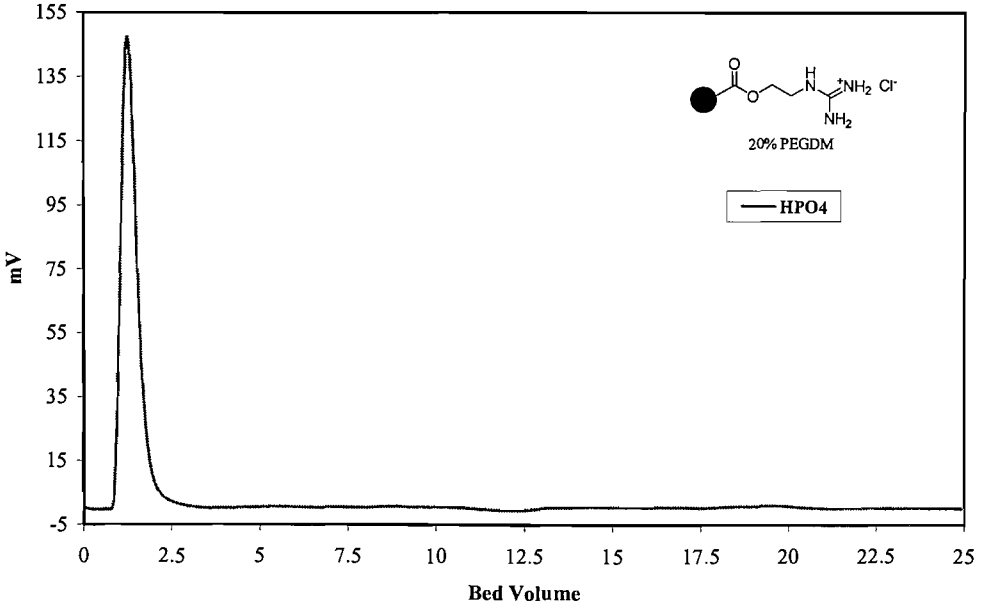

Ion exchange of PO4 on 31 with NaClO4 0.5M, flowrate 0.40 mL/min, column 60x5 mm

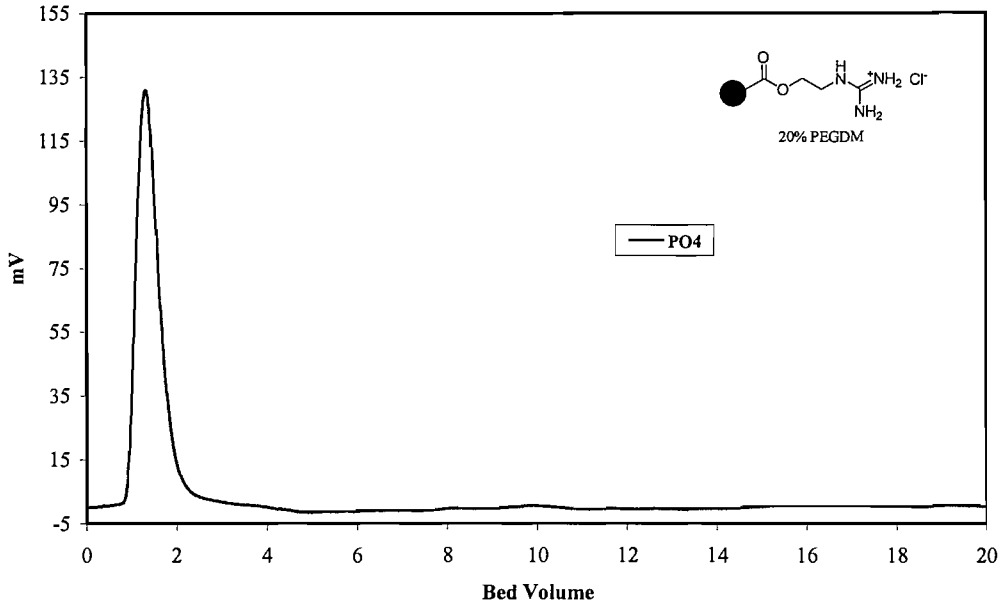

Ion exchange of AMP on 31 with NaClO4 0.5M, flowrate 0.40 mL/min, column 60x5 mm

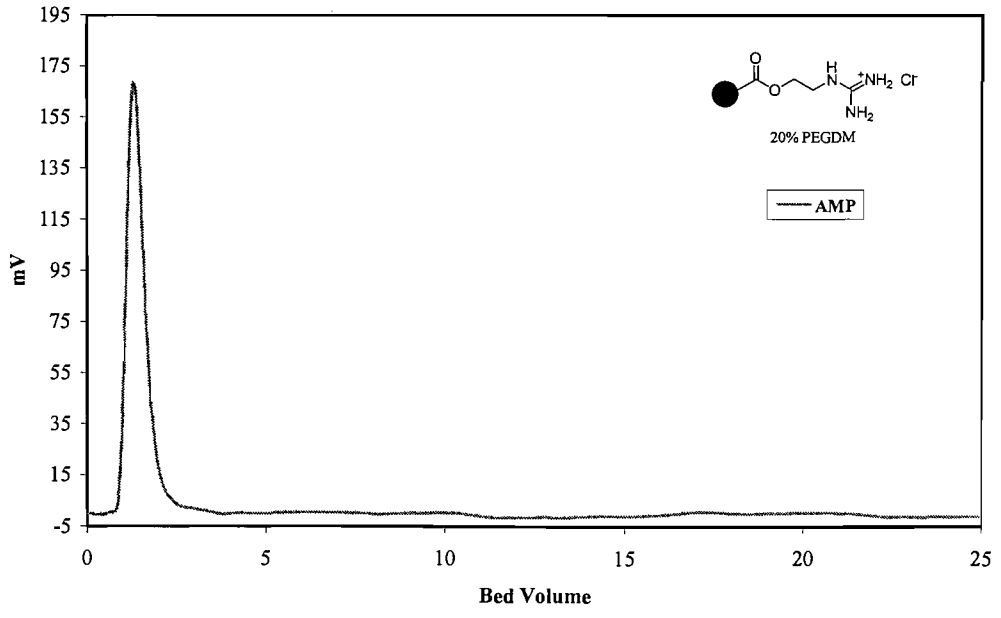

Ion exchange of ADP on 31 with NaClO4 0.5M, flowrate 0.40 mL/min, column 60x5 mm

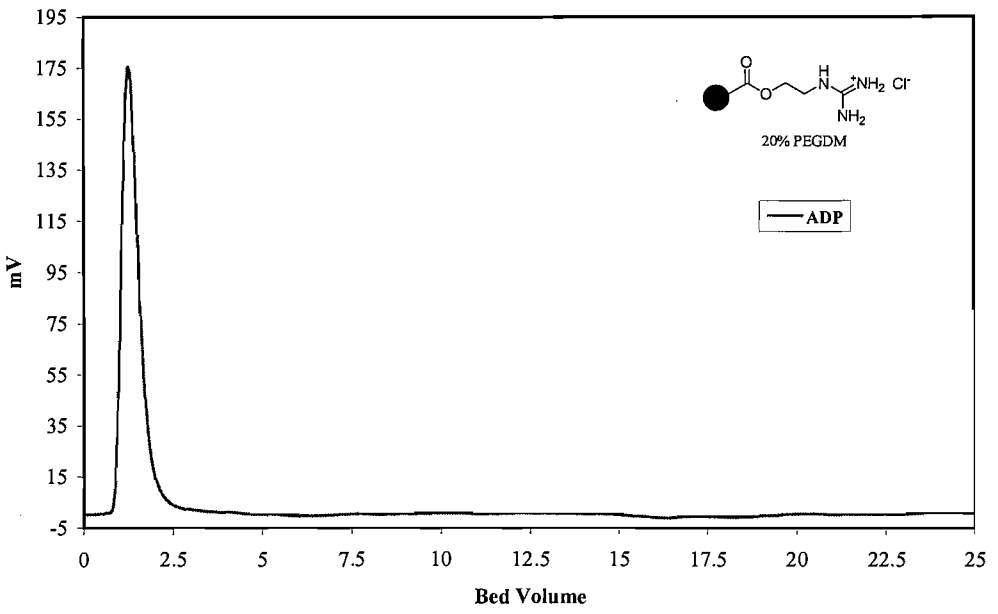

Ion exchange of ATP on 31 with NaClO4 0.5M, flowrate 0.40 mL/min, column 60x5 mm

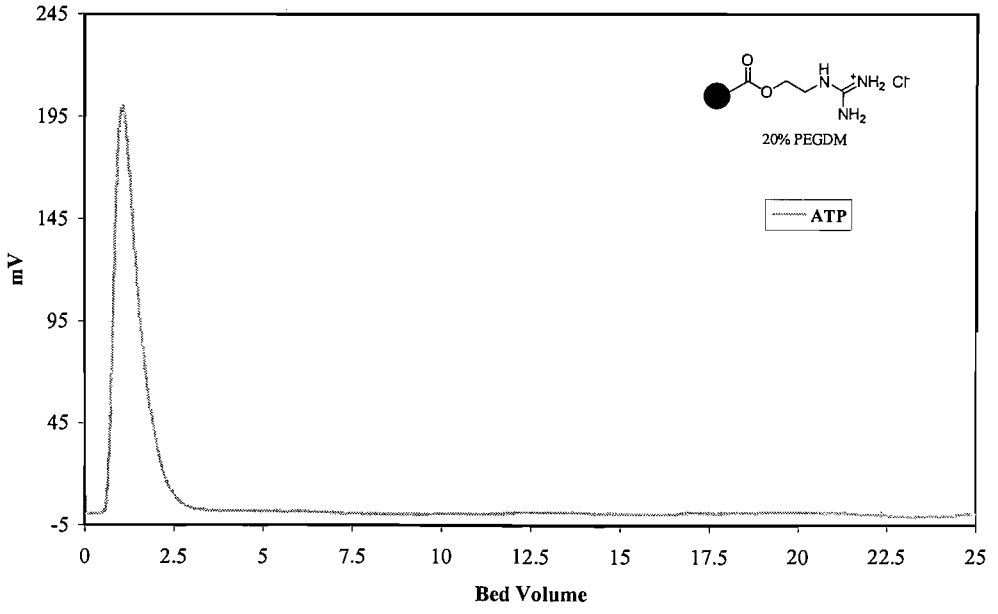

A.3.3 Silica gel derivatives

A.3.3.1 Silica supporting ammonium **61**

A.3.3.1.1 Separation in 0.05M $NaClO_4$

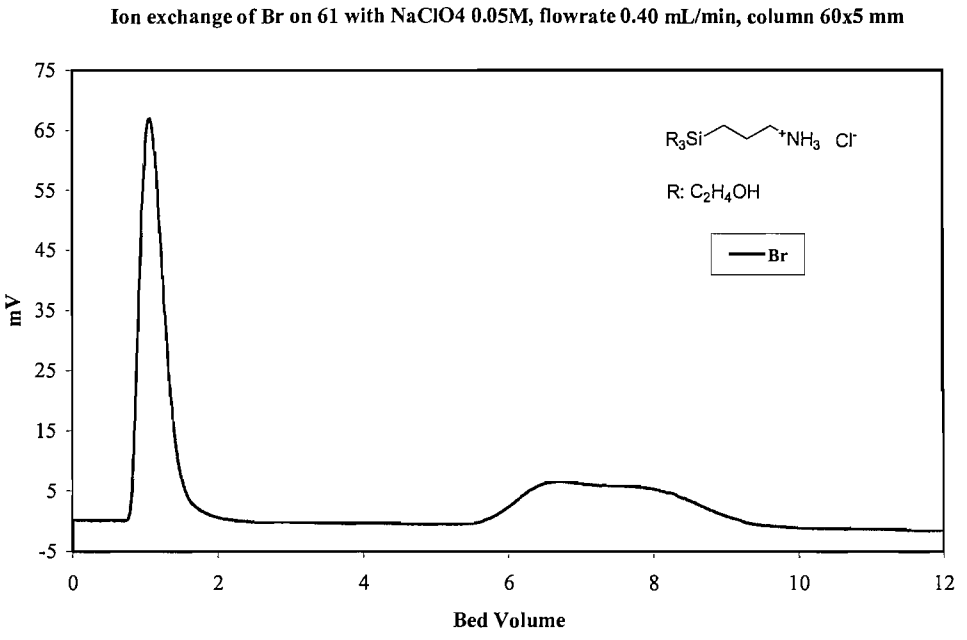

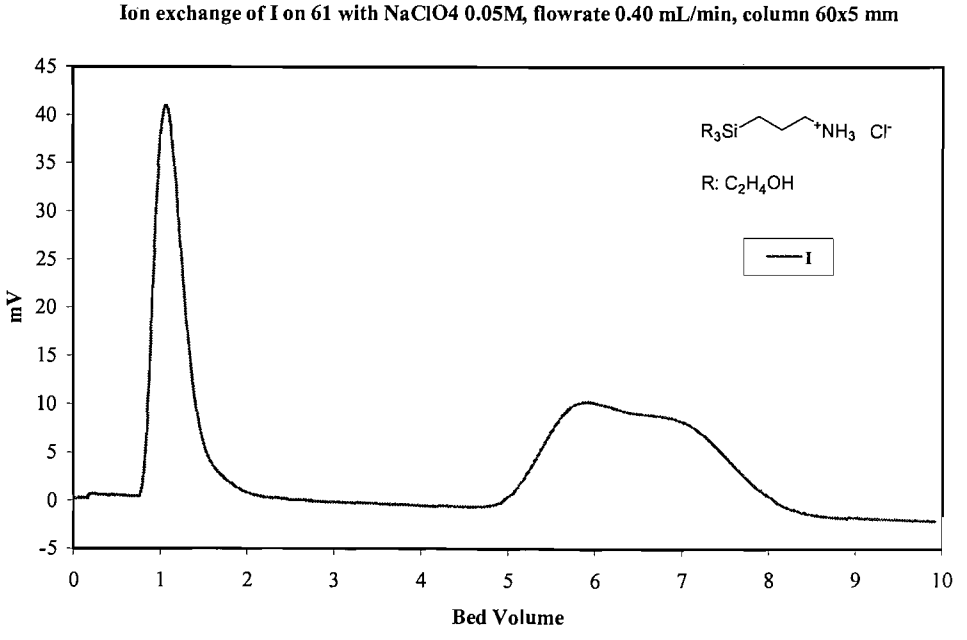

Ion exchange of NO3 on 61 with NaClO4 0.05M, flowrate 0.40 mL/min, column 60x5 mm

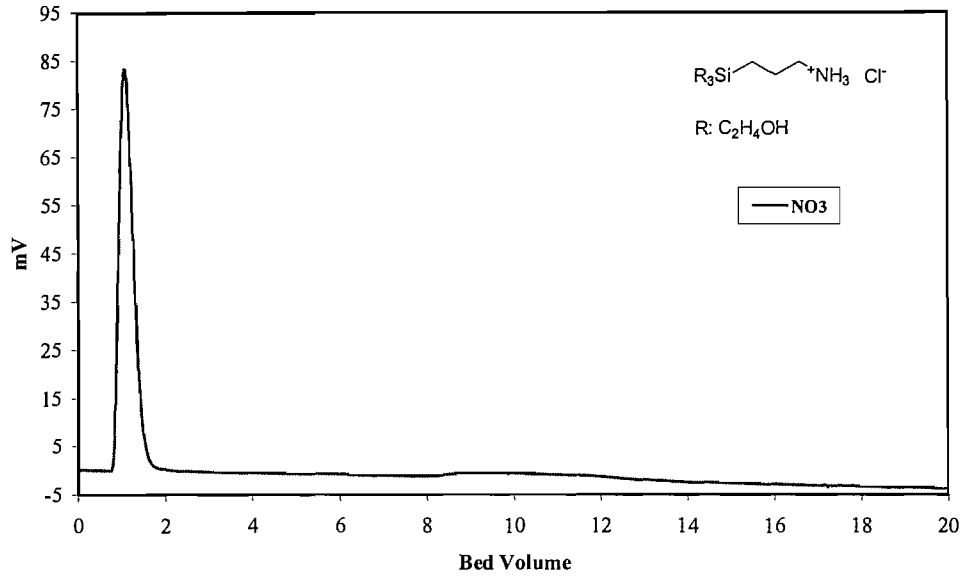

Ion exchange of SCN on 61 with NaClO4 0.05M, flowrate 0.40 mL/min, column 60x5 mm

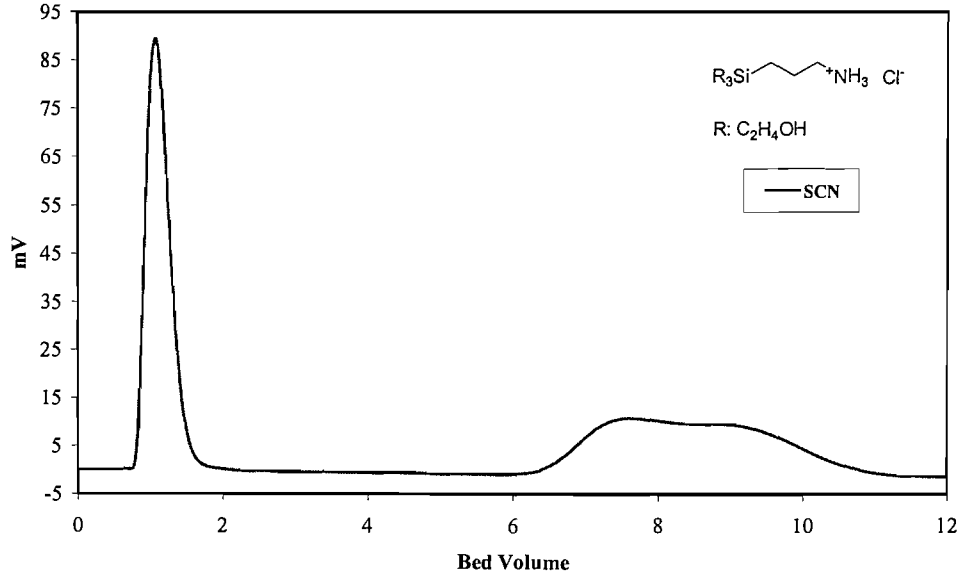

Ion exchange of S2O3 on 61 with NaClO4 0.05M, flowrate 0.40 mL/min, column 60x5 mm

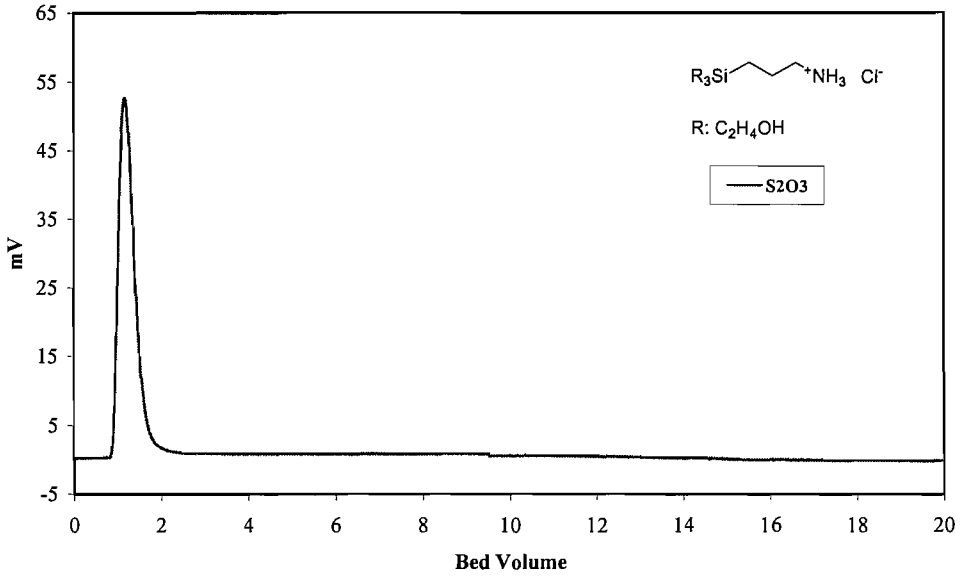

Ion exchange of ADP on 61 with NaClO4 0.05M, flowrate 0.40 mL/min, column 60x5 mm

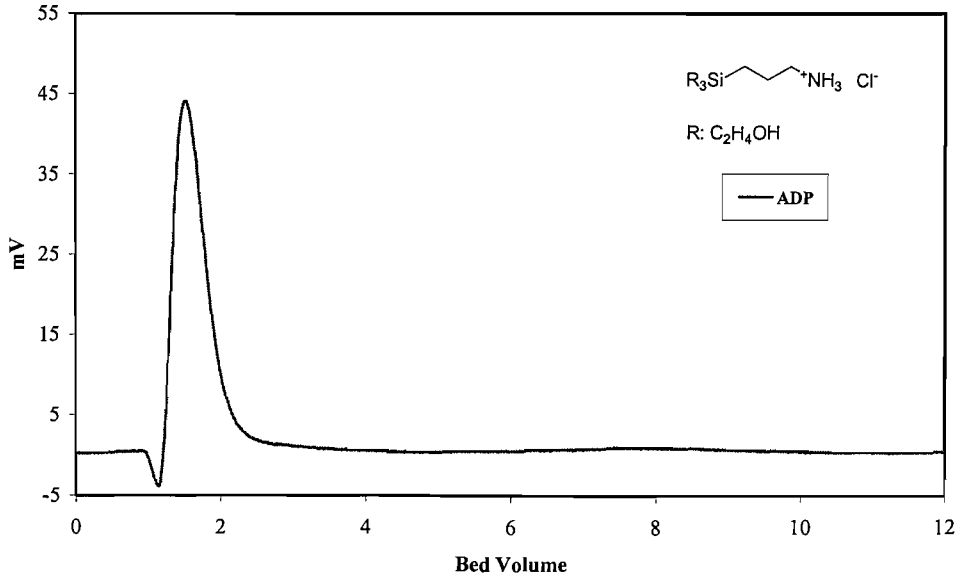

A.3.3.1.2 Separation in 0.5M $NaClO_4$

Ion exchange of Br on 61 with NaClO4 0.5M, flowrate 0.40 mL/min, column 60x5 mm

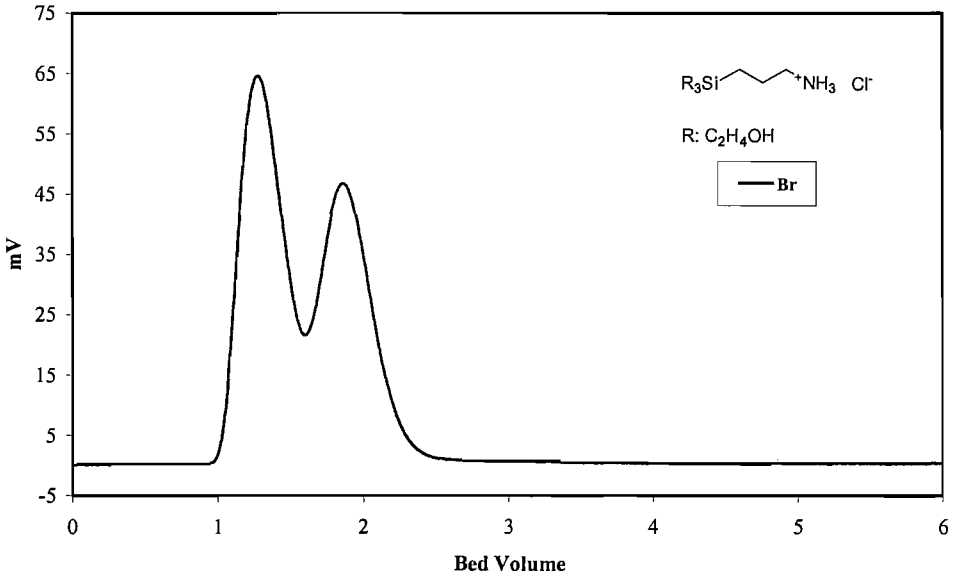

Ion exchange of I on 61 with NaClO4 0.5M, flowrate 0.40 mL/min, column 60x5 mm

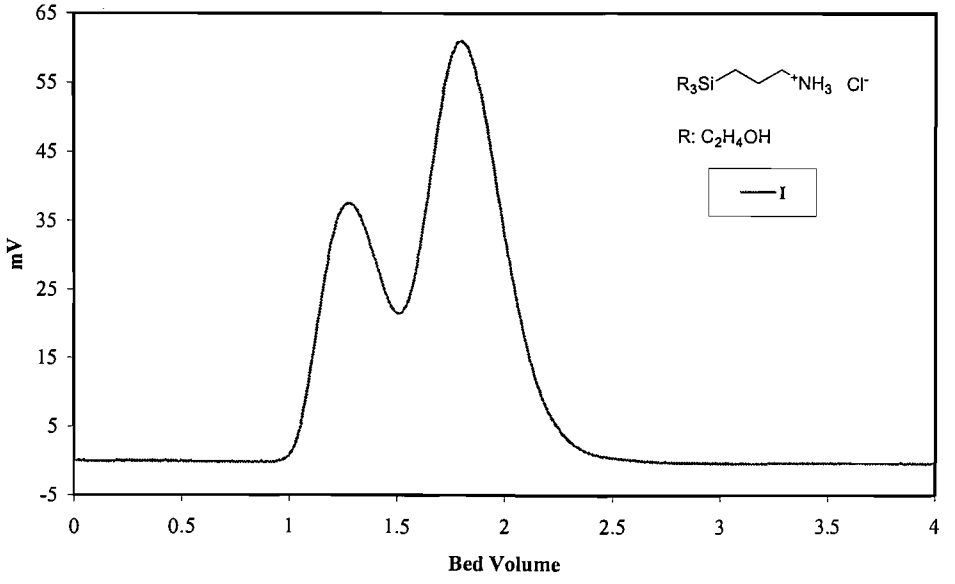

Ion exchange of NO3 on 61 with NaClO4 0.5M, flowrate 0.40 mL/min, column 60x5 mm

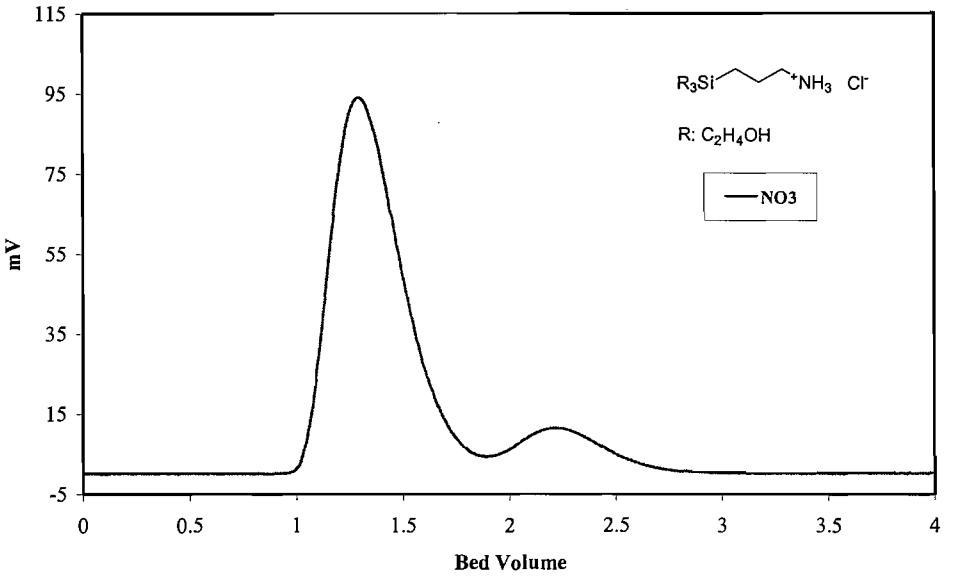

Ion exchange of SCN on 61 with NaClO4 0.5M, flowrate 0.40 mL/min, column 60x5 mm

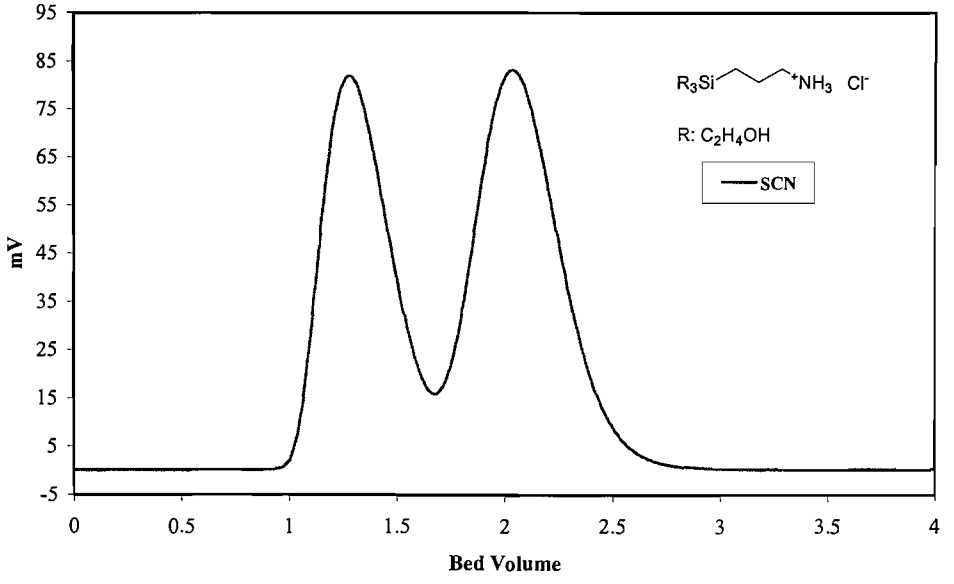

Ion exchange of S2O3 on 61 with NaClO4 0.5M, flowrate 0.40 mL/min, column 60x5 mm

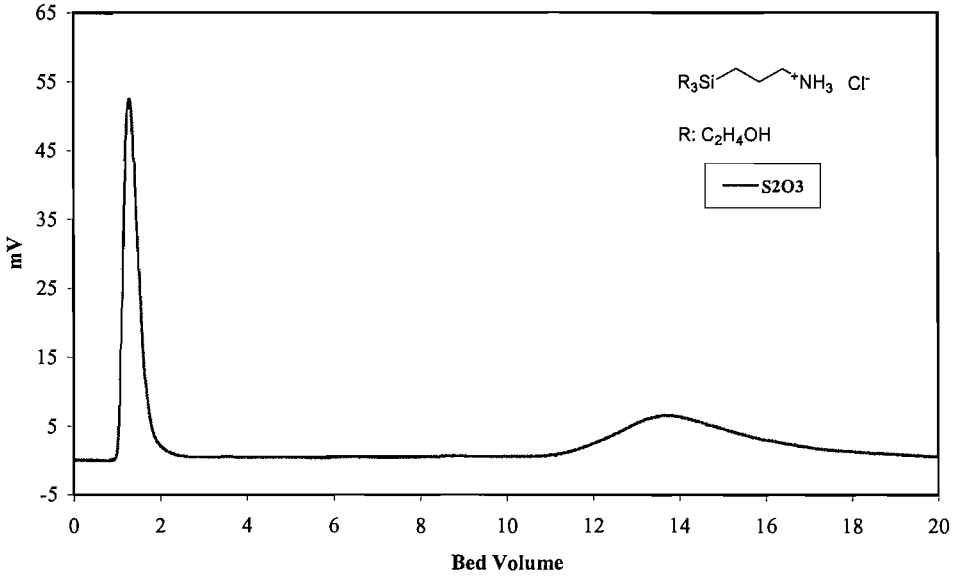

Ion exchange of SO4 on 61 with NaClO4 0.5M, flowrate 0.40 mL/min, column 60x5 mm

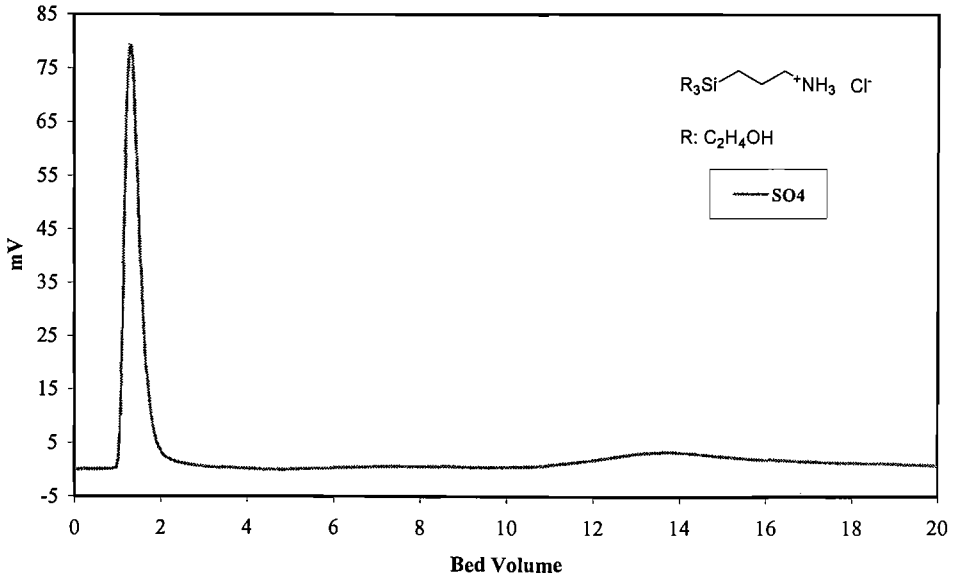

Ion exchange of HPO4 on 61 with NaClO4 0.5M, flowrate 0.40 mL/min, column 60x5 mm

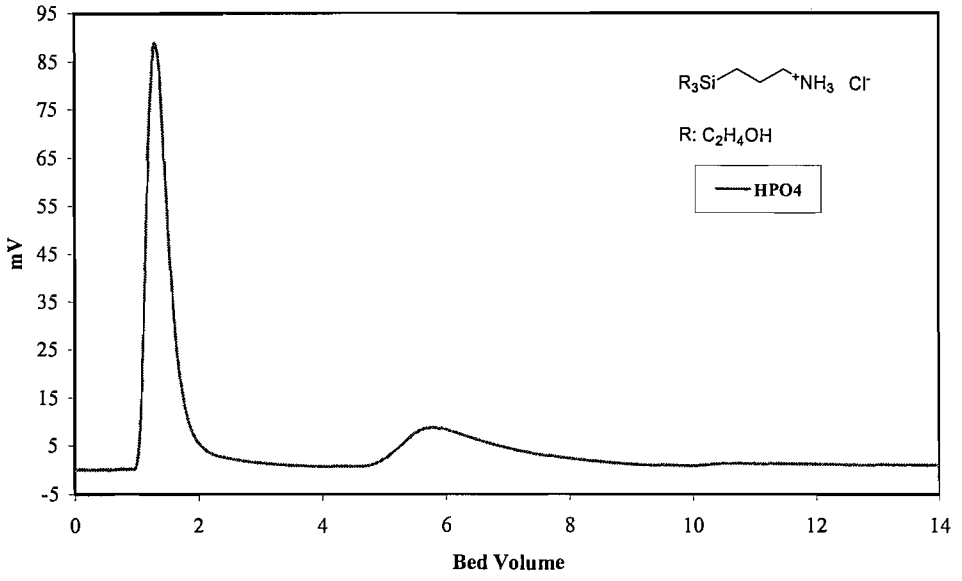

Ion exchange of H2PO4 on 61 with NaClO4 0.5M, flowrate 0.40 mL/min, column 60x5 mm

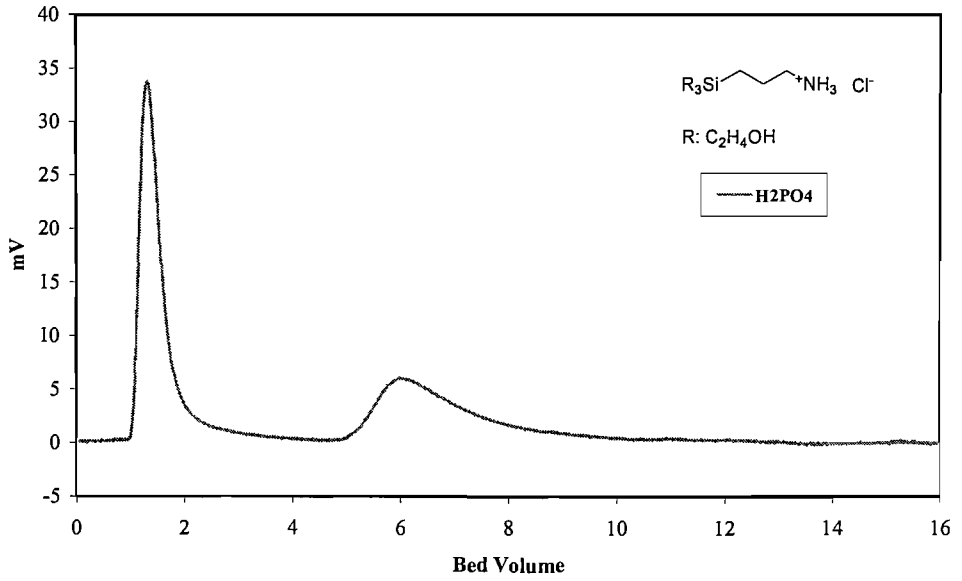

Ion exchange of AMP on 61 with NaClO4 0.5M, flowrate 0.40 mL/min, column 60x5 mm

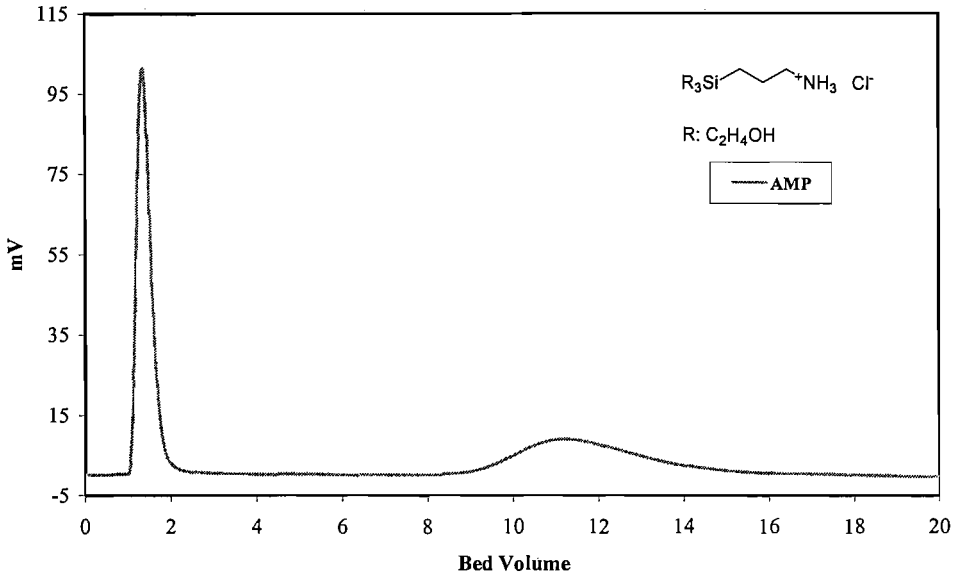

Ion exchange of ADP on 61 with NaClO4 0.5M, flowrate 0.40 mL/min, column 60x5 mm

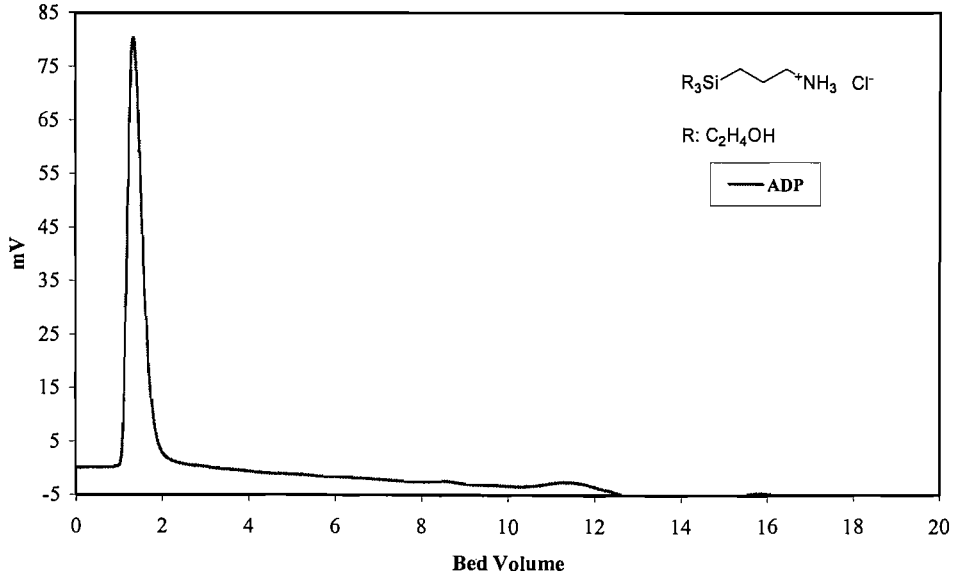

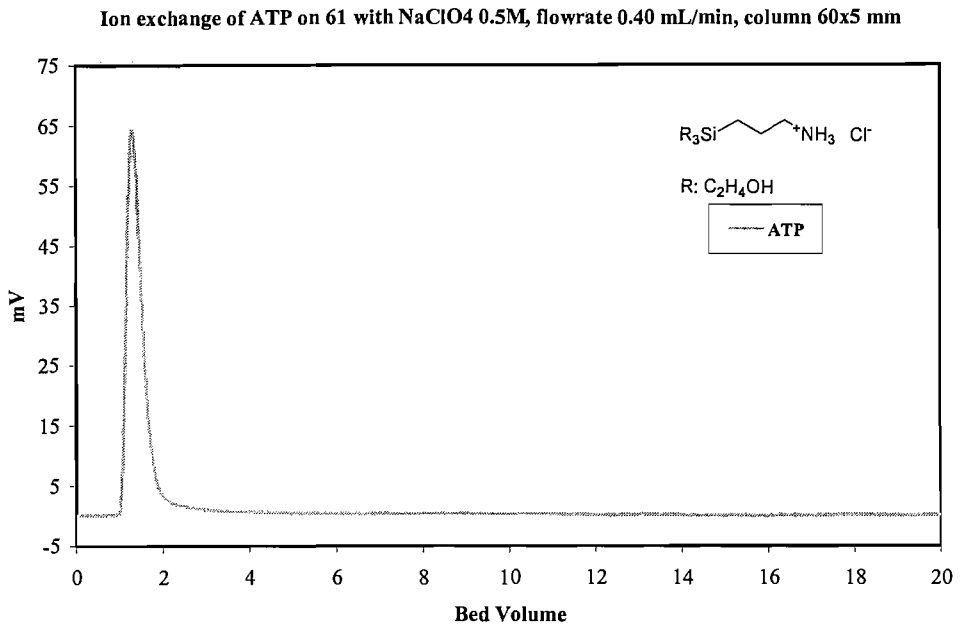

A.3.3.2 Silica supporting guanidinium group **28**

A.3.3.2.1 Separation in 0.05M $NaClO_4$

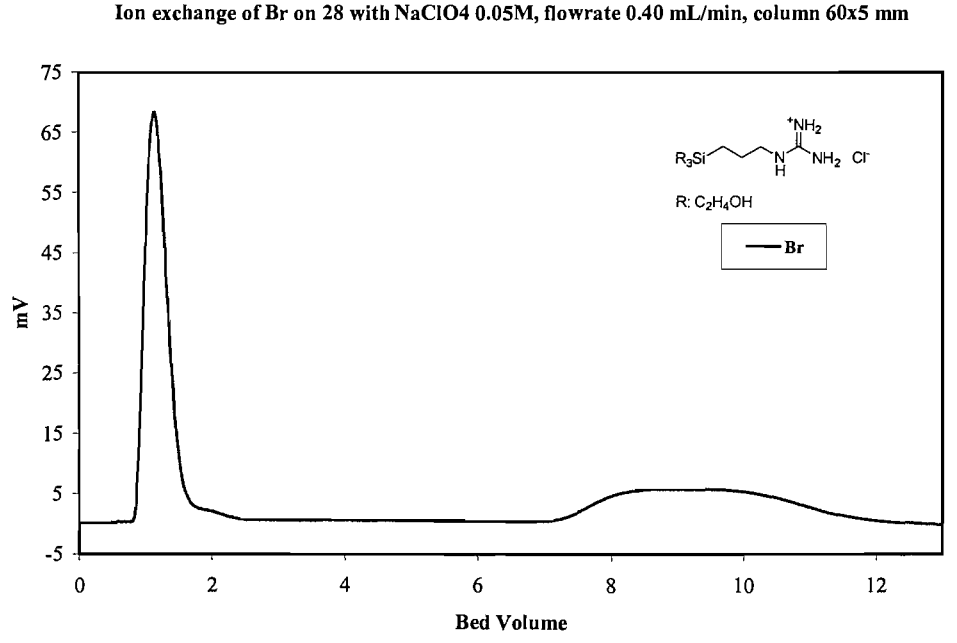

Ion exchange of I on 28 with NaClO4 0.05M, flowrate 0.40 mL/min, column 60x5 mm

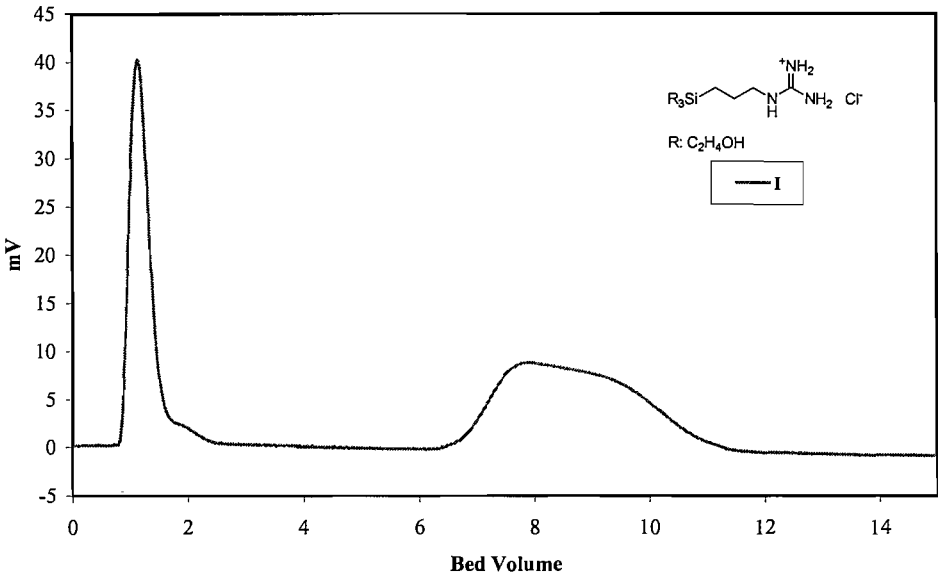

Ion exchange of NO3 on 28 with NaClO4 0.05M, flowrate 0.40 mL/min, column 60x5 mm

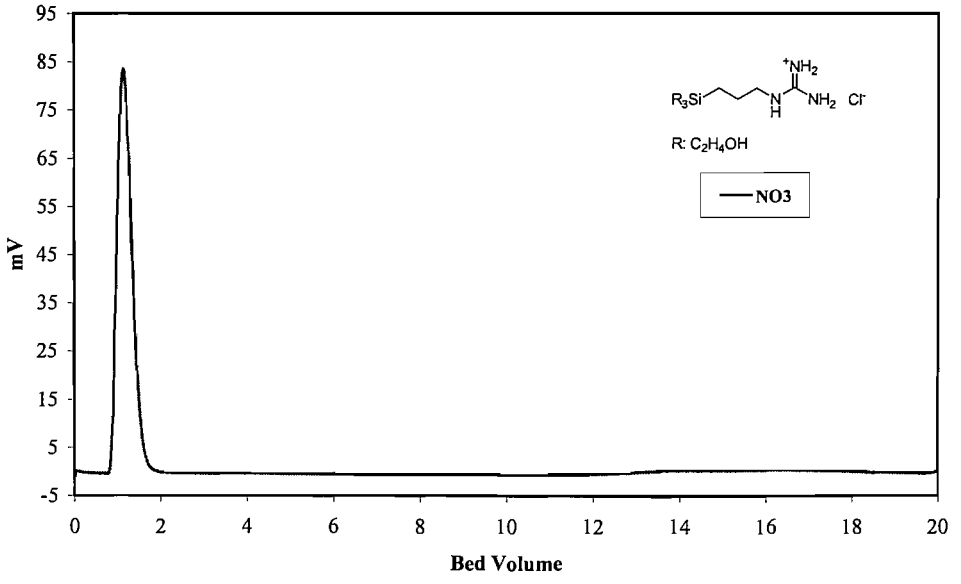

Ion exchange of S2O3 on 28 with NaClO4 0.05M, flowrate 0.40 mL/min, column 60x5 mm

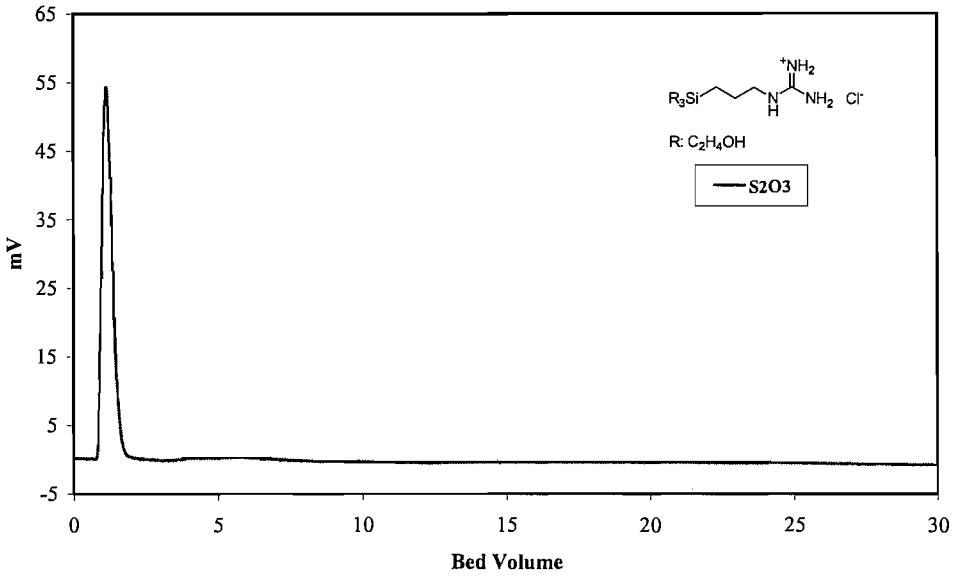

Ion exchange of SCN on 28 with NaClO4 0.05M, flowrate 0.40 mL/min, column 60x5 mm

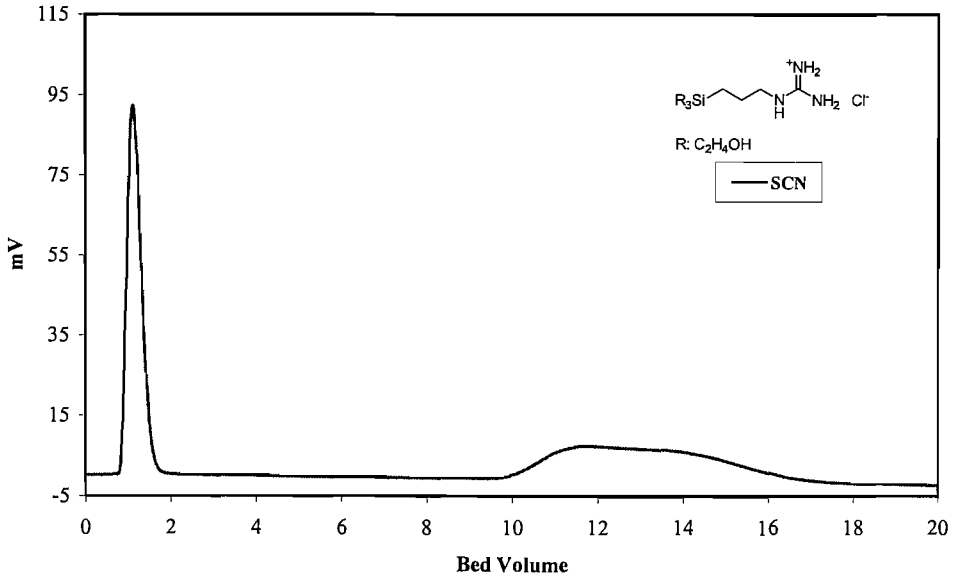

Ion exchange of HPO4 on 28 with NaClO4 0.05M, flowrate 0.40 mL/min, column 60x5 mm

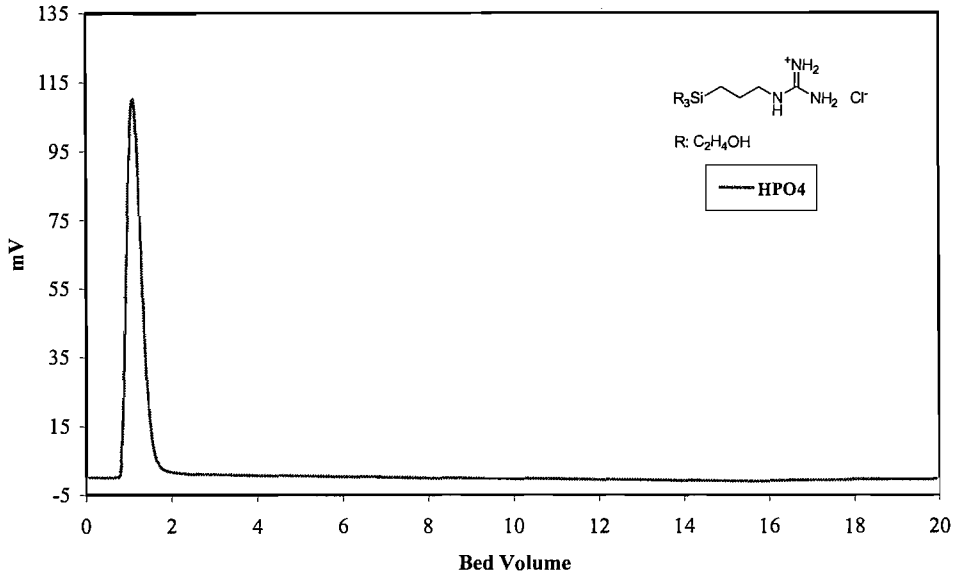

Ion exchange of H2PO4 on 28 with NaClO4 0.05M, flowrate 0.40 mL/min, column 60x5 mm

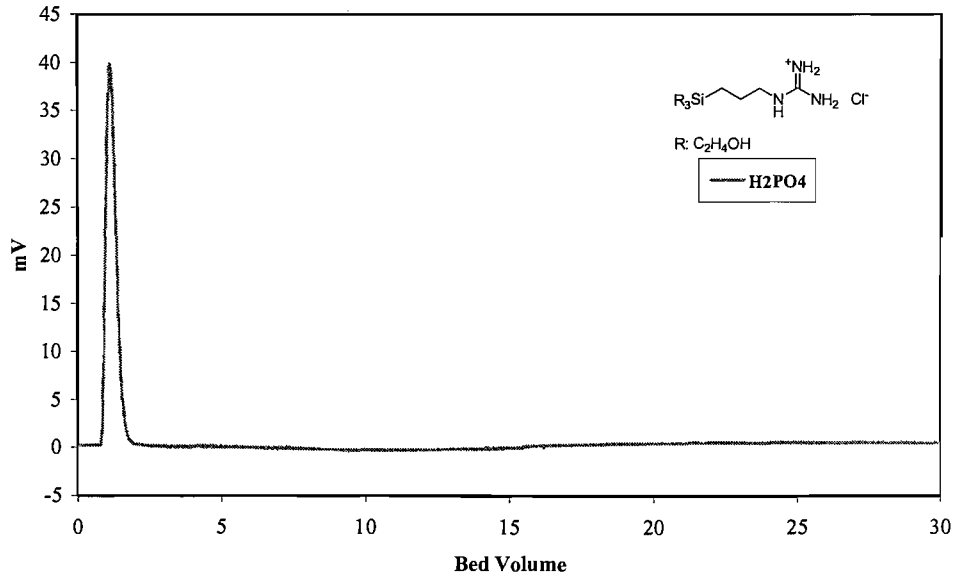

A.3.3.2.2 Separation in 0.5M $NaClO_4$

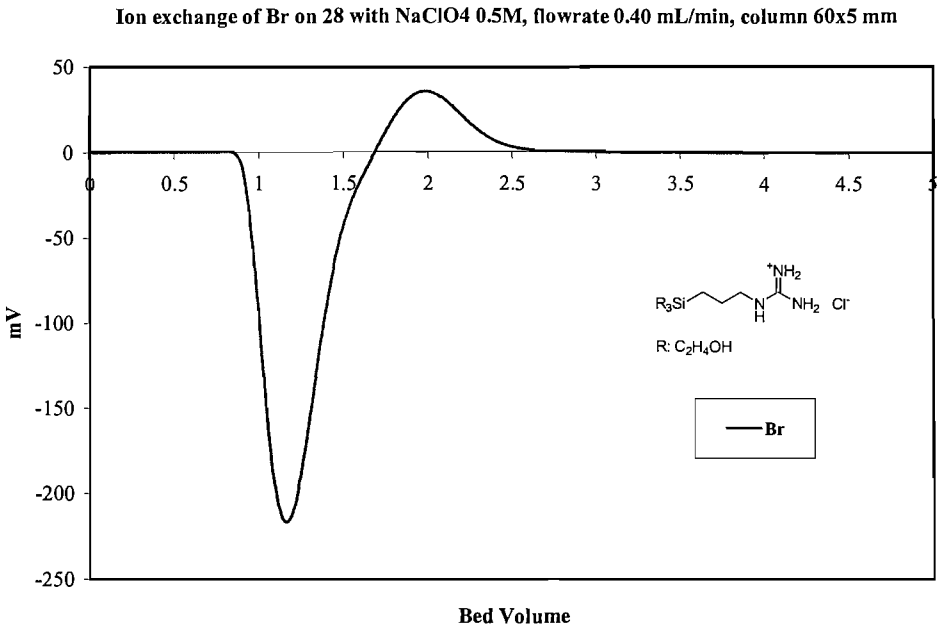

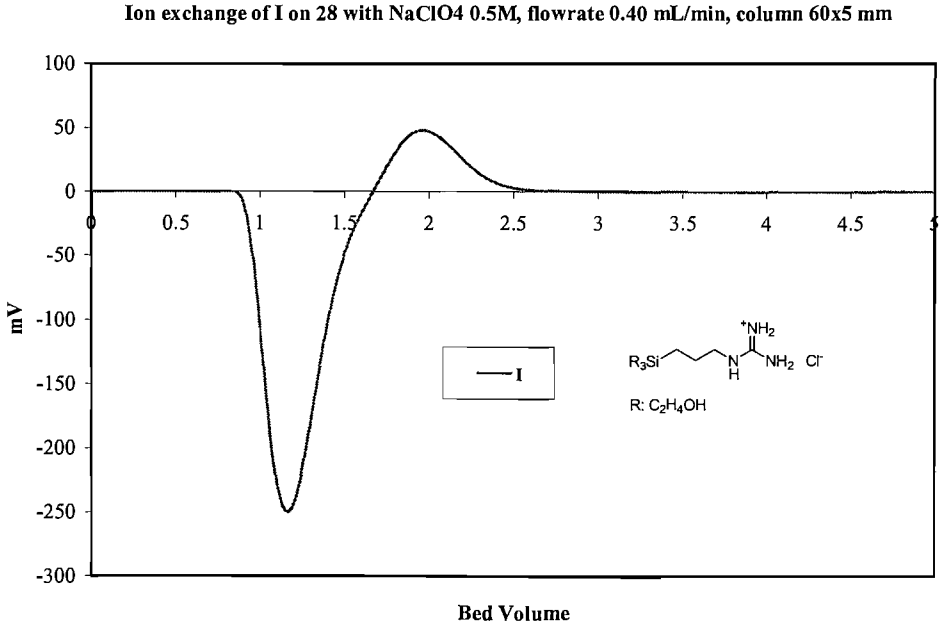

Ion exchange of NO3 on 28 with NaClO4 0.5M, flowrate 0.40 mL/min, column 60x5 mm

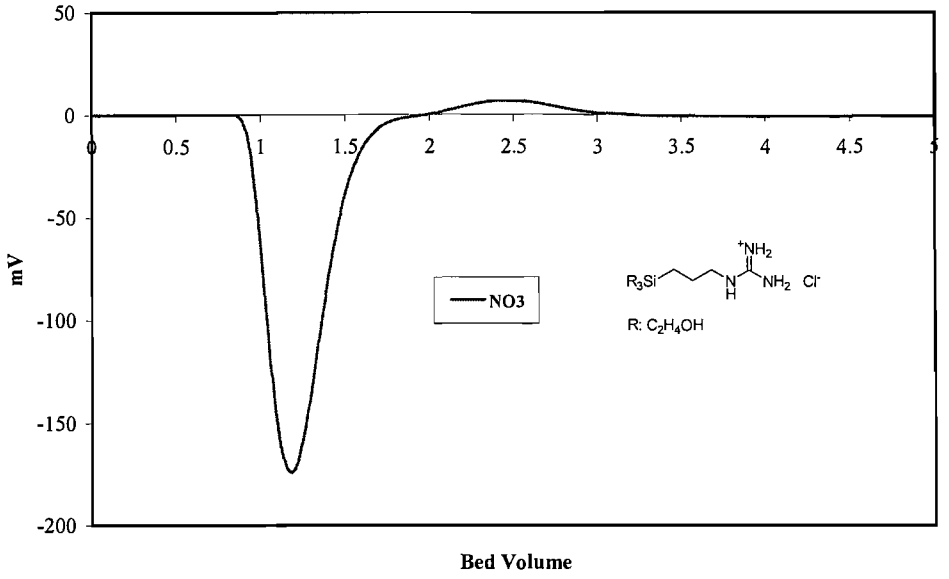

Bed Volume

Ion exchange of S2O3 on 28 with NaClO4 0.5M, flowrate 0.40 mL/min, column 60x5 mm

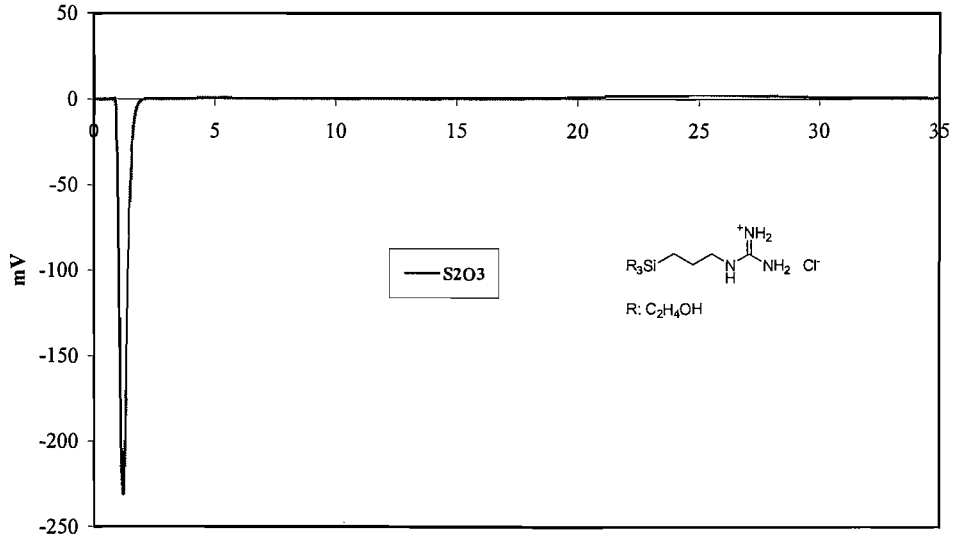

Bed Volume

Ion exchange of SO4 on 28 with NaClO4 0.5M, flowrate 0.40 mL/min, column 60x5 mm

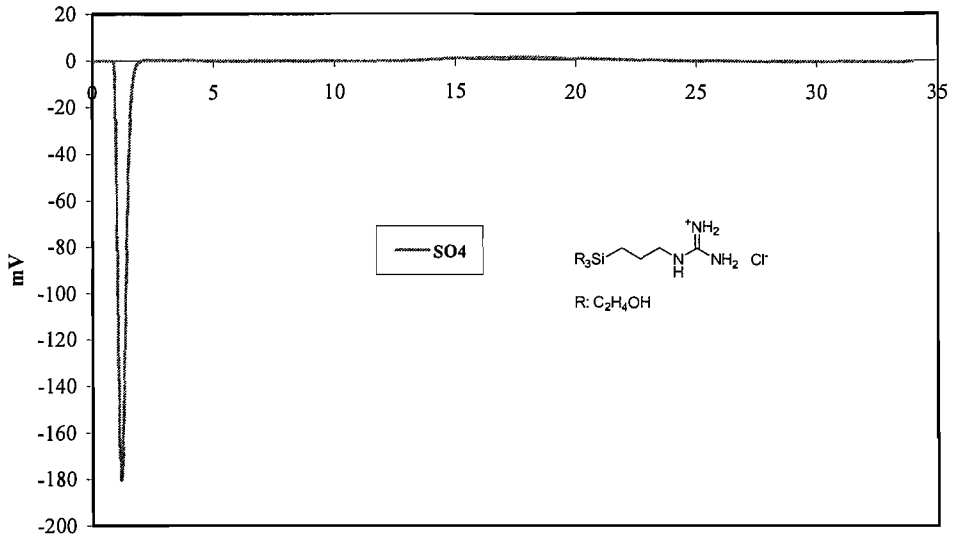

Bed Volume

Ion exchange of SCN on 28 with NaClO4 0.5M, flowrate 0.40 mL/min, column 60x5 mm

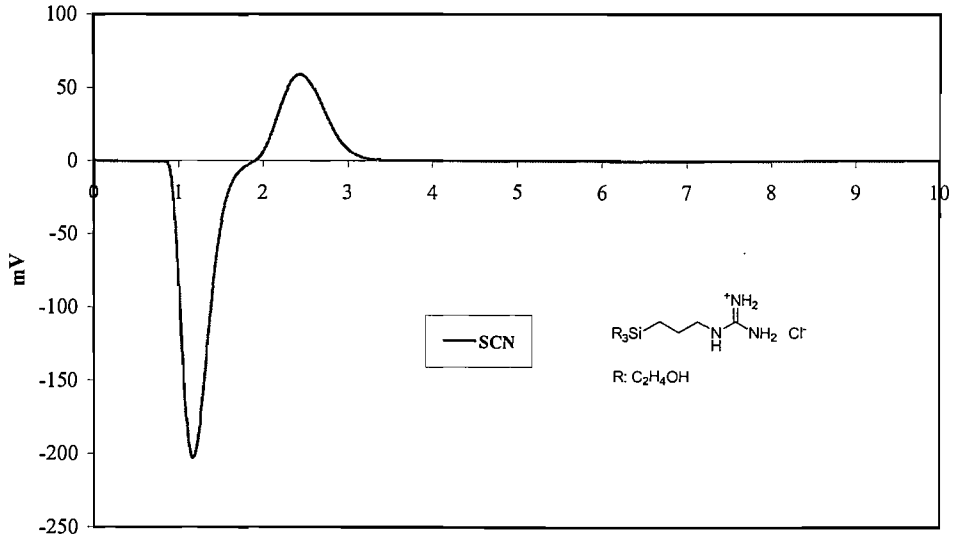

Bed Volume

Ion exchange of HPO4 on 28 with NaClO4 0.5M, flowrate 0.40 mL/min, column 60x5 mm

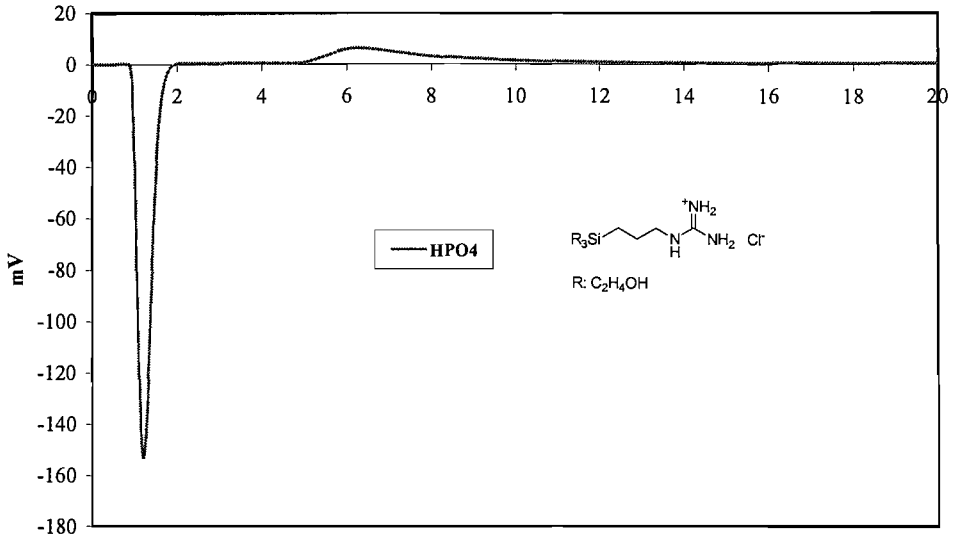

Bed Volume

Ion exchange of H2PO4 on 28 with NaClO4 0.5M, flowrate 0.40 mL/min, column 60x5 mm

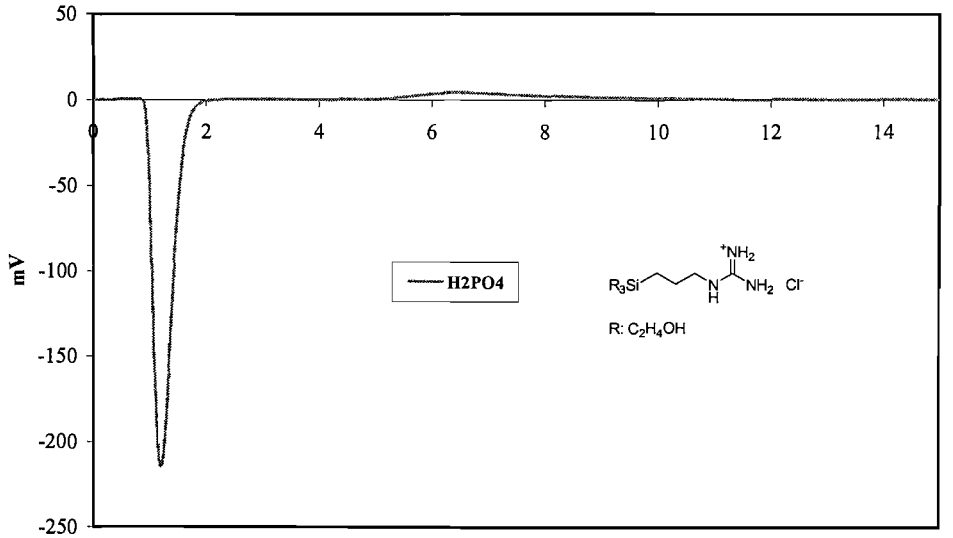

Bed Volume

Ion exchange of PO4 on 28 with NaClO4 0.5M, flowrate 0.40 mL/min, column 60x5 mm

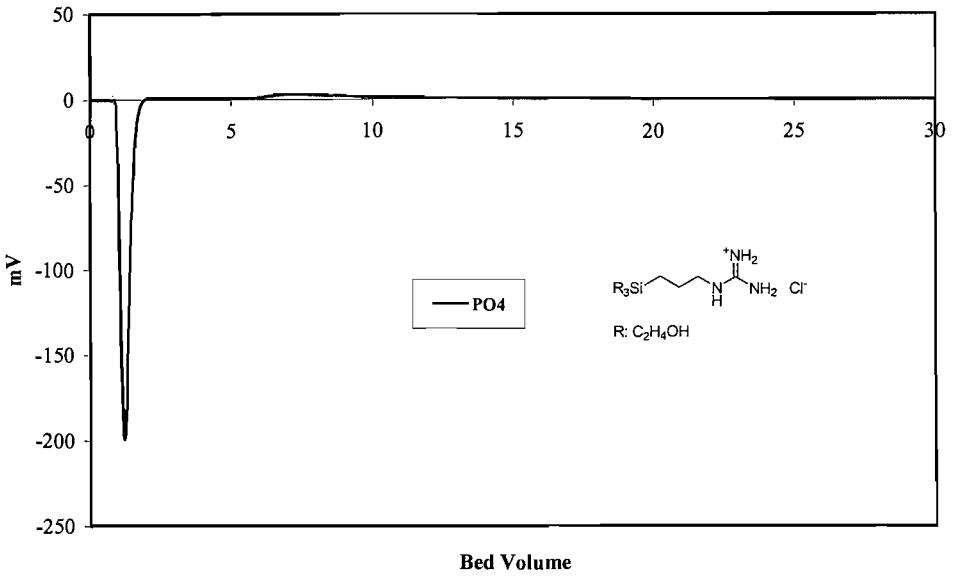

Bed Volume

Ion exchange of AMP on 28 with NaClO4 0.5M, flowrate 0.40 mL/min, column 60x5 mm

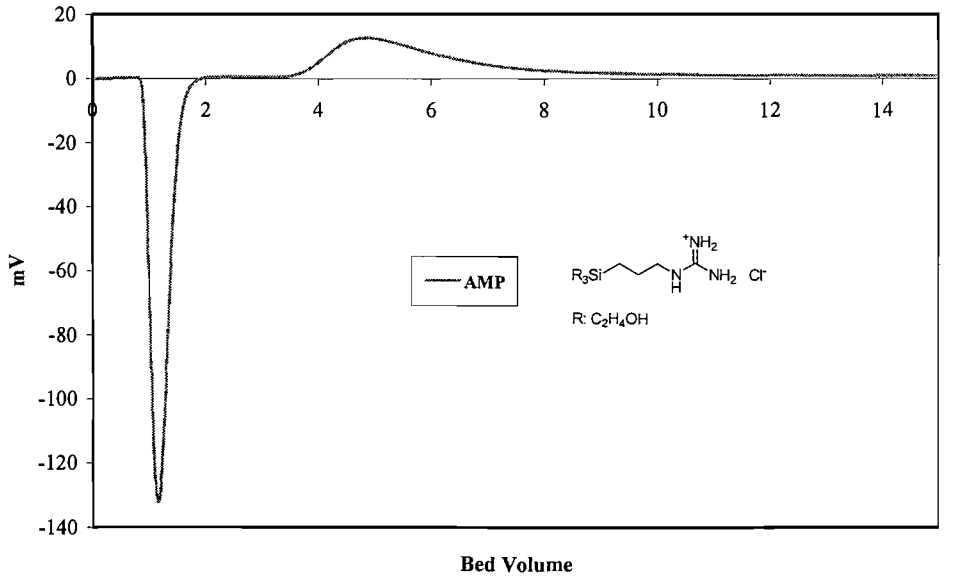

Bed Volume

Ion exchange of ADP on 28 with NaClO4 0.5M, flowrate 0.40 mL/min, column 60x5 mm

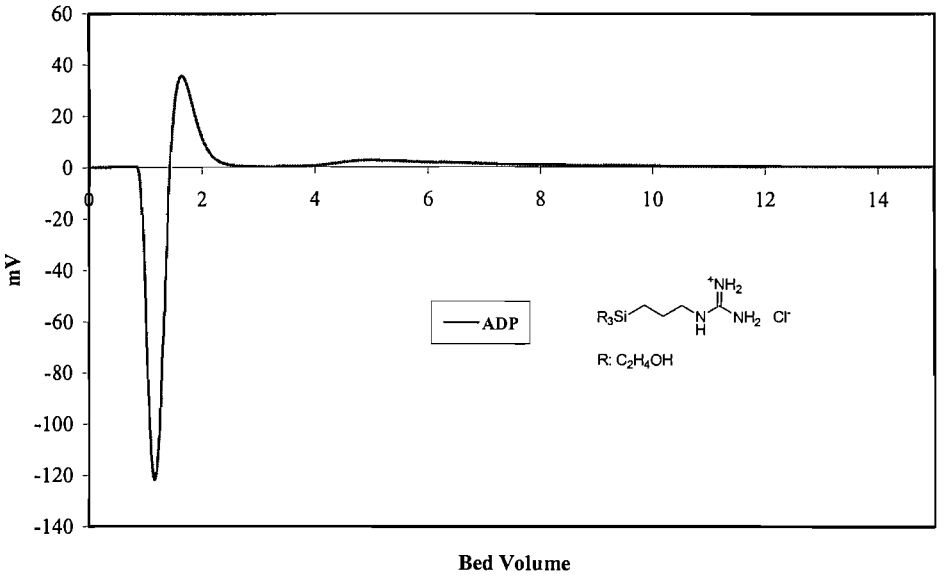

Ion exchange of ATP on 28 with NaClO4 0.5M, flowrate 0.40 mL/min, column 60x5 mm

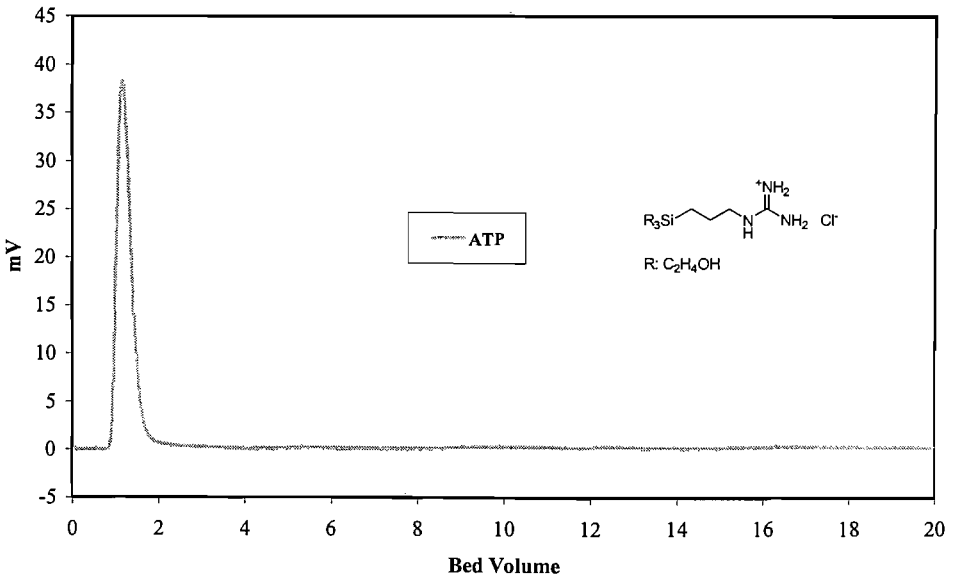

A.3.3.3 Silica supporting TBD **33**

A.3.3.3.1 Separation in 0.05M $NaClO_4$

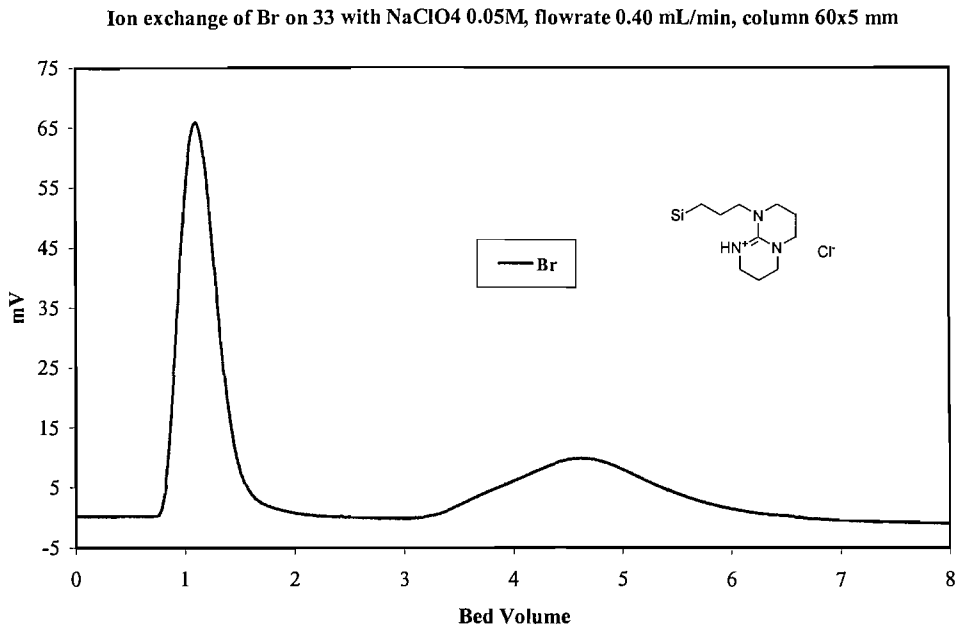

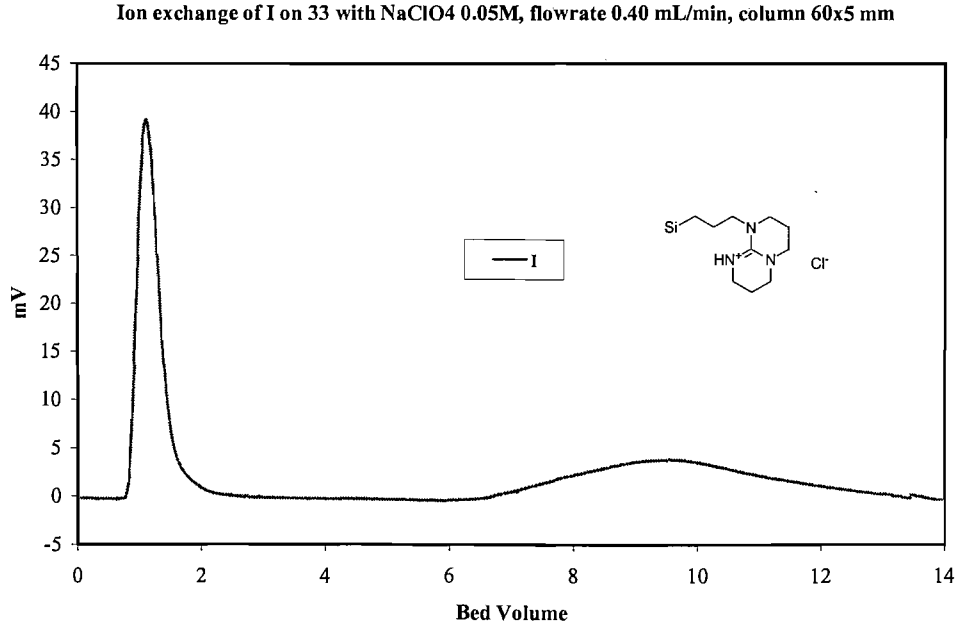

Ion exchange of NO3 on 33 with NaClO4 0.05M, flowrate 0.40 mL/min, column 60x5 mm

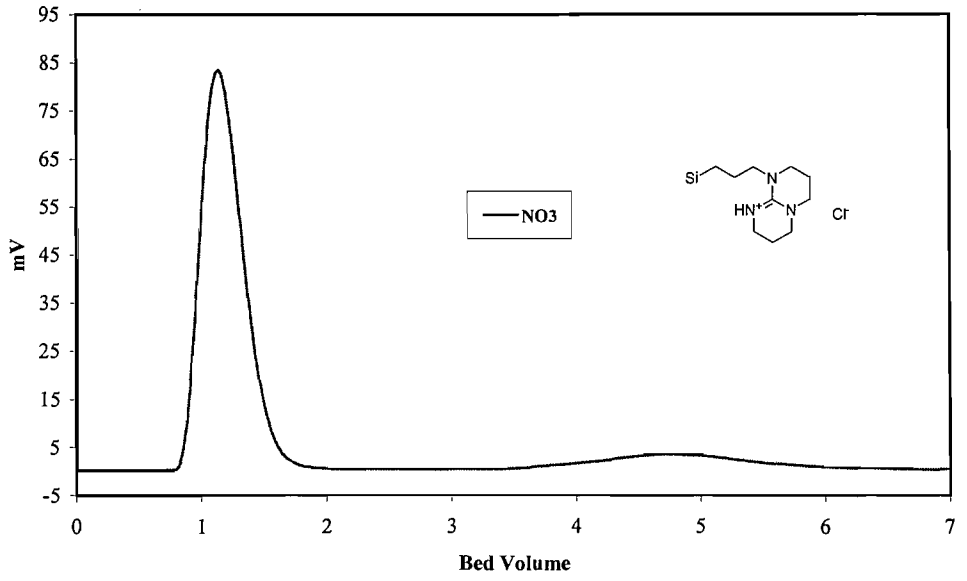

Ion exchange of S2O3 on 33 with NaClO4 0.05M, flowrate 0.40 mL/min, column 60x5 mm

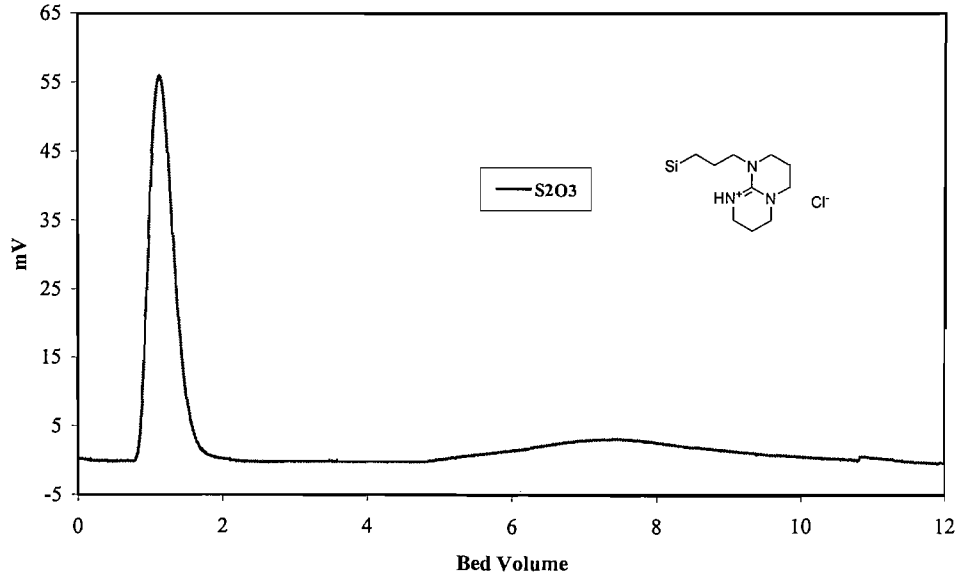

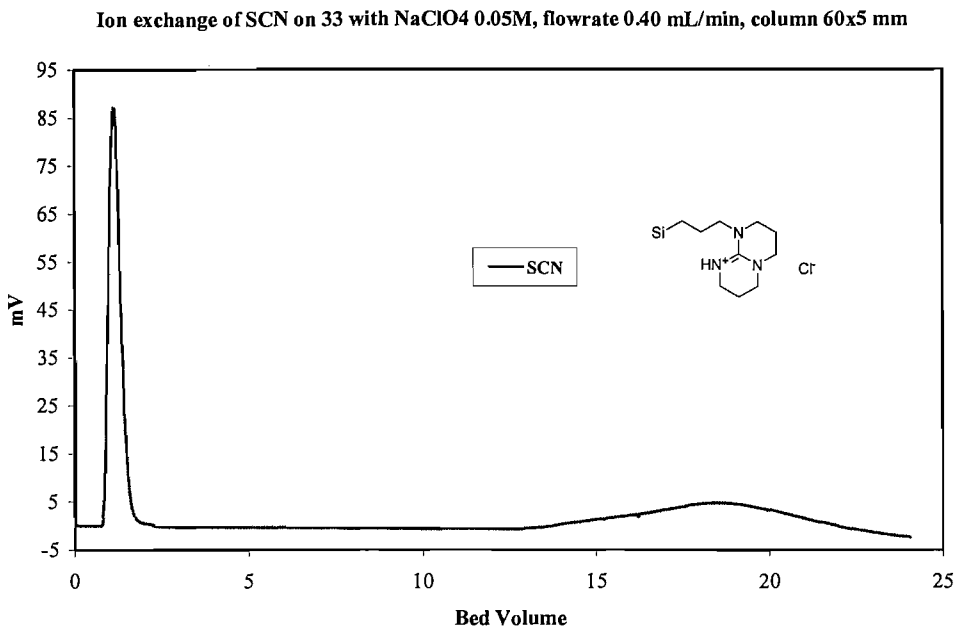

A.3.3.3.2 Separation in 0.5M $NaClO_4$

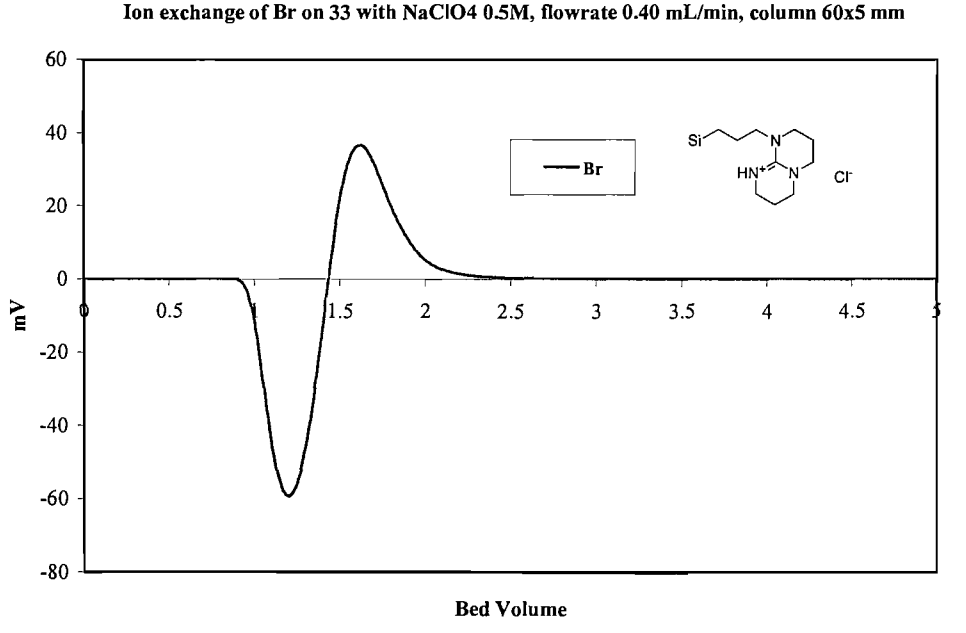

Ion exchange of I on 33 with NaClO4 0.5M, flowrate 0.40 mL/min, column 60x5 mm

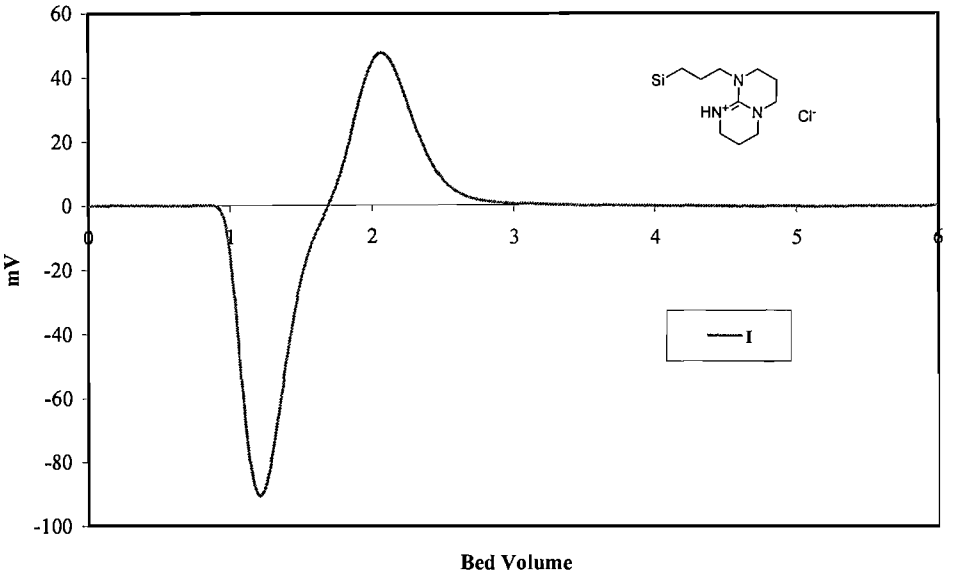

Ion exchange of SCN on 33 with NaClO4 0.5M, flowrate 0.40 mL/min, column 60x5 mm

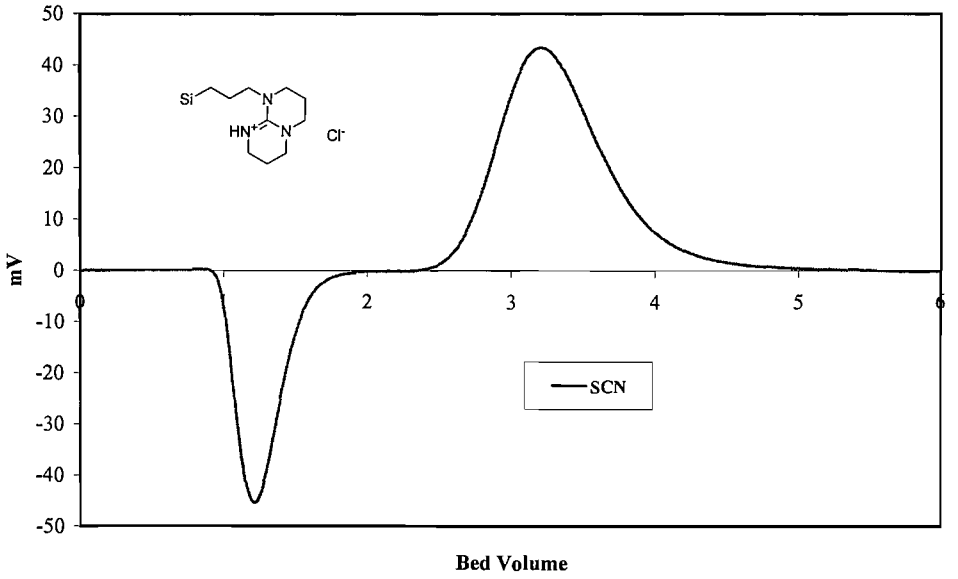

Ion exchange of NO3 on 33 with NaClO4 0.5M, flowrate 0.40 mL/min, column 60x5 mm

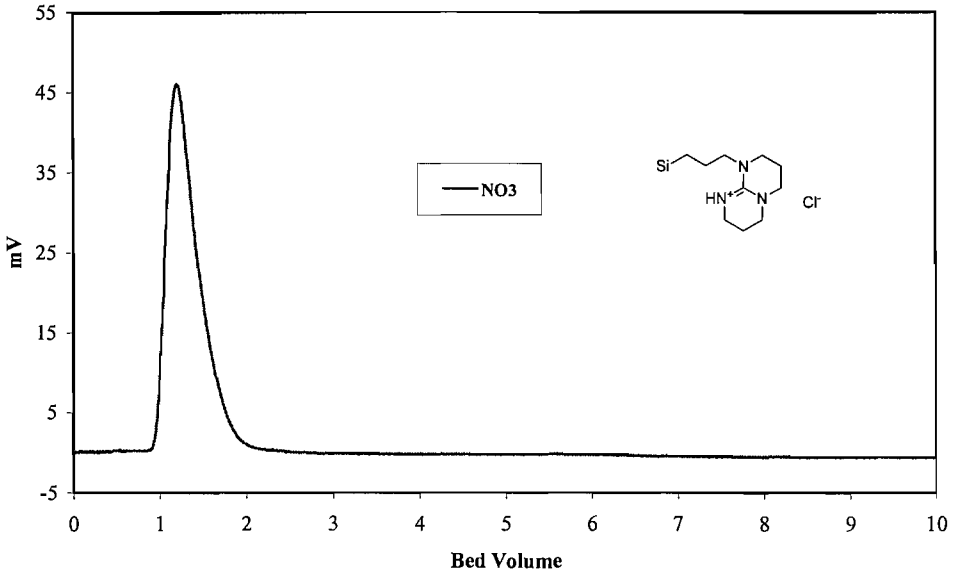

Ion exchange of S2O3 on 33 with NaClO4 0.5M, flowrate 0.40 mL/min, column 60x5 mm

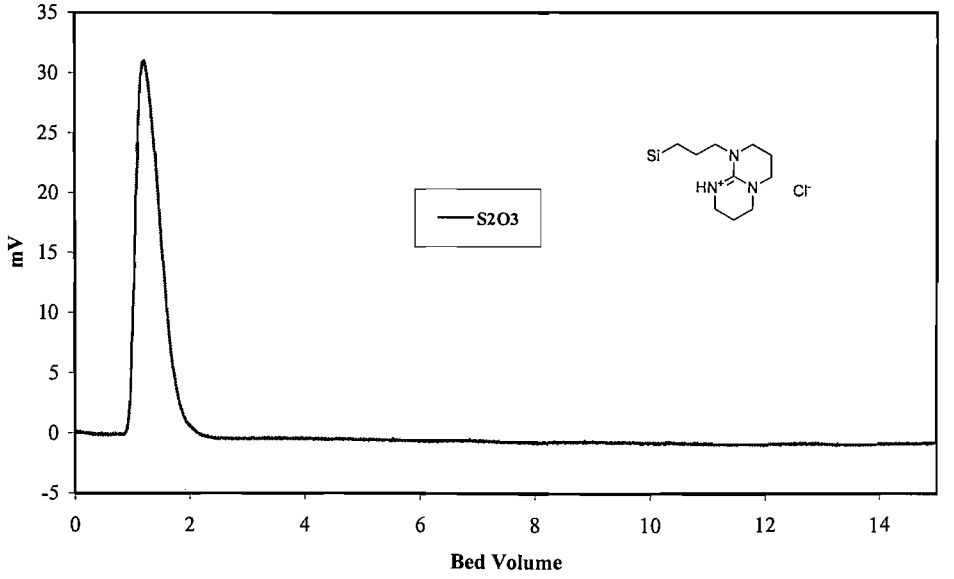

Ion exchange of SO4 on 33 with NaClO4 0.5M, flowrate 0.40 mL/min, column 60x5 mm

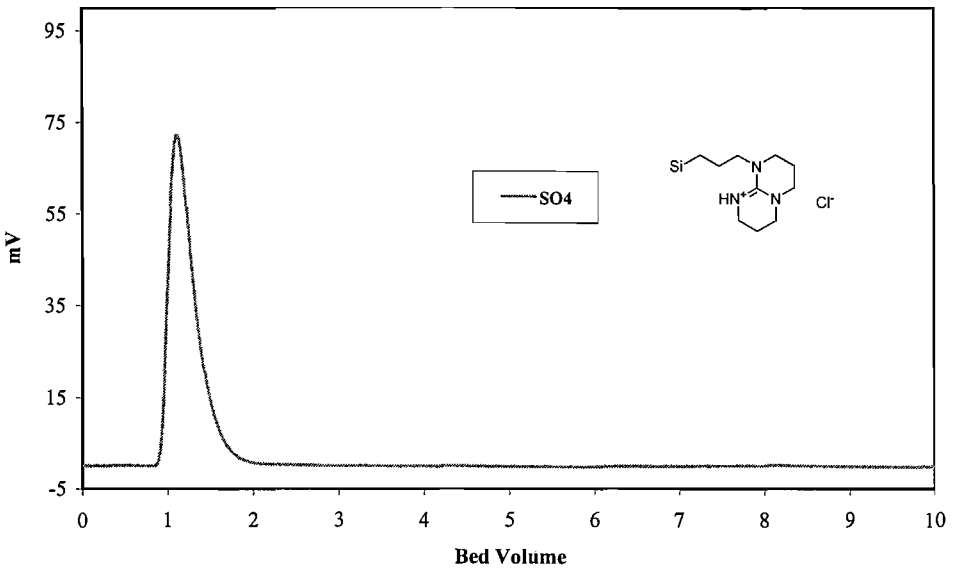

Ion exchange of H2PO4 on 33 with NaClO4 0.5M, flowrate 0.40 mL/min, column 60x5 mm

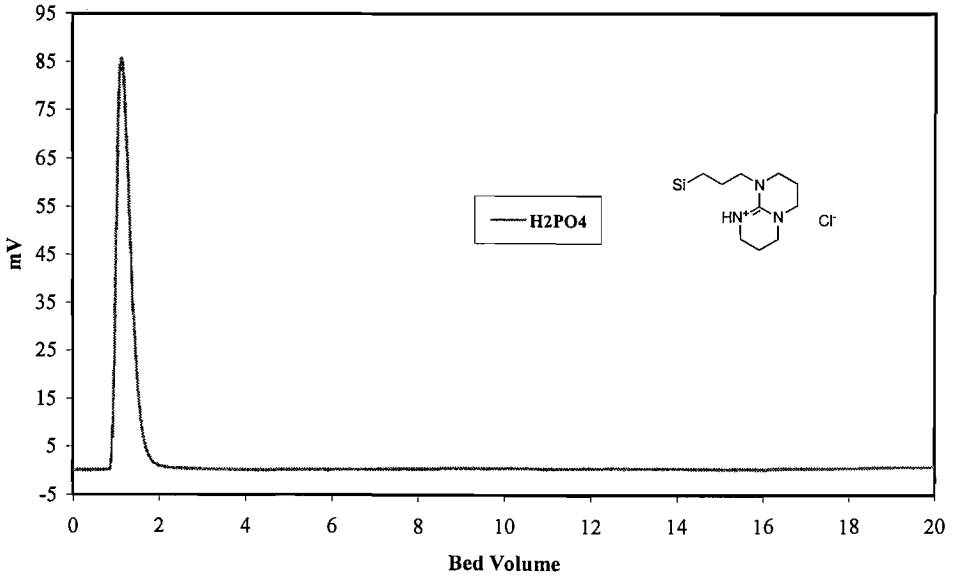

Ion exchange of HPO4 on 33 with NaClO4 0.5M, flowrate 0.40 mL/min, column 60x5 mm

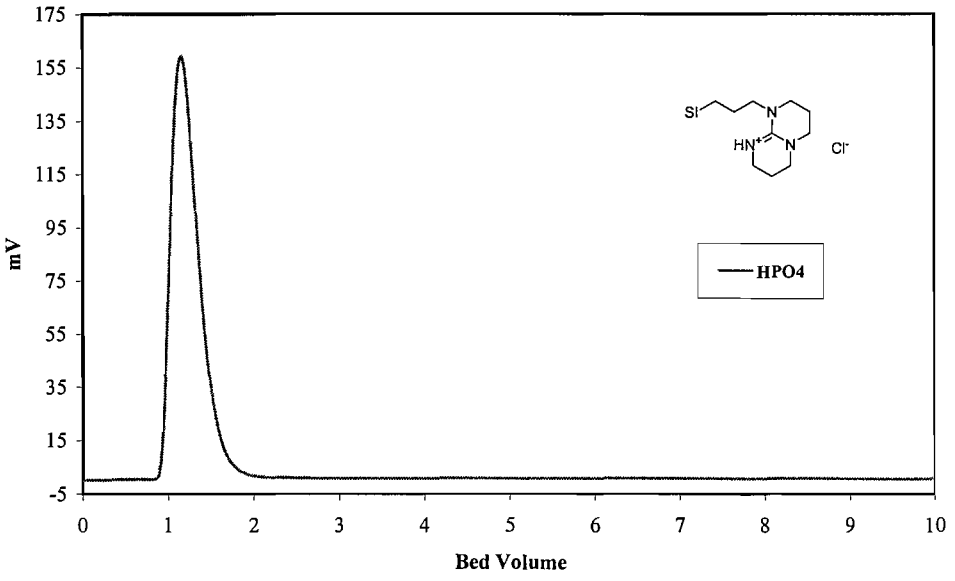

Ion exchange of PO4 on 33 with NaClO4 0.5M, flowrate 0.40 mL/min, column 60x5 mm

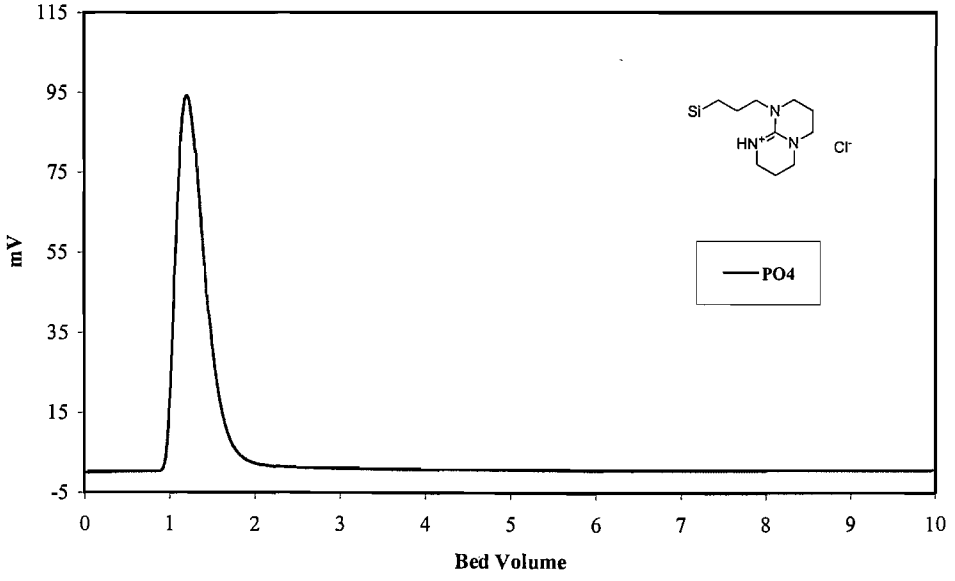

Ion exchange of AMP on 33 with NaClO4 0.5M, flowrate 0.40 mL/min, column 60x5 mm

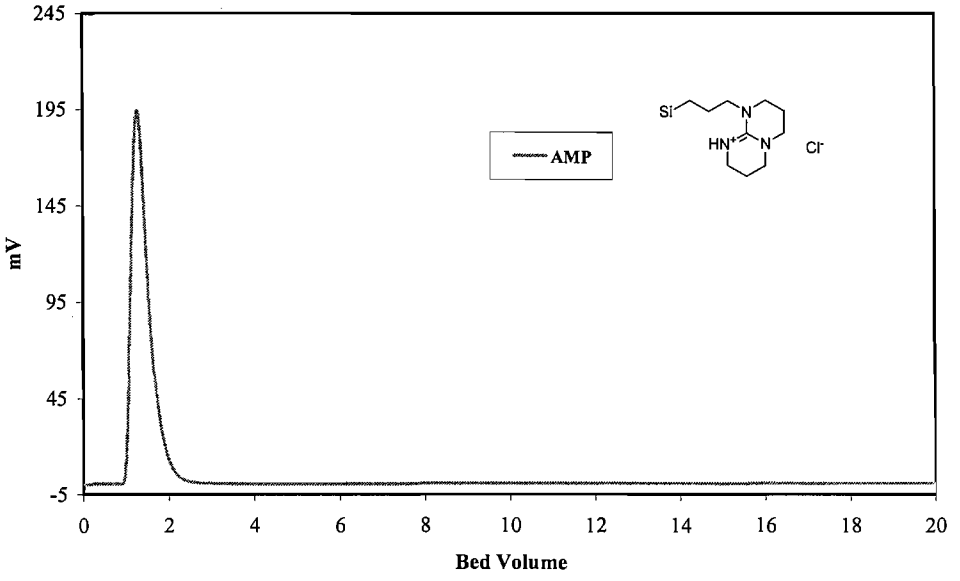

Ion exchange of ADP on 33 with NaClO4 0.5M, flowrate 0.40 mL/min, column 60x5 mm

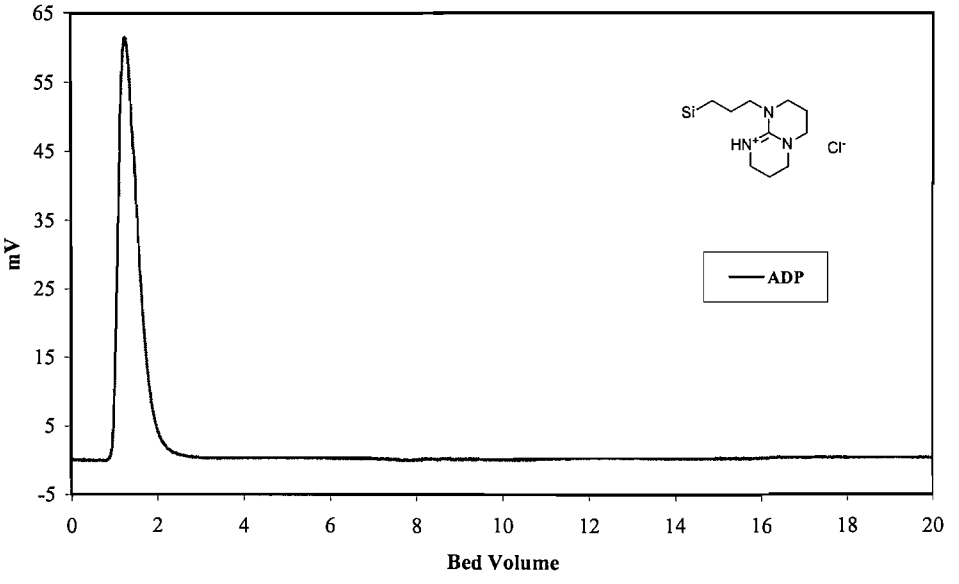

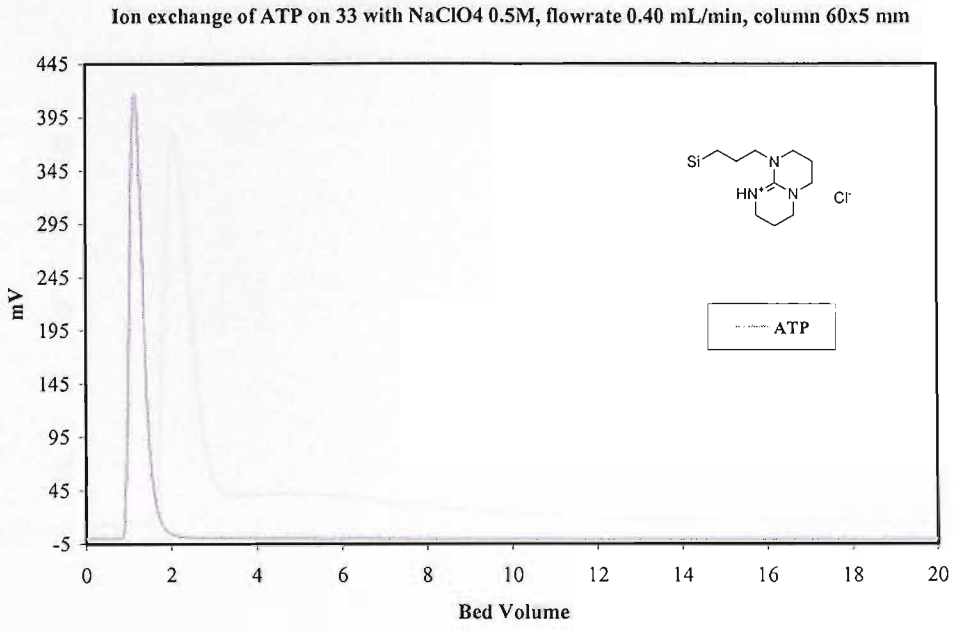

A.3.4 Double arm guanidinium resins 43

A.3.4.1 Separation in 0.5M $NaClO_4$

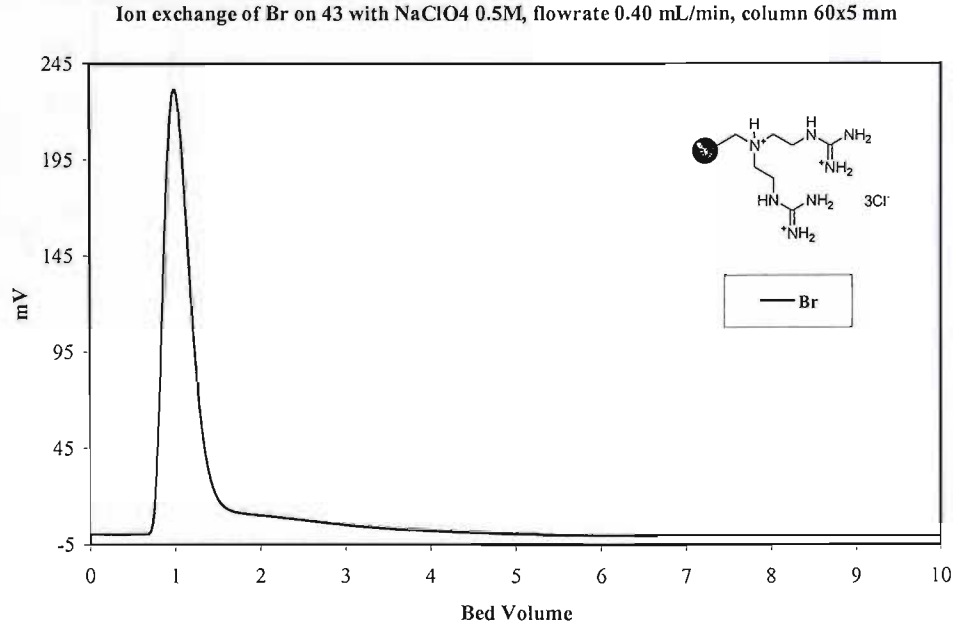

Ion exchange of I on 43 with NaClO4 0.5M, flowrate 0.40 mL/min, column 60x5 mm

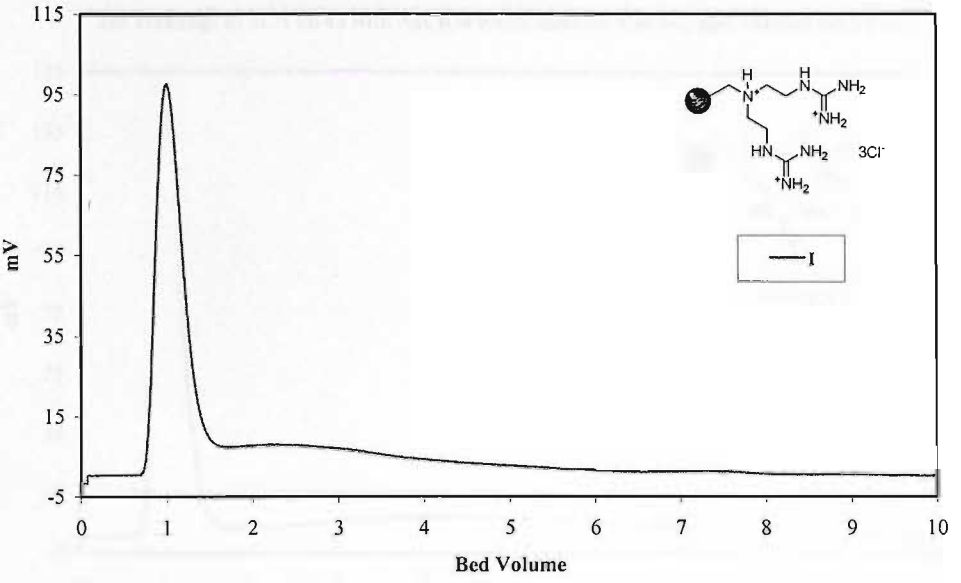

Ion exchange of NO3 on 43 with NaClO4 0.5M, flowrate 0.40 mL/min, column 60x5 mm

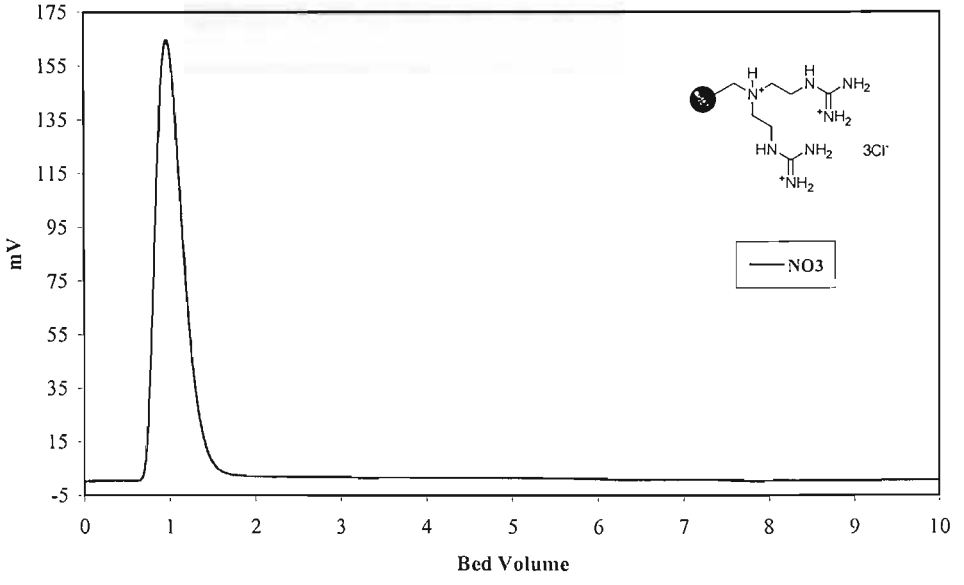

Ion exchange of SCN on 43 with NaClO4 0.5M, flowrate 0.40 mL/min, column 60x5 mm

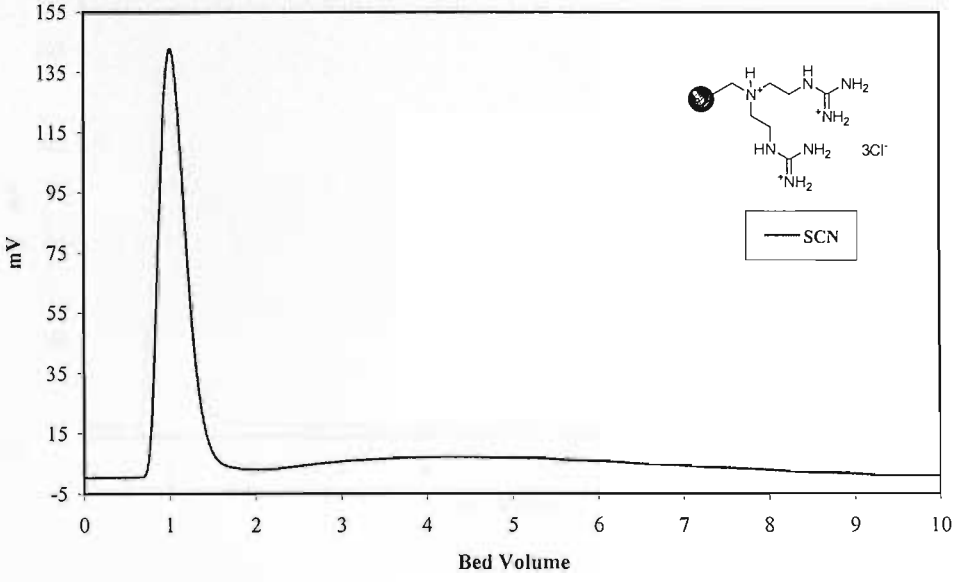

Ion exchange of S2O3 on 43 with NaClO4 0.5M, flowrate 0.40 mL/min, column 60x5 mm

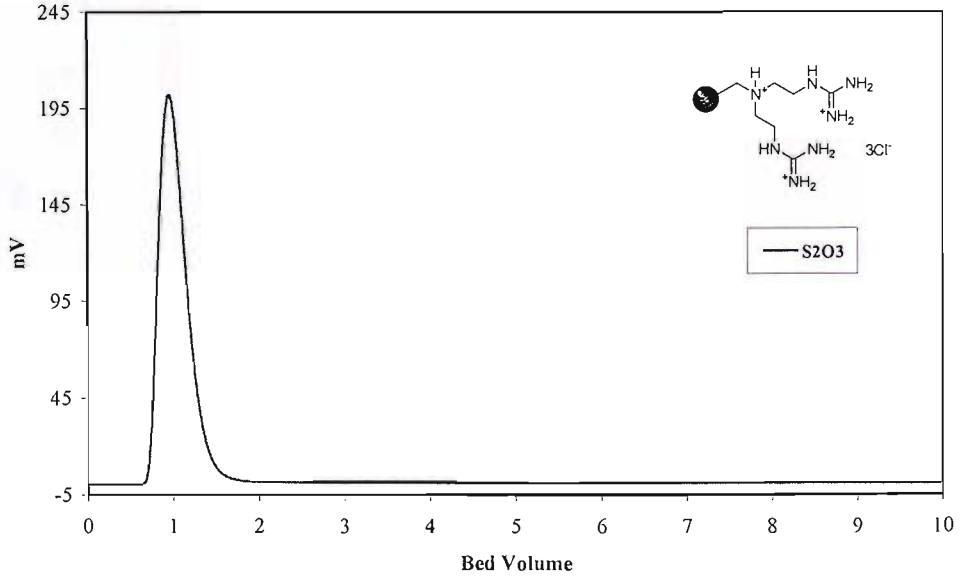

Ion exchange of SO4 on 43 with NaClO4 0.5M, flowrate 0.40 mL/min, column 60x5 mm

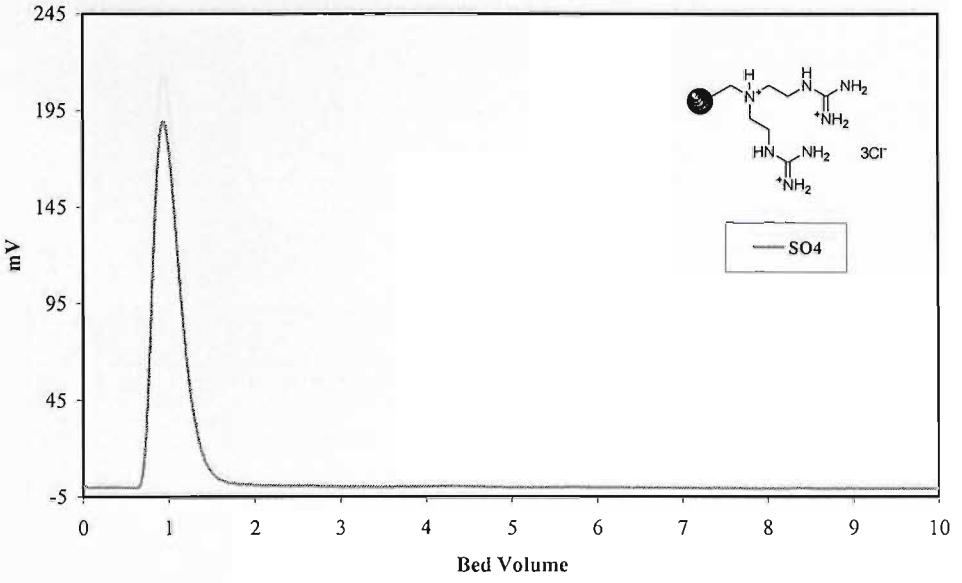

Ion exchange of H2PO4 on 43 with NaClO4 0.5M, flowrate 0.40 mL/min, column 60x5 mm

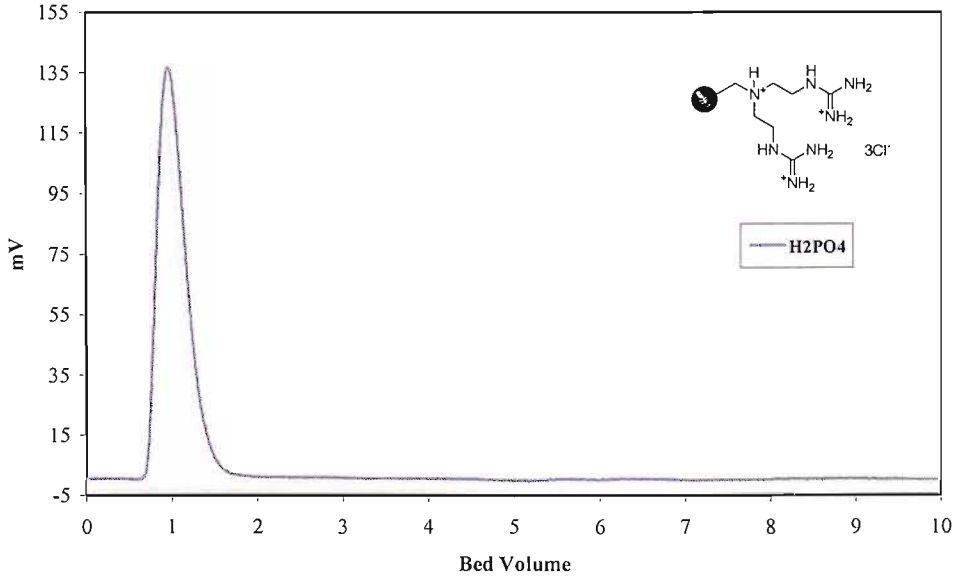

Ion exchange of HPO4 on 43 with NaClO4 0.5M, flowrate 0.40 mL/min, column 60x5 mm

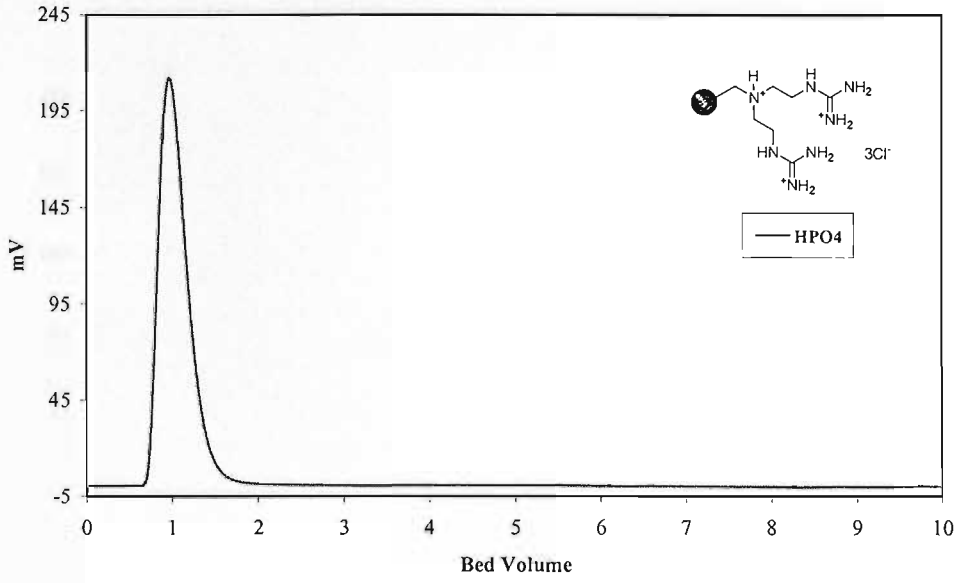

Ion exchange of PO4 on 43 with NaClO4 0.5M, flowrate 0.40 mL/min, column 60x5 mm

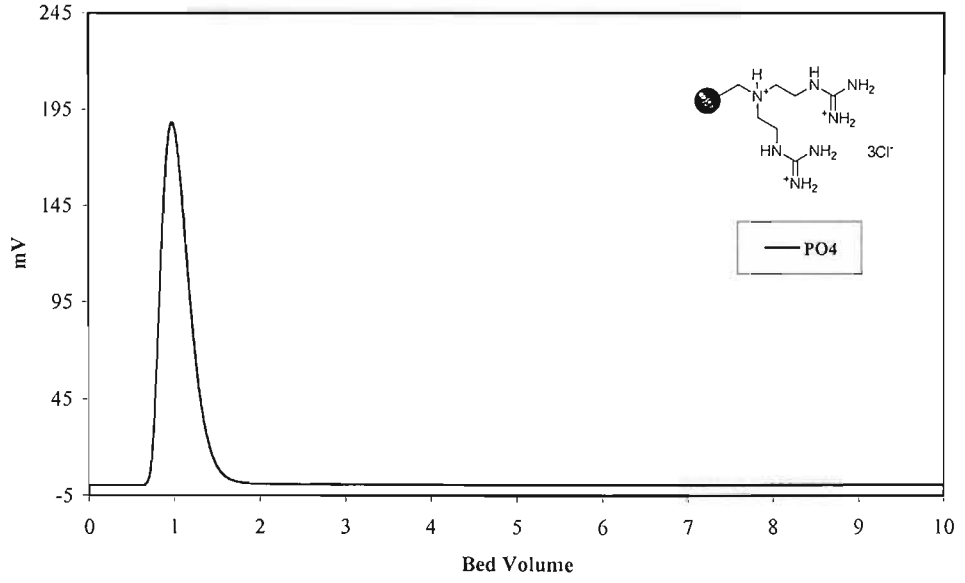

Ion exchange of AMP on 43 with NaClO4 0.5M, flowrate 0.40 mL/min, column 60x5 mm

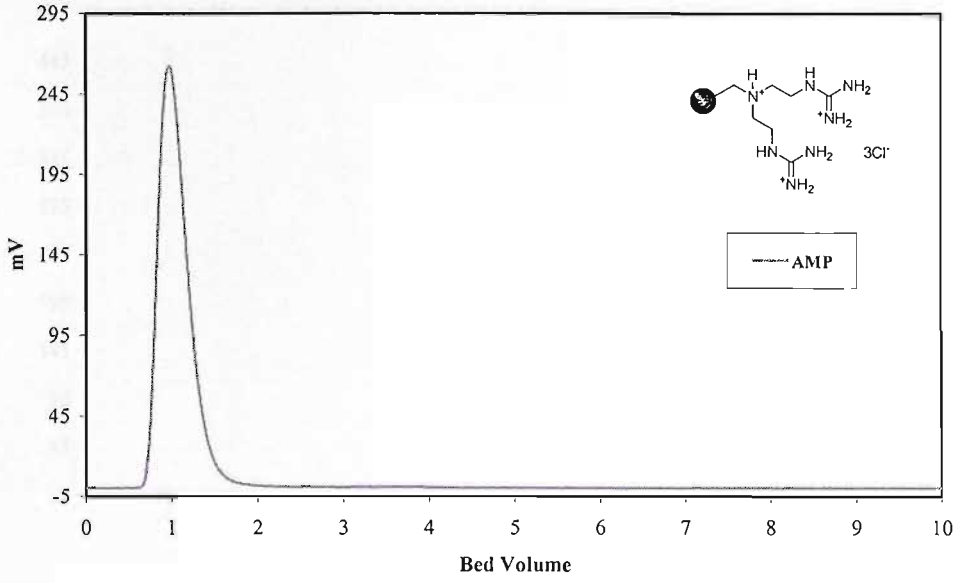

Ion exchange of ADP on 43 with NaClO4 0.5M, flowrate 0.40 mL/min, column 60x5 mm

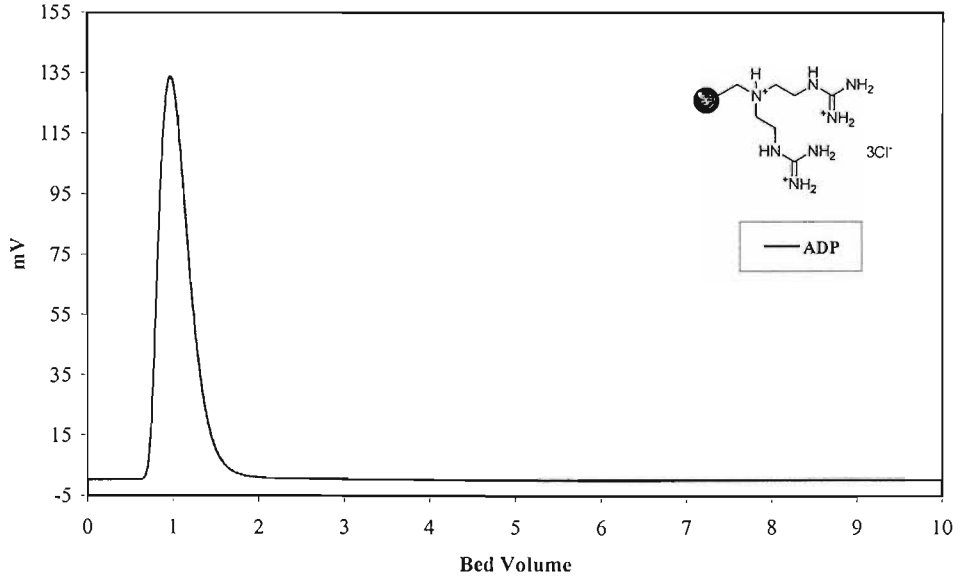

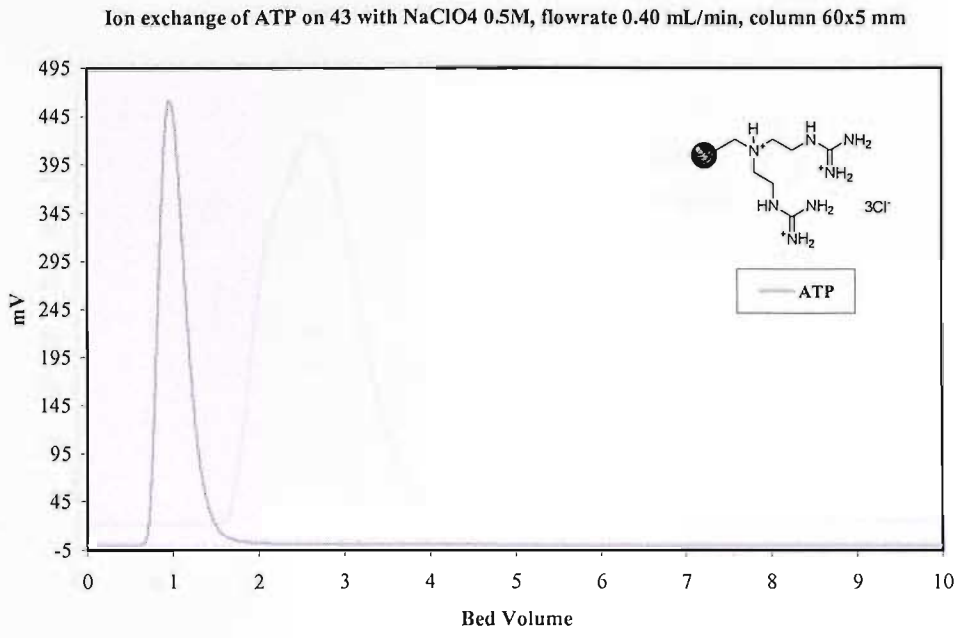

A.3.5 Thiourea resin derivatives

A.3.5.1 Silica supporting thiourea group **51**

A.3.5.1.1 Separation in 0.5M $NaClO_4$

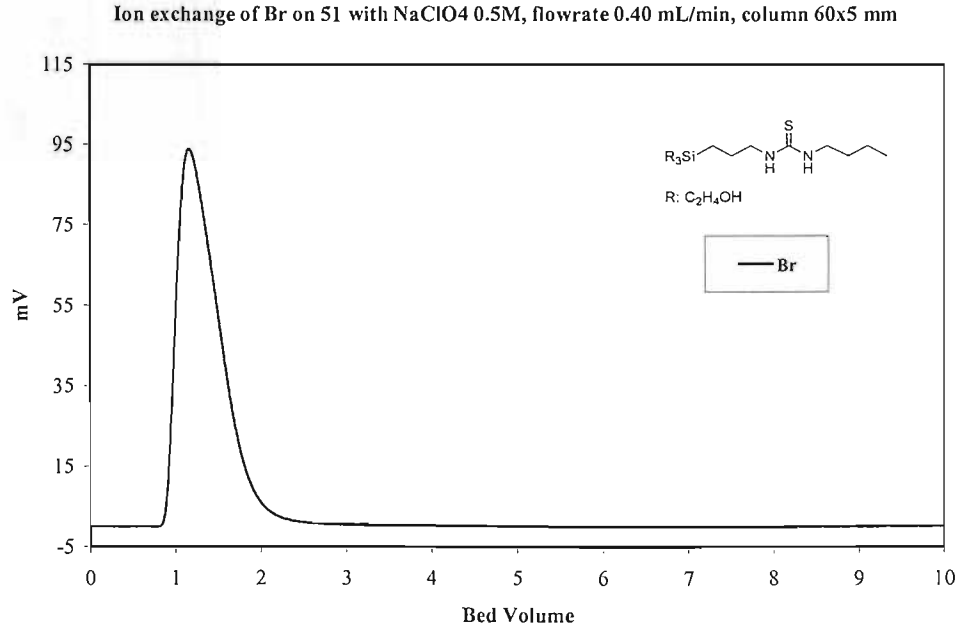

Ion exchange of I on 51 with NaClO4 0.5M, flowrate 0.40 mL/min, column 60x5 mm

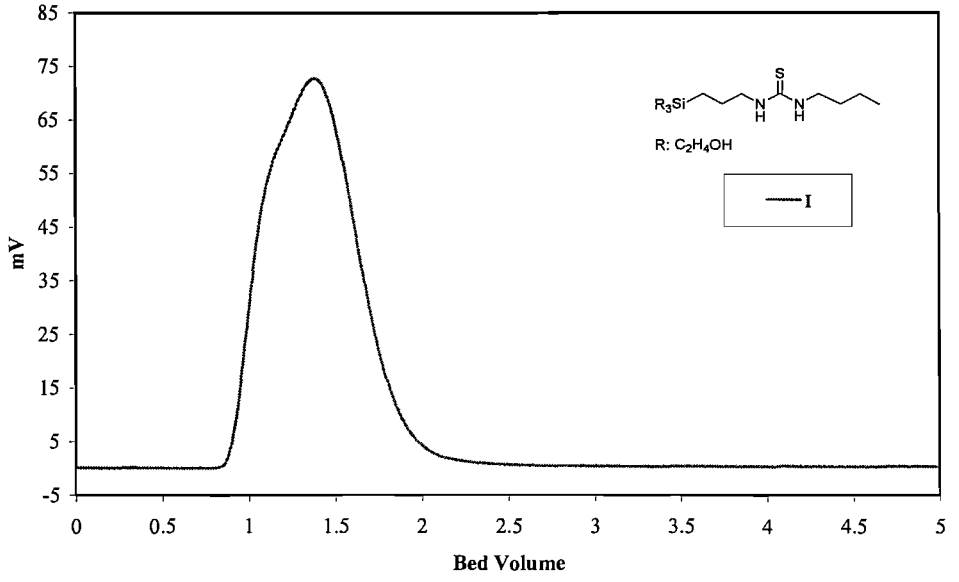

Ion exchange of NO3 on 51 with NaClO4 0.5M, flowrate 0.40 mL/min, column 60x5 mm

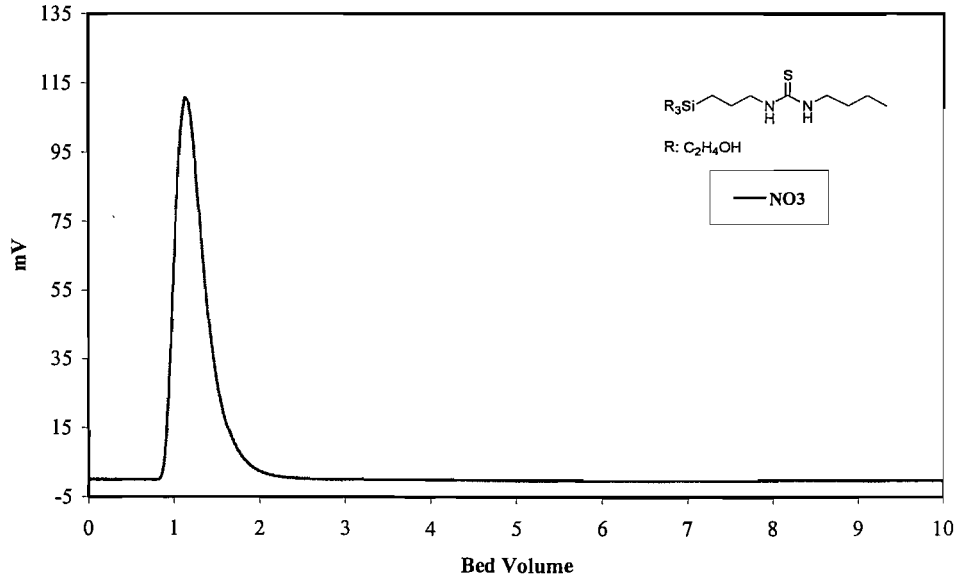

Ion exchange of SCN on 51 with NaClO4 0.5M, flowrate 0.40 mL/min, column 60x5 mm

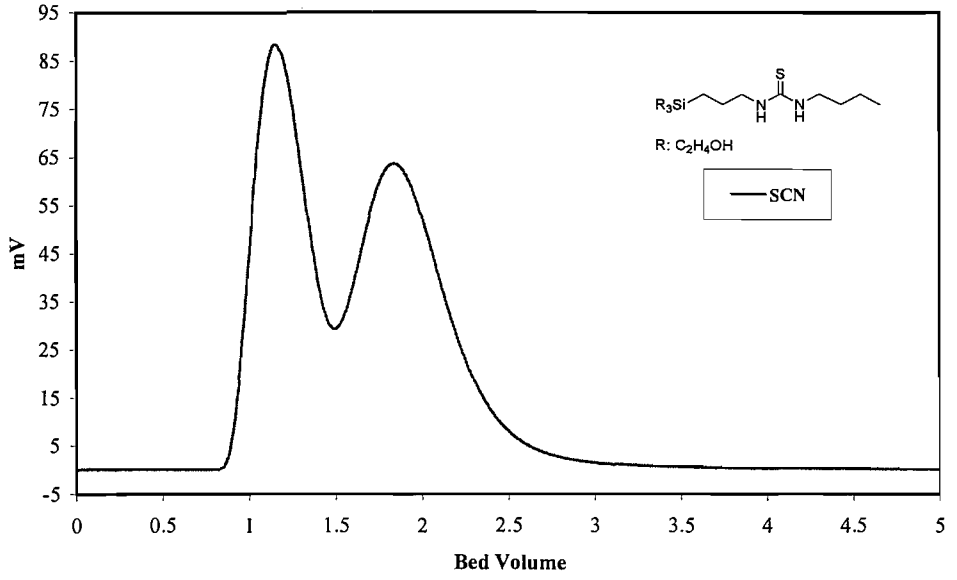

Ion exchange of S2O3 on 51 with NaClO4 0.5M, flowrate 0.40 mL/min, column 60x5 mm

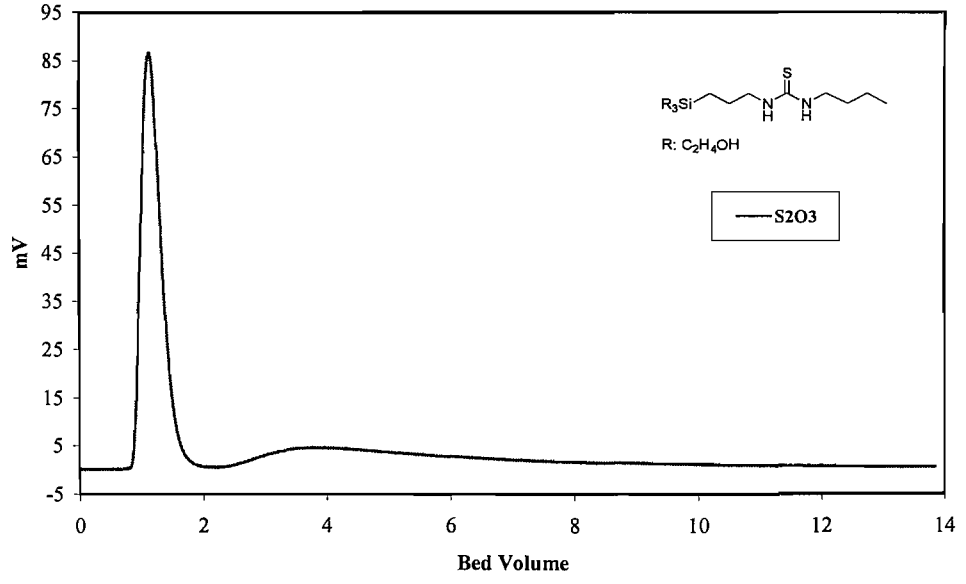

Ion exchange of SO4 on 51 with NaClO4 0.5M, flowrate 0.40 mL/min, column 60x5 mm

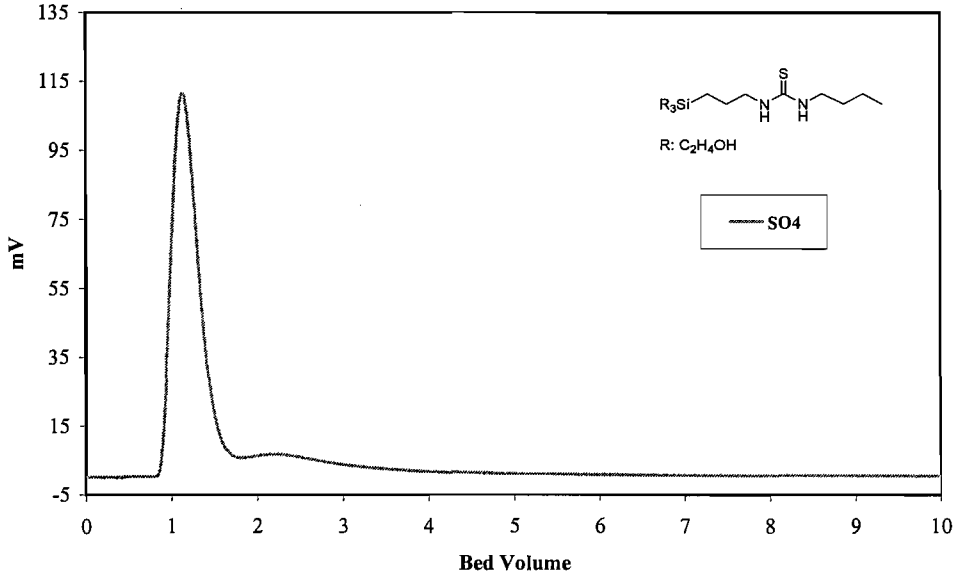

Ion exchange of H2PO4 on 51 with NaClO4 0.5M, flowrate 0.40 mL/min, column 60x5 mm

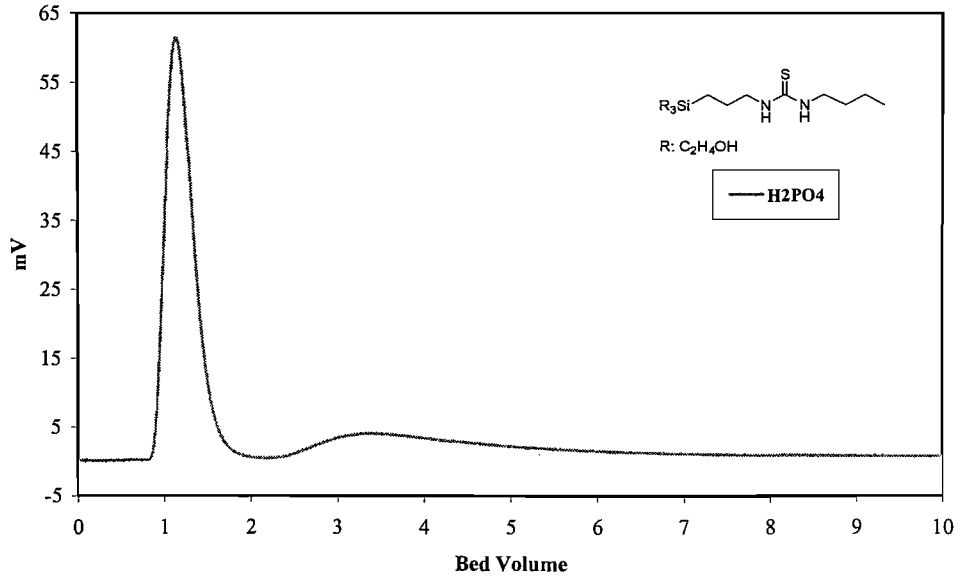

Ion exchange of HPO4 on 51 with NaClO4 0.5M, flowrate 0.40 mL/min, column 60x5 mm

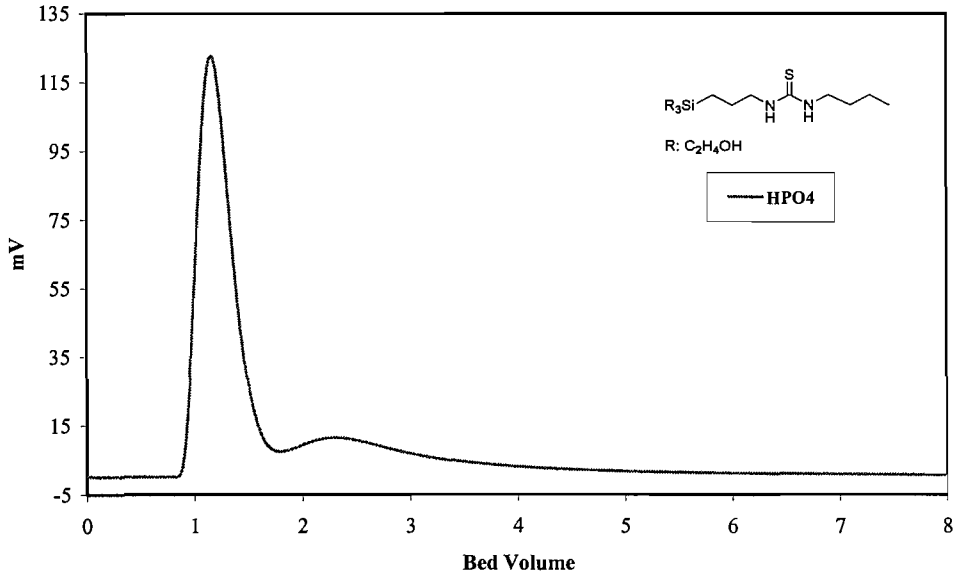

Ion exchange of PO4 on 51 with NaClO4 0.5M, flowrate 0.40 mL/min, column 60x5 mm

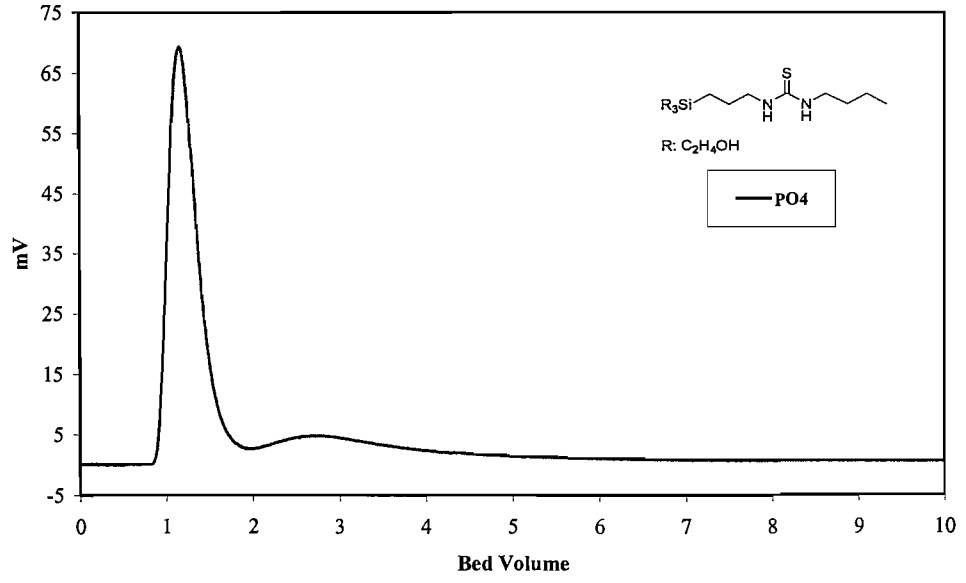

Ion exchange of AMP on 51 with NaClO4 0.5M, flowrate 0.40 mL/min, column 60x5 mm

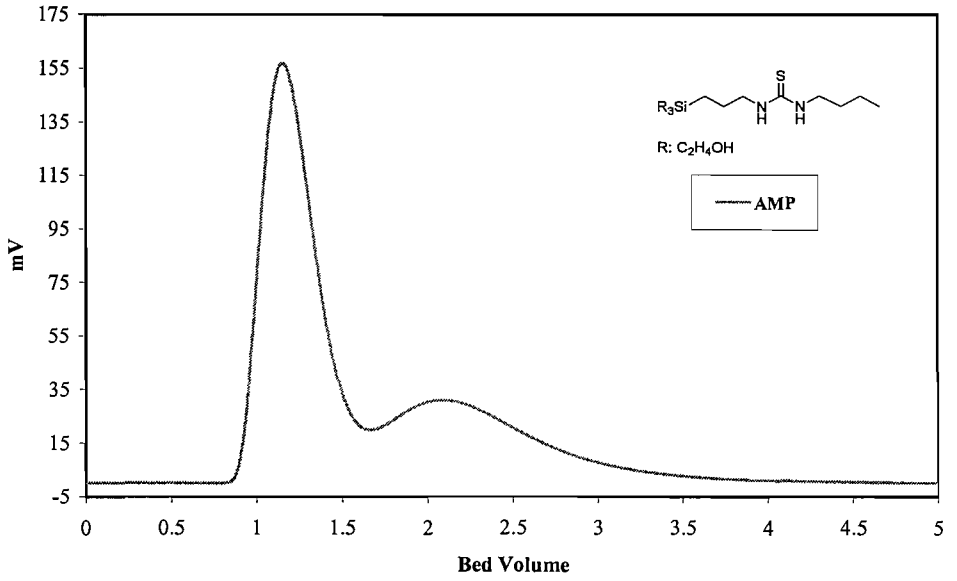

Ion exchange of ADP on 51 with NaClO4 0.5M, flowrate 0.40 mL/min, column 60x5 mm

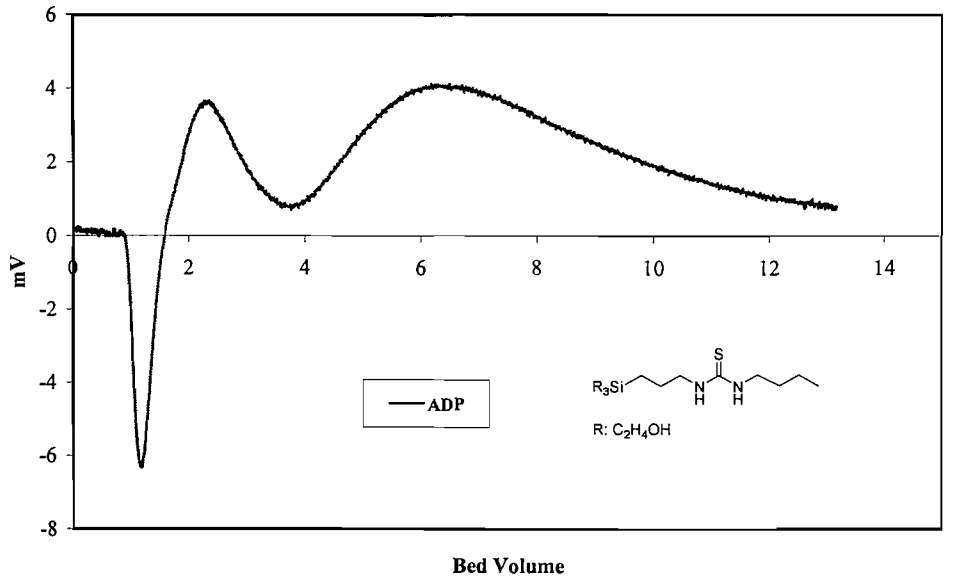

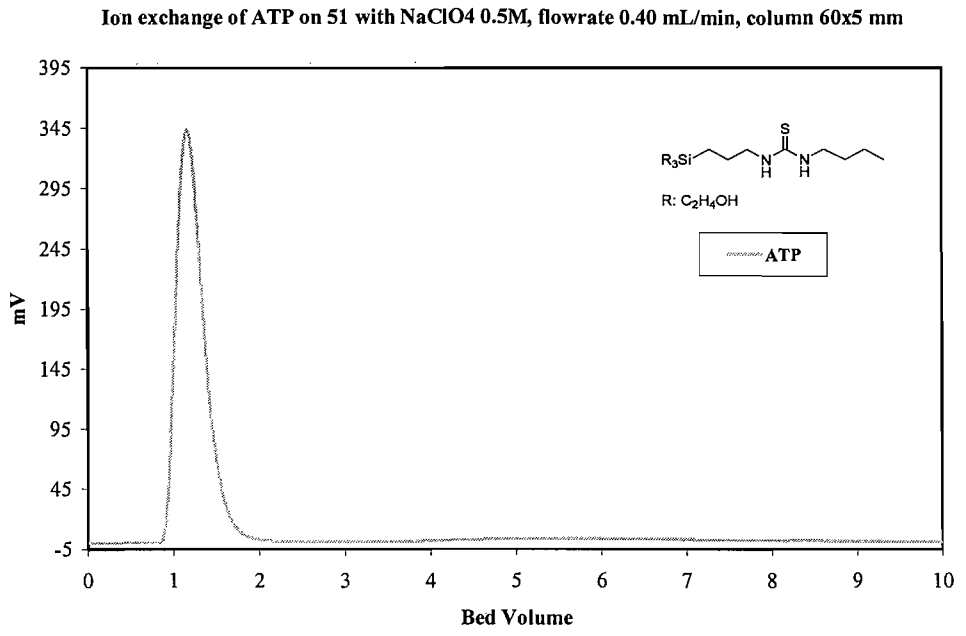

A.3.5.2 Methacrylate supporting thiourea group **52**

A.3.5.2.1 Separation in 0.5M $NaClO_4$

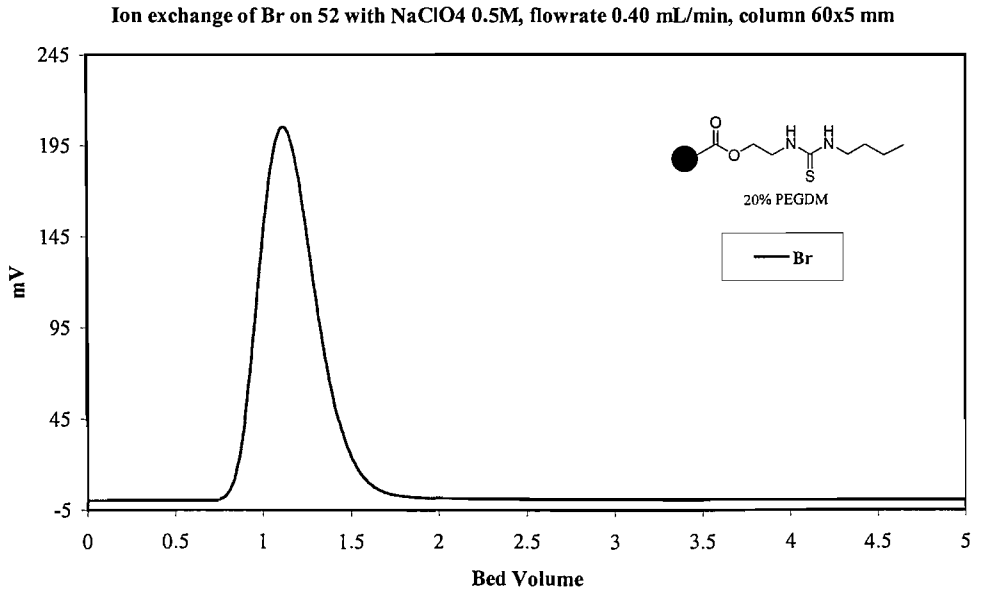

Ion exchange of I on 52 with NaClO4 0.5M, flowrate 0.40 mL/min, column 60x5 mm

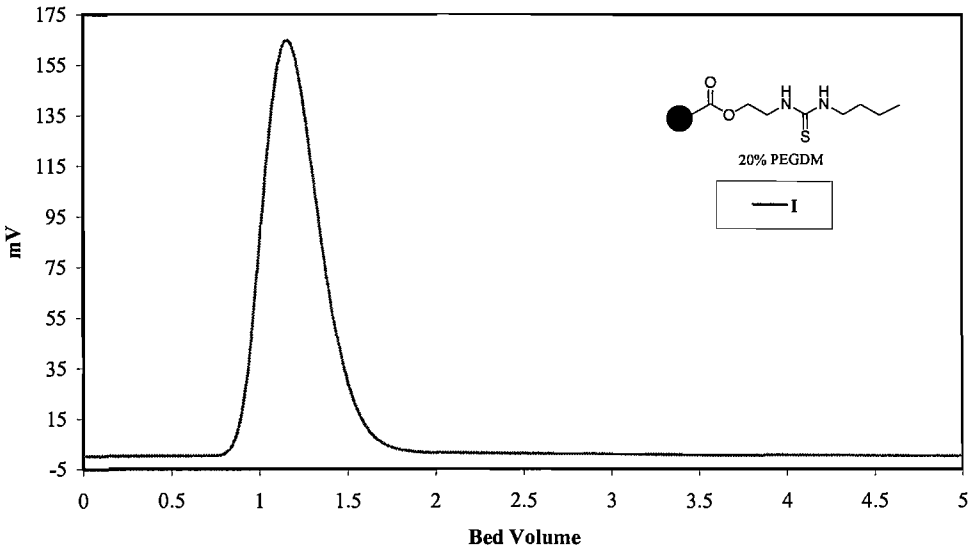

Ion exchange of SCN on 52 with NaClO4 0.5M, flowrate 0.40 mL/min, column 60x5 mm

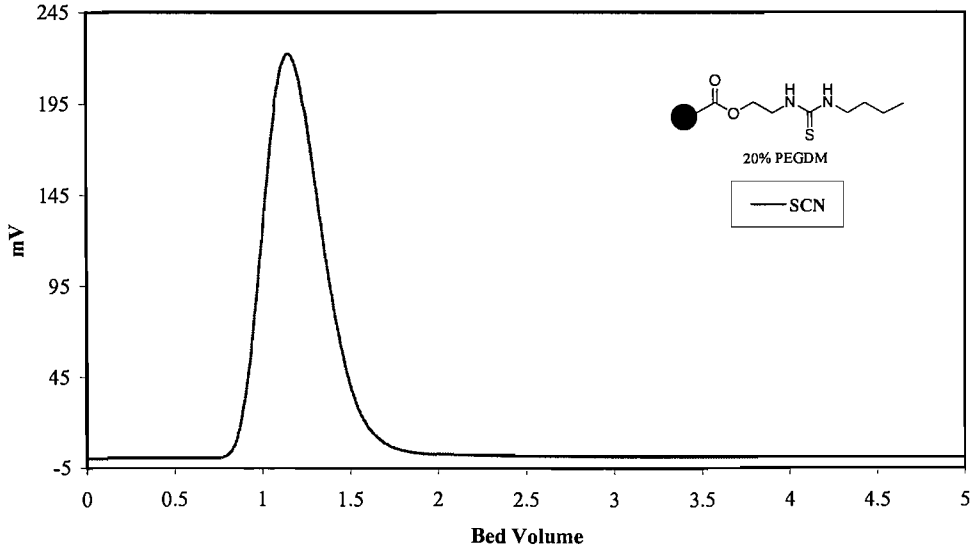

Ion exchange of S2O3 on 52 with NaClO4 0.5M, flowrate 0.40 mL/min, column 60x5 mm

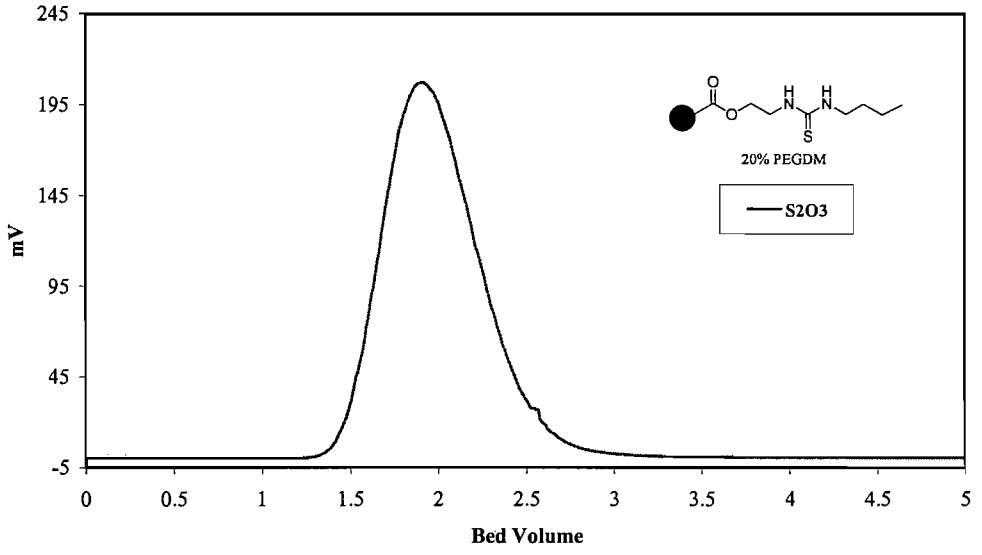

Ion exchange of SO4 on 52 with NaClO4 0.5M, flowrate 0.40 mL/min, column 60x5 mm

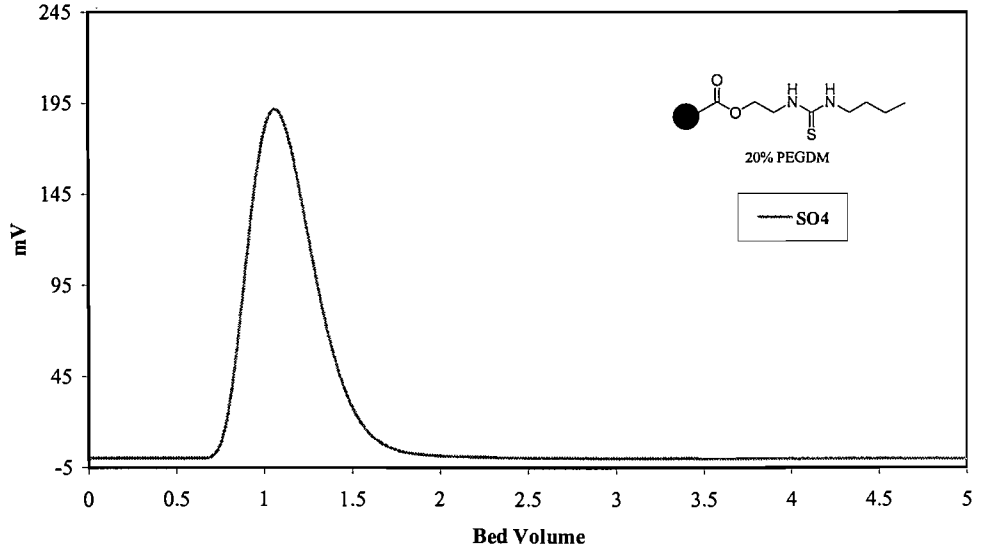

Ion exchange of H2PO4 on 52 with NaClO4 0.5M, flowrate 0.40 mL/min, column 60x5 mm

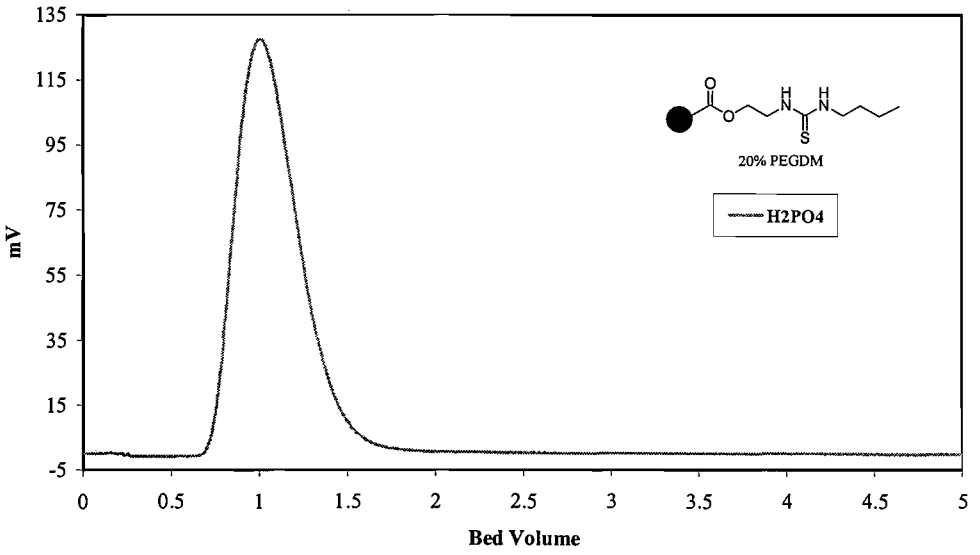

Ion exchange of HPO4 on 52 with NaClO4 0.5M, flowrate 0.40 mL/min, column 60x5 mm

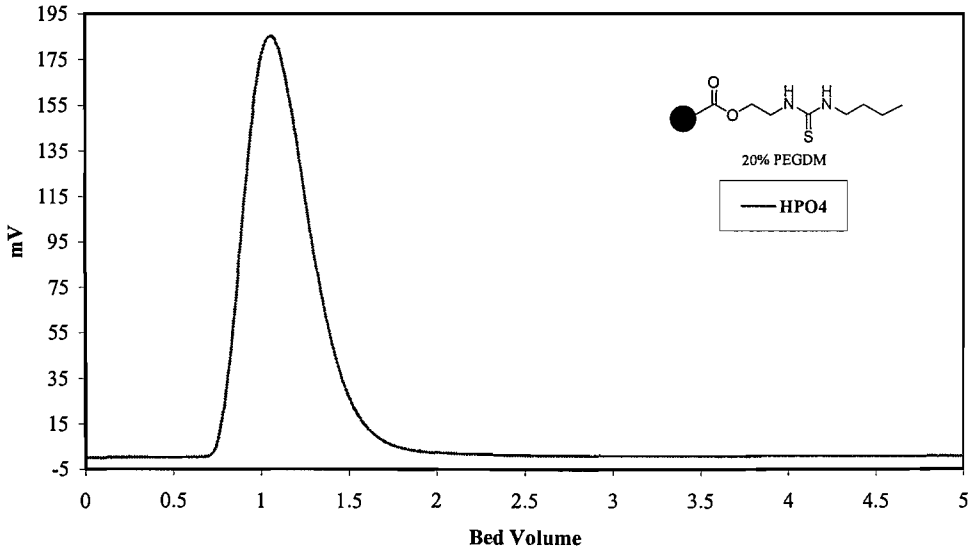

Ion exchange of PO4 on 52 with NaClO4 0.5M, flowrate 0.40 mL/min, column 60x5 mm

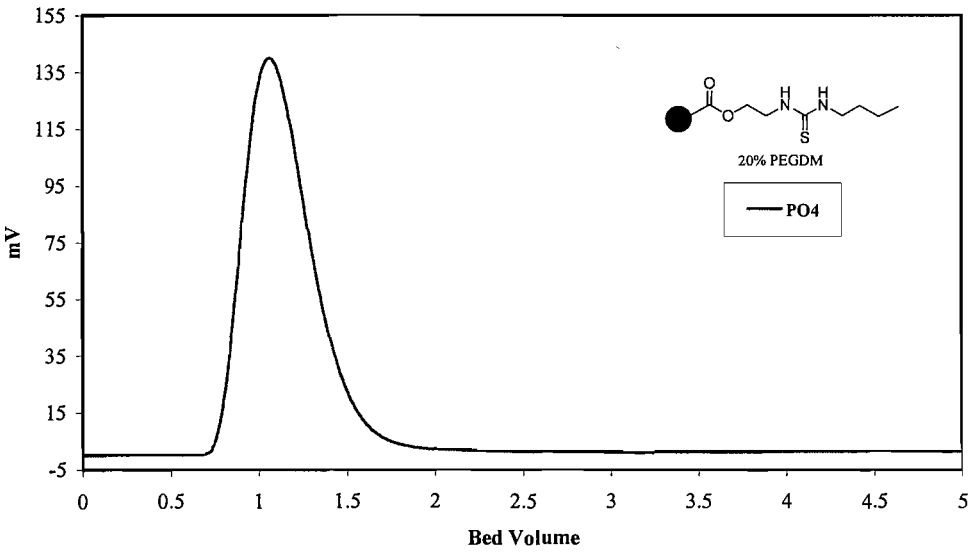

Ion exchange of AMP on 52 with NaClO4 0.5M, flowrate 0.40 mL/min, column 60x5 mm

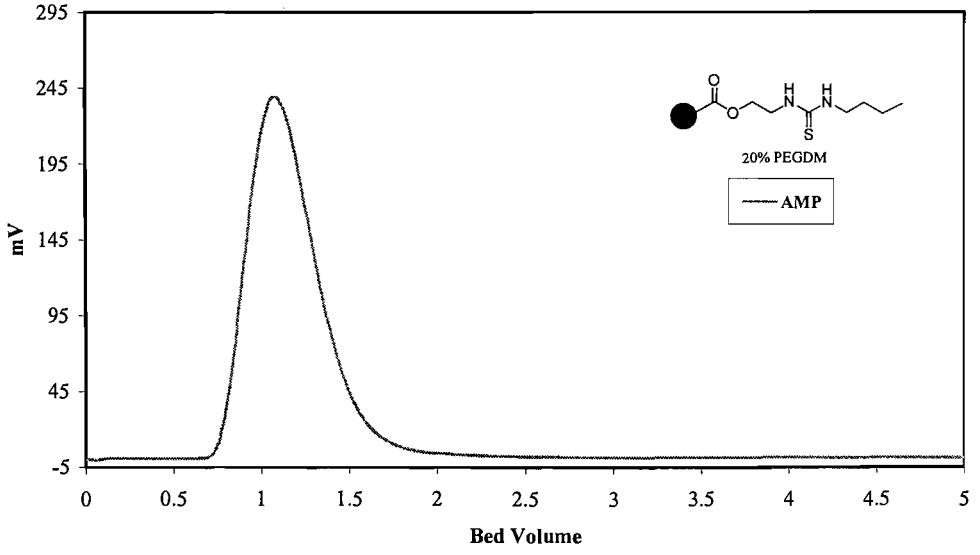

Ion exchange of ADP on 52 with NaClO4 0.5M, flowrate 0.40 mL/min, column 60x5 mm

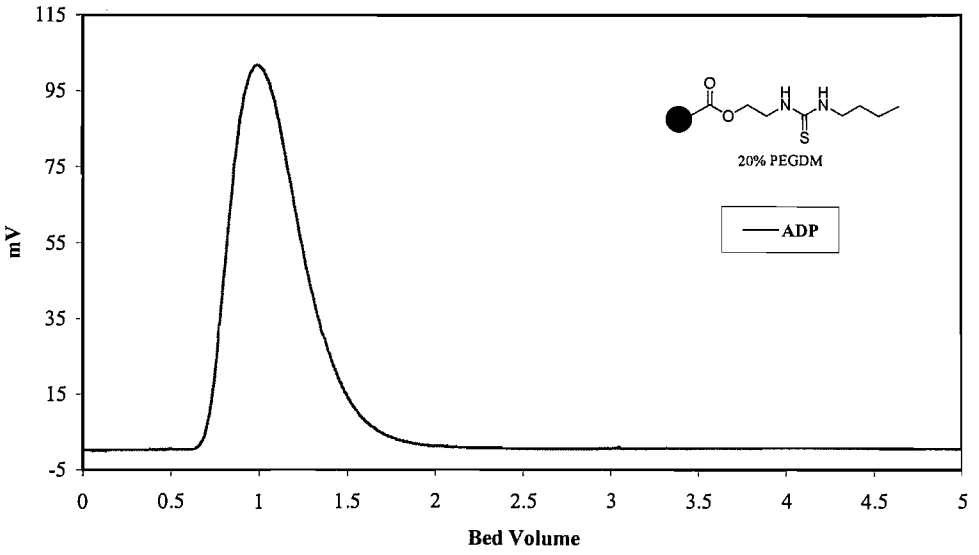

Ion exchange of ATP on 52 with NaClO4 0.5M, flowrate 0.40 mL/min, column 60x5 mm

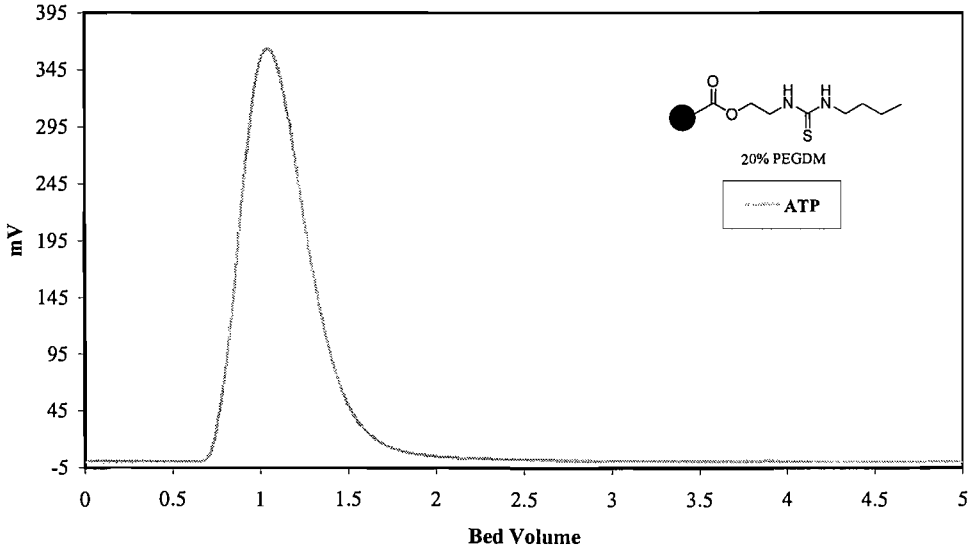

A.4 Elemental analysis templates

Example 1

Sample analysed by Medac Ltd.

Microanalysis	Carbon %	Hydrogen %	Nitrogen %
Found 1	83.45	7.54	4.53
Found 2	83.48	7.53	4.52

Elemental analysis results of the starting material (aminomethyl polystyrene resin).

Aminomethyl polystyrene	
Carbon %	89.53
Hydrogen %	7.84
Nitrogen %	2.00

Loading starting material=1.43 mmol/gram of resin.

Guanidinium group (part added).

Adding part	
Carbon %	15.11
Hydrogen %	5.07
Nitrogen % ($\%N_{Adding\ Part}$)	35.23
Mw	79.51

With the per cent Nitrogen % found in the above sample by Medac Ltd. the mass of attached part was calculated.

$$\textbf{Mass of attached part} = (\%N_{exp} - \%N_{Starting\ Material}) / (\%N_{Adding\ Part} - \%N_{exp})$$

Conversion of amine to guanidinium group can be calculated as follows:

% Conversion = [*Mass of attached part* / ((Loading x Mw)/1000)] x 100

The total mass (resin and the attached part) of carbon, hydrogen and nitrogen can be easily calculated:

Total mass of Carbon = ($\%C_{SM}$ /100) + (*Mass of attached part* x ($\%\ C_{AP}$ /100)

Total mass of hydrogen = ($\%H_{SM}$ /100) + (*Mass of attached part* x ($\%\ H_{AP}$ /100)

Total mass of Nitrogen = ($\%N_{SM}$ /100) + (*Mass of attached part* x ($\%\ N_{AP}$ /100)

With the total mass of each element the expected elemental analysis can be calculated.

Carbon % = [*Total Carbon mass* / (1 + *Mass of attached part*)] x 100

Hydrogen % = [*Total Hydrogen mass* / (1 + *Mass of attached part*)] x 100

Nitrogen % = [*Total Nitrogen mass* / (1 + *Mass of attached part*)] x 100

Example 2

Sample analysed by Medac Ltd.

Microanalysis	Carbon %	Hydrogen %	Nitrogen %
Found 1	51.35	7.41	5.22
Found 2	51.23	7.42	5.20

Elemental analysis results of the starting material (Macroprep epoxide).

Macroprep epoxide	
Carbon %	58.13
Hydrogen %	7.31

Loading starting material = 4 mmol/gram of resin.

Guanidinium group (part added).

Adding part	
Carbon %	12.50
Hydrogen %	6.30
Nitrogen % ($\%N_{Adding\ Part}$)	44
Mw	95.5

With the per cent Nitrogen % found in the above sample by Medac Ltd. the mass of attached part was calculated.

$$\textbf{Mass of attached part} = (\%N_{exp}) / (\%N_{Adding\ Part} - \%N_{exp})$$

Conversion to epoxide can be calculated as follows:

$$\textbf{\% Conversion} = [\textit{Mass of attached part} / ((\text{Loading} \times \text{Mw})/1000)] \times 100$$

The total mass (resin and the attached part) of carbon, hydrogen and nitrogen can be easily calculated as:

$$\textbf{Total mass of Carbon} = (\%C_{SM} /100) + (\textit{Mass of attached part} \times (\% C_{AP} /100)$$

$$\textbf{Total mass of Hydrogen} = (\%H_{SM} /100) + (\textit{Mass of attached part} \times (\% H_{AP} /100)$$

$$\textbf{Total mass of Nitrogen} = (\textit{Mass of attached part} \times (\% N_{AP} /100)$$

With the total mass of each element the expected elemental analysis can be calculated.

$$\textbf{Carbon \%} = [\textit{Total Carbon mass} / (1 + \textit{Mass of attached part})] \times 100$$

$$\textbf{Hydrogen \%} = [\textit{Total Hydrogen mass} / (1 + \textit{Mass of attached part})] \times 100$$

$$\textbf{Nitrogen \%} = [\textit{Total Nitrogen mass} / (1 + \textit{Mass of attached part})] \times 100$$

Example 3

Sample analysed by Medac Ltd.

Microanalysis	Carbon %	Hydrogen %	Chlorine %
Found 1	73.92	6.30	17.44
Found 2	73.87	6.27	17.55

Composition of the starting material of the polymer.

Composition	Carbon % (C_{comp})	Hydrogen % (H_{comp})
DVB	92.26	7.74
Styrene	92.26	7.74

VBC Composition	(VBC_{comp})
% C	70.83
% H	5.94
% Cl	23.23

Composition of each starting material that has been used to synthesised the polymer.

Composition	$\%_{material}$
Styrene	15
DVB	5
VBC	80

With the experimental Chlorine % found in the above sample by Medac Ltd. the loading of the resin was calculated.

$$\textbf{Loading} = [(\%Cl_{exp})/ (100 \times 35.5)] \times 1000$$

With the theoretical composition of each element the expected elemental analysis can be calculated.

Carbon % = [(%C_{mat} Styrene /100) x (%C_{comp} Styrene)] + [(%C_{mat} DVB /100) x (%C_{comp} DVB)] + [(%C_{mat} VBC /100) x (%C_{comp} VBC)]

Hydrogen % = [(%H_{mat} Styrene /100) x (%H_{comp} Styrene)] + [(%H_{mat} DVB /100) x (%H_{comp} DVB)] + [(%H_{mat} VBC /100) x (%H_{comp} VBC)]

Chlorine % = [(%Cl_{mat} VBC /100) x (%Cl_{comp} VBC)]

References

(1) Lehn, J. M. *Angew. Chem.-Int. Edit. Engl.* **1988**, *27*, 89.

(2) Fischer, E. *Ber. Dtsch. Chem. Ges.* **1894**, 2985.

(3) Sessler, J. L.; Sansom, P. I.; Andrievsky, A.; Kral, V. In *Supramolecular Chemistry of Anions*; Bianchi, A., Bowman-James, K., García-España, E., Eds.; Wiley-VCH: New York, 1997.

(4) Chakrabarti, P. *J. Mol. Biol.* **1993**, *234*, 463.

(5) Mangani, S.; Ferraroni, M. In *Supramolecular Chemistry of anions*; Bianchi, A., Bowman-James, K., García-España, E., Eds.; Wiley-VCH: New York, 1997.

(6) Scheele, J.; Timmerman, P.; Reinhoudt, D. N. *Chem. Commun.* **1998**, 2613

(7) Glidewell, C. *Chem. Br.* **1990**, *26*, 137.

(8) Moss, B. *Chem. Ind.* **1996**, *13*, 407.

(9) Holloway, J. M.; Dahlgren, R. A.; Hansen, B.; Casey, W. H. *Nature* **1998**, *395*, 785.

(10) Voet, D.; Voet, J. G.; Pratt, C. W. *Fundamentals of Biochemistry*; Wiley: New York, 1999.

(11) Simmons, H. E.; Park, C. H. *J. Am. Chem. Soc.* **1968**, *90*, 2428.

(12) Higgins, C. *Nature* **1992**, *358*, 536-536.

(13) Calnan, B. J.; Tidor, B.; Biancalana, S.; Hudson, D.; Frankel, A. D. *Science* **1991**, *252*, 1167.

(14) Ledvina, P. S.; Tsai, A. L.; Wang, Z. M.; Koehl, E.; Quiocho, F. A. *Protein Sci.* **1998**, *7*, 2550.

(15) He, J. J.; Quiocho, F. A. *Protein Sci.* **1993**, *2*, 1643.

(16) Steed, J. W.; Atwood, J. L. *Supramolecular Chemistry*; John Wiley & Sons: Chichester, 2000.

(17) Hofmeister, F. *Arch. Exp. Pathor. Pharmakol.* **1888**, *24*, 247.

(18) Choi, K. H.; Hamilton, A. D. *J. Am. Chem. Soc.* **2001**, *123*, 2456.

(19) Sansone, F.; Baldini, L.; Casnati, A.; Lazzarotto, M.; Ugozzoli, F.; Ungaro, R. *Proc. Natl. Acad. Sci. U. S. A.* **2002**, *99*, 4842.

(20) Beer, P. D.; Gale, P. A.; Hesek, D. *Tetrahedron Lett.* **1995**, *36*, 767.

(21) Galan, A.; Andreu, D.; Echavarren, A. M.; Prados, P.; Demendoza, J. *J. Am. Chem. Soc.* **1992**, *114*, 1511.

(22) Liu, F.; Lu, G. Y.; He, W. J.; Wang, Z. S.; Zhu, L. G. *Chin. J. Chem.* **2001**, *19*, 317.

(23) Linton, B. R.; Goodman, M. S.; Fan, E.; van Arman, S. A.; Hamilton, A. D. *J. Org. Chem.* **2001**, *66*, 7313.

(24) Benito, J. M.; Gomez-Garcia, M.; Blanco, J. L. J.; Mellet, C. O.; Fernandez, J. M. G. *J. Org. Chem.* **2001**, *66*, 1366.

(25) Sasaki, S.; Mizuno, M.; Naemura, K.; Tobe, Y. *J. Org. Chem.* **2000**, *65*, 275.

(26) Lee, K. H.; Hong, J. I. *Tetrahedron Lett.* **2000**, *41*, 6083.

(27) James, A. T.; Martin, A. J. P. *Biochem. J.* **1952**, *50*, 679.

(28) Bungay, H. R. *Basic Biochemical Engineering.*; BiLine Associates, 1993.

(29) Harris, D. C. *Quantitative Chemical Analysis.*; W. H. Freeman and Company, 1995.

(30) Small, H.; Stevens, T. S.; Bauman, W. C. *Anal. Chem.* **1975**, *47*, 1801.

(31) Gjerde, D. T.; Fritz, J. S. *Ion Chromatography*; 2nd ed.; Hüthig: Heidelberg, 1987.

(32) Haddad, P. R.; Jackson, P. E. *Ion Chromatography*; Elsevier: Amsterdam, 1990.

(33) Weiss, J. *Ion Chromatography*; 2nd ed.; VCH: Weinheim, 1995.

(34) Tarter, J. G. *Ion Chromatography*; Marcel Decker: New York, 1987.

(35) Hirayama, N.; Umehara, W.; Makizawa, H.; Honjo, T. *Anal. Chim. Acta.*

2000, *409*, 17.

(36) Horie, H.; Yamauchi, Y.; Kohata, K. *J. Chromatogr. A* **1998**, *817*, 139.

(37) Woodman, J. S. In *Coffee*; Clarke, R. J., Macrae, R., Eds.; Elsevier: Essex, 1985; Vol. 1, pp 266-287.

(38) Alcáraz, A.; Fernández-Cáceres, P. L.; Martín, M. J.; Pablos, F.; González, A. G. *Talanta.* **2003**, *61*, 95.

(39) Brown, D. M.; Pietrzyk, D. J. *J. Chromatogr.* **1989**, *466*, 291.

(40) Pietrzyk, D. J.; Senne, S. M.; Brown, D. M. *J. Chromatogr.* **1991**, *546*, 101.

(41) Gan, D. C.; Tarter, J. G. *J. Chromatogr.* **1987**, *404*, 285.

(42) Tarter, J. G. *J. Chromatogr.* **1986**, *367*, 191.

(43) Iskandarani, Z.; Miller, T. E. *Anal. Chem.* **1985**, *57*, 1591.

(44) Small, H.; Miller, T. E. *Anal. Chem.* **1982**, *54*, 462.

(45) Karim, K. J. B. A.; Ji-Ye; Takeuchi, T. *J.Chromatogr. A.* **2003**, *995*, 153.

(46) "An Introduction to Platinum Group Metals," 2004.

(47) Kendall, T. "Platinum 2004 Interim Review," Johnson Matthey, 2004.

(48) Christie, T.; Challis, A. "Mineral Commodity Report 5 - Platinum Group Metals," Institute of Geological and Nuclear Sciences Ltd, 1994.

(49) Basolo, F.; Pearson, R. G. *Mechanisms of Inorganic Reactions*; 2nd ed.; Wiley: London, 1967.

(50) Basolo, F.; Charr, J.; Gray, H. B.; Pearson, R. G.; Shaw, B. L. *J. Chem. Soc.* **1961**, 2207.

(51) Grant, R. A. In *Precious Metals Recovery and Refining Seminar*; Manzeik, L., Ed.: Scottsdale, Arizona, USA, 1989, 1990.

(52) Buslaeva, T. M.; Simanova, S. A. *Russ. J. Coord. Chem.* **1999**, *25*, 151.

(53) Cleare, M. J.; Grant, R. A.; Charlesworth, P. "Separation of the platinum group metals by use of selective solvent extraction techniques," Johnson Matthey Research Centre.

(54) Gindin, L. M.; Bobikov, P. I.; Kouba, E. F. *Izv. Sib. Otd. Akad. Nauk. SSSR.* **1961**, *10*, 84.

(55) Dolgikh, V. I.; Bobikov, P. I.; Borbat, V. F.; Kouba, E. F.; Gindin, L. M. *Tsevt. Metall.* **1964**, 9.

(56) Kuzmichev, G. V.; Blednov, B. P.; Dul'nyeva, W. E. *Tsevt. Metall.* **1970**, *43*, 62.

(57) Vasileva, A. A.; Gindin, L. M.; Kurbatova, N. V. *Izv. Sib. Otd. Akad. Nauk.*

SSSR, Ser Khim. **1971**, *2*, 67.

(58) Dolgikh, V. I.; Bobikov, P. I.; Borbat, V. F.; Ferberg, M. B.; Gindin, L. M. *Tsevt. Metall.* **1970**, *43*, 87.

(59) Savchenko, V. I.; Makaryan, I. A. *Platinum Metals Rev.* **1999**, *43*, 74.

(60) Rehkämper, M.; Halliday, A. N. *Talanta.* **1997**, *44*, 663.

(61) Schmuckler, G.; Technion Research and Development Foundation Ltd.: Israel, 1989, p 8.

(62) Limoni-Relis, B.; Schmuckler, G. *Sep. Sci. Technol.* **1995**, *20*, 337.

(63) Ge, X.; Wendler, I.; Schramel, P.; Kettrup, A. *React. Funct. Polym.* **2004**, *61*, 1.

(64) Strecker, A. *Liebigs Ann.* **1861**, *118*, 151.

(65) Patai, S.; Rappoport, Z. *The Chemistry of Amidines and Imidates*; Wiley: Chichester, 1991; Vol. 2.

(66) Häfelinger, G.; Kuske, F. K. H. In *The Chemistry of Amidines and Imidates*; Patai, S., Rappoport, Z., Eds.; Wiley: Chichester, 1991; Vol. 2, p chapt. 1.

(67) Gund, P. *J. Chem. Educ.* **1972**, *49*, 100.

(68) Krygowski, T. M.; Cyranski, M. K.; Anulewicz-Ostrowska, R. *Pol. J. Chem.* **2001**, *75*, 1939.

(69) Pauling, L.; Brockway, L. O.; Beach, J. Y. *J. Am. Chem. Soc.* **1935**, *57*, 2705.

(70) Pauling, L. *Nature of the Chemical Bond*; Universty Press: Ithaca, NY, 1942.

(71) Amekraz, B.; Tortajada, J.; Morizur, J. P.; Gonzalez, A. I.; Mo, O.; Yanez, M.; Leito, I.; Maria, P. C.; Gal, J. F. *New J. Chem.* **1996**, *20*, 1011.

(72) Olah, G. A.; Burrichter, A.; Rasul, G.; Hachoumy, M.; Prakash, G. K. S. *J. Am. Chem. Soc.* **1997**, *119*, 12929.

(73) Taft, R. W.; Raczynska, E. D.; Maria, P. C.; Leito, I.; Gal, J. F.; Decouzon, M.; Drapala, T.; Anvia, F. *Pol. J. Chem.* **1995**, *69*, 41.

(74) Tortajada, J.; Leon, E.; Luna, A.; Mo, O.; Yanez, M. *J. Phys. Chem.* **1994**, *98*, 12919.

(75) Olah, G. A.; White, A. H. *J. Am. Chem. Soc.* **1968**, *90*, 6087.

(76) Williams, G.; Hardy, M. L. *J. Chem. Soc.* **1963**, 2560.

(77) Olah, G. A. *A Life of Magic Chemistry*; Wiley: New York, 2001.

(78) Hulanicki, A. *Reactions of Acids and Bases in Analytical Chemistry*; Warsaw and Ellis Horwood: Chichester, 1987.

(79) Yamamoto, Y.; Kojima, S. In *The Chemistry of Amidines and Iminates*; Patai,

S., Rappoport, Z., Eds.; Wiley: Chichester, 1991; Vol. 2, p chapt. 10.

(80) Perrin, D. D. *Dissociation Constants of Organic Bases in Aqueous Solution*; Butterworths: London, 1965; Vol. Supplement, 1972.

(81) Alder, R. W. *Chemical Reviews* **1989**, *89*, 1215.

(82) Schwesinger, R. *Angew. Chem.-Int. Edit. Engl.* **1987**, *26*, 1164.

(83) Schwesinger, R. *Nachr. Chem. Tech. Lab.* **1990**, *38*, 1214.

(84) Perreault, D. M.; Cabell, L. A.; Anslyn, E. V. *Bioorg. Med. Chem.* **1997**, *5*, 1209.

(85) Schmidtchen, F. P.; Berger, M. *Chem. Rev.* **1997**, *97*, 1609.

(86) Atwood, J. L.; Steed, J. W. In *Supramolecular Chemistry of Anions*; Bianchi, A., Bowman-James, K., García-España, E., Eds.; Wiley-VCH, New York, 1997, pp 147-216.

(87) Jubian, V.; Dixon, R. P.; Hamilton, A. D. *J. Am. Chem. Soc.* **1992**, *114*, 1120.

(88) Echavarren, A.; Galan, A.; Lehn, J. M.; de Mendoza, J. *J. Am. Chem. Soc.* **1989**, *111*, 4994-4995.

(89) Metzger, A.; Lynch, V. M.; Anslyn, E. V. *Angew. Chem.-Int. Edit. Engl.* **1997**, *36*, 862.

(90) Dixon, R. P.; Geib, S. J.; Hamilton, A. D. *J. Am. Chem. Soc.* **1992**, *114*, 365.

(91) Bishop, R. B. *Practical Polymerisation for Styrene*; Cahners Publ. Co.: New York, 1971.

(92) Sherrington, D. C. *Chem. Commun.* **1998**, 2275.

(93) Alesso, S. M.; Yu, Z. R.; Pears, D.; Worthington, P. A.; Luke, R. W. A.; Bradley, M. *J. Comb. Chem.* **2001**, *3*, 631.

(94) Kolarz, B. N.; Jermakowicz-Bartkowiak, D.; Jezierska, J.; Apostoluk, W. *React. Funct. Polym.* **2001**, *48*, 169.

(95) Rittner, W. F.; Gulko, A.; Schmuckler, G. *Talanta.* **1970**, *17*, 807.

(96) Gulko, A.; Rittner, W. F.; Ron, G.; Weissman, A.; Schmuckler, G. *J. Inorg. Nucl. Chem.* **1971**, *33*, 761.

(97) Gulko, A.; Feigenbaum, H.; Schmuckler, G. *Anal. Chim. Acta.* **1972**, *59*, 397.

(98) Bernatowicz, M. S.; Wu, Y. L.; Matsueda, G. R. *J. Org. Chem.* **1992**, *57*, 2497.

(99) Zikos, C. C.; Ferderigos, N. G. *Tetrahedron Lett.* **1995**, *36*, 3741.

(100) Striegler, S. *Tetrahedron* **2001**, *57*, 2349.

(101) Delair, T.; Marguet, V.; Pichot, C.; Mandrand, B. *Colloid Polym. Sci.*

1994, *272*, 962.

(102) Mitchell, A. R.; Erickson, B. W.; Ryabtev, M. N.; Hodges, R. S.; Merrifield, R. B. *J. Am. Chem. Soc.* **1976**, *98*, 7357.

(103) Cai, J. Q.; Wathey, B. *Tetrahedron Lett.* **2001**, *42*, 1383.

(104) Moine, L.; Sherrington, D. C.; Grant, R. A.; Anglo Platinum Limited: GB, 2003, p 25.

(105) Gamcsik, M. P.; Hamill, T. G.; Colvin, M. *J. Med. Chem.* **1990**, *33*, 1009.

(106) Vlácil, F.; Vins, I.; Malicek, O. *Collect. Czech. Chem. Commun.* **1983**, *48*, 2255.

(107) Reynolds. *J. Chem. Soc.* **1869**, *22*, 1.

(108) Azman, A.; Lukman, B.; Hadzi, D. *J. Mol. Struct.* **1969**, *4*, 468.

(109) Zaidi, S. A. A.; Siddiqi, Z. A. *J. Inorg. Nucl. Chem.* **1975**, *37*, 1808.

(110) Olah, G. A.; Burrichter, A.; Rasul, G.; Christe, K. O.; Surya Prakash, G. K. *J. Am. Chem. Soc.* **1997**, *119*, 4345.

(111) Al-Bazi, S. J.; Freiser, H. *Solvent. Extr. Ion Exch.* **1988**, *6*, 1067.

(112) Diamantatos, A.; Verbeek, A. A. *Anal. Chim. Acta.* **1977**, *91*, 287.

(113) Rakovskii, E. E.; Shvedova, N. V.; Berliner, L. D. *J. Anal. Chem. USSR.* **1974**, *29*, 1946.

(114) Rakovskii, E. E.; Shvedova, N. V.; Berliner, L. D. *J. Anal. Chem. USSR.* **1975**, *30*, 1942.

(115) Siddhanta, S.; Das, H. R. *Talanta.* **1985**, *32*, 457.

(116) Uheida, A.; Zhang, Y.; Muhammed, M. *Solvent Extr. Ion Exch.* **2002**, *20*, 717.

(117) Uheida, A.; Zhang, Y.; Muhammed, M. *Solvent Extr. Ion Exch.* **2003**, *21*, 827.

(118) Parrish, J. R. *Chem. & Ind.* **1956**, 137.

(119) Koster, G.; Schmuckler, G. *Anal. Chim. Acta.* **1967**, *38*, 179.

(120) Warshawsky, A.; Fieberg, M. M. B.; Mihalik, P.; Murphy, T. G.; Ras, Y. B. *Sep. Purif. Meth.* **1980**, *9*, 209.

(121) Warshawsky, A.; Fieberg, M. M. B. *Nat. Inst. Metal. Tech.* **1971**, *Memo C82/70/3.*

(122) Warshawsky, A.; Fieberg, M. M. B.; Ras, Y. B. *Nat. Inst. Metal.* **1971**, *Rep. No. 1364.*

(123) Warshawsky, A.; Ras, Y. B. *Nat. Inst. Metal.* **1971**, *Rep. No. 1377.*

(124) Obrecht, D. *Helv. Chim. Acta.* **1997**, *80*, 65.

(125) Cotter, R. J.; Keogh, M. J.; Union Carbide Corporation: USA, 1975, p 5.

(126) Edwards, R. I.; Riele, W. A. M.; Bernfield, G. J. In *Handbook of Inorganic Chemistry*; Acres, G. J. K., Ed.; Springer Verlag: Berlin, 1986; Vol. A1, pp 1-23.

(127) Grant, R. A.; Smith, C. S. "Solvent Extraction of Ruthenium by a Mono N-Substituted Amide," Jonhson Matthey Technology Centre, 1996.

(128) Arpalahti, J.; Lippert, B. *Inorg. Chim. Acta.* **1988**, *153*, 51.

(129) Nakajima, K.; Kajino, T.; Monoyama, M.; Kojima, M. *Inorg. Chim. Acta.* **2001**, *312*, 67.

(130) Cotton, F. A.; Wilkinson, G. *Advanced Inorganic Chemistry*; Wiley Interscience: Chichester, 1988.

(131) Kavallieratos, K.; de Gala, S. R.; Austin, D. J.; Crabtree, R. H. *J. Am. Chem. Soc.* **1997**, *119*, 2325.

(132) Camiolo, S.; Gale, P. A.; Hursthouse, M. B.; Light, M. E.; Shi, A. J. *Chem. Commun.* **2002**, 758-759.

(133) Gale, P. A.; Navakhun, K.; Camiolo, S.; Light, M. E.; Hursthouse, M. B. *J. Am. Chem. Soc.* **2002**, *124*, 11228.

(134) Coles, S. J.; Frey, J. G.; Gale, P. A.; Hursthouse, M. B.; Light, M. E.; Navakhun, K.; Thomas, G. L. *Chem. Commun.* **2003**, 568.

(135) Hamilton, A. D.; Chang, S.-K. *J. Am. Chem. Soc.* **1988**, *110*, 1318.

(136) Hamilton, A. D.; Vanengen, D. *J. Am. Chem. Soc.* **1987**, *109*, 5035.

(137) Feibush, B.; Figueroa, A.; Charles, R.; Onan, K. D.; Feibush, P.; Karger, B. L. *J. Am. Chem. Soc.* **1986**, *108*, 3310.

(138) Hossain, M. A.; Llinares, J. M.; Powell, D.; Bowman-James, K. *Inorg. Chem.* **2001**, *40*, 2936.

(139) Hossain, M. A.; Kang, S. O.; Llinares, J. M.; Powell, D.; Bowman-James, K. *Inorg. Chem.* **2003**, *42*, 5043.

(140) Hynes, J. M. *J. Chem. Soc., Dalton., Trans.* **1993**, 311.

(141) Szumna, A.; Jurczak, J. *Eur. J. Org. Chem.* **2001**, 4031.

(142) Bisson, A. P.; Lynch, V. M.; Monahan, M. K. C.; Anslyn, E. V. *Angew. Chem.-Int. Edit. Engl.* **1997**, *36*, 2340.

(143) Gale, P. A.; Camiolo, S.; Tizzard, G. J.; Chapman, C. P.; Light, M. E.; Coles, S. J.; Hursthouse, M. B. *J. Org. Chem.* **2001**, *66*, 7849.

(144) Navakhun, K.; Gale, P. A.; Camiolo, S.; Light, M. E.; Hursthouse, M. B. *Chem. Commun.* **2002**, 2084.

(145) Gale, P. A.; Camiolo, S.; Chapman, C. P.; Light, M. E.; Hursthouse, M. B. *Tetrahedron Lett.* **2001**, *42*, 5095.

(146) Camiolo, S.; Gale, P. A.; Hursthouse, M. B.; Light, M. E. *Tetrahedron Lett.* **2002**, *43*, 6995.

(147) Denuault, G.; Gale, P. A.; Hursthouse, M. B.; Light, M. E.; Warriner, C. N. *New J. Chem.* **2002**, *26*, 811.

(148) Camiolo, S.; Coles, S. J.; Gale, P. A.; Hursthouse, M. B.; Tizzard, G. J. *Supramol. Chem.* **2003**, *15*, 231.

(149) Friedman, M. *J. Org. Chem.* **1965**, *30*, 589.